Report of Meteorological Laboratory *Vol.2 Nos.1—4*

STUDIES ON TYPHOON AND CONVECTION

By

Tetsuya FUJITA

JUNE 1952

Kyushu Institute of Technology

Tobata City, Japan

Report of Meteorological Laboratory *Vol. 2 Nos. 1~4*

STUDIES ON TYPHOON AND CONVECTION

By

Tetsuya FUJITA

JUNE 1952

Kyushu Institute of Technology

Tobata City, Japan

STUDIES ON TYPHOON AND CONVECTION

by Tetsuya Fujita

CHAPTER I

PRESSURE DISTRIBUTION WITHIN TYPHOON

CONTENTS

CHAPTER I PRESSURE DISTRIBUTION WITHIN TYPHOON

§ 1 Introduction

The pressure traces recorded at the time of a typhoon passage are well-shaped, suggesting that they might be shown by a mathematical expression. Y. Horiguchi studied the pressure field within the typhoon of Aug. 1924, concluding that the pressure is represented by the formula: $(760 - P)(r + 1.7) = 68.1$, where r is the distance from the typhoon center measured in 100 km. unit. It was known that this formula shows the pressure distribution within the typhoon studied by Horiguchi, but the formula is not so convenient when we attempt to represent the pressure curves for the other typhoons.

Introducing a variable x, the dimensionless quantity defined as the ratio r/r_0, K. Takahashi(26) presented the equation,

$$P = P_\infty - \frac{\Delta P}{1 + x} \qquad (x = r/r_0) \qquad \cdots\cdots (1)$$

where P is the pressure r km. from the center, P_∞ the pressure undisturbed by the typhoon, ΔP the depth of the pressure funnel, and r_0 the constant for each typhoon. It has been proved that this formula is capable of representing the pressure curves in the outer areas of typhoons. There remained, however, a fundamental problem that we must admit the existence of the finite pressure gradient at the center.

The pressure distribution in the vicinity of the center bas been studied by many writers, leading them to the conclusion that the pressure increases parabolically with the radius. Of course, in the outer area where the pronounced convergence is predominant, it is believed that the absolute angular momentum for each air parcel is

liable to be conserved. In the inner area, however, the parcels involved are rather stagnant, and they circulate as if they were fixed on a solid disc, on account of the internal friction and the eddy transfer of momentum. These motions of the air result in the initiation of a constant vorticity ζ in the vicinity of the center.

Now, we consider the case where the air flows along the circular isobar with the tangential velocity v_θ, the vorticity is written thus:

$$\zeta = \frac{1}{r}\frac{\partial}{\partial r}(r\, v_\theta) \qquad (2)$$

From the equation, it is known that the velocity v_θ is to be proportional to the radius, namely,

$$v_\theta = k\, r \qquad (3)$$

where, k is the constant having the value $\frac{1}{2}\zeta$,

whence, $$\zeta = \frac{1}{r}\frac{\partial}{\partial r} k\, r^2 = 2k$$

If the wind around the center be the cyclostrophic, we have

$$\frac{v_\theta^2}{r} = \frac{1}{\rho}\frac{\partial P}{\partial r}$$

Using the relation, $v_\theta = \frac{1}{2}\zeta\, r$, we obtain the pressure, thus:

$$P = P_\infty - \Delta P + \frac{\rho \zeta^2}{8} r^2 \qquad (4)$$

V. Bjerknes presented an expression,

$$P = P_\infty - \frac{\Delta P}{1+x^2} \qquad (x = r/r_0) \qquad (5a)$$

In the vicinity of the center, where x is very small, this formula can be reduced to

$$P = (P_\infty - \Delta P) + \Delta P\, x^2 \qquad (5b)$$

This equation shows that the pressure in center increases parabolically. In the outer area, however, the pressure approaches rapidly to P_∞, namely, the second term in the right side of the original equation is reduced to $\Delta P/x^2$. On the other hand, when x is very large Takahashi's equation is reduced to $P_\infty - \Delta P/x$ and it is known that the

typhoons in our country are well- represented by his equation.

§ 2 Examination of the Practical Pressure Distribution

In order to find out the equation which could represent the pressure curves for typhoons, it is very important to examine the pressure of many typhoons. The writer analysed the pressure field using the method presented hereunder.

The pressure curve of a typhoon through her center may be termed the profile. The profile would change, according to the direction, therefore, it will be better to define that the profile is the mean value of the ones along various directions. When the reporting stations are scattered uniformly in the typhoon areas, the profile can be drawn by plotting the pressure for each station. In the practical case, however, the stations are concentrated on the islands and the continent which do not cover the typhoon areas perfectly. The mean value along the circle with the radius R will be defined thus:

$$\overline{P}_R = \frac{1}{2\pi} \int_0^{2\pi} P_{R\theta}\, d\theta \qquad (6)$$

where, $P_{R\theta}$ is the pressure on the ring R km. from the center.

Using this method, many profiles for typhoons in their various stages were obtained, among which the case in Typhoon Jane of 3 Sept. 1950 is reproduced in Fig. 1.

In the practical computation of $\overline{P}_R$, it is desirable to obtain a great number of pressures on the circle. This is very laborious, therefore, the writer chose the pressures at the 36 points on the circle in Fig. 1, in order to calculate the value of $\overline{P}_R$ easily. The result was pretty much satisfactory and proved that Takahashi's equation is very capable for the representation of the outer field of

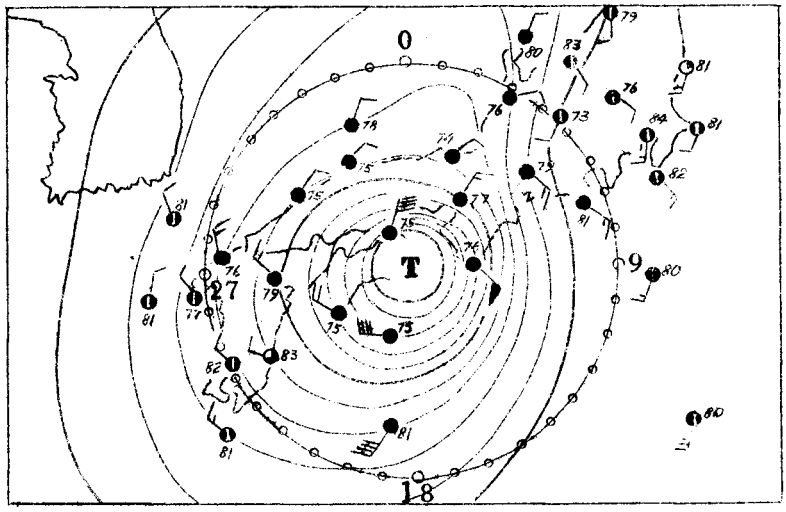

Fig. 1. To determine the mean pressure along the circle of the radius, 500 km. The circle is devided into every 10 degree segments. Typhoon Jane of 3 Sept. 1950.

typhoon.

Taking the above-mentioned characteristics of profiles into consideration, the writer obtained the equation which coincides with the equation by Takahashi in the outer area, and with that by Bjerknes in the vicinity of the center, that is,

$$P = P_\infty - \frac{\Delta P}{\sqrt{1+x^2}} \qquad (x = r/r_0) \qquad \text{(7a)}$$

This equation can be reduced to the formulas:

$$P = (P_\infty - \Delta P) + \frac{1}{2}\Delta P\, x^2 \qquad \text{(inner area)} \qquad \text{(7b)}$$

$$P = P_\infty - \Delta P/x \qquad \text{(outer area)} \qquad \text{(7c)}$$

There happened, however, an important problem how to connect the parabola in the center with the hyperbola extending to the infinite distance. Of course, the above-mentioned equation by the writer is one of the equations which would join the two curves.

Now it is likely that the pressure curves for typhoons are not so simple that they could be represented by the equations containing

only three constants, P_∞ , ΔP, and r_0.

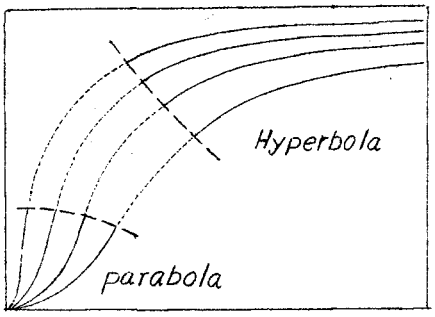

Fig. 2. Showing the curves which join the parabolas with hyperbolas.

To obtain a reasonable curve by connecting the two thick curves in Fig. 2, it is necessary to introduce a new constant by which the shape of the curve could be changed. The shape of the profile is closely related to the position of the inflexion point at which the profiles for inner and for outer areas could be connected continuously.

After the examination of profiles, it was known that the pressure ratio, $(P_{\text{infl.}} - P_{\text{center}}) : \Delta P$ is not always constant for each typhoon. By the way, the writer computed the pressure ratio for the equations, thus:

the ratio 0.000 for $P = P_\infty - \dfrac{\Delta P}{1 + x}$

the ratio 0.250 for $P = P_\infty - \dfrac{\Delta P}{1 + x^2}$

the ratio 0.184 for $P = P_\infty - \dfrac{\Delta P}{\sqrt{1 + x^2}}$

These results show that the ratios are constant for each equation, suggesting that it is not always able to represent the profile for an arbitrary typhoon.

§ 3 Radius Ratio of Pressure Profile

According to the discussion above, it is desirable to introduce the new constant which would change the pressure ratio presented before. In the practical case, however, it is very difficult to determine the location of the inflexion point on the curve accurately.

The writer, therefore, considered the ratio of two radii Rn and Rm corresponding to the pressures $\frac{2}{3}\Delta P$ and $\frac{1}{3}\Delta P$ lower than P_∞, instead of the value of $(P_{infl} - P_{center}) : \Delta P$ which could not be evaluated before the location of the inflexion point was given. As shown in Fig. 3, the value Rn/Rm will easily be obtained. Thus, the ratio Rn/Rm may be termed the radius ratio of a pressure profile.

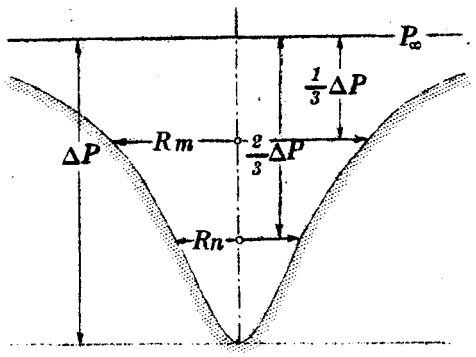

Fig. 3. How to determine the radius ratio Rn/Rm for a typhoon profile.

After the evaluation of the radius ratio for the formulas by many authors, it was known that the ratio for Takahashi's equation is minimum and that for Bjerknes' maximum.

According to the study of the practical pressure traces, the radius ratios are known to be about 0.10 - 1.0 for typhoons, and 1.0 - 10 for continental cyclones. In the redevelopment stage of a typhoon into an extra-tropical or continental cyclone, gradually the ratio increases. In this respect, Takahashi's equation is most suitable for the tropical storms having a steep funnel.

The variation of the radius ratio for the Muroto Typhoon of 21 Sept. 1934, which passed across Shikoku, Kinki, and Ou Districts, is shown below.

Time (MST)	5	6	7	8	9	10	11	12	13	14	15	16
Rn/Rm	0.17	0.17	0.16	0.17	0.23	0.30	0.31	0.33	0.36	0.38	0.41	0.41

21 September 1934

It will be seen in the table that the radius ratio changed rapidly, so that we must make an equation of wide range in the ratio, in order

to represent the profiles for the typhoon presented here.

§ 4 Cyclone Function

The writer obtained the function containing the new constant related to the radius ratio of the pressure curves, thus:

$$\Psi = \frac{1}{\sqrt{1 + \left(x \frac{x+1}{x+a}\right)^2}} \qquad (8a)$$

where, a is the constant capable of changing the radius ratio from 0.065 to 0.635. Therefore, it is clear that this function has an good adaptability from typhoon to continental cyclone in various stages.

Emphasizing the characteristic of the present function, it may be suitable to term this function "the Cyclone Function" together with the symbol Ψ. Using this symbol, the pressure of a typhoon can be written as follows: $P = P_\infty - \Psi \Delta P = f(P_\infty, \Delta P, a, r_0)$ (8b) It will become evident, in the following discussion, how completely this formula accounts for not only the pressure field, but also the pressure tendency, filling and deepening, expansion and shrink of isobars, and the temperature distribution within typhoons.

The four constants in formula (8a) are the important ones by which the shape of the pressure curves can perfectly be determined. Therefore, it is convenient to give them following names.

P_∞ ..... Undisturbed Pressure

ΔP ..... Pressure Depth

a ..... Cyclone Constant

r_0 ..... Unit Radius

THE VALUES OF

$$\Psi = f(x,a) = \frac{1}{\sqrt{1+\left(x\frac{x+1}{x+a}\right)^3}} \qquad \text{P 9 – 15}$$

$$\frac{\partial\Psi}{\partial x} = \Psi'_x = -\Psi^3\,\frac{x^4+(1+2a)x^3+3ax^2+ax}{(x+a)^3} \qquad \text{P 16 – 22}$$

$$\frac{\partial\Psi}{\partial a} = \Psi'_a = \Psi^3\,\frac{x^2(x+1)^2}{(x+a)^3} \qquad \text{P 23 – 29}$$

The values of Ψ'_x, which are always negative, are tabulated omitting the negative signes. All the quantities are shown in three figures, according to the following manner.

True Values	Tabular Values
13.8	138
7.26	726
0.377	377
0.0694	694
0.00213	213
0.000971	971
0.000057	057
0.000006	006

Computed February 1952 ·

x \ a	.00	.01	.02	.03	.04	.05	.06	.07	.08	.09	.10	.11	.12	.13	.14	.15
0.02	700	827	890	926	947	960	969	976	979	983	986	988	990	991	992	993
0.04	693	768	821	860	887	907	923	935	945	952	958	964	968	971	975	977
0.06	686	740	782	816	843	865	883	898	910	920	929	936	943	948	953	957
0.08	679	721	757	786	811	833	850	866	879	891	901	910	918	925	931	936
0.1	673	707	737	763	786	807	824	840	853	865	876	886	894	902	909	915
0.2	640	658	676	692	707	721	734	747	759	770	781	791	800	808	817	824
0.3	609	622	634	646	657	668	678	688	698	707	716	724	733	740	748	756
0.4	581	590	600	609	618	626	634	643	651	658	666	673	680	687	694	700
0.5	555	562	570	577	584	591	598	605	612	618	625	631	637	643	649	655
0.6	530	536	543	549	555	561	566	572	578	584	589	594	600	605	610	616
0.7	507	512	518	523	528	533	538	543	548	553	558	563	567	572	577	581
0.8	485	490	495	500	504	508	513	517	522	526	530	534	539	543	547	551
0.9	466	470	474	478	482	486	490	494	497	501	505	508	512	516	519	523
1.0	447	451	454	458	462	465	468	473	475	479	481	485	488	492	495	498
1.2	414	417	419	423	425	428	431	434	436	439	442	445	447	450	452	455
1.4	385	387	389	392	394	396	399	401	403	405	408	410	412	414	417	419
1.6	359	361	363	365	367	369	370	372	374	376	378	380	382	384	386	388
1.8	336	338	340	341	343	345	346	348	350	351	353	354	356	358	359	361
2.0	316	318	319	320	322	323	325	326	327	329	330	332	333	335	336	337
2.2	298	299	301	302	303	304	306	307	308	309	311	312	313	314	315	317
2.4	282	283	284	285	287	288	289	290	291	292	293	294	295	296	297	298
2.6	268	269	269	270	271	272	273	274	275	276	277	278	279	280	281	282
2.8	255	255	256	257	258	259	260	260	261	262	263	264	235	266	266	267
3.0	243	243	244	255	246	246	247	248	249	249	250	251	252	253	253	254
3.2	232	232	233	234	234	235	236	236	237	238	238	239	240	240	241	242
3.4	222	222	223	224	224	225	225	226	227	227	228	228	229	230	230	231
3.6	213	213	214	214	215	215	216	217	217	218	218	219	219	220	220	221
3.8	204	204	205	205	206	206	207	207	208	209	209	210	210	211	211	212
4.0	196	197	197	198	198	198	199	199	200	200	201	201	202	202	203	203
4.2	189	189	190	190	190	191	191	192	192	193	193	193	194	194	195	195
4.4	182	183	183	183	184	184	185	185	185	186	186	187	187	187	188	188
4.6	176	176	177	177	177	178	178	178	179	179	180	180	180	181	181	181
4.8	170	170	171	171	171	172	172	172	173	173	173	174	174	174	175	175
5.0	164	165	165	165	166	166	166	167	167	167	168	168	168	169	169	169
5.5	152	152	153	153	153	153	154	154	154	154	155	155	155	156	156	156
6.0	141	142	142	142	142	143	143	143	143	144	144	144	144	144	145	145
6.5	132	132	133	133	133	133	133	134	134	134	134	134	135	135	135	135
7.0	124	124	124	125	125	125	125	125	125	126	126	126	126	126	126	127
7.5	117	117	117	117	117	118	118	118	118	118	118	119	119	119	119	119
8.0	110	111	111	111	111	111	111	111	112	112	112	112	112	112	112	112
8.5	105	105	105	105	105	105	105	106	106	106	106	106	106	106	106	107
9.0	100	100	100	100	100	100	100	100	100	101	101	101	101	101	101	101
9.5	948	949	950	951	952	953	954	955	956	957	958	959	960	961	962	963
10.0	905	906	907	908	909	910	910	911	912	913	914	915	916	917	918	919
11.0	830	831	832	832	833	834	835	835	836	837	838	838	839	840	841	841
12.0	767	768	768	769	770	770	771	771	772	773	773	774	775	775	776	776
13.0	712	713	713	714	714	715	715	716	716	717	718	718	719	719	720	720
14.0	665	665	666	666	667	667	668	668	669	669	670	670	671	671	672	672
15.0	624	624	625	625	626	626	626	627	627	628	628	629	629	629	630	630
16.0	587	587	588	588	588	589	589	590	590	590	590	591	591	592	592	593
17.0	555	555	556	556	556	557	557	557	558	558	558	559	559	559	559	560
18.0	526	526	527	527	527	527	528	528	528	529	529	529	529	530	530	530
19.0	498	498	499	499	499	499	500	500	500	500	500	501	501	502	502	502

x \ a	.16	.17	.18	.19	.20	.21	.22	.23	.24	.25	.26	.27	.28	.29	.30	.32
0.02	994	994	995	996	996	996	997	997	997	997	998	998	998	998	998	998
0.04	979	981	982	984	985	986	987	989	989	990	991	991	992	992	993	994
0.06	961	964	967	969	971	974	975	977	978	979	981	982	983	984	985	986
0.08	940	945	949	952	955	958	961	963	965	967	969	971	972	974	975	977
0.1	921	926	931	935	939	942	946	949	951	954	956	958	960	962	964	967
0.2	832	838	845	851	857	863	868	873	878	882	887	890	894	898	901	907
0.3	763	769	776	782	788	794	800	805	810	815	720	825	829	834	838	846
0.4	707	713	719	725	731	736	742	747	752	757	762	767	772	776	781	789
0.5	661	666	672	677	682	687	693	697	702	707	711	716	720	725	729	736
0.6	621	626	630	635	640	645	649	654	658	663	667	672	675	680	684	692
0.7	586	590	594	599	603	607	612	616	620	624	628	632	636	639	643	651
0.8	555	559	563	567	571	574	578	582	586	589	593	596	600	603	607	614
0.9	527	531	534	537	541	545	548	551	554	558	561	565	568	571	574	581
1.0	502	505	508	511	514	518	521	524	526	530	533	536	539	542	545	551
1.2	458	460	463	466	469	471	474	476	479	482	484	486	489	492	494	499
1.4	421	423	426	428	430	432	434	436	439	441	443	445	447	449	451	455
1.6	390	392	393	395	397	399	401	403	404	406	408	410	412	414	416	419
1.8	363	364	366	367	369	371	373	374	375	377	379	380	382	383	385	388
2.0	339	340	341	343	344	345	347	348	350	351	353	354	355	357	358	361
2.2	318	319	320	321	323	324	325	326	327	329	330	331	332	334	335	337
2.4	299	300	301	302	304	305	306	307	308	309	310	311	312	313	314	316
2.6	283	284	285	286	287	288	289	289	290	291	292	293	294	295	296	298
2.8	268	269	270	271	272	272	273	274	275	276	276	277	278	279	280	281
3.0	255	255	256	257	258	259	259	260	261	261	262	263	264	264	265	267
3.2	242	243	244	245	245	246	247	247	248	249	249	250	251	251	252	253
3.4	232	232	233	233	234	235	235	236	236	237	238	238	239	239	240	241
3.6	222	222	223	223	224	224	225	225	226	227	227	228	228	229	229	230
3.8	212	213	213	214	214	215	215	216	216	217	217	218	218	219	219	220
4.0	204	204	204	205	205	206	206	207	207	208	208	209	209	210	210	211
4.2	196	196	196	197	197	198	198	199	199	200	200	200	201	201	202	203
4.4	188	189	189	190	190	190	191	191	192	192	192	193	193	194	194	195
4.6	182	182	182	183	183	184	184	184	185	185	185	186	186	186	187	188
4.8	175	176	176	176	177	177	177	178	176	178	179	179	179	180	180	181
5.0	170	170	170	170	171	171	171	172	172	172	173	173	173	174	174	175
5.5	156	157	157	157	157	158	158	158	158	159	159	159	160	160	160	161
6.0	145	145	146	146	146	146	146	147	147	147	147	148	148	148	148	149
6.5	135	136	136	136	136	136	137	137	137	137	137	138	138	138	138	139
7.0	127	127	127	127	128	128	128	128	128	128	129	129	129	129	129	130
7.5	119	119	120	120	120	120	120	120	121	121	121	121	121	121	121	122
8.0	113	113	113	113	113	113	113	114	114	114	114	114	114	114	115	115
8.5	107	107	107	107	107	107	107	108	108	108	108	108	108	108	108	109
9.0	101	101	102	102	102	102	102	102	102	102	102	102	103	103	103	103
9.5	964	965	966	967	968	969	970	971	972	973	974	975	976	977	978	980
10.0	919	920	921	922	923	924	925	926	927	928	928	929	930	931	932	934
11.0	842	843	844	844	845	846	847	847	848	849	850	850	851	852	853	854
12.0	777	778	778	779	780	780	781	781	782	783	783	784	785	785	786	787
13.0	721	721	722	722	723	724	724	725	725	726	726	727	727	728	729	730
14.0	673	673	673	674	674	675	675	676	676	677	677	678	678	679	679	680
15.0	631	631	631	631	632	632	633	633	634	634	635	635	635	636	636	637
16.0	593	593	594	594	594	595	595	596	596	596	597	597	597	598	598	599
17.0	560	560	561	561	561	562	562	562	563	563	563	564	564	564	565	565
18.0	531	531	531	532	532	532	532	533	533	533	534	534	534	534	535	535
19.0	502	503	503	503	503	504	504	504	504	505	505	505	506	506	506	506

x \ a	.34	.36	.38	.40	.42	.44	.46	.48	.50	.52	.54	.56	.58	.60	.65	.70
0.02	999	999	999	999	999	999	999	999	999	100	100	100	100	100	100	100
0.04	994	995	995	996	996	996	997	997	997	997	998	998	998	998	998	999
0.06	988	989	990	991	991	992	993	993	994	994	995	995	995	995	996	996
0.08	979	981	982	984	985	986	987	988	989	990	991	991	992	992	993	994
0.1	970	973	975	977	978	979	981	982	983	984	985	986	987	988	989	991
0.2	914	919	924	928	932	936	940	943	946	949	951	953	955	957	962	966
0.3	854	860	867	873	879	884	889	894	898	930	907	911	914	917	925	931
0.4	797	805	812	819	826	832	838	843	849	854	859	864	868	873	882	891
0.5	746	753	761	768	775	781	788	794	800	805	811	816	821	826	837	848
0.6	700	707	714	721	728	735	741	747	753	759	765	770	776	781	793	804
0.7	658	665	672	678	685	692	698	704	709	716	721	726	732	736	750	762
0.8	621	627	634	640	647	652	658	665	670	676	681	687	692	697	709	721
0.9	587	593	599	605	611	616	623	628	633	639	644	649	654	659	671	683
1.0	556	562	568	573	579	584	590	594	600	605	610	615	620	624	636	647
1.2	504	509	514	518	523	528	532	537	542	546	551	555	559	563	574	584
1.4	460	464	468	472	476	480	484	488	492	496	500	504	507	511	521	530
1.6	423	426	430	433	437	440	444	447	451	454	458	461	464	468	476	484
1.8	391	394	397	400	403	406	409	412	415	419	421	424	427	430	437	446
2.0	363	366	369	371	374	377	379	382	385	387	390	392	395	398	404	410
2.2	339	342	344	347	349	351	354	356	358	360	363	365	367	370	375	381
2.4	318	320	322	325	327	329	331	333	335	337	338	342	343	345	350	355
2.6	300	301	303	305	307	309	311	312	314	316	318	320	322	323	328	332
2.8	283	285	286	288	290	291	293	295	296	298	300	301	303	304	308	312
3.0	268	270	271	273	274	276	277	279	280	281	283	285	286	287	291	295
3.2	255	256	257	259	260	261	263	264	265	267	268	269	271	272	275	279
3.4	243	244	245	246	247	249	250	251	252	254	255	256	257	258	261	264
3.6	231	232	234	235	236	237	238	239	240	241	243	244	245	246	249	251
3.8	221	222	223	224	225	226	227	228	229	230	231	232	233	234	237	239
4.0	212	213	214	215	216	217	217	218	219	220	221	222	223	224	226	229
4.2	203	204	205	206	207	208	209	209	210	211	212	213	214	215	217	219
4.4	196	196	197	198	199	200	200	201	202	203	204	204	205	206	208	210
4.6	188	189	190	190	191	192	193	193	194	195	196	196	197	198	199	201
4.8	181	182	183	183	184	185	186	186	187	188	188	189	190	190	192	194
5.0	175	176	177	177	178	178	179	180	180	181	182	182	183	184	185	187
5.5	161	162	162	163	163	164	164	165	165	166	166	167	168	168	169	171
6.0	149	150	150	151	151	152	152	152	153	153	154	154	155	155	156	158
6.5	139	139	140	140	141	141	141	142	142	143	143	143	144	144	145	146
7.0	130	130	131	131	131	132	132	132	133	133	133	134	134	134	135	136
7.5	122	122	123	123	123	124	124	124	125	125	125	125	126	126	127	128
8.0	115	115	116	116	116	116	117	117	117	118	118	118	118	119	119	120
8.5	109	109	109	110	110	110	110	111	111	111	111	112	112	112	113	113
9.0	103	103	104	104	104	104	105	105	105	105	105	106	106	106	107	107
9.5	982	984	986	988	990	992	994	996	998	100	100	100	100	100	101	101
10.0	936	937	939	941	943	945	946	948	950	952	954	955	957	959	964	968
11.0	856	857	859	860	862	863	865	866	868	869	871	872	874	875	879	883
12.0	788	790	791	792	793	795	796	797	799	800	801	802	804	805	808	811
13.0	731	732	733	734	735	736	737	738	739	741	742	743	744	745	748	751
14.0	681	682	683	684	685	686	687	688	689	689	690	691	692	693	696	698
15.0	638	638	639	640	641	642	643	643	645	645	646	647	648	649	651	653
16.0	600	600	601	602	603	603	604	605	606	606	607	608	608	609	611	613
17.0	566	567	567	568	568	569	570	570	571	572	572	573	574	574	576	577
18.0	536	536	537	538	538	539	539	540	541	541	542	542	543	543	545	546
19.0	507	508	508	509	509	510	510	511	512	512	513	513	514	514	516	517

x \ a	.75	.80	.85	.90	.95	1.0	1.1	1.2	1.3	1.4	1.5	1.6	1.7	1.8	1.9	2.0
0.02	100	100	100	100	100	100	100	100	100	100	100	100	100	100	100	100
0.04	999	999	999	999	999	999	100	100	100	100	100	100	100	100	100	100
0.06	997	998	998	998	998	998	999	999	999	999	999	100	100	100	100	100
0.08	995	995	996	996	997	997	998	998	998	999	999	999	999	999	999	999
0.1	992	993	994	994	995	995	996	997	997	998	998	998	998	999	999	999
0.2	969	972	975	977	979	980	983	986	987	989	990	991	992	993	994	994
0.3	937	942	947	951	955	957	963	968	972	975	977	979	981	983	985	986
0.4	899	906	912	918	923	928	937	943	950	955	959	963	966	969	972	974
0.5	857	866	874	881	888	894	905	914	923	930	936	941	946	951	954	957
0.6	815	824	833	842	850	857	870	882	892	902	909	917	923	928	934	938
0.7	773	784	794	802	811	819	834	847	859	870	880	888	896	902	909	915
0.8	733	743	753	763	772	781	797	811	825	837	848	857	866	875	882	889
0.9	694	705	715	725	734	743	760	776	789	803	815	826	836	845	853	861
1.0	658	669	678	688	698	707	724	740	754	768	780	792	803	813	823	832
1.2	594	604	614	623	631	640	657	673	687	702	714	728	739	751	761	771
1.4	539	548	556	565	573	581	597	612	626	640	653	666	678	690	701	711
1.6	492	500	507	515	523	630	545	558	572	585	597	610	621	633	644	654
1.8	451	459	465	472	479	486	499	511	524	536	548	559	570	581	592	602
2.0	417	423	429	435	441	447	459	470	482	493	504	514	525	535	545	555
2.2	387	392	398	403	409	414	424	435	445	455	465	475	485	494	503	512
2.4	360	365	370	375	380	384	394	404	413	422	431	440	449	458	466	474
2.6	337	341	346	350	354	359	367	376	384	393	401	409	417	425	433	441
2.8	317	320	325	328	332	336	344	352	360	367	375	382	390	397	404	411
3.0	298	302	305	309	313	316	323	330	337	344	351	358	365	371	378	385
3.2	282	285	289	292	295	298	305	311	318	324	330	337	343	349	355	361
3.4	267	270	273	276	279	282	288	294	300	305	311	317	323	328	334	339
3.6	254	257	260	262	265	268	273	279	284	289	294	300	305	310	316	320
3.8	242	244	247	249	252	255	259	264	269	274	279	284	289	293	298	303
4.0	231	233	236	238	240	243	247	252	256	260	265	269	274	278	283	287
4.2	221	223	225	227	230	232	236	240	244	248	252	257	261	265	269	273
4.4	212	214	216	218	220	222	226	229	233	237	241	245	249	253	256	260
4.6	203	205	207	209	211	212	216	220	223	227	230	234	238	241	245	248
4.8	195	197	199	201	202	204	207	211	214	217	221	224	227	231	234	237
5.0	188	190	191	193	195	196	199	202	206	209	212	215	218	221	224	227
5.5	172	173	175	176	178	179	182	184	187	190	192	195	198	200	203	206
6.0	159	160	161	162	163	164	167	169	171	173	176	178	180	183	185	187
6.5	147	148	149	150	151	152	154	156	158	160	162	164	166	168	170	172
7.0	137	138	139	140	141	141	143	145	147	148	150	152	153	155	157	159
7.5	128	129	130	131	131	132	134	135	137	138	140	141	143	144	146	148
8.0	121	121	122	123	123	124	125	127	128	129	131	132	134	135	136	138
8.5	114	114	115	116	116	117	118	119	121	122	123	124	125	127	128	129
9.0	108	108	109	109	110	110	112	113	114	115	116	117	118	119	120	121
9.5	102	103	103	104	104	105	106	107	108	109	110	111	111	112	113	114
10.0	973	977	982	986	991	995	100	101	102	103	104	105	106	107	108	109
11.0	886	890	894	898	901	905	912	920	927	935	942	949	957	964	971	979
12.0	814	817	821	824	827	830	836	843	849	856	862	868	875	881	888	894
13.0	753	756	759	762	764	767	772	778	783	789	794	799	805	810	816	821
14.0	700	703	705	707	710	712	717	722	726	731	736	741	746	750	755	760
15.0	655	657	659	661	663	665	669	673	677	681	686	690	694	698	702	706
16.0	615	617	618	620	622	624	628	631	635	638	642	646	649	653	656	660
17.0	579	581	582	584	585	587	590	594	597	600	604	607	610	613	617	620
18.0	548	549	551	552	554	555	557	561	563	566	569	572	575	577	580	583
19.0	518	520	521	522	524	525	528	530	533	536	539	541	544	547	549	552

x \ a	2.1	2.2	2.3	2.4	2.5	2.6	2.7	2.8	2.9	3.0	3.2	3.4	3.6	3.8	4.0	4.2
0.02	100	100	100	100	100	100	100	100	100	100	100	100	100	100	100	100
0.04	100	100	100	100	100	100	100	100	100	100	100	100	100	100	100	100
0.06	100	100	100	100	100	100	100	100	100	100	100	100	100	100	100	100
0.08	999	100	100	100	100	100	100	100	100	100	100	100	100	100	100	100
0.1	999	999	999	999	999	999	999	100	100	100	100	100	100	100	100	100
0.2	995	995	996	996	996	997	997	997	997	997	998	998	998	998	999	999
0.3	987	988	989	990	991	991	992	992	993	993	994	995	995	996	996	996
0.4	976	978	979	980	982	983	984	985	986	987	988	989	990	991	992	993
0.5	961	964	966	968	970	972	974	975	976	978	980	982	983	985	986	988
0.6	942	946	949	952	955	957	960	962	964	966	969	972	975	977	979	980
0.7	920	926	929	934	937	940	943	946	949	952	956	960	964	967	969	972
0.8	895	901	907	912	917	921	925	928	931	935	940	946	950	954	957	961
0.9	868	876	882	888	894	898	904	908	912	916	923	929	935	940	944	948
1.0	840	848	855	862	868	874	879	884	890	894	903	910	917	923	928	933
1.2	781	790	798	806	814	821	828	835	841	847	858	867	876	884	892	898
1.4	721	731	740	749	757	766	773	781	788	795	807	819	830	840	849	858
1.6	665	675	684	693	702	710	719	727	734	742	756	769	781	792	803	813
1.8	612	622	631	640	649	658	666	674	682	690	705	718	731	743	755	766
2.0	564	573	582	591	600	608	616	624	632	640	655	669	682	695	707	718
2.2	521	530	539	547	555	564	570	579	586	594	609	623	636	649	661	673
2.4	483	491	499	507	515	523	530	537	545	552	566	579	593	605	617	629
2.6	449	456	464	471	478	486	493	500	506	513	527	540	552	565	576	588
2.8	418	425	432	439	446	453	459	466	472	479	491	503	515	527	539	550
3.0	391	398	404	410	417	423	429	435	441	447	459	471	482	493	504	515
3.2	367	373	379	385	391	396	402	408	413	419	430	441	452	462	472	483
3.4	345	351	356	361	367	372	378	383	388	393	404	414	424	434	444	453
3.6	326	331	336	341	346	351	356	360	365	370	380	389	399	408	417	426
3.8	308	312	317	322	326	331	336	340	345	350	359	367	376	385	393	402
4.0	292	296	300	305	309	313	318	322	326	330	339	347	355	363	371	379
4.2	277	281	285	289	293	297	301	305	309	313	321	328	336	343	351	359
4.4	264	268	271	275	279	283	286	290	294	297	305	312	319	326	334	340
4.6	252	255	259	262	266	269	273	276	280	283	290	297	303	310	317	323
4.8	241	244	247	250	254	257	260	263	267	270	276	282	289	295	301	308
5.0	230	233	236	239	243	246	249	252	255	258	264	270	275	281	287	293
5.5	208	211	213	216	219	221	224	226	229	231	237	242	247	252	257	262
6.0	189	192	194	196	198	201	203	205	207	210	214	218	223	227	232	236
6.5	174	176	178	180	182	183	185	187	189	191	195	200	203	207	211	214
7.0	160	162	164	165	167	169	171	172	174	176	179	183	186	189	193	196
7.5	149	151	152	154	155	157	158	160	161	163	166	169	172	175	178	180
8.0	139	140	142	143	144	146	147	148	150	151	154	156	159	162	164	167
8.5	130	131	133	134	135	136	137	139	140	141	143	146	148	151	153	155
9.0	122	124	125	126	127	128	129	130	131	132	134	137	139	141	143	145
9.5	115	116	117	118	119	120	121	122	123	124	126	128	130	132	134	136
10.0	109	110	111	112	113	114	115	116	117	118	119	121	123	124	126	128
11.0	98	99	100	101	102	103	103	104	105	106	107	108	110	111	113	114
12.0	90	90	91	91	92	93	93	94	95	95	97	98	99	101	102	103
13.0	82	83	83	84	84	85	85	86	87	87	88	89	90	91	93	94
14.0	76	76	77	77	78	78	79	79	80	80	71	82	83	84	85	86
15.0	71	71	71	72	72	73	73	73	74	74	75	76	77	78	78	79
16.0	66	66	67	67	67	68	68	69	69	69	70	71	71	72	73	74
17.0	62	62	63	63	63	63	64	64	64	65	65	66	67	67	68	69
18.0	58	58	59	59	59	60	60	60	61	61	61	62	63	63	64	64
19.0	55	55	56	56	56	56	57	57	57	57	57	58	58	59	59	60

x \ a	4.4	4.6	4.8	5.0	5.2	5.4	5.6	5.8	6.0	6.5	7.0	7.5	8.0	8.5	9.0	9.5
0.02	100	100	100	100	100	100	100	100	100	100	100	100	100	100	100	100
0.04	100	100	100	100	100	100	100	100	100	100	100	100	100	100	100	100
0.06	100	100	100	100	100	100	100	100	100	100	100	100	100	100	100	100
0.08	100	100	100	100	100	100	100	100	100	100	100	100	100	100	100	100
0.1	100	100	100	100	100	100	100	100	100	100	100	100	100	100	100	100
0.2	999	999	999	999	999	999	999	999	999	100	100	100	100	100	100	100
0.3	997	997	997	998	998	998	998	998	998	999	999	999	999	999	999	999
0.4	993	994	994	995	995	996	996	996	996	997	997	998	998	998	998	999
0.5	989	989	990	991	992	992	993	993	994	995	995	996	996	997	997	997
0.6	982	983	984	986	987	987	988	989	990	991	992	993	994	995	995	996
0.7	974	976	977	979	980	981	982	983	984	987	988	990	991	992	993	993
0.8	964	966	969	970	972	974	975	977	978	981	983	985	987	988	989	990
0.9	952	955	957	960	963	965	967	969	971	975	977	980	982	984	985	987
1.0	938	941	945	949	952	954	957	959	962	966	970	974	976	979	980	982
1.2	902	910	915	920	924	928	932	936	939	946	952	957	961	965	968	971
1.4	865	872	879	886	891	897	902	906	911	920	928	935	941	947	951	955
1.6	822	830	839	846	853	860	866	872	877	890	900	910	917	924	931	936
1.8	776	786	795	803	812	819	827	834	840	855	868	879	889	898	906	913
2.0	729	740	750	759	768	777	782	792	800	817	832	845	857	868	878	886
2.2	684	695	705	715	725	734	742	751	759	778	794	809	823	835	847	857
2.4	640	651	661	672	682	691	700	709	717	737	755	771	786	800	813	825
2.6	599	610	620	631	640	650	659	668	677	697	715	733	749	764	778	791
2.8	560	571	582	591	601	610	620	629	637	658	677	695	712	728	743	756
3.0	525	535	545	555	564	573	583	591	600	621	640	659	676	692	707	721
3.2	493	505	512	521	530	539	548	557	565	585	605	623	640	657	683	687
3.4	462	472	481	490	498	507	515	524	532	552	571	589	606	622	638	653
3.6	435	444	453	461	469	478	486	494	502	521	539	556	574	590	605	620
3.8	410	419	427	435	443	450	458	466	473	492	510	527	543	559	575	589
4.0	387	395	403	410	418	425	433	440	447	465	482	499	515	530	545	560
4.2	366	374	381	388	395	402	409	416	423	440	456	472	488	503	516	531
4.4	347	354	361	368	375	381	388	394	401	417	433	448	463	477	491	505
4.6	330	336	343	350	356	362	368	374	381	396	411	425	439	453	467	480
4.8	314	320	326	332	337	344	350	356	361	376	390	404	418	431	444	457
5.0	299	305	310	316	322	327	333	339	344	358	371	385	398	410	423	435
5.5	267	272	277	282	287	292	296	301	306	318	330	342	353	365	376	387
6.0	240	245	249	253	258	262	266	270	275	285	296	307	316	326	336	346
6.5	218	222	226	230	233	237	241	245	248	258	267	276	285	294	303	312
7.0	199	203	206	209	213	216	219	223	226	234	243	251	259	267	275	283
7.5	183	186	189	192	195	198	201	204	207	215	222	229	236	243	251	258
8.0	170	172	175	178	180	183	186	188	191	198	204	210	217	223	230	236
8.5	158	160	162	165	167	170	172	174	177	183	189	194	200	206	212	218
9.0	147	150	152	154	156	158	160	162	164	170	175	180	186	191	196	203
9.5	138	140	142	144	146	148	150	152	154	158	163	168	173	178	182	187
10.0	130	132	133	135	137	139	140	142	144	148	153	157	162	166	170	175
11.0	116	117	119	120	122	123	125	126	128	131	135	139	143	146	150	154
12.0	105	106	107	108	110	111	112	113	115	118	121	124	127	130	133	137
13.0	952	962	973	984	995	101	102	103	104	107	109	112	115	117	120	123
14.0	873	882	892	901	910	920	929	939	948	972	995	102	104	107	109	111
15.0	805	813	822	830	838	847	855	864	872	892	913	933	954	974	995	102
16.0	747	755	762	769	776	784	791	799	806	824	842	861	879	897	915	933
17.0	696	703	709	715	722	729	735	742	749	766	782	798	814	830	846	863
18.0	653	659	665	671	677	682	688	693	700	714	729	744	758	772	787	802
19.0	614	620	625	630	635	640	646	651	656	669	683	696	709	722	735	748

x \ a	10	12	14	16	18	20	25	30	35	40	45	50	60	70	80	90
0.02	100	100	100	100	100	100	100	100	100	100	100	100	100	100	100	100
0.04	100	100	100	100	100	100	100	100	100	100	100	100	100	100	100	100
0.06	100	100	100	100	100	100	100	100	100	100	100	100	100	100	100	100
0.08	100	100	100	100	100	100	100	100	100	100	100	100	100	100	100	100
0.1	100	100	100	100	100	100	100	100	100	100	100	100	100	100	100	100
0.2	100	100	100	100	100	100	100	100	100	100	100	100	100	100	100	100
0.3	100	100	100	100	100	100	100	100	100	100	100	100	100	100	100	100
0.4	999	100	100	100	100	100	100	100	100	100	100	100	100	100	100	100
0.5	998	999	100	100	100	100	100	100	100	100	100	100	100	100	100	100
0.6	996	997	998	999	999	999	100	100	100	100	100	100	100	100	100	100
0.7	994	996	997	998	998	999	999	999	100	100	100	100	100	100	100	100
0.8	991	994	996	997	997	998	999	999	999	100	100	100	100	100	100	100
0.9	988	991	994	995	996	997	998	999	999	999	999	100	100	100	100	100
1.0	984	988	991	993	995	996	997	998	999	999	999	999	100	100	100	100
1.2	973	980	985	988	991	992	995	997	998	998	999	999	999	100	100	100
1.4	959	970	977	982	985	988	992	995	996	997	998	998	999	999	999	100
1.6	941	956	966	973	978	982	988	992	994	995	996	997	998	999	999	999
1.8	919	939	952	962	969	975	983	988	991	993	994	996	997	998	998	999
2.0	894	919	936	949	957	964	976	983	987	990	992	994	996	997	998	998
2.2	866	896	917	932	944	953	969	977	981	986	989	991	994	995	997	997
2.4	835	870	895	914	928	939	958	970	977	982	985	988	992	994	995	996
2.6	803	842	871	893	911	923	947	961	970	977	981	984	989	992	994	995
2.8	769	812	845	870	890	909	934	951	963	970	976	980	986	990	992	994
3.0	735	781	817	846	869	887	919	940	953	963	970	975	982	987	990	992
3.2	701	749	788	819	844	866	903	927	943	955	963	969	978	983	987	990
3.4	667	717	758	792	819	842	884	912	931	945	955	963	973	979	984	987
3.6	633	686	729	764	794	818	866	896	919	935	946	955	968	975	980	985
3.8	603	654	698	736	768	794	845	880	905	923	937	947	962	971	977	981
4.0	573	625	669	707	740	768	823	862	890	912	925	938	954	965	973	978
4.2	545	596	640	679	713	742	801	843	874	896	914	927	946	959	968	974
4.4	518	568	612	652	686	716	778	823	857	882	901	916	938	952	963	970
4.6	493	542	585	625	660	691	754	802	838	866	887	905	929	945	956	965
4.8	469	517	559	599	634	665	731	781	819	849	873	891	919	937	950	959
5.0	447	493	535	573	608	640	707	759	800	832	857	877	907	928	942	953
5.5	398	440	479	515	549	581	649	706	750	787	816	841	878	904	922	936
6.0	356	394	430	464	496	527	594	651	698	738	722	800	844	875	898	916
6.5	321	355	388	419	449	478	543	599	648	691	726	757	806	844	871	893
7.0	291	323	351	380	408	434	496	551	600	643	681	713	767	809	841	866
7.5	265	293	320	346	371	396	454	507	555	598	636	670	727	772	807	837
8.0	243	268	292	316	340	363	417	467	513	555	593	628	687	735	774	806
8.5	223	246	269	291	312	333	383	430	474	515	552	587	647	697	739	770
9.0	207	227	248	268	287	307	353	398	439	478	515	548	609	660	703	740
9.5	192	211	229	248	266	284	327	368	407	445	479	512	572	623	668	706
10.0	179	196	213	230	247	263	303	342	379	414	447	479	537	588	633	672
11.0	157	172	186	200	214	229	263	297	329	360	390	419	474	523	567	607
12.0	140	152	164	177	189	201	231	260	288	316	343	369	419	465	509	547
13.0	125	136	147	157	168	178	204	230	255	280	304	327	372	415	455	492
14.0	114	123	132	141	151	160	183	205	227	249	271	292	332	371	409	444
15.0	104	112	120	128	136	144	164	184	204	223	243	261	298	334	368	401
16.0	951	102	110	117	124	131	149	167	184	202	219	236	269	301	333	363
17.0	879	943	101	107	114	120	136	152	168	183	199	214	244	274	302	330
18.0	816	874	932	989	105	110	125	139	153	167	181	195	222	249	275	301
19.0	761	813	865	917	969	102	115	129	141	153	166	179	204	228	252	276

x \ a	.00	.01	.02	.03	.04	.05	.06	.07	.08	.09	.10	.11	.12	.13	.14	.15
0.02	350	461	475	410	357	275*	228	191	160	137	118	103	901	798	710	636
0.04	346	196	248	261	253	236	217*	197*	179*	162*	146	133	121	110	101	937
0.06	343	110	152	173	184	184	178	171	163	153	144*	134*	126*	118*	110	103
0.08	338	800	111	130	141	146	147	146	142	137	132	127	122	116*	110*	105
0.1	334	642	863	102	113	120	123	125	124	123	120	117	114	110	106	102
0.2	314	399	474	535	589	634	670	700	725	745	761	771	780	783	785	784
0.3	294	334	370	404	433	461	484	506	527	544	559	573	584	592	603	611
0.4	274	297	319	340	360	377	394	410	424	437	449	460	471	481	490	497
0.5	257	271	286	300	313	325	338	350	361	371	382	390	399	407	416	423
0.6	238	248	260	271	281	289	297	306	316	324	331	338	346	352	359	367
0.7	222	230	238	246	255	262	268	275	282	288	294	300	306	312	317	322
0.8	206	212	218	225	231	237	243	249	255	260	265	270	275	280	285	289
0.9	192	197	202	207	212	217	222	227	231	235	239	243	249	252	256	259
1.0	178	182	186	192	196	200	204	208	212	215	218	221	225	229	232	236
1.2	156	159	162	165	168	170	173	176	179	181	184	187	190	192	194	197
1.4	137	139	141	143	145	147	150	152	154	156	158	160	162	164	166	168
1.6	120	122	124	125	127	129	130	132	133	134	136	138	140	142	143	145
1.8	106	108	109	110	112	113	114	116	117	118	119	120	122	123	124	126
2.0	947	957	968	978	988	999	101	102	103	104	105	106	107	108	109	110
2.2	847	856	864	873	882	891	899	908	917	925	934	942	950	958	966	974
2.4	763	770	777	784	791	799	806	813	820	827	834	840	847	853	860	866
2.6	694	699	705	710	715	721	726	731	736	742	747	753	758	764	769	775
2.8	630	635	639	644	648	653	657	661	666	671	675	680	685	690	694	699
3.0	574	578	582	586	590	594	597	601	605	609	613	617	621	625	629	633
3.2	525	528	531	534	537	541	544	547	550	553	556	560	563	567	570	574
3.4	481	484	487	489	492	495	498	501	503	506	509	514	515	518	521	524
3.6	444	446	448	451	453	455	457	459	462	464	466	469	471	474	477	480
3.8	408	410	412	415	417	419	421	423	426	428	430	432	434	436	438	441
4.0	377	379	381	383	385	387	389	391	393	395	397	399	401	403	405	407
4.2	352	354	355	357	359	361	362	364	366	367	369	371	373	374	376	378
4.4	325	327	328	330	331	333	334	336	337	339	341	342	344	345	347	348
4.6	306	307	309	310	311	312	314	315	317	318	319	321	322	323	325	326
4.8	286	287	288	290	291	292	293	295	296	297	298	299	300	302	303	304
5.0	264	265	266	267	269	270	271	272	273	274	275	277	278	279	280	281
5.5	229	230	231	232	232	233	234	235	236	237	238	238	239	240	241	242
6.0	196	197	197	198	199	199	200	201	202	202	203	204	204	205	206	206
6.5	173	174	175	175	175	176	176	177	177	178	179	179	180	180	181	181
7.0	152	152	153	153	154	154	155	155	156	156	157	157	158	158	158	159
7.5	136	137	137	137	138	138	139	139	139	139	140	140	140	141	141	142
8.0	121	121	122	122	122	123	123	123	123	124	124	124	125	125	125	126
8.5	109	109	109	110	110	110	111	111	111	111	112	112	112	112	113	113
9.0	985	987	990	992	994	996	999	100	100	101	101	101	101	101	102	102
9.5	895	897	899	901	903	905	907	909	911	913	915	917	919	920	922	924
10.0	815	817	818	820	822	824	825	827	829	830	832	834	935	837	839	841
11.0	686	687	689	690	691	693	694	695	696	698	699	700	702	703	704	706
12.0	586	587	588	589	590	591	592	593	594	595	596	597	598	599	600	601
13.0	505	506	507	507	508	509	510	511	511	512	513	514	515	516	516	517
14.0	441	442	442	443	444	444	445	445	446	447	447	448	449	449	450	451
15.0	389	390	390	391	391	392	392	393	393	394	394	395	395	396	396	397
16.0	344	344	345	345	346	346	347	347	348	348	348	349	349	350	350	351
17.0	308	308	309	309	309	310	310	311	311	311	312	312	312	313	313	313
18.0	277	277	278	278	278	279	279	279	279	280	280	280	281	281	281	282
19.0	247	247	248	248	248	248	249	249	249	249	250	250	251	251	251	251

The value prefixed by * is the maximum in each upright sequence.

x \ a	.16	.17	.18	.19	.20	.21	.22	.23	.24	.25	.26	.27	.28	.29	.30	.32
0.02	573	517	471	431	393	363	335	309	288	267	250	234	218	205	192	171
0.04	850	786	734	673	626	582	545	511	478	450	423	398	376	355	337	304
0.06	970	907	852	800	752	710	671	636	599	568	540	512	487	465	442	402
0.08	*997	*950	903	858	817	778	743	708	675	644	616	589	562	540	518	475
0.1	987	949	*911	*875	*843	*809	*778	*748	*719	690	663	637	614	591	570	528
0.2	781	776	770	762	754	747	738	727	717	*706	*695	*682	*670	*658	*645	*621
0.3	616	619	621	624	625	627	628	627	625	623	620	617	613	610	605	596
0.4	504	510	516	522	527	530	534	536	538	540	541	542	544	544	544	542
0.5	430	435	441	446	451	456	461	465	468	471	473	476	478	480	482	487
0.6	373	378	383	388	393	398	402	406	410	416	417	421	424	427	430	437
0.7	327	332	337	342	347	351	355	359	363	367	371	374	377	380	383	389
0.8	293	297	301	306	310	314	318	322	325	328	331	334	338	341	344	349
0.9	263	267	271	275	279	282	286	289	292	295	298	301	304	306	309	315
1.0	240	243	246	249	253	255	258	261	263	266	269	272	275	277	280	285
1.2	200	202	205	207	210	212	215	217	219	222	224	226	228	230	232	236
1.4	170	172	174	176	178	179	180	182	184	186	188	190	191	193	194	197
1.6	146	148	149	150	152	153	155	156	157	159	160	162	164	165	166	169
1.8	127	128	129	130	132	133	134	135	136	138	139	140	141	142	143	145
2.0	111	112	113	114	115	116	117	118	119	120	120	121	122	123	124	125
2.2	982	990	998	100	101	102	103	104	104	105	106	107	107	108	109	111
2.4	872	879	885	892	898	905	911	918	924	931	938	944	951	957	964	977
2.6	780	786	791	797	702	808	813	819	824	830	836	841	847	852	858	868
2.8	704	709	713	718	723	728	732	737	741	746	750	755	759	764	768	777
3.0	636	640	644	648	652	656	660	664	668	672	676	680	684	688	692	700
3.2	577	581	584	588	591	594	598	601	605	608	611	615	618	622	625	632
3.4	527	530	533	536	539	542	545	547	550	553	556	559	561	564	567	573
3.6	482	485	488	490	493	496	498	501	504	507	509	512	515	517	520	525
3.8	443	445	447	449	451	453	455	458	460	462	464	466	469	471	473	477
4.0	408	410	412	414	416	418	419	421	423	425	427	429	431	433	435	439
4.2	380	381	383	385	386	388	390	392	393	395	397	398	400	402	404	407
4.4	350	351	353	354	356	358	359	361	362	364	365	367	369	370	372	375
4.6	327	329	330	331	333	334	335	337	338	340	341	342	344	345	346	349
4.8	306	307	308	309	310	312	313	314	315	317	318	319	320	321	323	325
5.0	282	283	285	286	287	288	289	290	291	292	294	295	296	297	298	300
5.5	243	243	244	245	246	247	248	249	249	250	251	252	253	254	255	256
6.0	207	208	209	209	210	211	212	213	213	214	215	215	216	217	217	218
6.5	182	182	183	183	184	185	185	186	186	187	187	188	188	189	190	191
7.0	159	160	160	161	161	162	162	163	163	164	164	164	165	165	166	167
7.5	142	142	143	143	143	144	144	145	145	145	146	146	146	147	147	158
8.0	126	126	127	127	127	128	128	128	128	129	129	129	130	130	130	131
8.5	113	113	114	114	114	114	115	115	115	116	116	116	116	117	117	117
9.0	102	102	103	103	103	103	103	104	104	104	104	105	105	105	105	106
9.5	926	928	930	932	934	936	938	940	942	944	946	948	949	952	952	958
10.0	842	844	846	847	849	851	852	854	856	858	859	861	863	864	866	869
11.0	707	708	709	711	712	713	715	716	717	719	720	721	722	724	825	728
12.0	602	603	604	605	606	607	608	609	610	611	612	613	614	615	616	618
13.0	518	519	520	520	521	522	523	524	524	525	526	527	528	528	529	531
14.0	451	452	453	453	454	454	455	456	456	457	458	458	459	460	460	461
15.0	397	398	398	399	399	399	400	401	401	402	403	403	404	404	405	406
16.0	351	351	352	352	353	353	354	354	355	355	355	356	356	357	357	358
17.0	314	314	314	315	315	316	316	316	317	317	317	318	318	318	319	320
18.0	282	282	283	283	283	284	284	284	284	285	285	285	285	286	286	287
19.0	251	252	252	252	253	253	253	253	254	254	254	255	255	255	255	256

The value prefixed by * is the maximum in each upright sequence.

x \ a	.34	.36	.38	.40	.42	.44	.46	.48	.50	.52	.54	.56	.58	.60	.65	.70
0.02	154	139	126	114	104	957	880	813	757	704	652	609	571	533	458	399
0.04	275	250	228	209	192	177	164	152	142	132	124	116	109	102	886	775
0.06	368	338	311	287	265	247	230	214	200	188	177	166	156	147	128	113
0.08	439	406	377	350	326	304	285	267	251	236	223	210	199	188	165	146
0.1	493	460	430	402	376	353	332	313	295	279	264	250	238	226	199	178
0.2	*601*	577	563	533	511	493	474	456	439	422	406	390	375	359	330	303
0.3	586	575*	566*	552*	541*	529*	516*	504	491	480	468	457	445	433	406	381
0.4	540	537	533	529	525	518	511	504*	498*	491*	484*	477*	469*	461	441	422
0.5	489	489	490	490	488	486	485	483	480	476	473	469	465*	461*	448*	437
0.6	440	442	444	446	448	449	450	450	450	450	449	448	447	445	439	432
0.7	394	398	402	405	408	411	413	415	416	417	418	419	420	420	419	416
0.8	355	359	364	367	371	374	377	381	382	384	386	388	390	391	393	394
0.9	320	324	328	330	337	341	345	348	351	353	355	357	359	361	365	368
1.0	289	293	297	301	306	310	313	316	320	323	326	328	330	332	337	342
1.2	240	244	248	251	255	258	261	265	268	271	274	277	279	281	289	293
1.4	201	205	208	210	214	216	219	222	225	228	230	233	235	238	244	250
1.6	172	174	177	179	182	184	187	189	192	194	197	199	201	203	208	213
1.8	148	150	152	154	156	158	160	162	164	166	168	170	172	174	179	184
2.0	128	129	131	133	136	137	139	141	143	144	146	147	149	151	154	158
2.2	112	114	115	117	118	120	121	123	124	125	127	128	129	131	134	138
2.4	990	100	102	103	104	105	107	108	109	110	111	113	114	115	118	120
2.6	878	889	899	909	919	929	940	950	960	972	984	995	101	102	104	106
2.8	785	795	804	813	821	830	838	847	855	865	874	882	890	898	919	940
3.0	708	717	725	733	740	747	754	761	768	775	783	790	798	805	824	842
3.2	639	646	653	660	666	672	678	684	690	697	703	710	716	723	740	756
3.4	578	584	589	595	601	607	614	620	626	631	637	642	648	653	668	682
3.6	530	535	540	545	550	555	560	565	570	575	579	584	588	593	606	618
3.8	482	486	491	495	500	504	509	513	518	522	527	531	536	540	551	561
4.0	443	446	450	454	458	462	466	470	473	477	481	485	489	493	502	512
4.2	410	414	417	421	424	428	431	435	438	441	445	448	452	455	464	472
4.4	378	381	384	387	390	393	396	399	403	406	409	412	415	418	426	433
4.6	352	354	357	360	362	365	368	370	373	376	378	381	384	386	393	400
4.8	327	330	332	335	337	340	342	344	347	349	352	354	357	359	365	371
5.0	303	305	307	310	312	314	316	319	321	323	326	328	330	332	338	344
5.5	258	260	261	263	265	266	268	270	272	273	275	277	278	280	284	289
6.0	219	220	222	224	225	226	227	229	231	232	233	235	236	237	240	243
6.5	192	193	194	195	196	197	198	199	201	202	203	204	205	206	209	211
7.0	168	169	169	170	171	172	173	174	175	176	177	178	179	180	182	184
7.5	149	149	150	151	152	152	153	154	155	155	156	157	157	158	160	162
8.0	132	132	133	133	134	135	135	136	137	137	138	138	139	140	141	143
8.5	118	118	119	119	120	120	121	121	122	123	123	124	124	125	126	127
9.0	106	107	107	108	108	108	109	109	110	110	111	111	112	112	113	114
9.5	962	966	969	973	977	981	985	989	993	997	100	100	101	101	102	103
10.0	873	876	880	883	886	890	893	897	900	903	907	910	914	917	926	934
11.0	730	733	735	738	741	743	746	748	751	754	756	759	761	764	771	777
12.0	620	622	624	626	628	630	632	634	636	638	640	642	644	646	651	656
13.0	533	534	536	537	539	541	542	544	546	547	549	550	552	554	558	562
14.0	463	464	465	467	468	469	470	471	473	474	476	477	478	479	482	486
15.0	407	408	409	410	411	412	413	414	415	416	417	418	419	420	423	425
16.0	359	360	361	362	362	363	364	365	366	367	368	369	370	371	373	375
17.0	320	321	323	322	323	324	325	325	326	327	327	328	329	330	331	333
18.0	288	288	289	289	290	291	291	292	293	293	294	294	295	296	297	299
19.0	257	257	258	258	259	259	260	260	261	262	262	263	263	264	265	267

The value prefixed by * is the maximum in each upright sequence.

x \ a	.75	.80	.85	.90	.95	1.0	1.1	1.2	1.3	1.4	1.5	1.6	1.7	1.8	1.9	2.0
0.02	348	307	274	245	221	200	166	140	120	102	907	799	709	633	570	515
0.04	684	605	541	486	439	399	334	283	243	211	185	163	145	130	117	106
0.06	100	896	801	723	656	596	502	427	368	321	281	250	223	200	180	163
0.08	130	117	105	953	867	792	671	573	495	433	382	338	302	271	245	222
0.1	159	143	130	118	108	985	836	720	623	547	483	430	385	347	314	285
0.2	278	256	236	219	203	189	164	144	127	113	102	913	827	752	686	629
0.3	357	336	316	297	280	263	235	211	190	172	155	142	129	119	110	101
0.4	404	386	368	351	334	311	289	266	244	224	206	190	175	163	151	141
0.5	423	410	397	383	370	357	332	310	288	268	250	233	218	204	191	179
0.6	*424	*415	*406	*397	388	377	358	339	320	302	285	270	255	240	227	214
0.7	413	409	404	*397	*391	*385	*370	355	341	326	311	296	283	269	256	245
0.8	393	392	390	387	384	379	*370	*360	350	339	328	316	303	292	280	269
0.9	370	372	372	372	371	369	365	*360	*352	*344	*336	327	317	306	296	287
1.0	345	349	351	352	353	353	352	350	346	341	335	*328	*321	*313	306	298
1.2	298	302	306	310	312	315	319	322	322	322	321	319	316	*313	*309	*304
1.4	254	259	264	269	273	277	281	285	289	292	294	296	296	296	295	294
1.6	218	223	226	230	235	240	245	250	255	260	264	267	269	271	272	273
1.8	189	194	199	204	208	212	216	220	224	228	232	236	240	243	246	250
2.0	162	166	169	172	175	179	185	190	196	201	206	210	214	218	221	224
2.2	141	144	147	150	153	155	161	167	173	176	181	185	189	193	196	200
2.4	123	126	129	132	134	136	141	146	151	155	159	163	167	171	174	178
2.6	109	111	113	116	118	120	124	129	133	137	141	144	148	151	155	158
2.8	971	980	100	102	104	107	110	114	118	121	125	128	132	135	138	141
3.0	858	876	894	913	932	948	980	101	105	108	111	114	117	120	123	126
3.2	773	789	805	820	835	850	880	908	940	967	992	103	106	108	110	113
3.4	694	708	722	735	748	763	791	818	843	866	891	918	943	965	988	101
3.6	631	645	656	667	679	691	714	738	760	781	801	826	849	869	891	910
3.8	572	583	594	604	616	627	644	665	685	706	726	746	766	782	802	823
4.0	522	531	541	551	560	570	588	605	623	641	659	676	694	712	729	747
4.2	481	490	498	507	515	524	540	555	571	586	602	618	633	649	664	680
4.4	441	449	457	465	472	480	494	509	523	537	552	566	580	594	609	623
4.6	407	413	420	427	433	440	453	466	479	492	505	518	531	544	557	570
4.8	378	384	390	396	402	408	420	431	443	455	467	478	490	502	513	525
5.0	350	355	361	367	372	378	389	399	410	420	431	441	452	462	473	483
5.5	293	297	301	306	310	314	323	331	340	348	357	365	374	382	391	399
6.0	248	251	254	258	262	265	271	276	282	288	294	299	305	311	316	322
6.5	214	217	220	223	225	228	233	239	244	250	255	260	266	271	277	282
7.0	187	189	191	193	196	198	202	207	211	216	220	224	229	233	238	242
7.5	164	166	167	169	171	173	177	180	184	188	192	195	199	203	206	210
8.0	144	146	147	149	150	152	155	158	161	164	168	171	174	177	180	183
8.5	129	130	131	132	134	135	138	140	143	146	149	151	154	157	159	162
9.0	115	117	118	119	120	121	123	126	128	130	133	135	137	139	142	144
9.5	104	105	106	107	108	109	111	113	115	117	119	120	122	124	126	128
10.0	943	951	960	968	977	985	100	102	104	105	107	109	110	112	114	116
11.0	784	790	797	803	810	816	829	841	854	867	880	892	905	918	930	943
12.0	661	666	671	676	681	686	696	707	717	727	738	748	758	768	779	789
13.0	566	570	574	578	582	586	594	602	610	618	626	633	641	649	657	665
14.0	489	492	495	499	502	505	512	518	525	531	538	545	551	558	564	571
15.0	428	431	433	436	438	441	446	451	457	462	467	472	477	483	488	493
16.0	377	379	381	384	386	388	393	397	402	406	411	415	420	424	429	433
17.0	335	337	339	340	342	344	348	352	355	359	363	367	371	374	378	381
18.0	300	302	303	305	306	308	311	314	317	320	323	325	328	331	334	337
19.0	268	269	271	272	274	275	278	281	283	286	289	292	295	297	300	303

The value prefixed by * is the maximum in each upright sequence.

x \ c	2.1	2.2	2.3	2.4	2.5	2.6	2.7	2.8	2.9	3.0	3.2	3.4	3.6	3.8	4.0	4.2
0.02	467	426	390	360	331	307	284	264	247	231	203	180	161	145	131	118
0.04	963	880	808	742	687	635	590	549	514	480	423	375	336	302	273	248
0.06	149	136	125	115	106	985	916	854	798	747	659	585	524	471	426	387
0.08	203	186	171	158	146	136	126	118	110	103	910	810	725	653	591	538
0.1	261	239	220	202	188	175	163	152	142	133	118	105	940	849	767	700
0.2	579	535	494	458	426	398	372	348	327	308	275	245	221	200	182	166
0.3	936	869	808	755	707	661	621	584	551	520	465	419	379	345	314	288
0.4	131	123	115	108	101	954	898	848	805	760	684	620	564	515	472	435
0.5	169	159	150	141	133	126	119	113	107	102	925	845	770	708	651	602
0.6	203	192	182	173	165	157	149	142	135	129	118	108	995	916	846	785
0.7	234	223	213	203	194	185	177	169	162	177	143	132	122	113	105	983
0.8	258	248	238	229	220	211	203	195	188	181	168	156	145	135	126	118
0.9	277	268	259	250	242	234	226	218	211	204	190	178	167	157	147	138
1.0	291	283	275	267	259	251	244	237	230	223	211	199	187	176	166	157
1.2	*300	*295	*289	*284	279	273	268	263	257	252	241	230	219	209	200	191
1.4	292	290	287*	284*	281*	278*	275*	272*	268*	265	256	248	240	232	224	216
1.6	274	274	274	274	273	272	270	268	266	264*	260*	255*	249	243	237	231
1.8	251	252	253	254	255	256	256	256	255	254	253	251	248*	244*	240*	236
2.0	226	228	231	233	235	236	237	238	239	240	240	239	238	237	235	233
2.2	203	205	208	210	212	214	216	218	219	221	223	225	226	226	226	225
2.4	181	184	186	189	192	194	196	198	200	202	205	208	210	211	212	213
2.6	161	164	167	169	172	175	177	179	181	183	187	190	192	195	197	198
2.8	143	146	149	152	154	157	159	161	163	165	169	173	176	178	181	183
3.0	128	131	133	136	139	141	143	145	147	149	153	157	160	163	166	169
3.2	115	117	120	122	125	127	129	131	132	136	138	142	145	148	151	154
3.4	103	106	108	110	112	114	116	118	120	121	125	129	132	135	138	140
3.6	933	955	975	994	101	103	105	106	108	110	113	116	119	122	125	128
3.8	844	859	877	893	907	926	945	960	978	997	103	106	109	112	114	117
4.0	763	778	794	810	826	841	857	873	888	904	937	961	985	101	104	106
4.2	694	709	723	737	752	766	780	794	809	823	852	874	897	920	950	974
4.4	636	649	662	675	688	700	713	726	739	752	779	801	823	845	868	889
6.4	582	594	606	618	630	642	654	666	678	690	711	732	753	776	798	815
4.8	536	545	557	567	578	589	599	610	620	631	651	670	690	712	732	754
5.0	493	503	512	522	532	542	552	561	571	581	599	618	636	655	673	691
5.5	407	415	423	431	439	446	454	462	470	478	493	508	523	538	553	568
6.0	330	337	345	352	360	368	375	383	390	398	410	422	435	447	459	472
6.5	287	293	298	303	309	314	319	324	330	335	345	355	366	376	386	396
7.0	246	251	255	260	264	268	273	277	282	286	294	303	311	320	328	336
7.5	214	217	221	224	228	232	235	239	242	246	253	260	268	275	282	289
8.0	186	189	192	195	199	202	205	208	211	214	220	226	232	238	244	250
8.5	165	167	170	172	175	178	180	183	185	188	193	198	204	209	214	219
9.0	146	148	151	153	155	157	159	162	164	166	170	175	179	184	188	193
9.5	130	132	134	136	138	139	141	143	145	147	151	155	158	162	166	170
10.0	117	118	120	122	124	125	127	129	130	132	135	138	142	145	148	151
11.0	956	969	982	995	101	102	103	105	106	107	110	112	115	117	120	122
12.0	799	809	818	828	838	848	858	867	877	887	908	930	951	973	994	101
13.0	673	681	689	697	705	712	720	728	736	744	760	776	793	809	825	839
14.0	578	584	591	597	604	610	617	623	630	636	649	662	674	687	700	712
15.0	498	504	509	514	520	525	530	535	541	546	556	567	577	588	598	609
16.0	437	442	446	451	455	459	464	468	473	477	486	494	503	511	520	529
17.0	386	389	393	396	400	404	407	411	414	418	426	434	441	449	457	463
18.0	340	344	347	350	354	357	360	363	367	370	376	382	388	394	400	406
19.0	306	308	311	313	316	319	321	324	326	329	334	340	345	351	356	361

*The Values prefixed by * is the maximum in each upright Sequence.*

x \ a	4.4	4.6	4.8	5.0	5.2	5.4	5.6	5.8	6.0	6.5	7.0	7.5	8.0	8.5	9.0	9.5
0.02	109	990	908	838	777	720	669	625	584	498	429	374	329	292	260	234
0.04	226	207	190	176	162	151	140	131	122	104	900	785	691	613	547	492
0.06	354	324	298	275	255	236	220	205	192	164	142	124	109	966	861	775
0.08	490	450	415	383	354	329	306	286	268	229	198	173	152	135	120	108
0.1	639	586	540	498	461	429	400	374	349	299	258	226	199	177	158	142
0.2	152	140	129	120	111	104	967	903	847	730	633	555	490	435	390	351
0.3	265	245	226	211	196	183	171	160	150	130	113	992	877	781	701	632
0.4	401	372	345	321	299	280	262	246	232	200	175	154	137	122	110	994
0.5	558	517	481	450	521	394	371	348	329	286	249	220	196	176	158	143
0.6	730	680	635	596	559	524	493	465	439	383	336	298	266	239	215	196
0.7	917	857	801	753	707	665	628	593	561	494	435	387	346	312	282	256
0.8	111	104	980	919	866	820	775	735	697	613	543	485	436	392	356	324
0.9	130	122	115	109	103	980	927	881	840	745	660	593	533	483	438	401
1.0	149	141	133	126	120	114	108	103	987	874	784	707	638	580	527	483
1.2	182	173	166	159	152	145	139	133	128	115	104	945	862	789	723	666
1.4	208	200	193	186	179	173	167	161	155	142	130	119	109	101	928	860
1.6	225	219	213	207	201	195	189	183	177	165	153	142	131	122	114	106
1.8	*232*	228	223	218	213	208	204	199	194	182	171	161	151	142	133	125
2.0	230*	228*	225*	222*	219	215	211	207	204	194	185	175	166	158	149	141
2.2	224	223	221	220	218*	216*	213*	211*	208*	201	193	185	178	170	163	155
2.4	213	213	213	212	211	210	209	208	206*	201*	196	190	184	178	172	166
2.6	199	201	201	202	202	202	202	201	200	198	195*	191*	186*	182	177	170
2.8	185	187	188	189	190	191	192	192	192	191	190	188	185*	182*	179*	174
3.0	171	172	174	176	177	178	179	180	181	182	182	182	181	179	177*	174
3.2	157	159	161	163	164	166	168	170	172	173	174	174	174	174	173	171
3.4	143	146	148	150	152	154	156	158	160	162	164	165	166	166	167	166
3.6	130	133	136	138	140	142	143	145	147	151	154	156	158	159	159	160
3.8	119	122	125	127	129	130	132	134	136	140	143	146	148	150	152	152
4.0	109	111	114	116	118	120	122	124	125	129	133	136	139	141	143	145
4.2	990	102	104	106	108	110	112	113	115	120	123	126	129	132	134	136
4.4	910	933	952	973	995	101	103	104	106	110	114	118	121	123	126	128
4.6	838	858	879	901	916	931	946	962	985	102	106	109	112	115	118	120
4.8	772	790	805	823	840	858	875	890	900	944	977	101	104	107	110	112
5.0	709	727	739	758	773	789	804	820	836	872	907	938	969	995	102	105
5.5	582	597	611	624	637	650	663	676	690	721	751	779	807	833	860	884
6.0	485	497	511	519	530	541	552	563	574	600	626	651	677	701	725	747
6.5	405	516	427	435	445	454	464	473	483	506	528	550	571	592	613	632
7.0	344	354	362	369	377	385	394	402	410	429	448	467	486	504	521	539
7.5	295	302	308	316	323	330	337	343	350	367	385	400	416	432	448	463
8.0	257	263	270	273	279	285	291	296	302	317	331	345	360	373	386	400
8.5	224	229	234	238	243	248	253	259	264	276	288	300	312	324	336	246
9.0	197	202	206	211	215	219	223	227	231	241	252	262	273	284	294	304
9.5	174	178	182	185	189	193	197	200	204	214	223	232	240	249	258	267
10.0	154	158	161	164	167	171	174	178	181	189	197	205	213	221	229	237
11.0	124	127	129	131	134	137	140	143	146	152	158	164	170	176	182	188
12.0	103	104	106	108	110	113	115	118	120	125	130	134	139	144	149	153
13.0	852	866	879	893	911	929	948	966	984	102	106	110	113	117	121	124
14.0	724	737	749	761	775	789	804	818	832	864	896	929	961	993	103	106
15.0	620	630	641	652	663	674	684	695	706	733	761	788	816	843	870	898
16.0	538	547	556	565	575	585	595	605	615	635	655	676	696	716	736	757
17.0	469	476	482	488	496	505	513	522	530	549	567	586	604	623	641	660
18.0	413	419	426	432	438	444	451	457	463	480	496	513	530	546	563	579
19.0	366	372	377	382	389	395	402	408	415	427	440	452	465	477	489	502

x \ a	10	12	14	16	18	20	25	30	35	40	45	50	60	70	80	90
0.02	211	147	108	083	065	052	033	024	017	013	011	008	006	004	003	003
0.04	444	309	227	174	138	112	072	050	037	028	022	018	012	009	007	006
0.06	700	488	359	275	218	177	113	079	058	044	035	028	020	015	011	009
0.08	980	684	504	386	306	248	159	110	081	062	049	040	028	020	016	012
0.1	128	895	660	507	401	325	209	145	107	082	065	053	037	027	021	016
0.2	318	223	165	127	101	816	526	366	270	207	164	133	093	068	052	041
0.3	575	404	300	232	184	150	966	675	498	382	302	246	171	126	097	076
0.4	900	640	476	368	291	238	154	108	798	613	485	395	272	202	155	123
0.5	130	929	695	539	429	351	227	159	118	906	719	584	407	300	230	182
0.6	178	127	955	744	595	486	316	222	165	127	101	818	571	421	324	256
0.7	234	168	126	989	791	649	423	297	221	170	135	110	769	567	436	345
0.8	297	214	162	127	102	836	549	386	287	222	176	144	100	713	570	451
0.9	367	266	203	159	128	105	693	521	364	281	224	183	128	945	726	575
1.0	444	325	248	195	158	130	156	607	453	350	279	227	159	118	908	720
1.2	614	456	352	279	227	188	125	891	665	516	412	337	236	175	135	107
1.4	799	607	473	379	310	258	173	124	928	722	578	472	334	246	190	151
1.6	989	765	606	490	404	338	229	165	125	970	778	638	450	335	258	205
1.8	117	928	745	611	509	430	294	213	161	127	101	835	591	441	340	271
2.0	134	109	890	740	618	525	366	268	204	160	129	107	756	564	438	348
2.2	148	123	103	864	733	628	446	328	250	199	160	132	944	706	549	437
2.4	159	136	115	987	846	731	526	394	304	242	195	162	116	870	675	540
2.6	167	146	126	110	958	833	611	462	360	288	234	194	140	105	820	655
2.8	*171	153	135	120	106	942	698	534	420	336	276	230	166	126	980	787
3.0	*171	157	142	128	115	102	780	608	481	389	321	268	195	148	116	930
3.2	169*	159	144	134	122	110	861	682	545	444	368	309	226	172	135	109
3.4	165*	159	149	139	127	117	931	749	606	500	416	352	259	198	157	126
3.6	159	157*	150	141	132	122	100	813	670	556	466	396	295	226	179	145
3.8	153	152	148*	142*	135	126	105	875	730	611	518	442	332	256	203	164
4.0	145	148	146	141*	135	128	110	934	788	670	567	488	368	287	229	186
4.2	138	142	142	139*	135*	130	114	980	840	715	618	533	407	319	255	208
4.4	130	135	137	136	134	129	116	102	885	766	663	578	446	351	283	232
4.6	121	129	131	133	131	128*	118	105	922	809	708	623	485	385	311	257
4.8	114	122	125	128	128	126*	118	107	955	852	750	661	523	419	341	281
5.0	107	115	120	123	124	123*	118*	109	985	881	786	700	559	451	370	308
5.5	910	100	105	109	112	114	114*	109*	102	944	859	784	646	534	445	374
6.0	767	846	910	962	100	103	107	106*	102*	966	905	841	716	606	514	440
6.5	655	729	787	839	883	923	980	995	988	964*	919	870	767	669	579	503
7.0	559	630	677	730	775	811	884	922	937	930	912	875	796	713	632	557
7.5	479	538	590	636	676	717	794	845	875	884	879*	880*	810	740	671	605
8.0	415	464	508	553	596	633	710	766	805	827	835	835	805*	755	698	639
8.5	357	402	447	487	523	556	631	689	734	764	782	793	784	754*	713	653
9.0	315	351	392	427	457	492	560	622	667	702	730	743	756	741	710	673
9.5	276	310	343	376	406	436	501	556	603	644	671	693	716	715	701*	674
10.0	245	274	302	332	360	386	446	501	549	587	618	644	675	685	681	664
11.0	193	219	240	262	284	309	358	407	447	484	515	544	589	615	626	628
12.0	158	176	193	214	232	249	292	331	366	401	432	458	506	538	566	576
13.0	128	144	161	174	190	202	238	273	304	335	363	387	431	469	496	515
14.0	109	121	141	144	158	170	200	226	253	279	306	328	364	403	435	458
15.0	925	102	112	122	132	141	165	189	214	234	258	275	314	349	377	403
16.0	777	857	963	104	112	120	141	162	180	201	219	237	269	299	329	352
17.0	678	746	821	890	970	103	121	138	156	171	188	203	232	262	285	308
18.0	596	642	707	782	838	882	105	119	133	147	161	175	201	226	247	271
19.0	514	561	632	680	728	775	905	104	116	127	140	154	175	198	218	239

x \ a	.00	.01	.02	.03	.04	.05	.06	.07	.08	.09	.10	.11	.12	.13	.14	.15
0.02	*178	*874	*459	265	173	107	740	531	391	298	230	183	147	120	992	830
0.04	899	628	443*	321	236	177	136	106	845	680	555	459	383	323	275	235
0.06	605	477	377	301*	242*	197	161	133	111	932	791	676	582	502	438	382
0.08	456	384	324	273	230	196*	167	144	124	108	938	821	723	638	567	503
0.1	368	321	280	244	214	188	165*	146*	129*	114*	102	910	812	730	658	592
0.2	189	177	167	156	147	138	129	122	115	108	101*	957*	900*	846*	798*	751
0.3	127	123	118	114	110	106	102	978	940	905	872	840	809	779	749	720
0.4	961	937	914	891	868	846	824	802	781	761	741	722	703	684	666	648
0.5	767	753	739	725	712	699	686	673	660	647	635	623	611	599	587	576
0.6	635	627	618	610	601	593	584	576	567	559	550	542	534	526	518	511
0.7	539	533	527	521	515	510	504	498	492	486	480	475	469	464	458	453
0.8	463	459	455	451	447	443	439	435	431	427	423	419	415	412	408	404
0.9	406	403	400	397	394	391	388	385	382	379	376	373	370	368	365	362
1.0	358	356	354	352	349	347	345	343	341	339	337	334	332	330	328	326
1.2	286	285	284	282	281	280	279	277	276	275	274	273	271	270	269	268
1.4	234	233	232	232	231	230	229	229	228	227	226	226	225	224	223	223
1.6	196	196	195	195	194	194	193	193	192	192	191	191	190	190	189	189
1.8	166	166	165	165	165	164	164	164	163	163	163	162	162	162	161	161
2.0	142	142	142	141	141	141	141	140	140	140	140	139	139	139	139	139
2.2	123	123	123	123	122	122	122	122	122	122	121	121	121	121	121	121
2.4	107	107	107	107	107	106	106	106	106	106	106	106	106	106	106	105
2.6	954	953	952	951	951	950	949	948	947	946	946	945	944	943	942	941
2.8	850	849	849	848	847	847	846	845	845	844	844	843	842	842	841	840
3.0	760	760	759	759	758	758	757	757	756	756	755	755	754	754	753	753
3.2	684	684	683	683	682	682	682	681	681	681	680	680	679	679	679	678
3.4	621	621	620	620	620	619	619	619	619	618	618	618	617	617	617	616
3.6	564	564	564	563	563	563	563	562	562	562	562	561	561	561	561	560
3.8	514	514	514	513	513	513	513	513	512	512	512	512	512	512	511	511
4.0	471	471	471	471	470	470	470	470	470	470	470	469	469	469	469	469
4.2	433	433	433	433	433	432	432	432	432	432	432	432	432	432	431	431
4.4	400	400	400	400	400	400	400	399	399	399	399	399	399	399	399	399
4.6	370	370	370	370	370	370	370	369	369	369	369	369	369	369	369	369
4.8	343	343	343	343	343	343	343	343	343	342	342	342	342	342	342	342
5.0	320	320	320	320	320	320	320	320	320	320	320	319	319	319	319	319
5.5	270	270	270	270	270	270	270	270	270	270	270	270	270	270	270	269
6.0	231	231	231	231	231	231	231	231	231	231	231	231	231	231	231	231
6.5	200	200	200	200	200	200	200	200	200	200	200	200	200	200	200	200
7.0	174	174	174	174	174	174	174	174	174	174	174	174	174	174	174	174
7.5	153	153	153	153	153	153	153	153	153	153	153	153	153	153	153	153
8.0	136	136	136	136	136	136	136	136	136	136	136	136	136	136	136	136
8.5	122	122	122	122	122	122	122	122	122	122	122	122	122	122	122	122
9.0	110	110	110	110	110	110	110	110	110	110	110	110	110	110	110	110
9.5	989	989	989	989	989	989	989	989	989	989	989	989	989	989	988	988
10.0	897	897	897	897	897	897	897	897	897	897	897	897	897	897	897	897
11.0	749	749	749	749	749	749	749	749	749	749	749	749	749	749	749	749
12.0	635	635	635	635	635	635	635	635	635	635	635	635	635	635	635	635
13.0	544	544	544	544	544	544	544	544	544	544	544	544	544	544	544	544
14.0	472	472	472	472	472	472	472	472	472	472	472	472	472	472	472	472
15.0	415	415	415	415	415	415	415	415	415	415	415	415	415	415	415	415
16.0	366	366	366	366	366	366	366	366	366	366	366	366	366	366	366	366
17.0	326	326	326	326	326	326	326	326	326	326	326	326	326	326	326	326
18.0	292	292	292	292	292	292	292	292	292	292	292	292	292	292	292	292
19.0	261	261	261	261	261	261	261	261	261	261	261	261	261	261	261	261

The value prefixed by * is the muximum in each upright sequence.

x \ a	.16	.17	.18	.19	.20	.21	.22	.23	.24	.25	.26	.27	.28	.29	.30	.32
0.02	702	597	513	445	386	338	299	264	235	210	188	170	153	139	126	105
0.04	203	177	154	135	120	106	948	850	761	687	624	565	516	470	430	365
0.06	337	297	264	235	211	190	171	155	141	128	117	107	977	898	827	707
0.08	449	403	363	327	296	269	246	224	205	188	173	159	147	136	126	108
0.1	538	488	445	405	371	339	313	288	265	245	227	210	195	182	169	148
0.2	*710*	670	633	598	567	537	508	481	457	434	412	391	372	354	338	306
0.3	694	668*	643*	619*	596*	575*	555*	535*	515*	496	478	462	446	430	415	386
0.4	631	614	598	582	566	551	536	522	508	495*	482*	470*	458*	446*	435*	414
0.5	565	554	543	532	521	511	501	491	481	471	462	453	444	435	426	409
0.6	503	495	487	479	471	464	457	450	443	436	429	422	416	410	404	392
0.7	447	442	436	431	425	420	415	410	405	401	396	391	386	381	376	367
0.8	400	396	393	389	385	381	378	374	371	367	363	360	356	353	349	342
0.9	359	356	354	351	348	345	342	340	337	334	331	328	326	323	320	315
1.0	324	321	319	317	315	313	311	309	307	305	303	301	299	297	295	291
1.2	266	265	264	263	262	260	259	258	257	256	254	253	252	251	249	247
1.4	222	221	220	220	219	218	217	217	216	215	214	213	213	212	211	210
1.6	188	188	187	187	186	186	185	185	184	184	183	183	182	182	181	180
1.8	161	160	160	160	159	159	159	158	158	158	157	157	156	156	156	155
2.0	138	138	138	138	137	137	137	137	136	136	136	136	136	135	135	135
2.2	120	120	120	120	120	120	119	119	119	119	119	119	119	118	118	118
2.4	105	105	105	105	105	105	105	105	104	104	104	104	104	104	104	104
2.6	940	940	940	939	938	936	935	934	934	933	932	931	930	929	929	927
2.8	840	839	838	838	837	836	836	835	834	834	833	832	832	831	831	829
3.0	752	752	751	751	750	750	749	749	748	748	747	747	746	746	745	744
3.2	678	678	677	677	676	676	676	675	675	675	674	674	673	673	673	672
3.4	616	616	615	615	615	614	614	614	614	613	613	613	612	612	612	611
3.6	560	560	560	559	559	559	559	558	558	558	558	558	557	557	557	556
3.8	511	511	511	510	510	510	510	510	509	509	509	509	509	508	508	508
4.0	469	468	468	468	468	468	468	468	467	467	467	467	467	467	467	466
4.2	431	431	431	431	431	431	431	430	430	430	430	430	430	430	430	429
4.4	399	398	398	398	398	398	398	398	398	398	398	398	397	397	397	397
4.6	369	369	369	369	368	368	368	368	368	368	368	368	368	368	368	367
4,8	342	342	342	342	342	342	342	342	342	342	341	341	341	341	341	341
5.0	319	319	319	319	319	319	319	319	319	319	319	319	319	319	319	318
5.5	369	369	369	369	369	369	369	369	369	368	369	369	369	369	369	369
6.0	231	230	230	230	230	230	230	230	230	230	230	230	230	230	230	230
6.5	200	200	200	200	200	200	200	200	199	199	199	199	199	199	199	199
7.0	174	174	174	174	174	174	174	174	174	174	174	174	174	174	174	174
7.5	153	153	153	153	153	153	153	153	153	153	153	153	153	153	153	153
8.0	136	136	136	136	136	136	136	136	136	136	136	136	136	136	136	136
8.5	122	122	122	122	122	122	122	122	122	122	122	122	122	122	122	122
9.0	110	110	110	110	110	110	110	110	110	110	110	110	110	110	110	110
9.5	988	988	988	988	988	988	988	988	988	988	988	988	988	988	988	988
10.0	897	896	896	896	896	896	896	896	896	896	896	896	896	896	896	896
11.0	749	749	749	749	749	749	749	749	749	749	748	748	748	748	748	748
12.0	635	635	635	635	635	635	635	635	635	635	635	635	635	635	635	635
13.0	544	544	544	544	544	544	544	544	544	544	544	544	544	544	544	544
14.0	472	472	472	472	472	472	472	472	472	472	472	472	472	472	472	472
15.0	415	415	415	415	415	415	415	415	415	415	415	415	415	415	415	415
16.0	366	366	366	366	366	366	366	366	366	366	366	366	366	366	366	366
17.0	326	326	326	326	326	326	326	326	326	326	326	326	326	326	326	326
18.0	292	292	292	292	292	292	292	292	292	292	292	292	292	292	292	292
19.0	261	261	261	261	261	261	261	261	261	261	261	261	261	261	261	261

The value prefixed by * is the maximum in each upright sequence.

x \ a	.34	.36	.38	.40	.42	.44	.46	.48	.50	.52	.54	.56	.58	.60	.65	.70
0.02	890	756	649	561	487	427	376	332	295	264	238	214	193	174	138	112
0.04	310	267	230	200	176	155	137	122	109	977	882	797	723	656	524	426
0.06	609	528	460	404	356	316	282	251	226	204	185	167	152	139	112	910
0.08	945	828	729	643	571	510	456	410	370	335	305	277	253	232	188	154
0.1	130	114	101	902	805	721	650	588	533	484	441	404	370	340	277	230
0.2	279	255	233	213	195	180	166	153	142	132	122	113	106	983	834	711
0.3	360	331	315	296	277	260	244	229	215	203	192	181	171	161	140	123
0.4	*394	374	355	336	320	305	290	276	263	251	239	228	218	208	186	167
0.5	393*	377*	363*	349*	336	323	311	299	288	277	267	257	247	238	217	199
0.6	380	368	357	346	335*	325*	315*	305*	296*	287*	278	270	262	254	236	218
0.7	358	350	341	332	324	316	308	300	292	285*	278*	271*	264*	258*	243	228
0.8	335	329	322	315	309	302	296	289	283	278	272	267	262	256	242*	230
0.9	310	305	300	295	290	285	280	275	270	266	261	257	252	248	237	228
1.0	287	283	279	275	271	267	264	260	256	252	248	245	241	237	229	221
1.2	245	242	240	237	235	232	230	227	225	223	221	218	216	214	208	203
1.4	208	207	205	204	202	201	200	198	196	194	193	191	190	188	185	181
1.6	179	178	177	176	175	174	173	172	172	171	170	169	168	166	164	162
1.8	154	154	153	152	152	151	150	150	149	148	148	147	146	146	144	142
2.0	134	134	133	133	132	132	131	131	131	130	130	129	129	128	127	126
2.2	118	117	117	117	116	116	116	115	115	115	114	114	114	113	113	112
2.4	103	103	103	103	103	102	102	102	102	101	101	101	101	101	100	995
2.6	925	923	922	920	918	917	915	913	912	910	908	906	905	903	899	895
2.8	828	827	825	824	823	821	820	819	818	816	815	814	812	811	808	805
3.0	743	742	741	740	739	738	737	736	736	735	734	733	732	731	728	826
3.2	671	670	670	669	668	667	667	666	665	664	663	663	662	661	659	657
3.4	610	610	609	609	609	608	607	606	606	605	604	604	603	602	601	599
3.6	556	555	555	554	554	553	553	552	552	552	551	551	550	550	548	547
3.8	508	507	507	506	506	506	505	505	505	504	504	504	503	503	502	501
4.0	466	466	465	465	465	464	464	464	464	463	463	463	462	462	461	461
4.2	429	429	429	429	428	428	428	428	428	427	427	427	427	426	426	425
4.4	397	397	397	396	396	396	396	396	396	395	395	395	395	395	394	394
4.6	367	367	367	367	367	366	366	366	366	366	366	366	365	365	365	364
4.8	341	341	341	341	340	340	340	340	340	340	340	340	340	339	339	339
5.0	318	318	318	318	318	318	318	318	318	317	317	317	317	317	317	317
5.5	269	269	269	269	269	268	268	268	268	268	268	268	268	268	268	268
6.0	230	230	230	230	230	230	230	230	230	229	229	229	229	229	229	229
6.5	199	199	199	199	199	199	199	199	199	199	199	199	199	199	198	198
7.0	174	174	173	173	173	173	173	173	173	173	173	173	173	173	173	173
7.5	153	153	153	153	153	153	153	153	153	152	152	152	152	152	152	152
8.0	136	136	136	136	136	136	136	136	136	136	136	136	136	136	135	135
8.5	122	122	122	122	122	122	122	122	122	122	122	122	122	122	122	122
9.0	110	110	110	110	110	110	110	110	110	110	110	110	110	110	110	110
9.5	988	988	988	988	987	987	987	987	987	987	987	987	987	987	987	986
10.0	896	896	896	896	896	896	896	896	896	895	895	895	895	895	895	895
11.0	748	748	748	748	748	748	748	748	748	748	748	748	748	748	748	748
12.0	635	635	635	635	634	634	634	634	634	634	634	634	634	634	634	634
13.0	544	544	544	544	544	544	544	544	544	544	544	544	544	544	544	544
14.0	472	472	472	472	472	472	472	472	472	472	472	472	472	472	472	472
15.0	415	415	415	415	415	415	415	415	415	415	415	415	415	415	415	415
16.0	366	366	366	366	366	366	366	366	366	366	366	366	366	366	366	366
17.0	326	326	326	326	326	326	326	326	326	326	326	326	326	326	326	326
18.0	292	292	292	292	292	292	292	292	292	292	292	292	292	292	292	292
19.0	261	261	261	261	261	261	261	261	261	261	261	261	261	261	261	261

The value prefixed by * is the maximum in each upright sequence.

x \ a	.75	.80	.85	.90	.95	1.0	1.1	1.2	1.3	1.4	1.5	1.6	1.7	1.8	1.9	2.0
0.02	911	754	632	534	456	393	296	230	181	146	119	098	082	069	059	051
0.04	352	291	245	208	174	153	117	908	720	580	473	393	329	278	237	204
0.06	755	631	533	454	390	338	258	202	160	130	106	882	740	627	536	462
0.08	129	108	917	784	676	587	451	354	282	230	188	157	132	112	960	827
0.1	192	162	139	119	103	896	692	545	437	356	293	245	206	176	151	130
0.2	611	529	461	403	355	314	249	201	164	136	114	961	820	705	611	531
0.3	108	956	849	757	678	608	495	409	340	288	243	208	180	156	136	120
0.4	150	135	122	110	100	913	765	641	548	468	403	350	305	268	237	210
0.5	181	166	153	140	129	119	102	876	759	660	576	506	448	398	353	316
0.6	202	188	175	163	152	142	124	108	954	845	747	668	595	533	481	432
0.7	214	201	189	178	168	158	141	125	112	101	905	813	736	665	605	550
0.8	*219	207	197	188	178	169	153	138	126	114	104	944	861	791	723	664
0.9	218*	208*	200*	191	183	175	160	147	135	124	114	105	971	896	827	765
1.0	213	205	197	190*	184*	177*	164	152	141	131	122	113	105	979	914	853
1.2	197	192	187	182	177	172	162*	154*	145*	137*	129	122	115	109	103	975
1.4	178	174	170	167	164	160	154	147	141	135*	129*	123*	118*	113*	108	103
1.6	159	157	154	152	149	147	142	137	133	128	124	120	116	112*	108*	104
1.8	141	139	137	135	134	132	129	126	122	119	116	113	110	107	104	101
2.0	125	124	122	121	120	119	117	114	112	110	108	105	103	101	983	960
2.2	111	110	109	109	108	107	105	104	102	100	985	968	951	934	917	900
2.4	990	984	979	974	968	963	950	937	925	912	899	886	873	861	848	835
2.6	890	886	882	878	873	869	859	850	840	830	821	811	801	791	782	772
2.8	801	798	795	792	788	785	778	770	763	756	749	741	734	727	719	712
3.0	723	721	718	716	713	711	705	700	694	689	683	677	672	666	661	655
3.2	656	654	652	650	648	646	642	638	633	629	625	621	617	612	608	604
3.4	598	596	595	593	592	590	587	583	580	576	573	569	566	562	559	555
3.6	546	545	544	542	541	540	537	535	532	529	527	524	521	518	516	513
3.8	500	499	498	497	496	495	493	491	489	487	485	483	481	479	477	475
4.0	460	459	458	458	457	456	454	453	451	449	448	446	444	442	441	439
4.2	425	424	424	423	423	422	421	419	418	416	415	414	412	411	409	408
4.4	393	393	392	392	392	391	390	389	388	387	386	384	383	382	381	380
4.6	364	364	363	363	362	362	361	360	359	358	358	357	356	355	354	353
4.8	339	338	338	338	337	337	336	336	335	334	334	333	332	331	331	330
5.0	316	316	316	316	315	315	314	315	313	312	312	311	310	309	309	308
5.5	267	267	267	267	267	267	266	266	266	265	265	264	264	264	263	263
6.0	229	229	228	228	228	228	228	227	227	227	227	226	226	226	225	225
6.5	198	198	198	198	198	198	198	197	197	197	197	196	196	196	196	196
7.0	173	173	173	173	173	173	172	172	172	172	172	172	172	171	171	171
7.5	152	152	152	152	152	152	152	152	152	152	152	151	151	151	151	151
8.0	135	135	135	135	135	135	135	135	135	135	135	135	135	135	134	134
8.5	122	122	121	121	121	121	121	121	121	121	121	121	121	121	121	121
9.0	110	110	110	110	110	110	110	110	109	109	109	109	109	109	109	109
9.5	986	986	986	986	986	985	985	985	984	984	984	983	983	983	982	982
10.0	895	895	894	894	894	894	894	893	893	893	893	892	892	892	891	891
11.0	748	747	747	747	747	747	747	747	746	746	746	746	746	745	745	745
12.0	634	634	634	634	634	634	634	634	633	633	633	633	633	633	633	633
13.0	544	544	543	543	543	543	543	543	543	543	543	543	543	543	543	543
14.0	472	472	472	472	472	472	472	472	471	471	471	471	471	471	471	471
15.0	415	415	415	415	415	415	415	415	414	414	414	414	414	414	414	414
16.0	366	366	366	366	366	366	366	366	365	365	365	365	365	365	365	365
17.0	326	326	326	326	326	326	326	326	326	326	326	326	326	326	326	326
18.0	292	292	292	292	292	292	292	292	292	292	292	292	292	292	292	292
19.0	261	261	261	261	261	261	261	261	261	261	261	261	261	261	261	261

The value prefixed by * is the maximum in each upright sequence.

x \ a	2.1	2.2	2.3	2.4	2.5	2.6	2.7	2.8	2.9	3.0	3.2	3.4	3.6	3.8	4.0	4.2
0.02	044	038	033	029	026	023	021	019	017	015	012	010	009	007	006	006
0.04	177	154	135	119	106	094	084	076	068	062	051	042	036	031	026	023
0.06	401	351	308	272	241	215	192	173	156	141	117	098	082	070	060	052
0.08	720	630	554	490	434	388	348	312	282	255	212	177	150	128	110	095
0.1	113	992	873	772	686	613	549	496	448	405	337	282	238	204	175	152
0.2	461	410	364	324	289	260	234	211	191	174	146	123	104	895	774	674
0.3	106	938	838	750	674	607	550	498	454	415	348	296	253	218	189	165
0.4	187	167	149	134	122	110	100	914	838	766	646	552	475	411	360	315
0.5	284	256	231	209	190	173	158	145	133	123	104	899	775	676	591	522
0.6	391	356	323	294	269	246	227	209	192	178	153	132	115	101	886	784
0.7	502	461	421	387	355	328	302	280	259	241	209	182	159	140	124	110
0.8	610	561	519	480	445	412	383	355	330	309	269	237	209	185	165	147
0.9	709	660	612	570	531	493	463	432	404	379	335	295	262	234	209	188
1.0	796	744	697	652	610	571	535	503	474	446	397	354	317	284	256	231
1.2	925	875	825	783	742	702	667	634	601	571	518	467	424	387	352	320
1.4	986	943	901	863	827	791	757	725	695	666	610	561	517	476	439	406
1.6	*100	*970	*935	*901	868	837	810	781	752	725	677	630	586	546	510	476
1.8	985	957	929	*901	*873	*849	*824	*799	*775	*754	711	668	631	594	560	528
2.0	939	917	896	874	853	833	813	794	774	*754	*718	*684	650	619	588	559
2.2	883	867	850	834	817	801	786	770	755	739	710	682	*653	*626	*600	*576
2.4	823	810	798	785	773	761	748	736	723	711	688	665	642	619	596	*576
2.6	762	753	743	734	724	714	705	695	686	676	657	639	620	602	583	566
2.8	704	697	689	682	674	666	659	651	644	636	621	607	592	578	563	549
3.0	649	643	638	632	626	620	614	609	603	597	585	574	562	550	539	527
3.2	599	595	590	586	581	576	572	567	563	558	548	539	529	520	510	500
3.4	552	548	545	541	538	534	531	527	524	520	512	505	497	489	482	474
3.6	510	507	505	502	499	496	493	491	488	485	479	472	466	459	453	447
3.8	473	470	468	465	463	461	458	456	453	451	446	441	436	431	426	421
4.0	437	435	434	432	430	428	426	425	423	421	417	413	408	404	400	396
4.2	406	405	403	402	405	398	397	395	394	392	389	385	382	378	375	371
4.4	379	377	376	374	373	372	370	369	367	366	363	360	357	355	352	349
4.6	352	351	350	349	348	347	346	345	344	343	341	338	336	333	331	329
4.8	329	328	327	326	325	324	323	322	321	320	318	316	314	312	310	308
5.0	307	307	306	305	305	304	303	302	302	301	300	298	296	294	293	291
5.5	263	262	262	261	261	260	260	259	259	258	257	256	255	253	252	251
6.0	225	224	224	224	224	223	223	223	222	222	221	221	220	220	219	218
6.5	195	195	195	195	195	194	194	194	194	193	193	193	192	192	191	191
7.0	171	171	171	171	171	170	170	170	170	170	170	169	169	169	168	168
7.5	151	151	151	151	151	150	150	150	150	150	150	150	149	149	149	149
8.0	134	134	134	134	134	134	134	134	134	134	133	133	133	133	133	133
8.5	121	121	121	121	121	120	120	120	120	120	120	120	120	120	120	119
9.0	109	109	109	109	109	109	109	109	109	109	109	109	109	108	108	108
9.5	981	981	981	980	980	980	979	979	979	978	978	977	976	975	975	974
10.0	891	890	890	890	890	889	889	889	888	888	887	887	886	886	885	884
11.0	745	745	744	744	744	744	744	743	743	743	743	742	742	742	741	741
12.0	632	632	632	632	632	632	632	632	632	631	631	631	631	631	630	630
13.0	543	543	543	543	543	542	542	542	542	542	542	542	542	541	541	541
14.0	471	471	471	471	471	471	471	471	471	471	471	471	471	470	470	470
15.0	414	414	414	414	414	414	414	414	414	414	414	414	414	413	413	413
16.0	365	365	365	365	365	365	365	365	365	365	365	365	365	364	364	364
17.0	326	326	326	326	325	325	325	325	325	325	325	325	325	325	325	325
18.0	292	292	292	292	291	291	291	291	291	291	291	291	291	291	291	291
19.0	261	261	261	261	261	261	261	261	261	261	261	261	261	261	261	261

The value prefixed by * is the maximum in the upright sequence.

x \ a	4.4	4.6	4.8	5.0	5.2	5.4	5.6	5.8	6.0	6.5	7.0	7.5	8.0	8.5	9.0	9.5
0.02	005	004	004	003	003	003	002	002	002	002	001	001	001	001	001	000
0.04	020	017	015	013	012	011	010	009	008	006	005	004	003	003	002	002
0.06	046	040	035	031	028	025	022	020	018	014	011	009	008	006	005	005
0.08	083	073	064	057	051	045	041	037	033	026	021	017	014	012	010	008
0.1	133	117	103	091	081	073	065	059	053	042	034	028	023	019	016	014
0.2	590	519	459	409	364	327	294	267	241	191	154	126	104	087	074	063
0.3	145	128	114	101	908	817	736	666	605	482	389	320	265	223	189	161
0.4	277	246	219	196	176	159	143	130	118	945	766	631	526	442	375	322
0.5	463	410	366	329	297	267	242	220	201	161	131	108	904	764	651	558
0.6	698	622	558	502	454	410	373	340	310	250	205	170	142	120	103	884
0.7	986	884	794	717	648	588	536	490	449	365	300	249	209	177	152	131
0.8	132	119	107	972	881	804	734	673	618	503	416	347	292	249	213	184
0.9	170	153	138	126	115	105	963	885	815	670	554	464	393	336	288	250
1.0	209	190	173	158	145	133	122	112	104	854	713	601	510	438	377	327
1.2	293	270	248	228	210	194	180	167	155	129	109	927	795	687	596	521
1.4	374	346	321	299	278	260	242	225	220	178	152	131	113	988	863	759
1.6	445	416	390	365	342	321	301	283	266	230	198	173	151	133	117	104
1.8	498	471	444	419	397	375	355	336	317	277	243	214	190	168	150	134
2.0	533	508	484	460	437	417	397	377	360	319	284	253	227	203	183	165
2.2	552	530	507	485	466	446	427	410	392	355	319	287	260	235	214	194
2.4	*556	*536	*516	498	480	462	445	430	414	379	345	314	288	263	241	222
2.6	549	533*	516*	501*	485*	470*	455	440	427	394	363	335	309	286	264	245
2.8	535	521	507	493	480	468*	455*	443*	430*	401	374	348	324	303	282	263
3.0	515	503	492	480	469	458	448	437	426*	401*	378	355	334	313	294	276
3.2	491	481	472	462	453	445	436	428	419	397	376*	356*	337*	320	303	287
3.4	466	458	451	443	436	429	421	413	406	388	370	353	336*	320*	304*	290
3.6	440	434	427	421	415	409	404	398	392	376	361	346	332	318*	304*	290
3.8	416	411	406	401	396	391	385	380	375	362	350	337	324	312	301	289
4.0	392	387	383	379	375	371	366	362	358	348	337	327	317	306	296	285
4.2	368	364	361	357	354	350	347	343	340	331	323	314	305	296	288	279
4.4	346	343	340	337	334	332	329	326	323	316	308	301	293	286	278	271
4.6	326	324	321	319	317	314	312	309	307	301	294	288	282	275	269	262
4.8	306	304	302	300	298	296	294	292	290	285	279	274	269	263	258	252
5.0	289	288	286	285	283	281	279	278	276	272	267	262	257	253	248	243
5.5	250	249	248	247	246	244	243	242	241	238	235	231	228	225	222	219
6.0	218	217	217	216	215	214	214	213	212	209	207	205	203	201	199	196
6.5	190	190	189	189	188	188	187	187	186	185	184	182	181	179	177	176
7.0	168	168	167	167	167	166	166	165	165	164	163	162	161	160	159	158
7.5	149	148	148	148	148	148	147	147	147	146	146	145	144	143	143	142
8.0	132	132	132	132	132	132	131	131	131	130	130	129	129	128	128	127
8.5	119	119	119	119	119	119	118	118	118	118	117	117	117	116	116	115
9.0	108	108	108	108	108	108	107	107	107	107	106	106	106	105	105	104
9.5	973	972	972	971	970	970	969	969	968	966	963	961	958	956	953	951
10.0	884	883	883	882	881	881	880	879	879	877	875	874	872	870	868	867
11.0	740	740	739	739	739	738	738	737	737	736	735	734	732	731	730	729
12.0	630	629	629	629	629	628	628	628	628	627	626	626	625	624	623	623
13.0	541	541	541	541	541	541	540	540	540	539	539	538	537	536	536	536
14.0	470	470	470	470	470	470	470	469	469	469	469	468	468	467	467	466
15.0	413	413	413	413	413	413	413	413	412	412	412	412	411	411	411	410
16.0	364	364	364	364	364	364	364	364	364	363	363	363	363	363	362	362
17.0	325	325	325	325	325	325	325	325	325	324	324	324	324	324	323	323
18.0	291	291	291	291	291	291	291	291	291	290	290	290	290	290	289	289
19.0	261	261	261	261	261	261	261	261	261	261	261	261	260	260	260	260

The value prefixed by * is the maximum in upright sequence.

x \ a	10	12	14	16	18	20	25	30	35	40	45	50	60	70	80	90
0.02	000	000	000	000	000	000	000	000	000	000	000	000	000	000	000	000
0.04	002	001	001	000	000	000	000	000	000	000	000	000	000	000	000	000
0.06	004	002	001	001	001	001	000	000	000	000	000	000	000	000	000	000
0.08	007	004	003	002	001	001	000	000	000	000	000	000	000	000	000	000
0.1	012	007	004	003	002	001	001	000	000	000	000	000	000	000	000	000
0.2	054	032	020	014	010	007	004	002	001	001	001	000	000	000	000	000
0.3	139	082	052	035	025	018	009	005	003	002	002	001	001	000	000	000
0.4	278	164	105	071	050	037	019	010	007	005	003	002	001	001	001	000
0.5	482	287	185	125	089	065	034	020	013	008	006	004	003	002	001	001
0.6	772	456	294	201	143	105	055	032	020	014	009	007	004	003	002	001
0.7	114	681	441	302	215	159	083	049	031	021	015	011	006	004	003	002
0.8	160	971	632	433	310	229	120	071	045	031	022	016	009	006	004	003
0.9	217	133	868	597	428	318	167	099	063	043	030	022	013	008	006	004
1.0	286	176	115	796	575	426	226	133	086	058	041	030	018	011	008	005
1.2	457	285	190	132	961	714	382	227	146	099	071	052	030	019	013	009
1.4	671	428	288	203	148	111	599	359	231	158	112	083	049	031	021	015
1.6	923	602	411	292	215	163	886	535	347	237	169	125	074	047	032	022
1.8	120	800	556	401	298	238	125	761	496	340	243	180	107	068	046	033
2.0	149	102	720	528	394	303	170	104	684	471	339	251	149	096	065	046
2.2	177	124	898	665	505	392	224	138	909	632	455	339	202	130	088	063
2.4	203	147	108	817	626	490	284	179	119	830	597	446	267	172	118	083
2.6	227	168	127	970	757	596	354	224	151	106	767	574	345	223	153	109
2.8	245	187	144	112	887	718	430	276	187	132	964	724	439	285	195	139
3.0	260	203	160	127	102	815	509	333	227	162	119	897	545	356	244	105
3.2	270	216	174	140	114	938	592	393	272	195	144	109	669	438	302	216
3.4	276	226	185	152	125	104	674	455	319	231	172	131	808	531	370	264
3.6	*278	233	194	162	136	114	761	520	370	270	202	155	966	638	442	320
3.8	*278	236	200	171	145	124	839	587	422	311	236	181	114	758	528	381
4.0	275*	238	206	176	152	131	914	652	475	356	269	209	132	888	622	450
4.2	270*	238	207	181	158	138	985	714	529	397	306	239	153	103	726	528
4.4	263	234*	208	184	162	143	105	772	580	442	342	270	174	118	838	612
4.6	256	231	206*	185	165	147	110	826	628	485	379	302	197	135	957	705
4.8	247	226	203*	185*	167	149	115	875	675	528	417	333	221	152	109	803
5.0	238	219	201	183	166*	151	118	917	721	569	452	365	245	170	123	910
5.5	216	203	189	175	163*	151	123	100	814	660	539	445	308	220	160	120
6.0	194	185	175	166	156	146*	124	104	870	730	611	515	369	269	201	153
6.5	174	367	360	353	346	139	122*	105	905	779	666	572	424	319	243	188
7.0	157	152	146	141	135	130	117	103*	915	802	705	613	470	363	283	223
7.5	141	137	133	129	125	121	111	100	905*	809	723	643	508	402	321	258
8.0	127	124	121	119	116	113	104	962	880	800*	726	657	534	434	353	289
8.5	114	112	110	108	106	104	975	911	843	780	716*	658	549	456	380	312
9.0	104	103	101	994	976	957	909	859	807	754	701	650*	555	471	398	338
9.5	948	936	924	911	889	885	847	806	763	720	677	635*	555*	480	413	355
10.0	865	856	846	836	826	815	786	755	721	685	650	615	546*	480	421	368
11.0	728	723	717	711	705	698	680	660	638	613	590	566	517	469*	423*	379
12.0	622	619	615	611	607	603	591	577	562	547	531	514	479	444	409	375
13.0	535	533	531	528	525	522	514	506	496	486	475	463	439	414	388	361
14.0	466	465	464	462	460	458	453	446	440	433	425	417	399	381	362	342
15.0	410	409	407	406	404	403	399	395	390	385	380	374	362	348	334	320
16.0	362	361	360	360	359	358	355	352	349	346	342	338	329	319	308	297
17.0	323	322	322	321	321	320	318	315	313	310	307	304	298	291	283	275
18.0	289	289	288	288	287	287	286	284	282	280	278	276	271	266	260	253
19.0	260	260	260	259	259	259	258	257	256	254	252	250	246	242	238	233

The Values prefixed by * are the maximum in each upright sequence.

AUXILIARY TABLE OF THE CYCLONE FUNCTION (I)

(1) Using the pressure profile, at first we determine the radius ratio R_n/R_m, and choose the suitable cyclone constant for the given profile.

(2) The unit radius r_o can be obtained by the relation $r_o = R_m/X_m$, where, X_m is the quantity tabulated under the radius ratio.

(3) If we want to know the critical values, the quantities α, β; γ, δ; ε, ζ are available. As shown below, α, γ, ε are the maximum values of Ψ'_x, $x\Psi'_x$, Ψ'_a, respectively. And β, δ, ζ are the values of x where the each maximum occurs.

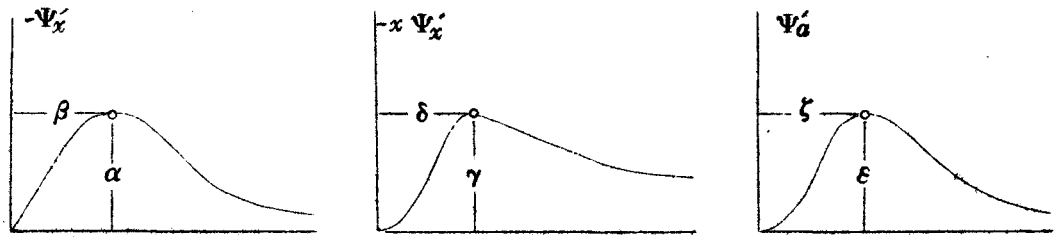

a		.00	.01	.02	.03	.04	.05	.06	.07	.08	.09	.10	.11	.12	.13	.14	.15
R_n/R_m		065	097	118	134	148	159	169	178	187	195	202	209	215	221	226	231
X_m		182	183	185	186	188	189	191	192	194	195	197	198	199	201	202	203
Ψ'_x	α	...	...	...	...	...	...	...	...	...	...	147	135	126	118	110	106
	β	...	...	...	...	...	...	...	...	...	...	048	052	057	063	068	074
$x\Psi'_x$	γ	192	195	198	201	204	207	210	213	216	219	222	225	228	231	234	238
	δ	170	165	160	157	154	150	147	143	140	137	133	130	127	124	122	119
Ψ'_a	ε	...	090	048	313	250	200	167	147	129	115	106	098	090	084	079	075
	ζ	...	001	003	042	054	066	080	093	107	125	141	156	171	186	202	216

a		.16	.17	.18	.19	.20	.21	.22	.23	.24	.25	.26	.27	.28	.29	.30	.32
R_n/R_m		236	241	246	251	256	260	263	267	271	275	278	281	284	287	290	297
X_m		204	205	207	208	209	210	211	213	214	215	216	217	219	220	221	223
Ψ'_x	α	100	095	091	087	084	081	079	077	075	073	071	069	068	066	065	062
	β	080	085	093	100	106	114	123	129	136	144	153	160	169	177	186	207
$x\Psi'_x$	γ	241	244	246	249	252	255	258	261	264	267	270	273	276	278	280	285
	δ	117	114	112	110	108	107	105	103	101	100	099	099	098	098	098	099
Ψ'_a	ε	072	068	065	062	060	058	056	054	052	051	490	475	462	450	438	414
	ζ	228	240	254	368	381	393	305	317	329	341	354	366	378	390	402	432

a		.34	.36	.38	.40	.42	.44	.46	.48	.50	.52	.54	.56	.58	.60	.65	.70
Rn/Rm		302	307	311	315	319	323	328	332	336	339	342	345	349	352	359	365
Xm		225	227	229	231	233	235	237	239	241	243	245	247	249	250	255	259
Ψ'_x	α	060	058	057	056	054	053	052	051	050	491	482	476	468	460	450	438
	β	226	243	262	277	295	315	332	353	370	387	402	422	440	455	483	053
$x\Psi'_x$	γ	290	295	299	304	308	312	315	319	322	326	329	333	336	339	346	353
	δ	100	102	103	105	107	108	110	111	112	113	114	116	118	119	121	125
Ψ'_a	ϵ	394	380	365	350	337	325	315	306	298	290	281	272	266	260	244	230
	ζ	452	470	490	510	535	550	570	592	603	062	064	066	068	071	074	078

a		.75	.80	.85	.90	.95	1.0	1.1	1.2	1.3	1.4	1.5	1.6	1.7	1.8	1.9	2.0
Rn/Rm		372	377	383	388	393	398	406	413	420	426	432	437	441	445	449	452
Xm		263	267	271	275	279	282	291	297	304	310	315	320	328	335	341	346
Ψ'_x	α	424	417	407	402	395	382	377	363	353	344	335	328	322	317	311	306
	β	056	060	063	066	069	072	078	083	088	095	098	103	106	111	114	118
$x\Psi'_x$	γ	359	365	371	376	381	386	395	402	410	416	422	428	434	439	444	449
	δ	129	132	134	137	140	144	148	152	156	160	165	169	173	176	180	184
Ψ'_a	ϵ	219	209	198	190	182	176	165	155	146	138	131	125	120	115	110	105
	ζ	081	085	089	092	095	099	105	111	117	123	128	132	137	142	147	151

a		2.1	2.2	2.3	2.4	2.5	2.6	2.7	2.8	2.9	3.0	3.2	3.4	3.6	3.8	4.0	4.2
Rn/Rm		456	459	462	465	468	471	473	475	477	478	482	486	490	494	497	500
Xm		352	357	362	367	372	377	382	387	392	396	405	417	423	431	440	448
Ψ'_x	α	303	297	294	289	285	281	277	274	271	267	262	256	252	246	243	238
	β	122	126	129	135	132	138	143	145	148	152	157	163	169	173	178	182
$x\Psi'_x$	γ	454	458	462	466	470	473	476	480	483	486	493	499	504	508	512	516
	δ	188	192	196	200	204	209	213	217	220	224	232	239	246	252	259	264
Ψ'_a	ϵ	101	097	094	091	088	085	082	080	078	076	072	068	065	063	060	058
	ζ	156	160	164	168	172	176	180	183	186	190	197	204	211	217	222	228

a		4.4	4.6	4.8	5.0	5.2	5.4	5.6	5.8	6.0	6.5	7.0	7.5	8.0	8.5	9.0	9.5
Rn/Rm		503	505	507	509	511	513	515	517	519	524	528	531	533	536	538	540
Xm		455	463	471	478	485	492	499	506	513	529	545	561	575	590	604	617
Ψ'_x	α	234	230	226	224	221	216	215	213	210	203	197	192	187	183	180	176
	β	187	192	197	203	206	211	214	218	223	233	244	252	262	270	280	288
$x\Psi'_x$	γ	519	523	527	530	533	537	540	542	545	552	558	563	568	573	577	580
	δ	270	276	281	288	292	298	303	309	316	329	341	353	363	373	383	393
Ψ'_a	ϵ	056	054	052	050	488	473	460	448	435	407	382	358	332	320	306	293
	ζ	233	239	243	249	255	261	266	271	276	287	289	309	320	331	341	352

a		10	12	14	16	18	20	25	30	35	40	45	50	60	70	80	90
Rn/Rm		542	546	550	553	556	568	574	579	583	586	589	591	595	598	601	603
Xm		631	691	727	770	810	849	933	102	109	116	122	129	140	150	160	169
Ψ'_x	α	173	160	151	143	136	131	119	110	103	097	092	088	082	076	072	068
	β	295	324	353	380	405	426	479	053	058	061	064	068	075	080	087	092
$x\Psi'_x$	γ	584	596	605	613	620	627	639	648	656	663	669	674	681	685	689	690
	δ	402	430	458	485	512	537	595	651	705	757	805	850	937	102	110	118
Ψ'_a	ϵ	280	240	210	185	167	152	125	105	093	081	073	067	056	484	425	380
	ζ	363	402	436	470	500	053	060	065	071	075	079	082	090	098	106	112

In the case where the formula is applied for the height of the constant pressure level, P_∞ and ΔP are changed into H_∞ and ΔH, respectively. They may be called thus:

H_∞ ..... Undisturbed Height

ΔH ..... Height Depth

The values of Ψ, $\frac{\partial \Psi}{\partial x}$, and $\frac{\partial \Psi}{\partial a}$ were computed for about 100 different values of a. The results are tabulated on pages 9 to 29, for the range of x from 0.02 to 19.0. The table is available when we desire to compute the typhoon curves, their gradients, winds, and temperatures.

When x is small, the cyclone function is expanded into the power series,

$$\Psi = \frac{1}{\sqrt{1 + \left(x\frac{x+1}{x+a}\right)^2}} \fallingdotseq 1 - \frac{1}{2a^2}x^2 - \frac{a-1}{a^3}x^3 \quad (x \ll a) \qquad (8c)$$

It is clear that the pressure near the center increases parabolically. In the case where x is very large, the function is reduced to

$$\Psi = \frac{1}{\sqrt{1 + \left(x\frac{x+1}{x+a}\right)^2}} \fallingdotseq \frac{1}{x} + \frac{a-1}{x^2} \quad (x \gg 1) \qquad (8d)$$

The cyclone function can be differentiated partially with respect to x and a. The results are given by

$$\frac{\partial \Psi}{\partial x} \equiv \Psi'_x = -\Psi^3 \frac{x^4 + (1+2a)x^3 + 3ax^2 + ax}{(x+a)^3} \qquad (9a)$$

$$\fallingdotseq -\frac{x}{a^2} - 3\frac{a-1}{a}x^2 \quad (x \ll a) \qquad (9b)$$

$$\fallingdotseq -\frac{1}{x^2} + \frac{2(a-1)}{x^3} \quad (x \gg 1) \qquad (9c)$$

$$\frac{\partial \Psi}{\partial a} \equiv \Psi'_a = \Psi^3 \frac{x^2(x+1)^2}{(x+a)^3} \qquad (10a)$$

$$\fallingdotseq \frac{x^2}{a^3} - \frac{3-2a}{a^4}x^3 \quad (x \ll a) \qquad (10b)$$

$$\fallingdotseq \frac{1}{x^2} \quad (x \gg 1) \qquad (10c)$$

In order to know the change in shape of the curve, represented

by the function with different values of a, three-dimensional feature of the curves is presented in Fig. 4, in which the value of Ψ in-

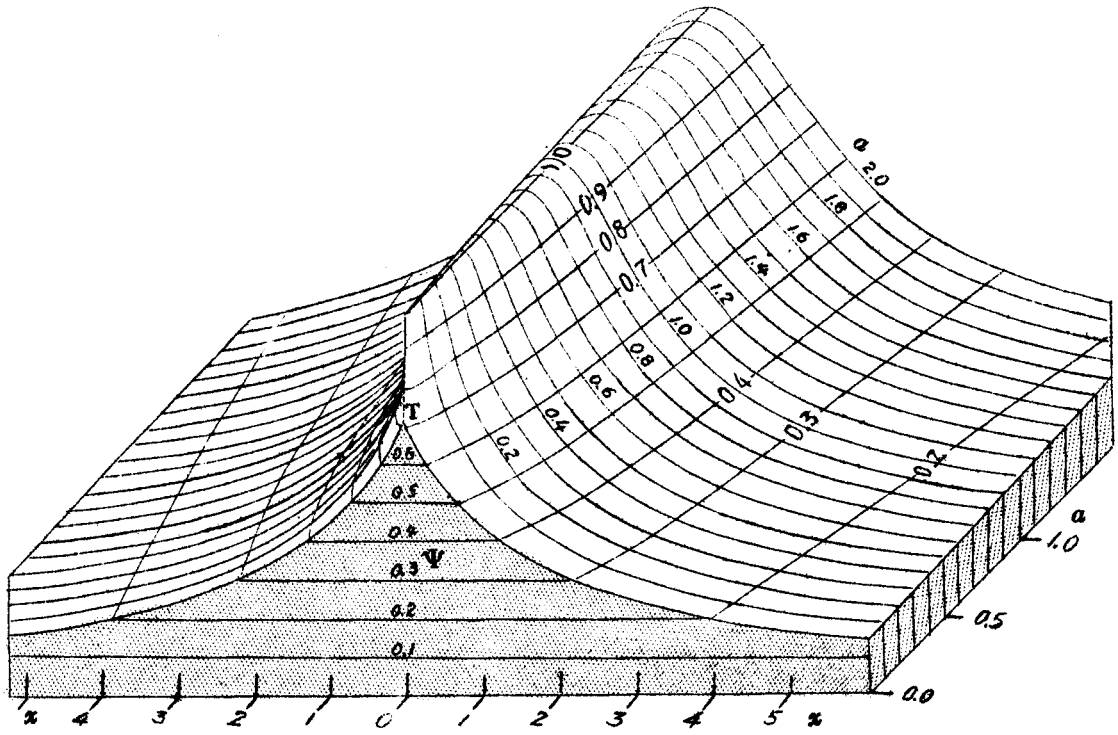

Fig. 4. Showing the curves for different cyclone constants.

creases upward, and at the top it reaches the value, 1.000. The figure shows that the radius of curvature near the top becomes larger as the cyclone constant increases. When $x = 0$, we have $\Psi = 0$, $\Psi'_x = 0$ and $\Psi''_x = -1/a^2$, then the radius of curvature at the top is given by

$$\left| \frac{(1 + \Psi'^2_x)^{\frac{3}{2}}}{\Psi''_x} \right| = a^2 \qquad (11)$$

When a is very small, the curve has a pointed top rather than rounded one. If the value of a in the cyclone function be zero, the curve changes into inverted-Y shape shown in Fig. 5. T is the triple point at which the three lines meet, and it is located at the altitude of 0.707 or $1/\sqrt{2}$. It is evident that all the curves must occupy the space above the hatched area in the figure.

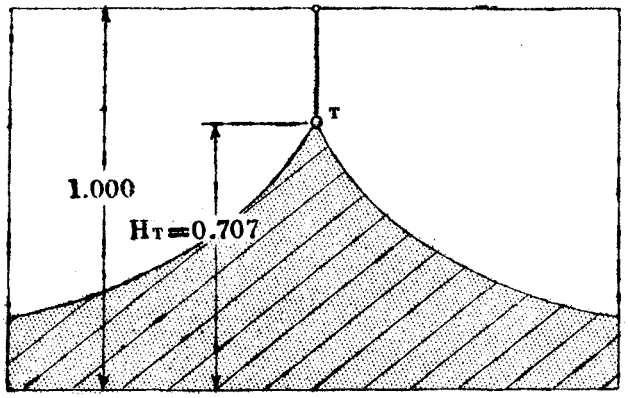

Fig. 5. The triple point which appears when $a = 0$. The area where no curve exists is shown by hatched area.

The shape of the curve for $a = 0$ will change if we introduce one more constant b into the cyclone function, thus:

$$\Psi^* = \frac{1}{\sqrt{1 + \left(x\frac{x+b}{x+a}\right)^2}} \quad (12a)$$

When $a = 0$, it will be reduced to

$$\Psi^*_{a=0} = \frac{1}{\sqrt{1 + (x+b)^2}} \quad (12b)$$

The values of this formula are tabulated and shown in Fig. 6.

b \ x	0.0	0.1	0.2	0.5	1.0	1.5	2.0	2.5	3.0	4.0	5.0	6.0	7.0	8.0	9.0	10
0.0	000	995	981	894	707	554	447	371	316	242	196	164	141	124	110	100
0.1	995	981	958	857	672	530	429	359	306	236	192	162	139	123	109	099
0.2	981	958	928	819	640	507	413	347	298	231	188	159	137	121	108	098
0.3	958	928	894	781	610	486	399	336	290	226	186	157	136	120	107	097
0.4	928	894	857	743	581	466	384	326	282	221	182	154	134	118	106	096
0.5	894	857	819	707	554	447	371	316	274	217	179	152	132	117	105	095
0.6	857	819	781	672	530	429	359	306	268	212	175	150	130	116	103	094
0.7	819	781	743	640	507	413	347	298	261	208	172	147	129	114	102	093
0.8	781	743	707	610	486	399	336	290	254	204	170	145	127	113	102	092
0.9	743	707	672	581	466	384	326	282	248	200	167	143	126	112	101	091
1.0	707	672	640	554	447	371	316	274	242	196	164	141	124	110	100	091
2.0	447	429	413	371	316	274	242	217	196	164	141	124	110	100	091	083
3.0	316	306	298	274	242	217	196	179	164	141	124	110	100	091	083	077
4.0	242	237	231	217	196	179	164	152	141	124	110	100	091	083	077	071
5.0	196	192	188	179	164	152	141	132	124	110	100	091	083	077	071	066
6.0	164	161	159	152	141	132	124	117	110	100	091	083	077	071	066	062
7.0	141	141	137	132	124	117	110	104	100	091	083	077	071	066	062	059
8.0	124	123	121	117	110	104	100	095	091	083	077	071	066	062	059	055
9.0	110	109	108	104	100	095	091	088	083	077	071	066	062	059	055	053
10.0	100	099	098	095	091	088	083	080	077	071	066	062	059	055	053	050

Table 2. Showing the values of $\Psi^*_{a=0}$.

It will be seen that the space, occupied by the curves with various cyclone constants, increases downward when b becomes ~~smaller~~ larger.

It is important problem to determine the value of b suitable to

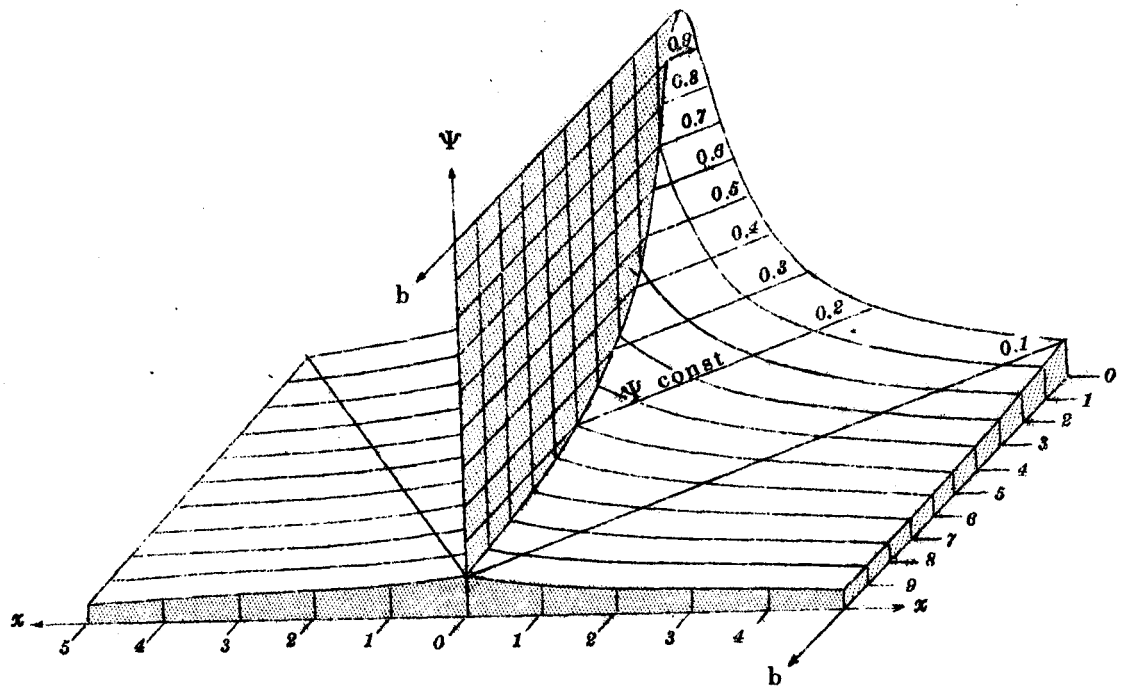

Fig. 6. Showing the cyclone function with the value of $a = 0$, and the different values of b.

the typhoon curves. After the analyses of many typhoon curves, the writer concluded that $b = 1$ is better.

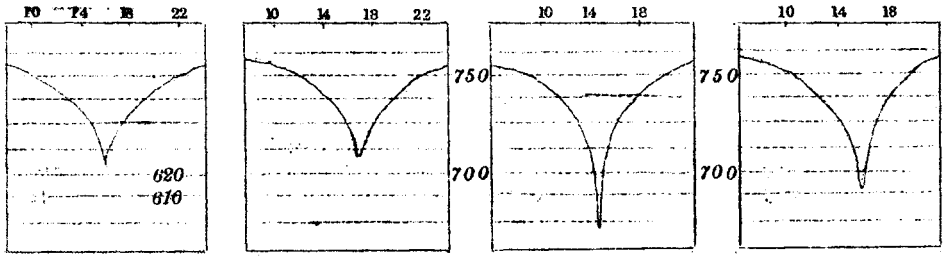

Fig. 7. Showing the pressuretraces recorded when the Makurazaki Typhoon attacked Kyushu.

According to the traces shown in Fig. 7, for example, the pressure drops rapidly in the vicinity of the center. This fact had been noticed by T. Namekawa and Z. Aoki(1), together with their notion of "Secondary Typhoon" imaginable inside the area of main typhoon. On the other hand, however, the writer's function is capable of

representing the pointed curve that they noticed.

§ 5 Deepening and Filling

In this section, the deepening and filling of typhoon pressure observed from the system moving with the typhoon are studied. When the pressure field is represented by the formula,

$$P = P_\infty - \Psi \Delta P$$

the deepening and filling taking place inside the typhoon areas may be known by differentiating the equation partially with respect to time, thus we have

$$\left(\frac{\partial P}{\partial t}\right)_r = \frac{dP_\infty}{dt} - \Psi \frac{d\Delta P}{dt} - \Delta P \frac{\partial \Psi}{\partial a}\frac{da}{dt} - \Delta P \frac{\partial \Psi}{\partial x}\frac{\partial x}{\partial r_0}\frac{dr_0}{dt} \qquad (13a)$$

Replacing the rate of change in the four constants by the notations with single dot, we have more simple formula,

$$\left(\frac{\partial P}{\partial t}\right)_r = \dot{P}_\infty - \Psi \dot{\Delta P} - \Delta P \Psi_a' \dot{a} + x \Delta P \Psi_x' \log \dot{r}_0 \qquad (13b)$$

(I) The undisturbed pressure P_∞ increases gradually as a typhoon enters the high pressure area in the middle latitude. The rate of change is about 20 mb/week, namely 1/5 mb/hr, which is negligiblly small in the ordinary case.

(II) As shown in Fig. 8, the rate of filling or deepening due to the change in ΔP is very large in the central area. Because it is multiplied by the value of Ψ, the cyclone function.

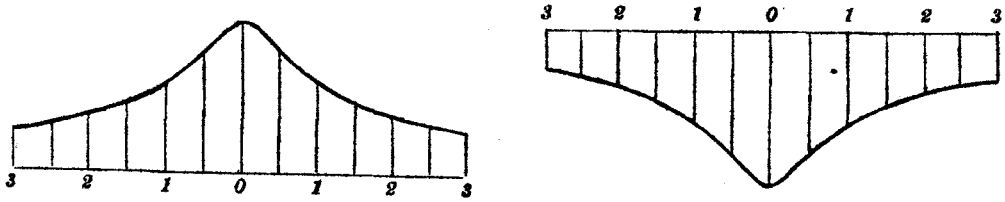

Fig. 8. The value of $-\Psi\dot{\Delta P}$ when $\dot{\Delta P}$ is negative (right), and the value of $-\Psi\dot{\Delta P}$ when $\dot{\Delta P}$ is positive.

(III) The change in a, the cyclone constant with respect to time produces the deepening or filling of $-\Delta P\Psi'_a\dot{a}$, whose value is zero both at the center and infinite distance. It is known that, in the development stage, the sign of $\dot{a}$ is negative, and that it changes into positive in earlier decaying stage. In decaying stage, usually $\dot{a}$ is about 0.1 per hour. This amount results in the value of $-\Delta P\Psi'_a\dot{a}$ of about 1 mb/hour when $\Delta P = 50$ mb., $a = 0.8$, and Ψ'_a is maximum. The shapes of the curves for deepening and filling cases are shown in Fig. 9.

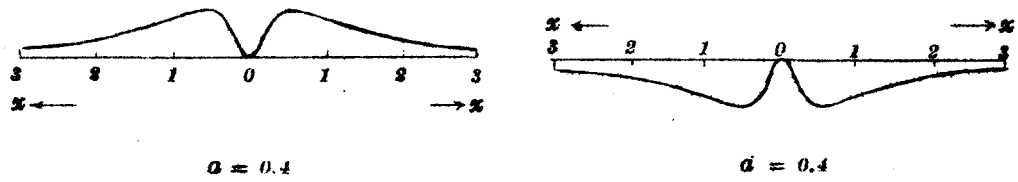

Fig. 9. Showing the value of $-\Delta P\Psi'_a\dot{a}$ in the development (left) and the decaying(right) stages.

(IIII) The unit radius r_0 increases from zero up to several hundred kilometers through formation, development, mature, and decaying stages. Therefore, $\dot{r}_0$ is positive showing that the value of $\Delta Px\Psi'_x\log\dot{r}_0$ is always negative. The deepening caused by the change in r_0 is shown in Fig. 10. It must be noticed here that the amount of deepening does not decrease in the outer area so rapidly as we have seen in the case of $\dot{a}$, because $x\Psi'_x$ decreases proportional to the reciprocal of the larger value of x.

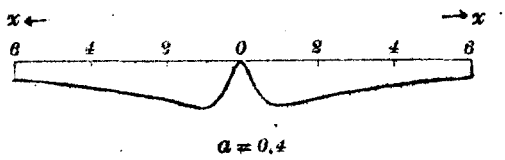

Fig. 10. Showing the value of $\Delta Px\Psi'_x\log\dot{r}_0$, which is usually negative in any stage of typhoon.

In the formation and development stage, the effect of filling

caused by $\dot{a}$ is partly cancelled by that of the deepening by $\dot{r}_0$. Therefore, the deepening due to $-\Psi\dot{\Delta P}$ is most prominient before a

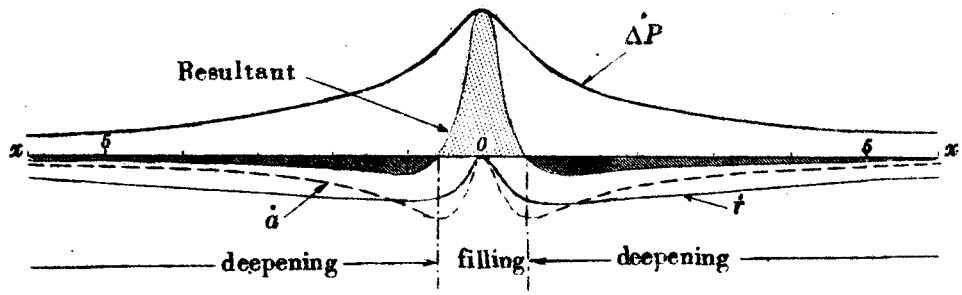

Fig. 11. Showing the distribution of filling and deepening for a decaying typhoon.

typhoon reaches its mature stage. On the other hand, in the decaying stage, values of $\dot{r}_0$ and $\dot{a}$ produce a pronounced deepening in the outer area, showing a remarkable contrast with the filling taking place in the vicinity of the center. The typical example of the pressure change inside a decaying typhoon is shown in Fig. 11.

There are two significant studies concerning the pressure change. One was carried out by Z. Aoki(1) being suggested by T. Namekawa in Kyoto University. He paid much attention to the fact that the center of typhoon decays rapidly, while the outer area remains almost unchanged. That fact led him to the conclusion that a well-developed typhoon must ~~be~~ consisted of two typhoons, the main and the secondary typhoon, and that the latter which is to be in the central area is rather small in area but very deep in pressure. To explain the rapid filling in the central area, he assumed that the secondary typhoon has the characteristic to decay rapidly.

The writer's function, however, would explain the fact that Z. Aoki had noticed. Because, when the cyclone constant is very small,

the shape of the funnel, as shown in Fig. 12, is supposed as if it

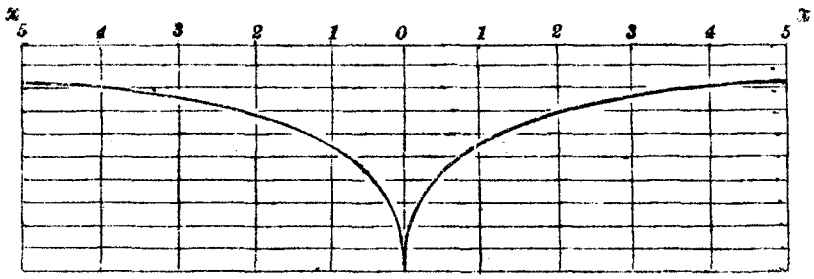

Fig. 12. The profile of typhoon with the cyclone constant $a = 0.02$.

~~were~~ consisted of two profiles for the main and the secondary typhoon.

The other study was completed by A. Kasahara. He introduced the filling-up index, a quantity showing the mass convergence inside a decaying typhoon. According to his study, the index is to be computed as the summation of the values of $\zeta_s/\sqrt{\lambda+\bar{\zeta}}$ multiplied by each of the four annular areas which are separated by the circles with the radii, 20km, 40km, 60km, and 80km from the center, where $\bar{\zeta}$, ζ_s, and λ denote the mean vorticity inside the frictional layer, relative vorticity at the surface, and the Coriolis' parameter, respectively. The filling-up index by Kasahara is supported also by the writer's theory, because it is evident that the filling-up takes place in the vicinity of center where the vorticity shows a large positive value.

The mass convergence inside a typhoon can be computed by integrating the rate of pressure rise around the center with respect to the area, thus:

$$\text{Rate of mass convergence} = \int_{\text{center}}^{\text{pivot}} \dot{P}\, dA = \int_{\text{center}}^{\text{pivot}} \dot{P}\, 2\pi r\, dr \qquad (14a)$$

where, the pivot is the point noticed by Kasahara, at which the filling changes into deepening.

Replacing r by xr_0, we have

$$\text{Rate of mass convergence} = \int_{\text{center}}^{\text{pivot}} 2\pi x \cdot r_0^2 \dot{P}\, dx = 2\pi r_0^2 \int_{\text{center}}^{\text{pivot}} x \dot{P}\, dx$$

$$= 2\pi r_0^2 \left(-\dot{\Delta P}\int x\Psi\, dx - \Delta P\, \dot{a}\int x\Psi_a'\, dx + \Delta P \dot{\log} r_0 \int x^2 \Psi_x' dx\right) \quad \text{(14b)}$$

whence, $$\dot{P} = -\Psi\dot{\Delta P} - \Delta P \Psi_a' \dot{a} + \Delta P x \Psi_x' \dot{\log} r_0$$

In order to carry out the integration from center to the pivot, graphical integration is preferable.

The pivot noticed by A. Kasahara may be re-emphasized here. It is the point or circle at/on which the filling or deepening is not taking place. Therefore, the value of x at the pivot must satisfy the formula, $\partial P/\partial t = 0$, namely,

$$\dot{P}_n - \Psi\dot{\Delta P} - \Delta P \Psi_a' \dot{a} + \Delta P x \Psi_x' \dot{\log} r = 0$$

It is evident that the several values of x would satisfy the equation. The smallest value of x, however, shows the most important point as the pivot.

§ 6 Expansion and Shrink of Isobars.

This is the rate of change in the isobar radii. If the pressure r km. from the center changes $-dP$, as shown in Fig. 13, the radius will expand dr, and there exists a relation,

$$-\frac{dP}{dt}\Big/\frac{dr}{dt} = \text{grad } P \quad \text{(15)}$$

therefore,

$$\frac{dr}{dt} = -\frac{dP}{dt}\Big/\text{grad } P = \frac{r_0}{\Psi_x' \Delta P}\dot{P}$$

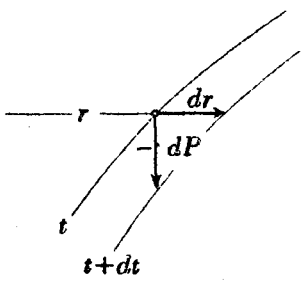

Fig. 13. In order to obtain the rate of expansion.

Using the formula(13), we have

$$\frac{dr}{dt} = \frac{r_0}{\Delta P}\frac{1}{\Psi_x'}\dot{P}_n - \frac{r_0}{\Delta P}\frac{\Psi}{\Psi_x'}\dot{\Delta P} - r_0\frac{\Psi_a'}{\Psi_x'}\dot{a} + x\dot{r}_0 \quad \text{(16a)}$$

The shape of each term in the right side is shown in Fig. 14.

In the vicinity of the center, the formula can be reduced to

$$\left(\frac{dr}{dt}\right)_{x\ll 1} = -\frac{r_0 a^2}{\Delta P}\frac{d}{dt}(P_\infty - \Delta P)\frac{1}{x} \quad (16b)$$

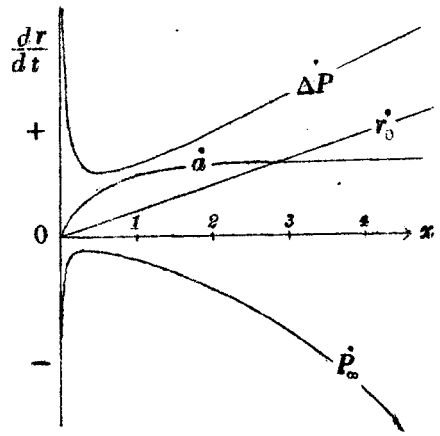

Fig. 14. Showing the effect of the positive rate of the four constants.

In the outer area, we get

$$\left(\frac{dr}{dt}\right)_{x\gg 1} = -\frac{r_0}{\Delta P}x^2\dot{P}_\infty + r_0 x\log\dot{\Delta P} + x\dot{r}_0 \quad (16c)$$

It is true, from these equations, that the radius of the isobar at the center changes quickly, when $P_\infty - \Delta P$, the central pressure, changes. And the smallest isobar enclosing the center would vanish or appear abruptly.

When x is very large, the value of $\dot{P}_\infty$ multiplied by x^2 may play an important rôle to change the radius of isobars, however, in the outer areas, this effect is not clear, since those areas are influenced by the other pressure systems.

The schematical figure showing the shrink and expansion taking place inside a typhoon is presented in Fig. 15. The most impor-

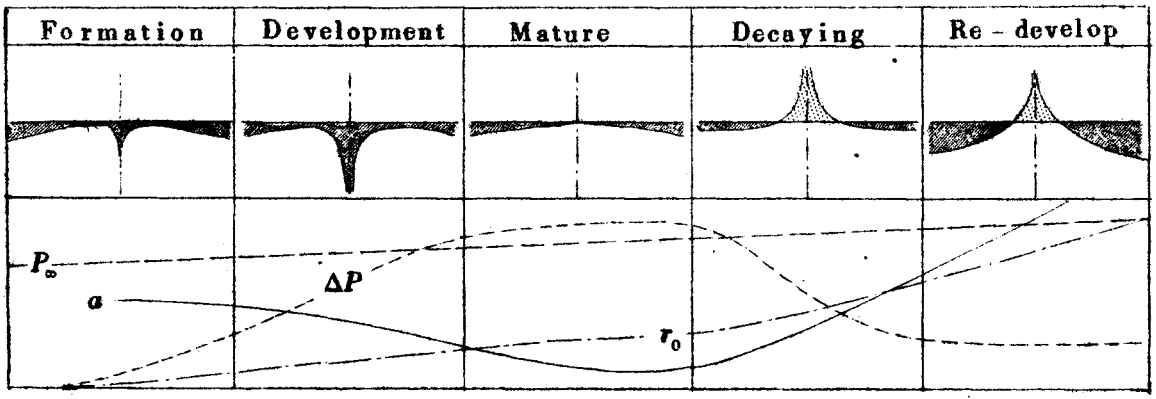

Fig. 15. Shrink and expansion of isobars for a typhoon in various stages(upper) and the change in four constants.

tant fact seen in the figure is the expansion of the isobars in the outer areas, which is seen in any stage of a typhoon.

§ 7 Pressure Tendency

The pressure tendency for a moving typhoon is given by the formula, $$\frac{dP}{dt} = \frac{\partial P}{\partial t} - (V \cdot grad P) \quad \text{---------- (17)}$$ which means that the tendency is produced by the change of the typhoon itself and also by its movement.

(A) TENDENCY DUE TO THE TYPHOON MOVEMENT

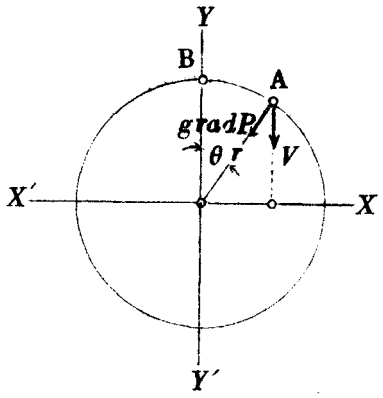

Fig. 16. To obtain the pressure tendency caused by the typhoon movement.

It is known that the tendency due to the typhoon movement is given by the inner product of two vectors; V, the relative velocity of a station to the typhoon center, and grad$P$, the pressure gradient at the station in discussion. If we measure the time from the moment when the station has passed across the line XX′, at a time t the station must be located at the distance r km. from the center and V_t km. from XX′ axis. Now, we call the station in discussion Station A, and the other one located on YY′ axis r km. from the center Station B. It will be seen that there exists a simple relation between the tendencies at the Station A and B. Because the tendency at A is

$$-(V \cdot \text{grad} P) = -V \frac{\Delta P}{r_0} \Psi_X' \cos\theta \quad \text{---------- (18a)}$$

$$= -V \frac{\Psi_X' \Delta P}{r_0} \cos\theta \times \cos\theta$$

$$= \text{Tendency at B} \times \frac{V_t}{r_0} \quad \text{---------- (18b)}$$

which tells us the relation,

$$\text{Tendency at A} = \text{Tendency at B} \times \frac{Vt}{r} \qquad (18c)$$

On the other hand, the tendency at B given by

$$-\frac{\Delta P}{r_0}\,\Psi_x'\,V \qquad (18d)$$

would easily be computed using the table of Ψ_x'. The tendencies for the different values of a are presented in Fig. 17.

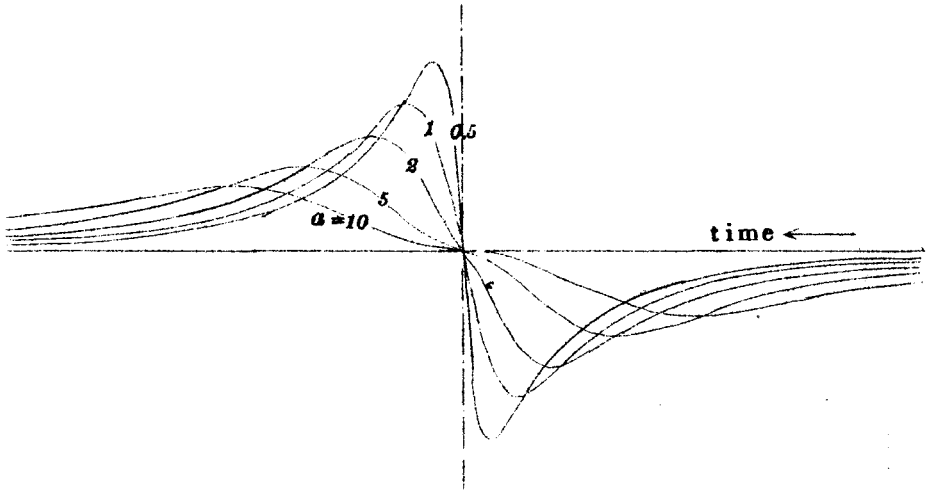

Fig. 17. Tendencies for the station on the axis YY'. It should be noticed that the curves have three inflexion points when $a > 1.0$.

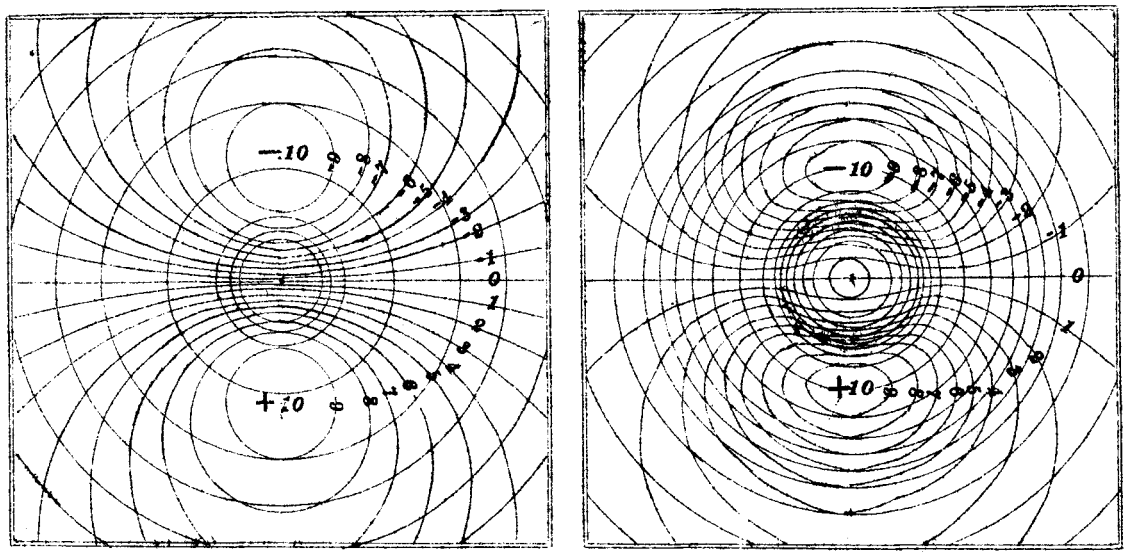

Fig. 17. Isallobars of the typhoon with $a = 0.5$(left) and those of the cyclone with $a = 5.0$(right).

Making use of the formulas (18), the isallobars in Fig. 18 were drawn. The most interesting and important difference between the isallobars for typhoon and continental cyclone is their shape in the inner area. As will be seen in the figure, the isallobars of the typhoon with the cyclone constant smaller than 1.0, have their shape of the left, and the cyclone with the constant larger than 1.0 are something like that of the right. This fact is very helpful in drawing the isallobars of moving system.

(B) TENDENCY DUE TO $\partial P/\partial t$

The other tendency represented by $\partial P/\partial t$ is caused by the deepening and filling of typhoon. This effect is prominent when the typhoon speed is rather slow. Especially when a typhoon stays at a constant location and deforms, whole tendency is given by this value.

According to the equation(13b), we know

$$\left(\frac{\partial P}{\partial t}\right)_r = \dot{P}_\infty - \Psi \dot{\Delta P} - \Delta P \, \Psi_a' \dot{a} + \Delta P \, x \Psi_x' \log \dot{r}_0$$

The first term $\dot{P}_\infty$ gives the constant tendency throughout the areas.

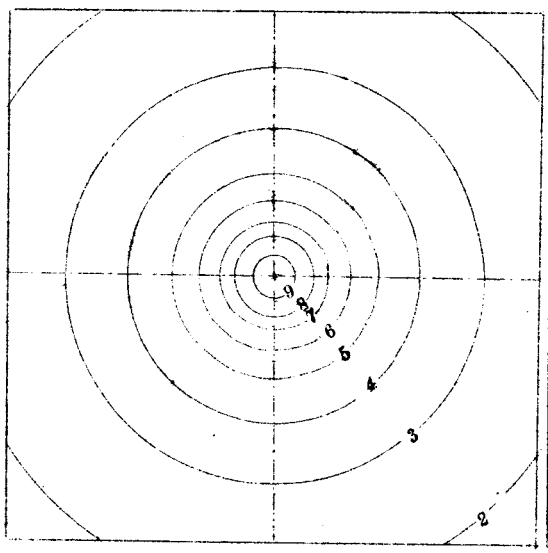

Fig. 19. Isallobars due to the change in $\dot{\Delta P}$. $(-\Psi \dot{\Delta P})$

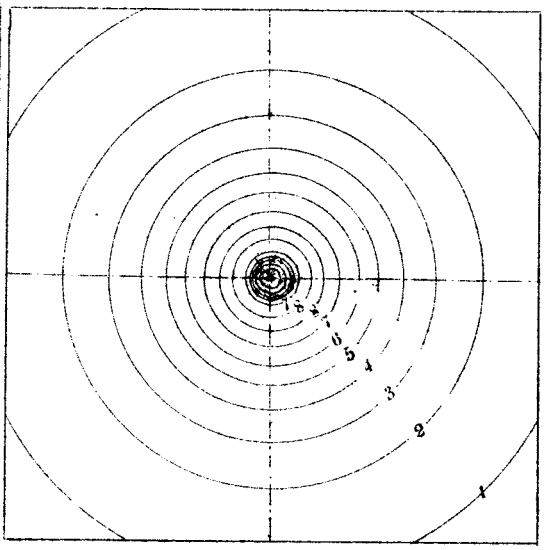

Fig. 20. Isallobars due to the change in $\dot{a}$. $(-\Delta P \Psi_a' \dot{a})$

The second and third ones form the isallobars shown in Figs. 19 & 20. Similar to the third one, the last term gives the tendency with the maximum amount encircling the center. Its shape will be seen in Fig. 21.

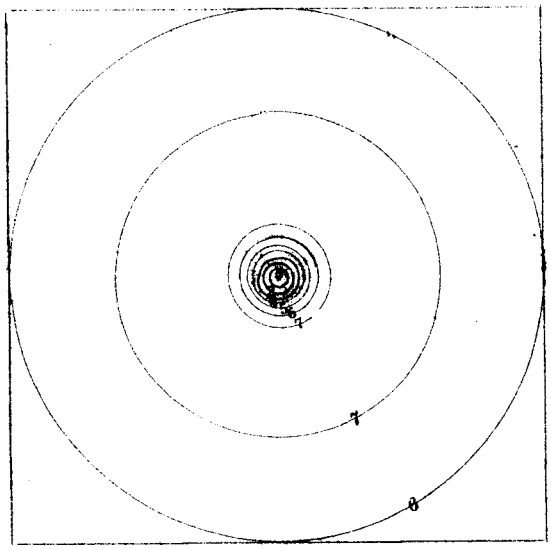

Fig. 21. Isallobars due to the change in r_0. $(+\Delta P \times \Psi_x \dot{} \log \dot{r}_0)$

In the practical case, the isallobars in Figs. 19, 20, and 21 must be superimposed upon those in Fig. 18. In her mature stage the effect of $\partial P/\partial t$ is very small, but when she enters the middle latitude, according to the rapid change in ΔP, a, and r_0, the isallobars deform appreciablly.

PROBLEM OF MINIMUM PRESSURE

One might consider that the minimum pressure at a station would occur when a typhoon passes the nearest distance from the station. This assumption, however, is not always accurate. Now we consider the case where a typhoon passes in the vicinity of a station, the tendency,

$$\frac{dP}{dt} = \frac{\partial P}{\partial t} - (V \cdot \mathrm{grad}\, P)$$

can be reduced to

$$\frac{dP}{dt} \fallingdotseq (\dot{P}_\infty - \dot{\Delta P}) + \frac{V^2 \Delta P}{a^2 r_0^2}\, t \qquad (\because x \ll 1) \qquad (19a)$$

The time of the occurrence of the minimum pressure is obtained, thus:

$$t = \frac{-a^2 r_0^2}{V^2 \Delta P} (\dot{P}_\infty - \dot{\Delta P}) = -\frac{a^2 r_0^2}{V^2 \Delta P}\, \dot{P}_0 \qquad (19b)$$

where, $\dot{P}_0$ is the change in the rate of the central pressure. The

result shows that the minimum pressure for a decaying typhoon ($\dot{P} > 0$) appears prior to the passage of the center.

If the central pressure of a typhoon, having the values, $a = 0.5$, $r_0 = 100$km, $\Delta P = 50$mb, and $V = 50$km/hr, increases at the rate of 5 mb. per hour, the minimum pressure would appear 1/10 hour before the passage of the center, namely, it occurs 5 km. ahead of the center. When the cyclone constant is two times larger, it will be seen about 10 km. ahead.

In the practical analyses of typhoon, we must always consider the fact that the minimum pressure and the passage of the center do not occur at the same time. For the illustration of this fact, an example of isallobars for a rapidly decaying typhoon is shown in Fig. 22. It will be understood that the $\partial P/\partial t = 0$ line, on which the minimum pressure is to be observed does not pass through the center.

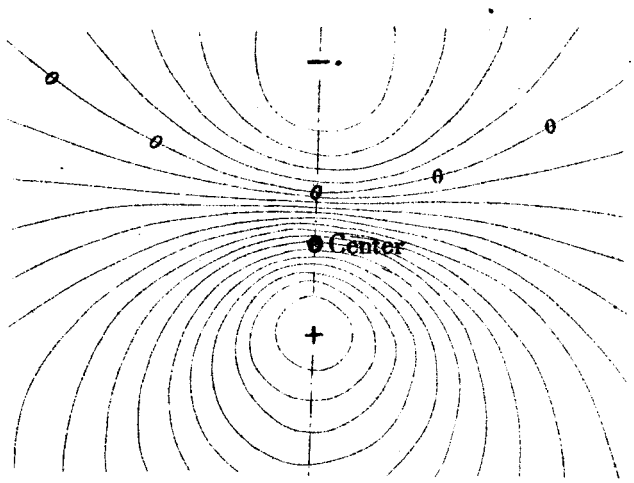

Fig. 22. Showing the isallobars of a typhoon when her central pressure increases rapidly.

§ 8 Standard and Anomalous Pressure

(I) STANDARD PRESSURE

To obtain the standard pressure, we must compute the mean pressure defined by the formula (6). We plot the pressure for the

different radii on the section paper and draw the reasonable pressure profile satisfying the plotted points. As will be seen in Fig. 23, the pressures for the reporting stations are very helpful in drawing the profile; however, it should always be kept in mind that the stations concentrated inside a local area indicated by the arrow have sometimes a bad influence for drawing the profile.

After drawing the profile, we determine the horizontal line for P_∞, making use of the characteristic of the pressure profile that approaches to P_∞ line inversely proportional to the distance from the center. Then we read the depth of the funnel ΔP.

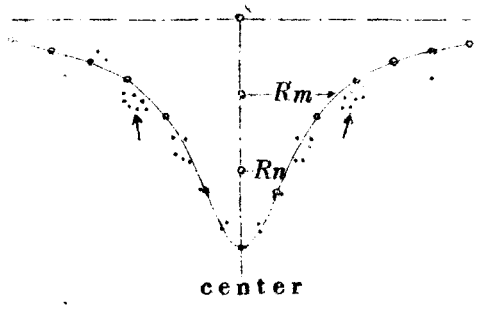

Fig. 23. Drawing the pressure profile of a typhoon.
○ —— mean pressure, · —— pressure for reporting stations.

Next we compute the radius ratio Rm/Rn and find out the suitable cyclone constant using the tables in pages 30 and 31.

The unit radius r_0 is given by the relation,

$$r_0 = Rm / Xm$$

where, Xm is the parameter tabulated on the same pages.

Using the four constants P_∞, ΔP, a, r_0, and also the table of Ψ, the pressure; $P = P_\infty - \Psi \Delta P$ can be computed, which is the standard pressure for the typhoon under discussion.

(Ⅱ) ANOMALOUS PRESSURE

The observed pressure subtracted by the standard pressure may be called the anomalous pressure. The characteristic of the anomaly becomes evident by drawing the isallobars for the anomalous pressure.

Should the anomaly chart be drawn on the steering level of typhoon, it would show the general current by which the storm is to be steered. To know the general current, the surface anomaly chart is not always suitable, but in the case where the storm areas are not occupied perfectly by cold air-masses, surface anomaly isobars are something like those of the steering level.

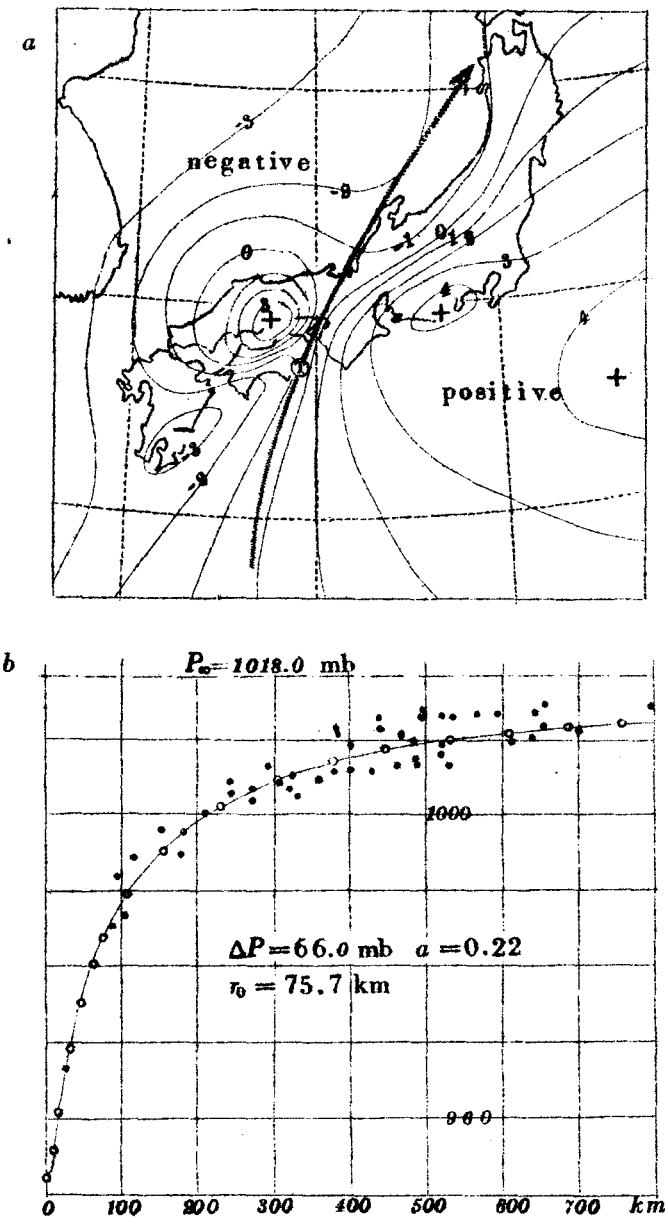

Fig. 24. Anomalous pressure chart(a) for Typhoon Jane of 3 Sept. 1950, and her profile(b) at the same time.

The anomaly chart for Typh.Jane of 3 Sep. 1950 is presented in Fig. 24a. And at that time she had the profile shown in Fig. 24b. It will be seen that the isobars show the general current especially in the warm sector. In the cold sector, however, the general current is screened by the cold air-masses north west of the typhoon. The pronounced positive anomaly over West

Japan is produced by the shallow cold air-masses caused by the heavy rains in that area.

In the mountain areas such as Japan and Philippines we see sometimes positive anomaly. In Fig. 25 the typical anomaly over Japan is shown. Such anomaly is supposed to be caused by the convergence of the circulating airs which results in the topographical filling. On account of the topographical positive anomaly, a travelling cyclone over Japan Islands, in many cases, has split into two depressions on both offings of the Islands.

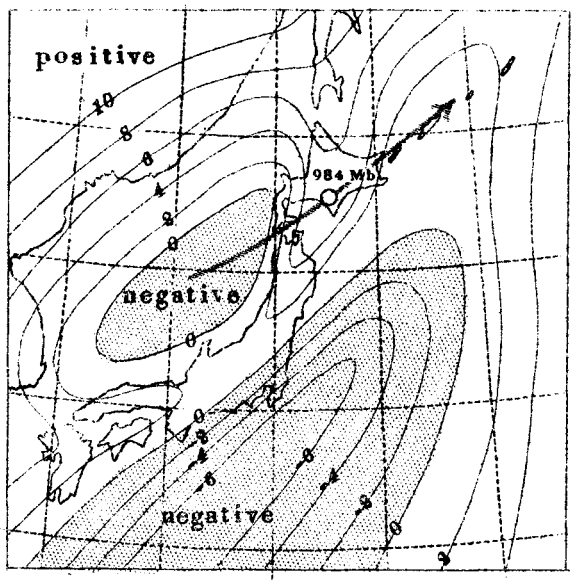

Fig. 25. Positive anomaly caused by the mountains over Japan Islands. Continental cyclone at 9h Oct.30 1949

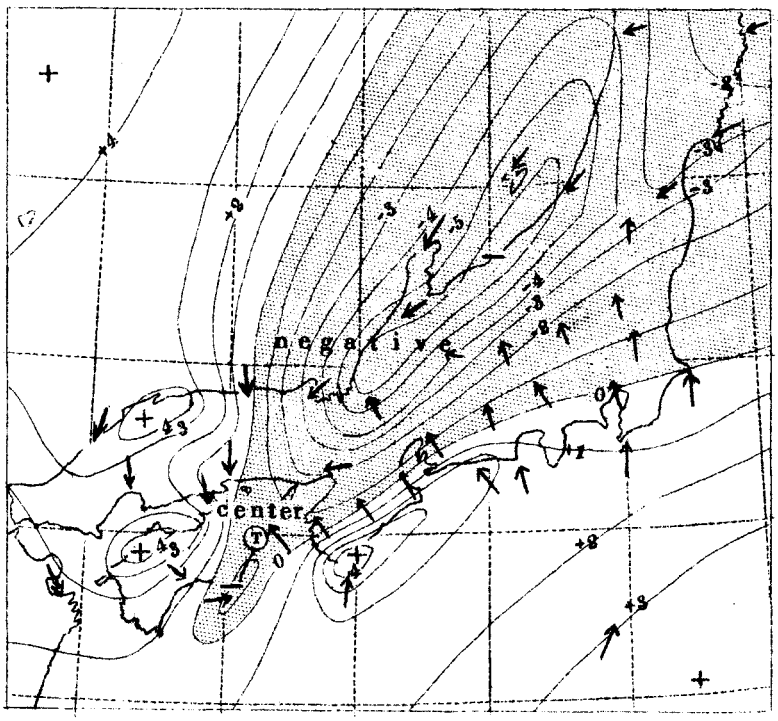

Fig.26. Negative anomaly(Typh. Muroto in 1934)

Negative anomaly is seen in föhn regions in typhoon areas. An example in North Japan at the time of the Muroto Typhoon

of 21 Sept. 1934 is represented in Fig. 26. The insolation reaching the earth's surface through the fine weather inside the föhn area sometimes heats the ground, consequently promoting the negative anomaly in the daytime. Similar to the topographical anomaly, this anomaly does not reach the higher altitude, vanishing usually below the level of 700 mb.

It must be pointed out here that the small depressions which are used to be drawn on the isobar chart of the typhoon over a complicated topography are not the small secondary typhoons followed by cyclonic winds but the apparent lows without any relation to the profound nature of the storm. Thus, the pressure anomaly tells us of many interesting problems on the pressure field, but there exist other anomalies caused by a travelling depression. It will be discussed in section 10 in detail.

§ 9 Pressure Oscillations

"This section has been studied in cooperation with K. Otani(19) in Fukuoka Meteorological Observatory."

In this section we only discuss the case where the density of the air is approximately equal in horizontal directions. Under this assumption, the air pressure in horizontal flow coincides with the weight of the air column.

At the time of a storm passage, sometimes it happens that barometers oscillate about several millimeters so that we can not read the pressure accurately. In reading the scale it has been taught to read the mean position of the mercury meniscus oscillating up and down. We have long been desiring to know the nature of the oscillations, and recently we have studied the traces of wind and pressure

at the top of Mt. Seburi, leading us to the conclusion that the oscillations are closely related to the suction of air in the barometer room, and that the mean position of the mercury top does not indicate the pressure in the open air.

As shown in Fig. 27, the pressure oscillates whenever the wind speed is higher than 15 m/sec, meanwhile the pressure itself decreases proportional to the square of the speed. The other example recorded at the time of Typhoon Kezia is also shown in the next page. These figures do not always suffice our need, therefore, one of us has made the traces of wind and pressure recorded on a rapidly rotating drum, by using Dines'pressure tube anemometer, the optical lever connected to the axis of aneroid pressure recorder, and statoscope. The results thus obtained are presented in Figs. 29 and 30, in which the squares of the wind speeds multiplied by half of air density are compared with the pressure drawn upside down. As will be seen in the figure, there exist long period oscillation(order of minutes) and short period one(order of seconds), which may be called the long and the short period gustiness, respectively. The long period gusts in wind are correlated to the pressure gusts, but the shorter ones are not always correlated with them.

Now we consider the causes of pressure oscillation from various angles.

(A) TOPOGRAPHICAL EFFECT

The pressure within a current prevailling over a hill does not coincide with the weight of the air column, because, as shown in Fig. 31, the horizontal upstream currents are accelerated along the hillside, meanwhile the pressure drops untill they reach the maximum speed. Isobars for the practical pressure subtracted by the net

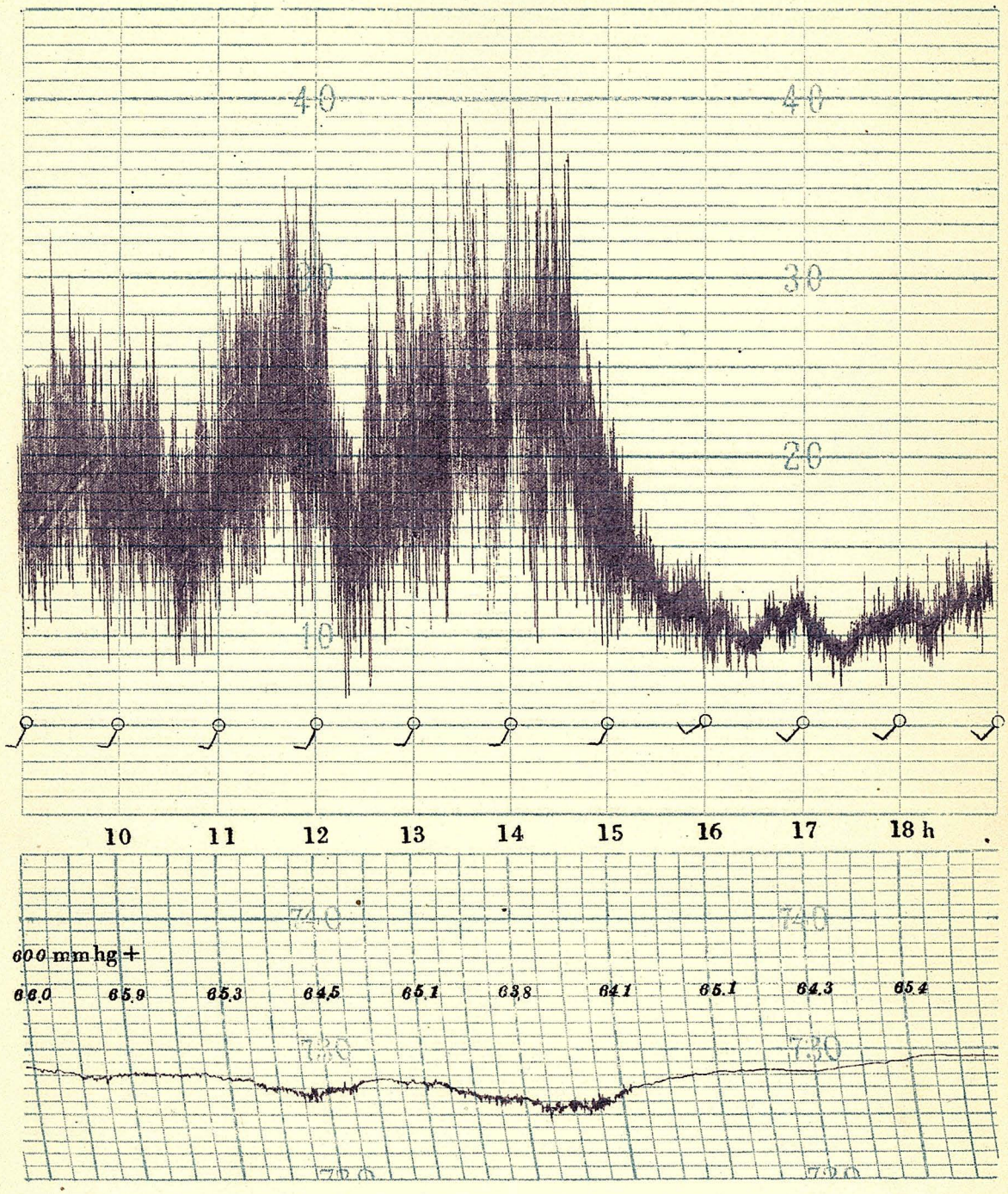

Fig. 27. Pressure drops associated with the long period wind gusts occurring at the time of the cold-frontal passage on 12 May 1949. It will be seen that the barometer oscillated when the wind speed is higher than 15 m/sec. (Mt. Seburi Weather Station, 1954 m)

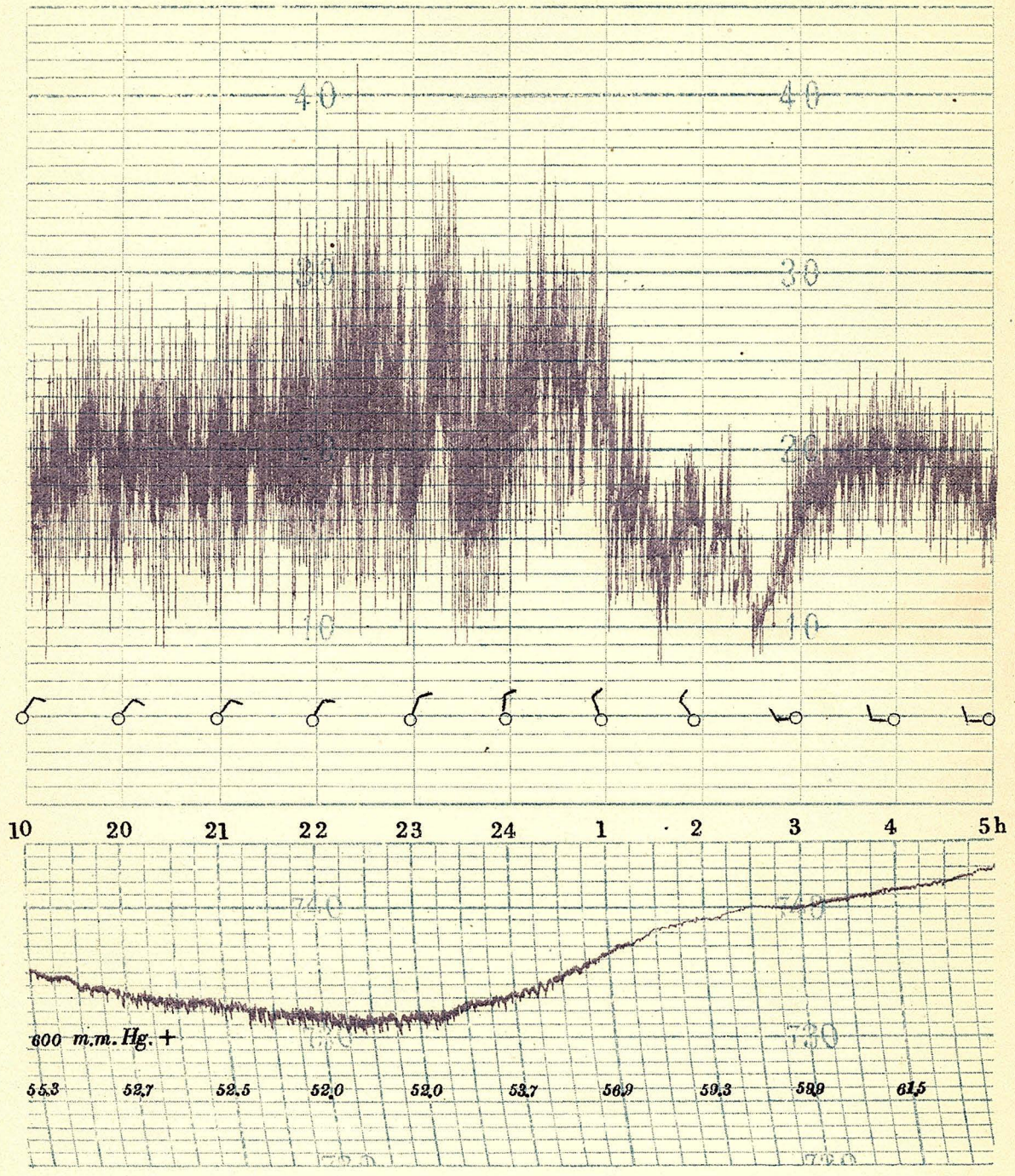

Fig. 28. Gusty winds and the short period pressure oscillations recorded at the time of Typhoon Kezia. This type of oscillations were recorded, without exception, by the pressure recorder. (Mt. Seburi Weather Station, 1054 m)

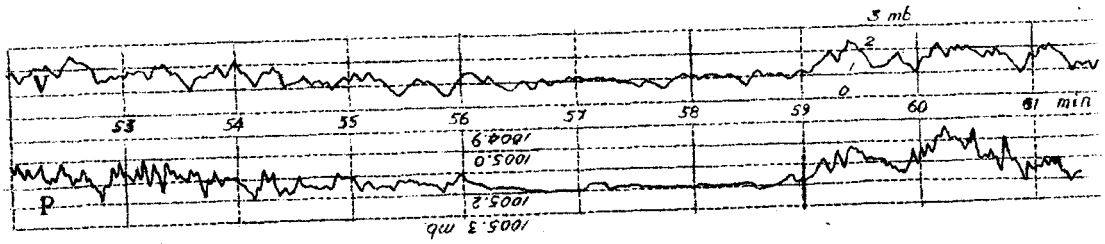

0952 ⟶ 1001 15 October, 1951

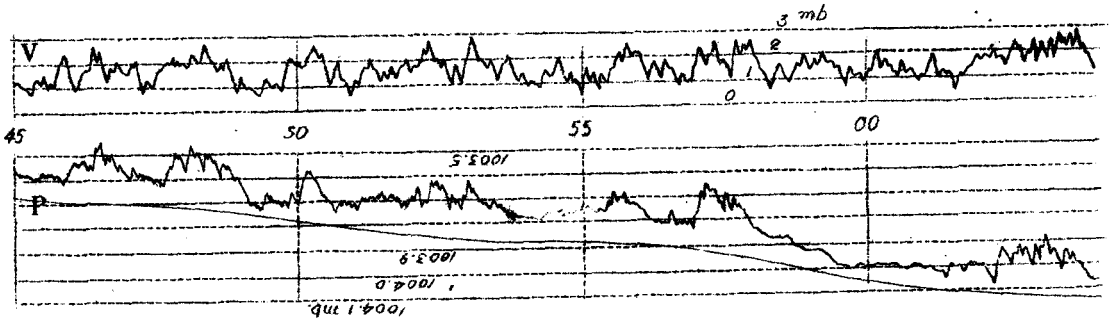

0845 ⟶ 0905 15 October, 1951

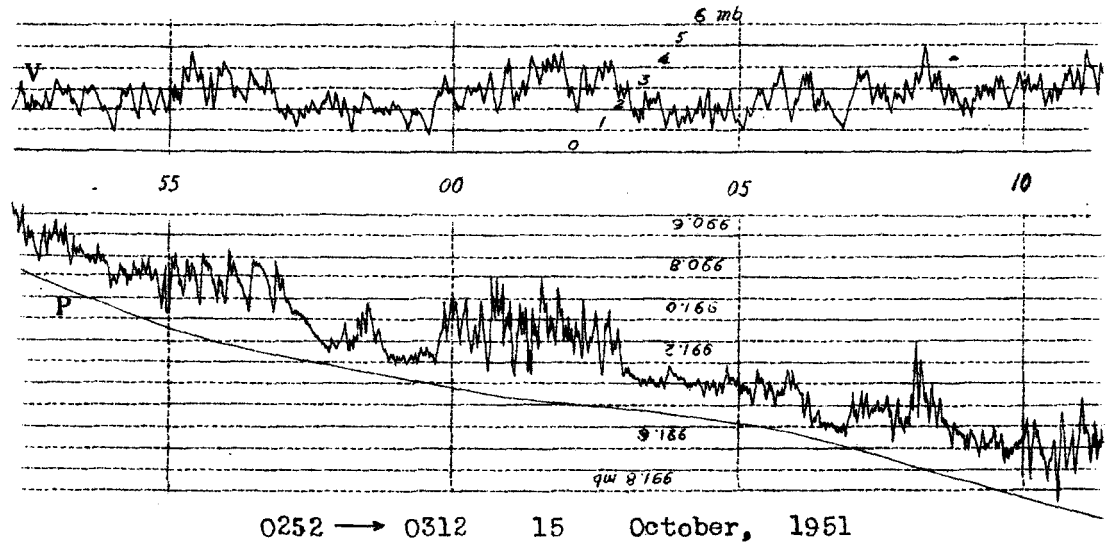

0252 ⟶ 0312 15 October, 1951

Fig. 29. Comparison of the pressure oscillations and the wind gusts transcribed in the $\frac{1}{2}\rho V^2$ scale. Fukuoka Meteorological Observatory. recorded by Statoscope.

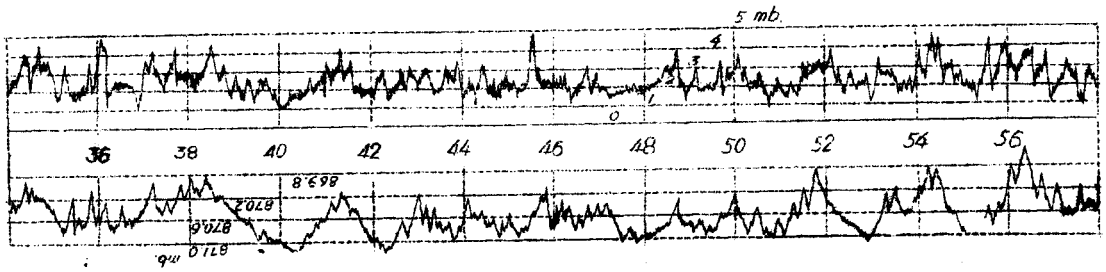

2034 → 2058 13 Sept, 1950

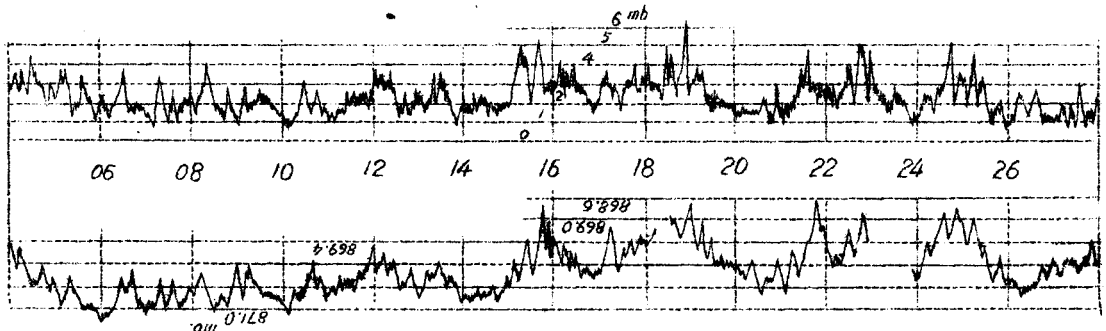

2104 → 2128 13 Sept, 1950

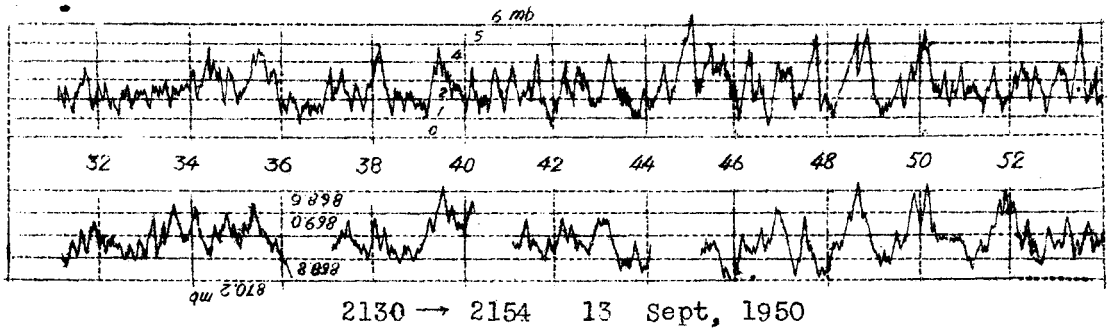

2130 → 2154 13 Sept, 1950

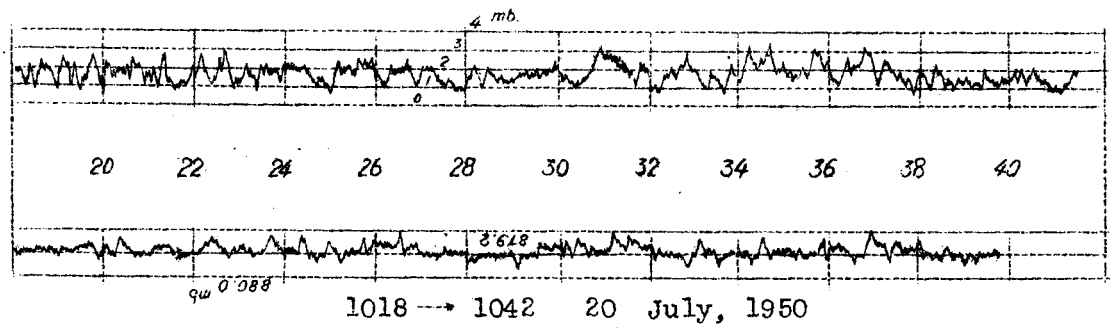

1018 → 1042 20 July, 1950

Fig. 30. Comparison of the pressure oscillations and the wind gusts transcribed in the $\frac{1}{2}\rho V^2$ scale. Mt. Seburi Weather Station, 1054 m.

weight of the air column are drawn schematically in the figure. The low pressure area on the hill is always screened by the centrifugal force of the airs passing over along the convex paths. If the stream is irrotational, the pressure drop is to be computed, but in the practical case, the drop in the leeward side is rather difficult to be computed.

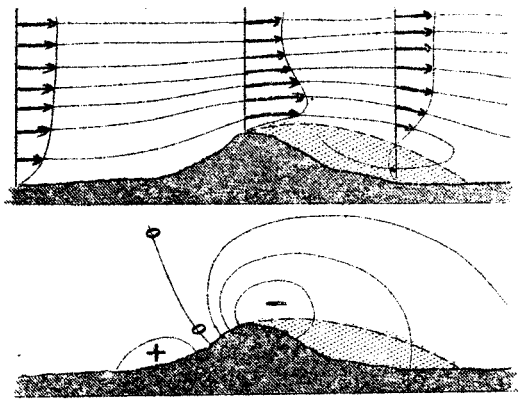

Fig. 31. Stream lines and the low pressure field caused by a small hill.

In the case where the station is located in the low pressure area on the hill, the observed pressure would be lower than the net weight appreciably. The decrease in pressure can be written, thus:

$$P_\alpha = \alpha \frac{1}{g} \rho V^2 \qquad (20)$$

where, V is the wind speed at the station under consideration, ρ the density, α the coefficient decided by the shape of the hill and the location of the barometer room. The wind oscillation with the wave length comparable to the scale of the hill will produce such a decrease in pressure. Typhoon winds of 30 m/sec with the period of 1 minute has the wave length of about 2 km., which is enough for the present case.

(B) SUCTION EFFECT

This effect occurs in the manner similar to that we see in the suction tube of Dines' anemometer. In the present case, the building of the weather station with doors and windows acts as if it were the suction tube. The pressure inside the room can, therefore, be given

by the formula: $P_\beta = \beta \frac{1}{2} \rho V^2$ ..... (21)

where, β is the constant determined by the way of presentation of the building in the storm. The pressure drop must be proportional to the square of the wind speed strictly.

The resultant effect of the above-mentioned pressure drop is written thus:

$$P_\alpha + P_\beta = \alpha \frac{1}{2} \rho V^2 + \beta \frac{1}{2} \rho V^2$$
$$= (\alpha + \beta) \frac{1}{2} \rho V^2 \quad \text{..... (22)}$$

in which the coefficient α and β have each frequency character de-

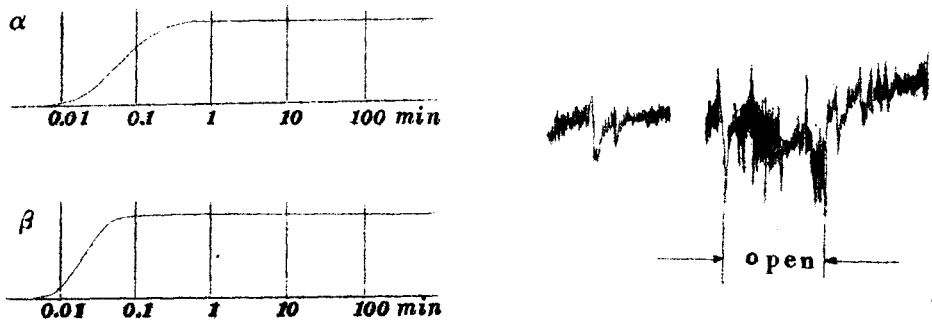

Fig. 32. Showing the frequency character of α and β (left), and the increase of gust when the door of barometer room is opened.

creasing for higher frequency. Schematically, the change in β and α with frequency is shown in Fig. 32 together with the practical example showing the increase of gust when the door of the barometer room is opened.

(C) EFFECT OF TURBULENCE

The shape of the eddies imbedded inside a typhoon current is not so evident, but it is reasonable to consider that the vortices develop, deform, or decay as they travel along their courses. On account of the internal friction or the resistance of the obstacles, eddies will be initiated successively inside the frictional layer.

The long-lived vortices must have long eddy line which is shown in Fig. 33.

How much would the pressure decrease when a vortex passes across a weather station ? This question can be answered by computing the pressure decrease in the model vortex shown in Fig.34. If the speed of the air with respect to the moving vortex center be ΔV, the speed V of the actual wind that would be recorded by the Dines' anemometer is obtained superposing the speed of the vortex center upon the speed ΔV.

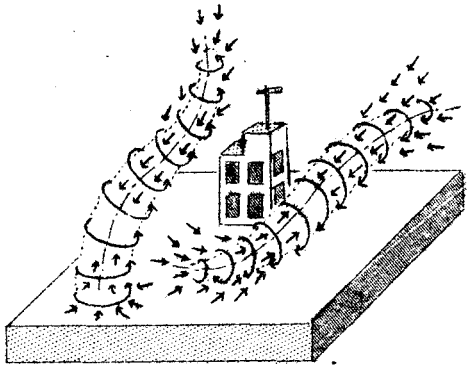

Fig. 33. Three-dimensional feature of practical vortices within typhoon wind. The airs enter inside the vortex from both ends of the vortex, where the centrifugal force of circulating air is not enough to prevent the entering air.

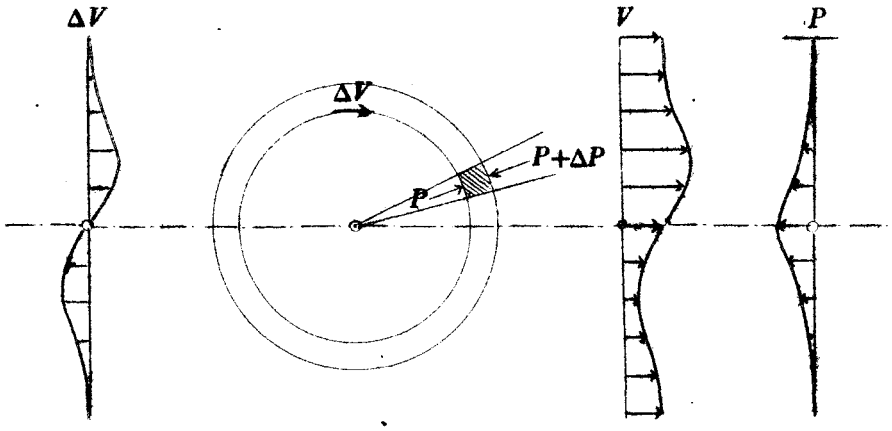

Fig. 34. Showing the distribution of wind relative to the vortex center (ΔV), and wind speed (V), and the pressure decrease inside the vortex.

The pressure decrease in the vortex is obtained, thus:

$$\frac{\Delta V^2}{r} = \frac{-1}{\rho}\frac{dP}{dr} \qquad \therefore dP = -\rho\,\Delta V^2 d(\log r)$$

Therefore, $$P_r = -\rho\int_{\infty}^{r}\Delta V^2\, d(\log r) \qquad (23)$$

In the case where the wind speed within a vortex, having the diameter of 40 m., is proportional to the radius, with the proportional constant of $\frac{1}{2}$ per second, pressure at the center is

$$-\rho\int_{2000}^{0}\frac{\left(\frac{r}{4}\right)^2}{r}dr = -\frac{1}{8}\rho\left[r^2\right]_{2000}^{0} = \frac{1}{2}\times 10^3\ dyne/cm^2 \fallingdotseq 0.5\ mb.$$

This value is conceivable in the practical cases.

In the turbulent layer, in which many vortices of various sizes exist, the pressure is different from the weight of air column which would increase homogeneously downward. The schematical pressure distribution is shown in Fig. 35. As the airs in the turbulent layer flow horizontally supporting the weight of the overlying atmosphere, the pressure free from the perturbation must satisfy the condition of static equilibrium. We must, therefore, consider the fact that there exist the positive and negative pressure perturbations inside the frictional layer. The most important characteristic of the pressure variation is that it does not vary parallel to the wind speed. The short period pressure oscillations uncorrelated to those

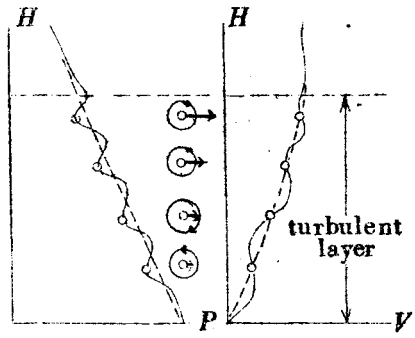

Fig. 35. Schematical distribution of pressure and wind velocity within turbulent layer involving vortices.

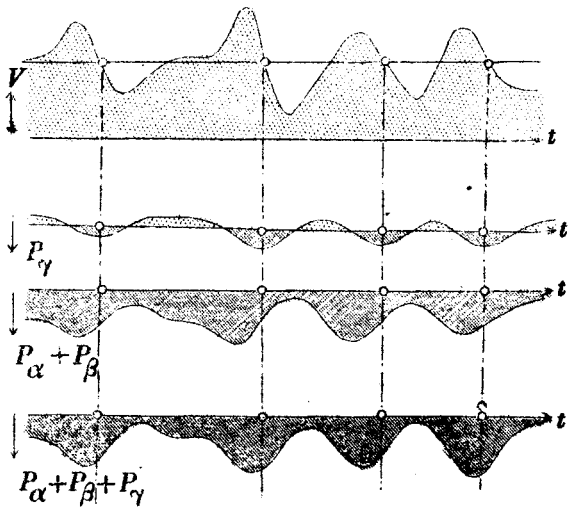

Fig. 36. Pressure decrease $(P_\alpha+P_\beta+P_\gamma)$ caused by the successive vortices circulating in the same direction. It will be seen that there is no good correlation between the speed and the pressure decrease.

of the wind are supposed to be caused by these vortices. The pressure oscillation due to the vortices circulating in the same direction is shown in Fig. 36. It will be understood that the pressure variations are not to be connected with those of the wind.

The pressure oscillations of this type do not lower the mean value of the pressure traces but they make the short period pressure oscillation more random.

Thus the pressure variation due to high winds can be represented by the formulas,

$$P = wP - \frac{1}{g}\rho(\alpha+\beta)V^2 - P_\eta \qquad (24a)$$

$$\overline{P} = \overline{wP} - \frac{1}{g}\rho(\alpha+\beta)\overline{V}^2 \qquad (24b)$$

where, P is the pressure inside the barometer room, wP the weight of the air column, the values $\overline{P}$, $\overline{wP}$, $\overline{V}^2$ show the mean.

DETERMINATION OF THE CONSTANT $(\alpha+\beta)$

The constant we now want to determine is very important, because wP can be computed by the relation,

$$\overline{wP} = \overline{P} + (\alpha+\beta)\frac{1}{g}\rho\overline{V}^2 \qquad (24c)$$

Should there be two stations at the foot and at the top of a hill which is not so high, it is possible to get the value as follows: At the surface station far from hills, the pressure decrease due to high wind is caused only by the suction of the station building, therefore, $\alpha=0$. After the examination of pressure traces at Fukuoka Meteorological Observatory, the value of β for such station is known to be about 0.1 - 0.2. Then, we have, $\overline{P}_A = \overline{wP} - 0.1 \times \frac{1}{g}\rho\overline{V}_A^2$

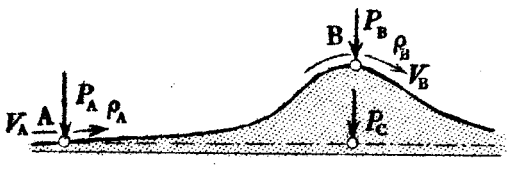

Fig. 37. Showing the pressure and wind for two station A and B.

$$\overline{Pc} = \overline{wP} - (\alpha_B + \beta_B)\frac{1}{g}\rho_B \overline{V_B^2}$$

where, P_A, P_C, and V_A, V_B are used in the meanings in Fig. 37.

Thus we have, $$\overline{P_A} - \overline{P_C} = (\alpha_B + \beta_B)\tfrac{1}{2}\rho_B \overline{V_B^2} - 0.1\,\tfrac{1}{2}\rho_A \overline{V_A^2} \quad \text{(25a)}$$

If the second term in the right side, which is about one tenth of the first one, can be neglected, we get

$$\overline{P_A} - \overline{P_C} = (\alpha_B + \beta_B)\tfrac{1}{2}\rho_B \overline{V_B^2} \quad \text{(25b)}$$

This formula shows us that the value of $(\alpha + \beta)$ is computed by pressure and wind for the two stations in Fig. 37.

EXAMPLE (I) Hosojima(top) and Nobeoka. (Typhoon Della of 1949)

As shown in Fig. 38, the constant $(\alpha + \beta)$ for Hosojime lighthouse weather station is about 0.6.

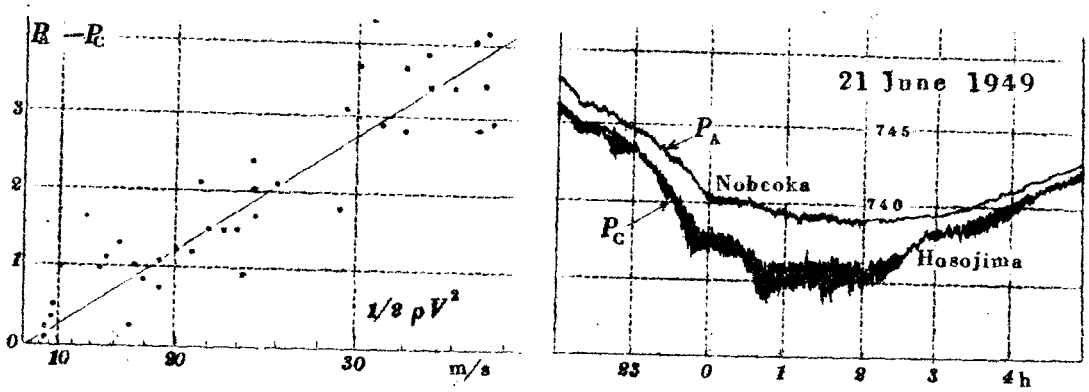

Fig. 38. Showing the coefficient $(\alpha + \beta)$ obtained by the pressure traces from Nobeoka and Hosojima.

EXAMPLE (II) Muroto-misaki(top) and Tsuro (Typhoon Jane of 1950)

Using the data in Fig. 39, the constant $(\alpha + \beta)$ for Murotomisaki Station was computed; it is about 0.5.

In the case where there are no surface stations, the pressure of which could be compared with that of the hill or mountain station, we correlate the long period pressure oscillations to the wind oscillations plotted in $\frac{1}{2}\rho V^2$ scale.

EXAMPLE (III) Mt. Fuji Weather Station (Typhoon Della of 1949)

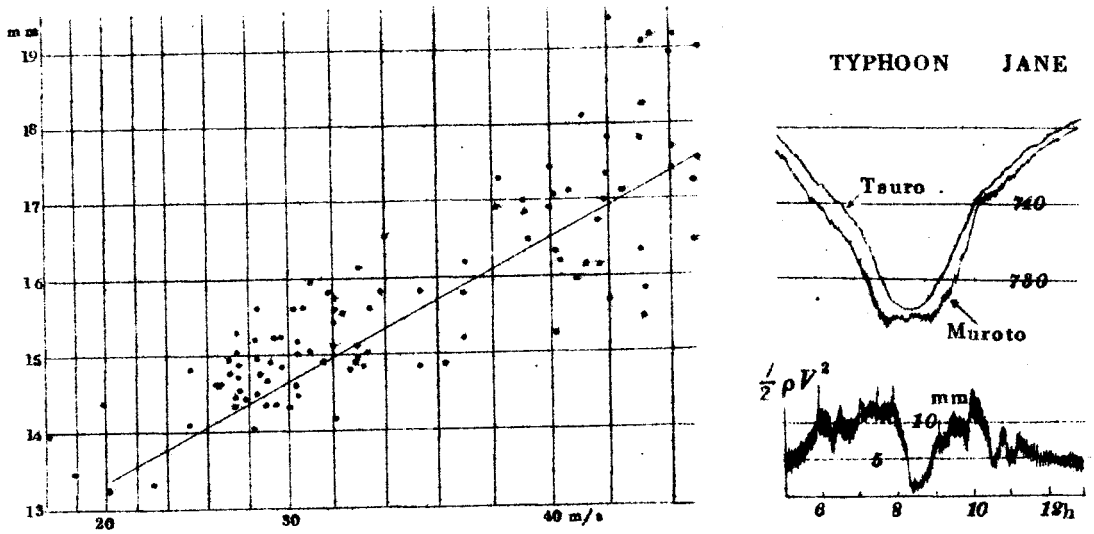

Fig. 39. Computation of $(\alpha+\beta)$ for Muroto-misaki Station.

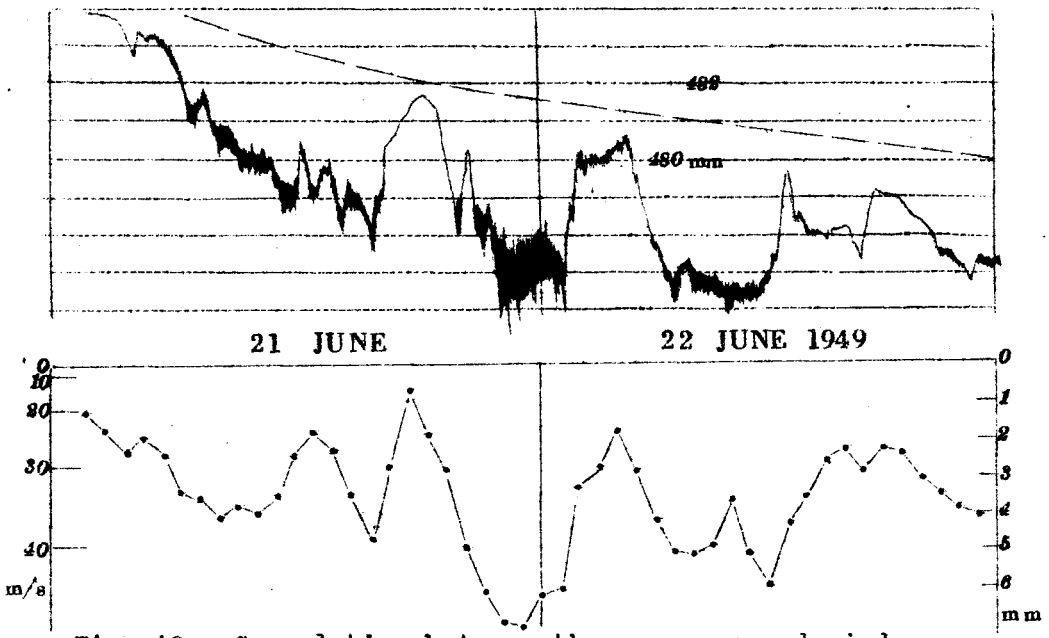

Fig. 40. Correlation between the pressure and wind drawn in $\frac{1}{2}\rho V^2$ scale. Mt. Fuji Weather Station.

As shown in Fig. 40, appreciable pressure drops associated with the high wind were observed at the top of Mt. Fuji Weather Station. Assuming the pressure indicated by the broken line in the figure, we obtain the value of

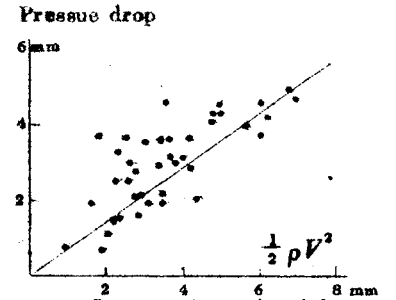

Fig. 41. Determination of $(\alpha+\beta)$ for Mt. Fuji Stat.

$(\alpha+\beta)$ for Mt. Fuji. The result, 0.7 is not so large comparing with the value in the two examples presented before. Therefore, it can be concluded that $(\alpha+\beta)$ for lighthouses and mountain stations are roughly 0.5 - 0.7.

Now it is possible to carry out the new correlation by which the weight of the air column, which may be called the " weight pressure", is obtainable. The pressure differences, which must be added to the observed pressure in order to obtain the weight of the air column are tabulated as the function of the constant $(\alpha+\beta)$ and wind speed.

Remarks	$(\alpha+\beta)$	10	15	20	25	30	35	40	45	50 m/s
Station in town	0.1	0.0	0.1	0.2	0.3	0.4	0.6	0.8	1.0	1.2
	0.2	0.1	0.2	0.4	0.6	0.9	1.2	1.5	2.0	2.4
Station on hill	0.3	0.1	0.3	0.6	0.9	1.3	1.8	2.3	2.9	3.6
	0.4	0.2	0.4	0.8	1.2	1.7	2.4	3.1	3.9	4.9
Lighthouse or mountain stat.	0.5	0.2	0.5	1.0	1.5	2.2	3.0	3.9	4.9	6.1
	0.6	0.3	0.7	1.2	1.8	2.6	3.5	4.6	5.9	7.3
	0.7	0.3	0.8	1.4	2.1	3.1	4.1	5.4	6.9	8.5

Table 3. Showing the correction of pressure due to high wind. The table is computed for 0°C, 760 mm. Hg.

The value of $(\alpha+\beta)$ for the station that needs the correction, is not always known, however, it will be assumed, according to the remarks in the table. We must not be nervous in the selection of the value of $(\alpha+\beta)$, because, even if the suitable value could be determined, there would remain unknown errors which can be known by the fact that the dots on the $P-\frac{1}{2}\rho V^2$ diagram are widely scattered. Thus we must recognize that there are numerous errors in pressure inside a storm area which are inevitable, and that there is no reason why we must draw the isobars within typhoons believing the 0.1 mb. of the reported pressures to which the correction discussed here was not made yet.

§ 10 Pressure Dips

The negative pressure anomaly supposed to occur in connection with the structure of typhoon is the pressure dip which has been pointed out by the writer. Pressure dip is a small travelling depression satisfying the following definition presented by the writer.

a. Pressure dip is a small trough-like depression,

b. which is not accompanied by cyclonic winds,

c. nor a sharp drop in temperature at the time of passage;

d. and the propagation of which must be recognized by referring to the pressure traces.

The mechanism of dip initiation was presented by Dr. Syono(23) early in 1940 in his study of the thunderstorms in the vicinity of Tokyo. The idea of the decrease in pressure due to a localized heavy rain had led him to the conclusion that the heavy rains in the intertropic frontal zone which could lower the pressure could play an important role to the initiation of tropical cyclones.

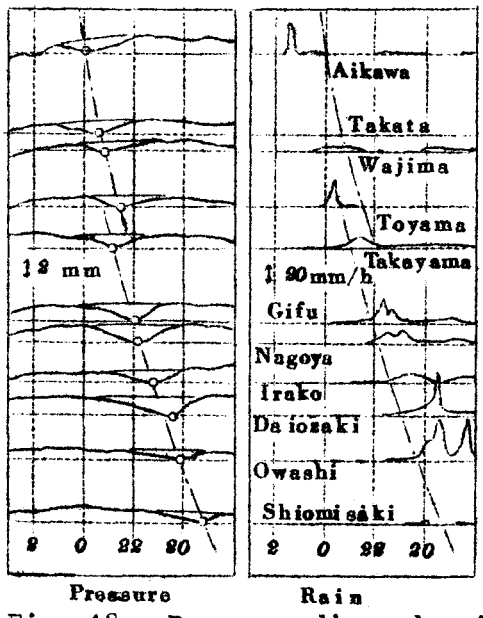

Fig. 42. Pressure dip and rain. (Typhoon Della of 21 June 1949)

As shown in Fig. 42, pronounced dip followed by a heavy rain is

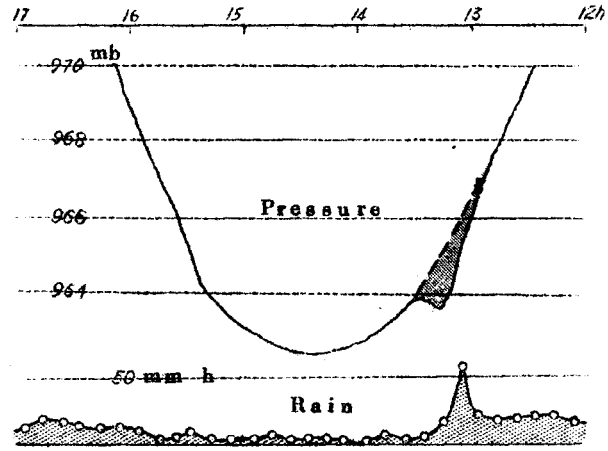

Fig. 43. Pressure dip and rain. (Typhoon Kezia of 13 Sept. 1950)

seen, which passed across central Japan from Shimonoseki to Aikawa. It was known that the weight of the precipitated rain was comparable to the weight decrease of air column, suggesting that the dip could be initiated by heavy rains. As has been analysed by K. Hashimoto (10), the pressure dip in the center of typhoon Kezia of 13 Sept. 1950 was accompanied by heavy rain shown in Fig. 43.

Thus, in many cases, dips are followed by heavy rains which would have initiated them. Sometimes, we come across the dip free from the rain. The largest dip within Typhoon Della shown in Fig. 44 was not followed by appreciable rain. At Iki station, the pressure drop by the dip was 6.7 mb., which might be the deepest one ever known. The initiation of this dip is not evident, but the writer presented the idea that a kind of dip can be initiated by the large mass of air inside the typhoon which gets out when the pressure gradient decreases according to the rapidly filling typhoon area. Of course, it is possible to

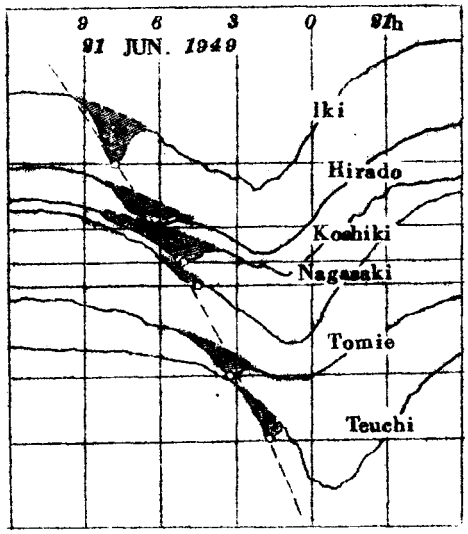

Fig. 44. Pressure traces showing the passage of Dip Z.

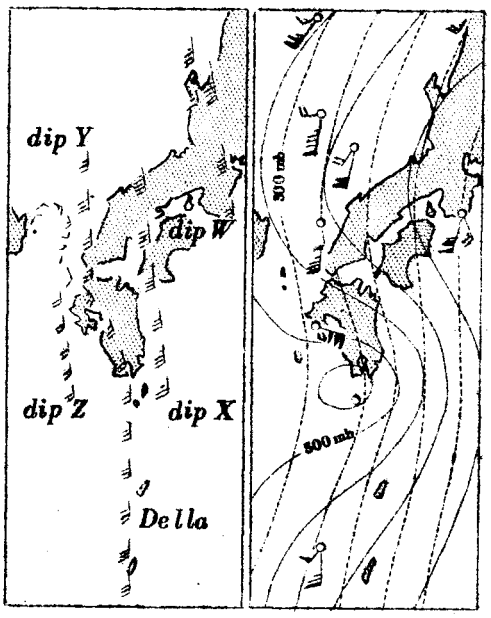

Fig. 45. Movement of the dips within Typhoon Della of 20 June 1949. In the right figure, the winds at the 500 mb. and 300 mb. levels are shown.

suppose that the rain which had produced the dip had already disappeared. The movement of dips is shown in Fig. 45. It will be seen that the speed of dip movement is larger in the right side of the typhoon center. The most mysterious fact of the movement is that dips move along the steering current of the typhoon affected not by the surface topography, and that they do not stray as the center of the main storm does.

Comparing the speed of the dips with that of the current at the 500 mb. and 300 mb. levels, it is evident that the current of 300 mb. level is about two times larger in speed while the speed on 500 mb. level is quite similar to that of the dip.

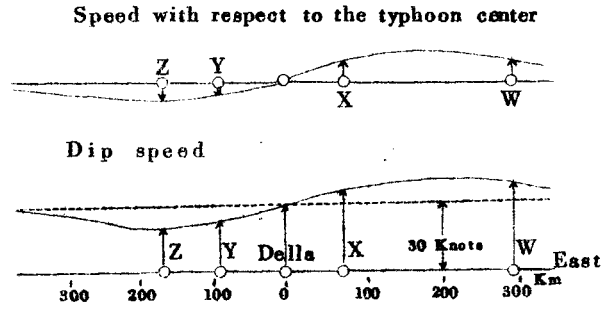

Fig. 46. Showing the steering speed of dips, X, Y, Z and W. The speed distribution shows us that dips move at the steering velocity given by both typhoon circulation and general circulation.

The relative velocities of the dips to the typhoon center and to the ground are shown in Fig. 46. It is evident that the dips under discussion had moved together with the general current of 30 knots, upon which the circulating wind around the typhoon is superposed.

These results show that a dip near the center must move with the similar speed to that of the typhoon center. This fact seems to be true, since we know examples of dip which moved together with the main depression forming two pressure minima in the bottom. The two minima in Typhoon Kezia are the good example.

As has been introduced, the pressure dips tell us great deal

about the unknown feature and the structure of typhoons, therefore, it is desirable to analyse the pressure field within typhoons using as many pressure traces as possible.

L I T E R A T U R E S

(1) Aoki Z. Theory of Main and Secondary Typhoons.
Report on Akune and Makurazaki Typhoons. C.M.O. of Japan 1949

(2) Aoki Z. Two Examples of Typhoons consisting of Main and Secondary Typhoons. Applied Physics of Japan Vol. 5 No. 9 1936

(3) Aoki Z. Theory of Main And Secondary Typhoons.
Applied Physics of Japan Vol. 10 No. 2 and 3 1941

(4) Byers H. R. The Thunderstorm.
U.S. Government Printing Office, Washington D.C. 1949

(5) Deppermann C. E. Notes on the Origin and Structure of Philippine Typhoons. Bull. Amer. Met. Soc. 28 1947

(6) Fuchi H. Influence of Topography upon the Speed and Direction of Winds. Bull. of C.M.O. of Japan 1933

(7) Fujita T. Micro-analysis of Typhoon Della.
Lectured at the Met. Research Meeting in Tokyo Oct. 1949

(8) Fujita T. Micro-analytical Study of Cold-front.
Geophysical Magazine of Japan Vol. 22 No. 3 1950

(9) Fujita T. Study on Pressure Dips within Typhoon Della.
Bull. of the Kyushu Institute of Technology. Vol. 2 1952

(10) Hashimoto K. On the Internal Regions of Typhoon in South Kyushu.
Report on Typhoon Kezia of Sept. 1949

(11) Horiguchi Y. Feature of Muroto Typhoon when she passed over Kinki District. Report on Muroto Typhoon of Sept. 1934 C.M.O. of Japan Mar. 1935

(12) Inoue E. On the Pressure Fluctuations in a Turbulent Fluid.
Geophysical Notes, Tokyo Univ. Vol. 3 No. 33 1950

(13) Kanaya K. On the Hydrodynamical Effect near the Center of Typhoon Jane. Report on Typhoon Jane of 1950. C.M.O. of Jap. 1951

(14) Kasahara A. On the Distribution of the Amount of Rain-fall and Filling-up of the "Kitty Typhoon". Geophysical Notes, Tokyo University Vol. 3 No. 30 1950

(15) Kasahara A. On the Filling-up of a Typhoon. Geophysical Notes Tokyo University. Vol. 2 No. 13 1949

(16) Masuda Y. and Takeuchi T. An Aerological Investigation of the Structure of Typhoon (Jane and Kezia) Papers in Meteorology and Geophysics. Vol. 2 Nos. 3-4 Dec. 1951

(17) Miyamoto M. Warm Front inside Typhoon Della. Report of Kobe Marine Observatory Mar. 1950

(18) Namekawa T. A View of the Structure of Muroto Typhoon Report of the University of Kyoto. 1936

(19) Otani K. On the Pressure Oscillations caused by Gusty Winds. Proceedings of the Western-Japan Meteorological Meeting. 1950

(20) Pierce C.H. The Meteorological History of the New England Hurricane of Sept. 21, 1938. Monthly Weather Review July 1939

(21) Syōno S. Relation between the Absolute Vorticity and the Absolute Angular Momentum and its Application. Geophysical Notes, Tokyo University Vol 2 No. 7 1949.

(22) Syōno S., Ogura Y., Gambo K., and Kasahara A. On the Negative Vorticity in a Typhoon. Journal of Meteor. Soc. Jap. Dec.1951

(23) Syōno S. Structure of Thunderstorms occurring in the Vicinity of Tokyo. Bull. of the C. M. O. of Jap. Vol. 17 Sept. 1940

(24) Syōno S. On the Tendency Equations. Lectured at the Laboratory. The pressure drop caused by heavy rains had been emphasized. 1946

(25) Syōno S. On the theory of the Formation of Tropical Storms. Completed in 1951 (Not yet published) In this paper, the effect of heavy rains is considered as a cause of the initiation of typhoons in earlier stages.

(26) Takahashi K. On the Distribution of Wind Speed within Typhoons. Memoirs of the C.M.O. of Jap. Vol. 35. Mar. 1951.

(27) Tepper M. A Proposed Mechanism of Squall-line; Pressure Jump Line. Journal of Meteorology Vol. 7 No. 1. 1950

(28) Watanabe T. Dynamical Study on Typhoon Eyes. Memoirs of the C.M.O. of Jap. Vol. 35. Mar. 1951.

(29) Watanabe T. Mechanism of Convergence inside Typhoon. Memoirs of the C.M.O. of Japan. Vol. 35. Mar. 1951.

CHAPTER II

TEMPERATURE DISTRIBUTION WITHIN TYPHOON

CONTENTS

CHAPTER II TEMPERATURE DISTRIBUTION WITHIN TYPHOON

§ 1 Height of Constant Pressure Levels

(I) Height of 1000 mb. level

Let P be the surface pressure within a typhoon, it is written, thus: $P = P_\infty - \Psi \Delta P$

where, P_∞ is the undisturbed pressure, Ψ the cyclone function, and ΔP the pressure depth. This formula can be changed into the one showing the height of the 1000 mb. level.

The air-temperature within a typhoon may be different from place to place. As shown in Table 4, the height of 1000 mb. level, corresponding to the given surface pressure, is not influenced too much by the temperature.

T°C / $P_{mb.}$	20	21	22	23	24	25	26	27	28	29	30	31
1020	+56	+ 56	+ 56	+ 56	+ 57	+ 57	+ 57	+ 57	+ 57	+ 57	+ 57	+ 58
1000	0	0	0	0	0	0	0	0	0	0	0	0
980	- 57	- 57	- 57	- 57	- 58	- 58	- 58	- 58	- 58	- 58	- 58	- 59
960	-116	-116	-116	-117	-117	-118	-118	-119	-119	-119	-120	-120
940	-174	-174	-175	-176	-176	-177	-177	-178	-178	-179	-180	-180
920	-236	-236	-237	-238	-238	-239	-240	-241	-241	-242	-243	-243
900	-297	-298	-299	-300	-301	-302	-303	-304	-305	-306	-307	-308

Table 4. Height of 1000 mb. level in 10 feet unit. The change in height due to the difference in temperature is so small that it could be neglected.

According to the observation by drop-sonde, the temperature in the eye at 1000 mb. level can be extrapolated to about 30°C. Therefore, it seems to be reasonable, in order to compute the height of 1000 mb. level, to assume that the air-temperature between sea and 1000 mb. level is 30°C. Because the maximum error for the height would occur only in the central area; while in the outer area, with the pressure nearly equal to 1000 mb., the temperature difference of

about 10°C is out of the question.

Now, we try to change the pressure formula into the height formula. Let ρ be the density of the air, g the gravity, R the gas constant, and T the air temperature, we have,

$$dH = -\frac{RT}{g}\frac{dP}{P} \qquad (26)$$

whence, $dP = -\rho g\, dH$, $P = \rho R T$.

Integrating both sides, we obtain

$$H^{1000} = \frac{RT}{g} \log \frac{P}{1000} \qquad (27a)$$

where, H^{1000} is the height of 1000 mb. level.

Substituting $P_\infty - \Psi\Delta P$, into P, we have

$$H^{1000} = \frac{RT}{g} \log \frac{P_\infty - \Psi\Delta P}{1000} \qquad (27b)$$

The right side can be expanded into the series,

$$H^{1000} = \frac{RT}{g} \log (1+y) = \frac{RT}{g}\left(y - \frac{y^2}{2} + \frac{y^3}{3} - \cdots\right)$$

In many cases, the value of y is less than 4/50, therefore, the square and the cube term in the parentheses are negligible. And the formula can be reduced to

$$H^{1000} = \frac{RT}{g}\frac{P_\infty - 1000}{1000} - \frac{RT}{g}\frac{\Psi\Delta P}{1000} \qquad (27c)$$

$$= H_\infty^{1000} - \Psi\,\Delta H^{1000} \qquad (27d)$$

where, H_∞^{1000} and ΔH^{1000} are the undisturbed height and the height depth of 1000 mb. level. Using the values: $R = 2.87 \times 10^6$ erg/g·deg, $g = 980$ dyne/g, and $T = 303$°K, we have

$$H_\infty^{1000} = 8.87\left(\frac{P_\infty}{1000} - 1\right) \times 10_m^3 = 2.91\left(\frac{P_\infty}{1000} - 1\right) \times 10^4\, ft \qquad (27e)$$

$$\Delta H^{1000} = 8.87\,\frac{\Delta P}{1000} \times 10^3\, m = 2.91\,\frac{\Delta P}{1000} \times 10^4\, ft \qquad (27f)$$

Thus the pressure formula can be changed into the height formula on 1000 mb. level.

(II) Height of Constant Pressure Level

Let us consider the typhoon on the P mb. pressure level, travelling along the straight line DD' at the speed of V km/hr.

The height at p, r km from the center is not only the function of r but also of the angle p O D in Fig. 47. It is represented by the formula,

$$H^p = H_\infty^p + \Psi^p \Delta H^p - G_r^p \sin\theta \qquad (28)$$

where, H_∞^p is the undisturbed height along the straight line DD' and G^p the height gradient of the general current. It is clear that the height H^p varies as much as $2G_r^p$ along the circle, but the mean height defined by the formula,

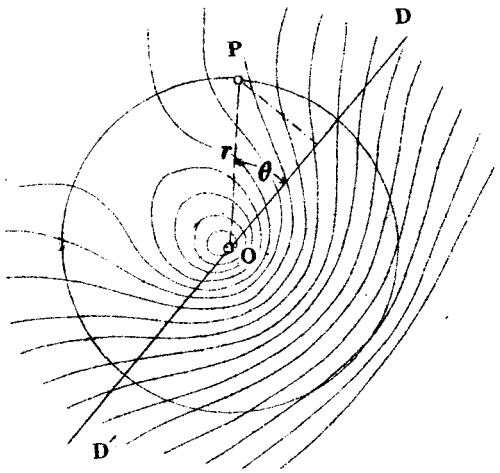

Fig. 47. Contours for a cyclone in a general current.

$$\overline{H_r} = \frac{1}{2\pi}\int_0^{2\pi} Hr \; d\theta \qquad (29a)$$

is given by the function of r, that is:

$$\overline{H_r}^p = \frac{1}{2\pi}\int_0^{2\pi} \left(H_\infty^p - \Psi^p \Delta H^p - G_r^p \sin\theta \right) d\theta$$

$$= H_\infty^p - \Psi^p \Delta H^p \qquad (29b)$$

It must be noticed here that the center from which the distance is to be measured is not the isobaric center but the tornado center that is not always seen on the chart.

Next we consider the distribution of mean temperature between two levels with the pressure P_1 and P_2 ($P_1 > P_2$). The height difference is given by subtracting

$$H^{P_1} = H_\infty^{P_1} - \Psi^{P_1} \Delta H^{P_1} - G^{P_1} r \sin\theta$$

from $$H^{P_2} = H_\infty^{P_2} - \Psi^{P_2} \Delta H^{P_2} - G^{P_2} r \sin\theta$$

we have, $$H^{P_2} - H^{P_1} = \left(H_\infty - \Psi \Delta H \right)_{P_1}^{P_2} - \left(G \right)_{P_1}^{P_2} r \sin\theta \qquad (30a)$$

The height can be replaced by the mean temperature on Emagram, using the relation,

$$\frac{R}{g} T \log \frac{P_1}{P_2} = H^{P_2} - H^{P_1}$$

If the shape of the typhoon is equal on two levels, the equation(30a) is reduced to

$$T = \left(H_\infty - rG\sin\theta\right)^{P_1}_{P_2}\frac{g}{R} \Big/ \log\frac{P_1}{P_2} \qquad (30b)$$

The formula shows that, if $G^{P_2} > G^{P_1}$, the temperature between the levels decreases toward the left (facing to the direction of movement) proportional to the distance from the path of the tornado center. And the value given by (30b) is the temperature not for the typhoon but for the steering current.

The temperature field for typhoon can be given by equating the values, $\left(H_\infty - \Psi\Delta H\right)^{P_2}_{P_1}$ and $\frac{R}{g}T\log\frac{P_1}{P_2}$, we have,

$$T = \frac{g}{R}\left[H_\infty - \Psi\,\Delta H\right]^{P_2}_{P_1} \Big/ \log\frac{P_1}{P_2} \qquad (30c)$$

When Typhoon Kezia of Sept. 1950 was on the southern ocean of Japan, the heights for 1000 and 700 mb. levels were shown by the constants: $H_\infty = 10230$ ft, $\Delta H = 1640$ ft, $a = 0.52$, $r_0 = 67$ km.....700 mb.

$H_\infty = 380$ ft, $\Delta H = 1790$ ft, $a = 0.20$, $r_0 = 67$ km....1000 mb.

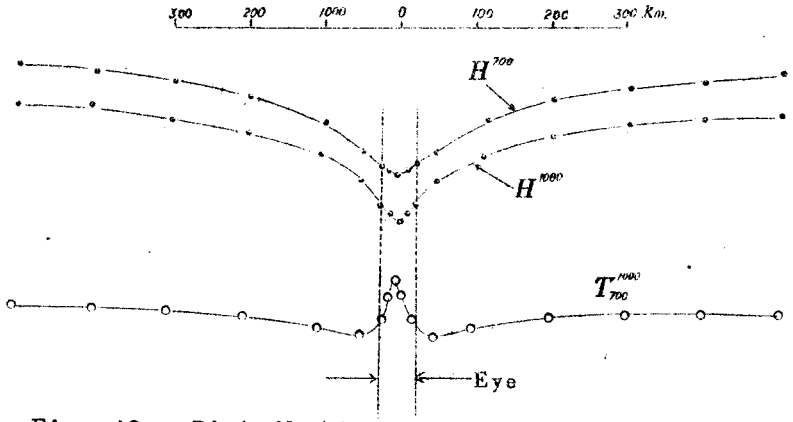

Fig. 48. Distribution of mean temperature computed by the heights of the 1000 and 700 mb. levels.

The height and the temperature computed by the cyclone function are shown in Fig. 48. The utmost interest seen in the figure is the high temperature in the eye which is surrounded by the low temperature area where the ring-shaped heavy rain would exist.

2 Radial Distribution of Temperature.

If the pressure inside a typhoon is in the condition of static equilibrium, using the relations

$$dP = -\rho g\, dH \qquad \rho = \frac{P}{RT}$$

we obtain the temperature, thus:

$$T = -\frac{g}{R} P \frac{\partial H}{\partial P} = -\frac{g}{R} \frac{\partial H}{\partial (\log P)}$$

Introducing the notation: $\overset{*}{H} = \dfrac{\partial H}{\partial (\log P)}$

we write, $$T = -\frac{g}{R} \overset{*}{H} \qquad \text{(31a)}$$

When the height of the constant pressure level is represented by the equation, $H = H_\infty - \Psi\, \Delta H$

we obtain, $$T = \frac{g}{R}\left(-H^*_\infty + \Psi \Delta^* H + \Delta H\, \Psi'_a\, \overset{*}{a} - \Delta H\, x \Psi'_x\, \log^* r_0\right) \qquad \text{(31b)}$$

which shows that the temperature consists of four terms.

(I) $-\dfrac{g}{R} H^*_\infty$

This term shows the temperature in the environment free from typhoon. Because when x is very large, the other terms in the parentheses are reduced to zero. Therefore, this term shows the temperature upon which the typhoon temperature is to be superposed. Thus we know, $$T_\infty = -\frac{g}{R} H^* \qquad \text{(31c)}$$

(II) $\dfrac{g}{R} \Psi\, \Delta^* H$

The temperature at the center obtained by substituting $x = 0$ in (31b) is

$$T = -\frac{g}{R} H^*_\infty + \frac{g}{R} \Delta^* H$$

$$= T_\infty + \frac{g}{R} \Delta^* H$$

Therefore, $$\frac{g}{R} \Delta^* H = T_0 - T_\infty = \Delta T \qquad \text{(31d)}$$

where, ΔT is the temperature difference between the center and the environment. Now, we write the present term as:

$$\Psi \frac{g}{R} \Delta^* H = \Psi\, \Delta T \qquad \text{(31e)}$$

And the temperature can be written thus:

$$T = T_\infty + \Psi \Delta T + \frac{g \Delta H}{R}\left(\Psi_a' a^* - x \Psi_x' log^* r_0\right) \qquad (31f)$$

In the case where the values of r_0 and a do not change along the vertical, the last two terms in the parentheses are reduced to zoro, viz., $T = T_\infty + \Psi \Delta T$ (31g) having somewhat similar distribution to that of the pressure or height. The distributions of temperature and height within such depressions are drawn in Fig. 49 & 50.

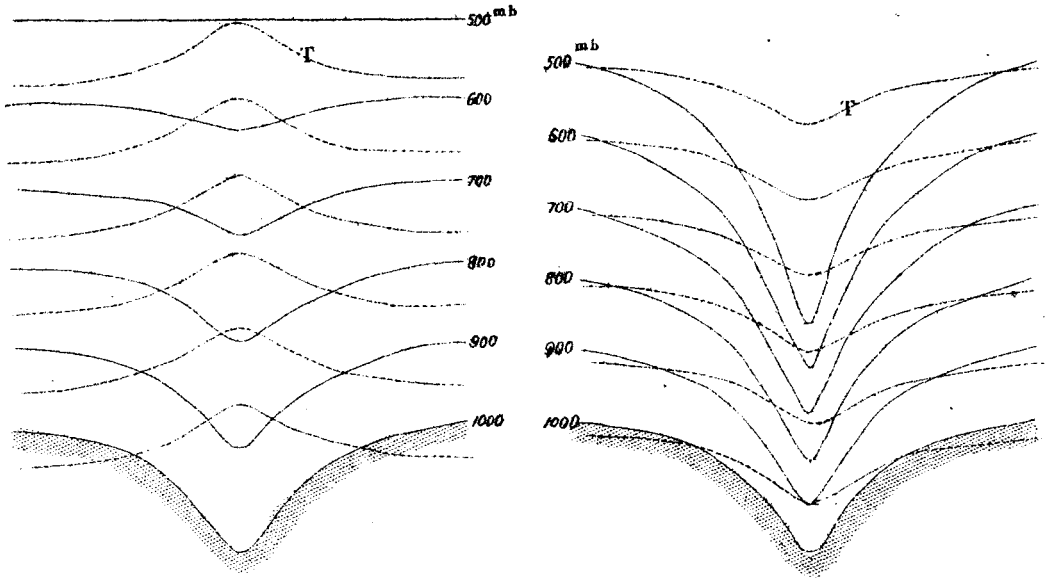

Fig. 49 & 50. Showing the distribution of height and temperature on constant pressure levels within the depression, the constants r_0 and a of which do not change along the vertical.

(III) In the practical case, r_0 and a change along the vertical direction, and "$log^* r_0$" plays a role to change the temperature in the annular area around the center. Because the value of $-x\Psi_x'$ is zero both at the center and the infinite distance. The temperature curve for this term is shown in Fig. 51. "a^*" plays the role similar to that of the previous term, and the curve of $-\Psi_a'$ is shown in Fig. 52.

Temperature distributions computed for various ΔT, a and r_0 are shown in Fig. 53, in which the resultant disturbances produced by the

vertical change of a and r_0 are represented by the stippled areas.

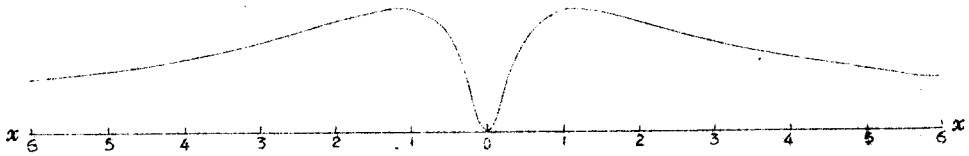

Fig. 51. The value of $-x\Psi_x'$ for $a=0.5$.

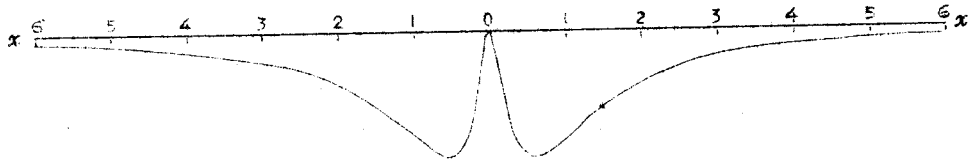

Fig. 52. The value of $-\Psi_a'$ for $a=0.5$.

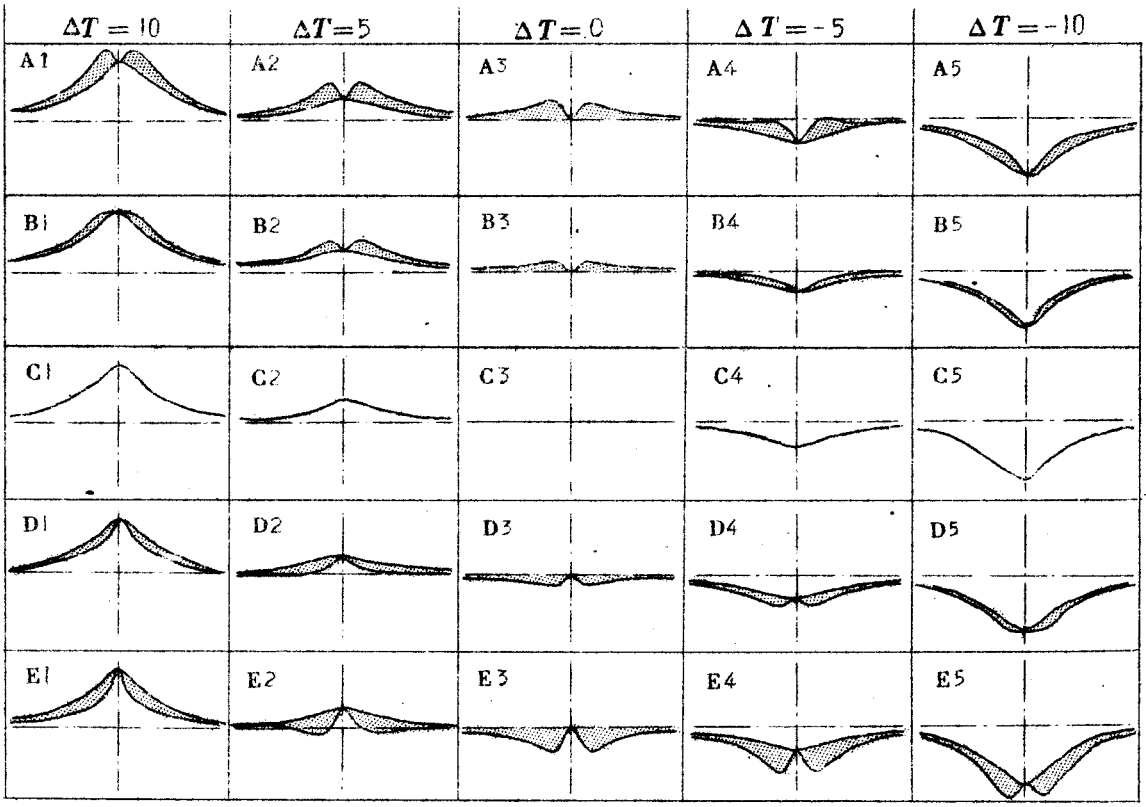

Fig. 53. Showing the possible temperature distribution within typhoon and cyclone, when they are represented by the formula(31b). The T_∞ is shown by the line passing through the center of each figure. The disturbance by $log^* r$ and $\overset{*}{a}$ is shown as the stippled areas.

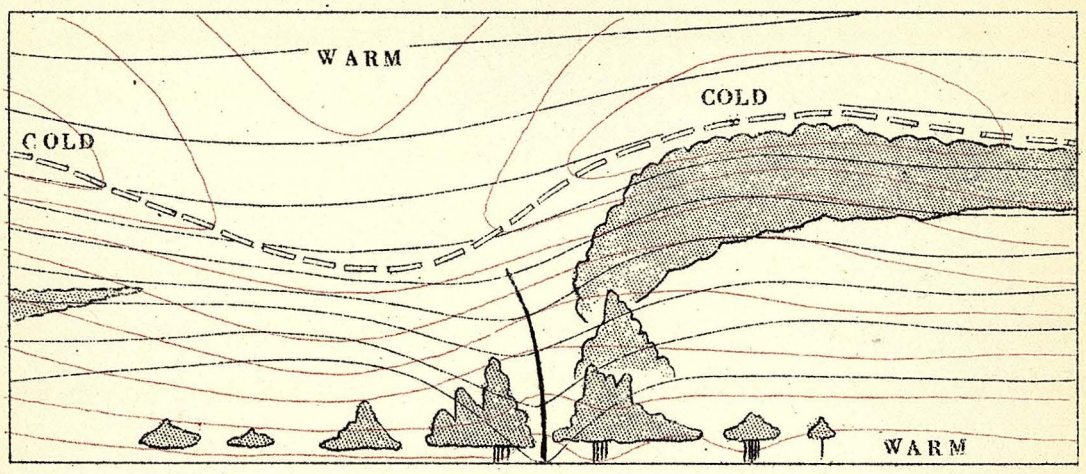

Fig. 54. Distribution of temperature and height in decaying stage.

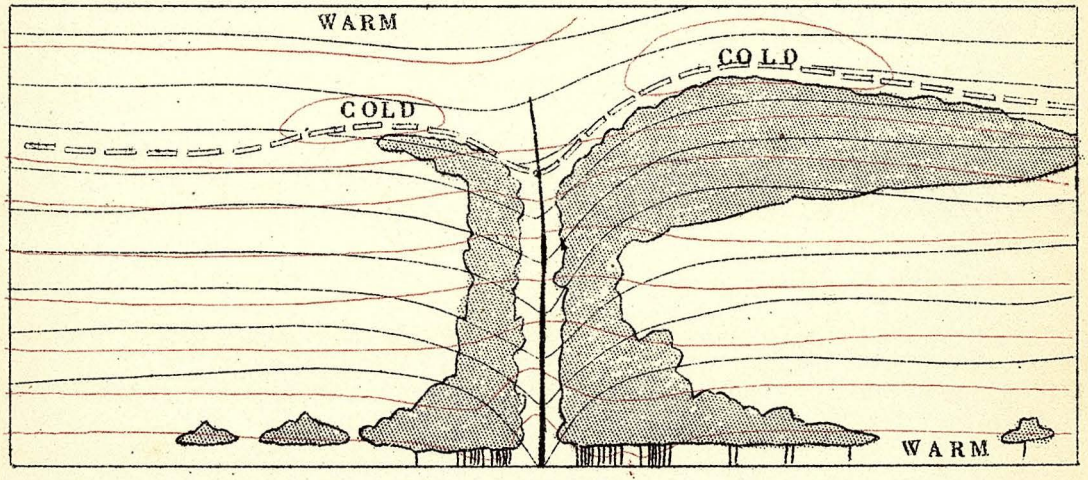

Fig. 55. Distribution of temperature and height in mature stage.

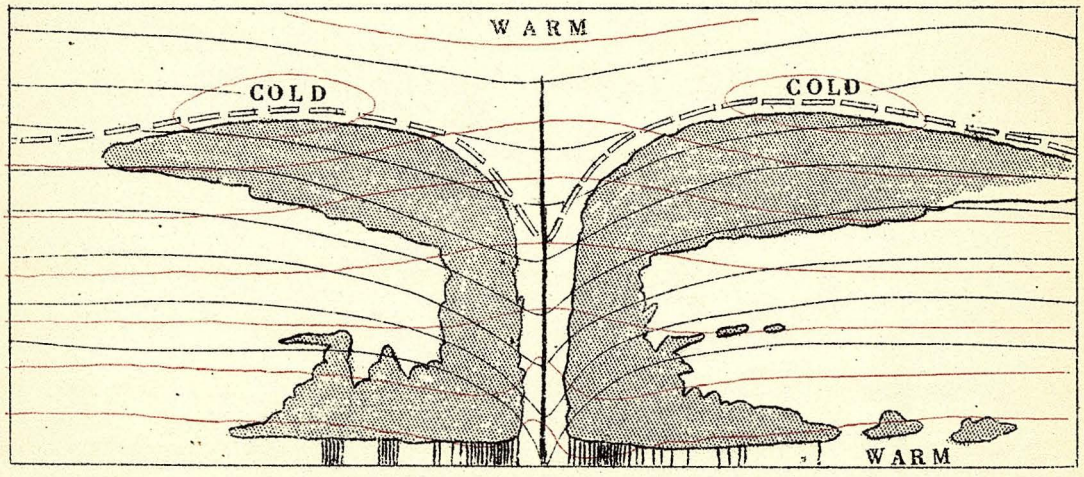

Fig. 56. Distribution of temp. and height in development stage.

According to the vertical section of model typhoons in Fig. 54, 55 and 56, which were drawn by the writer having basis on the observational facts, each of the temperature curves in Fig. 53 is to be found in them. In the figures, the cloud systems are represented by the hatched areas, height of constant pressure levels by black lines, and isotherms by red ones. In the lower level of typhoon, where the central temperature higher than those of the far environments is surrounded by colder areas caused by the ring-shaped heavy rains, the distribution is similar to that of the temperature curve E2. The curves C1 and C2 are seen in the middle levels with the pressure of 700-500 mb. In the mature stage, the upward currents around the center are very intense, and the temperature involved is sometimes much higher than that in the center,which is higher than the environments. This is the case that we call "cold-core cell", which is usually seen in the upper layers. In the middle or lower level, however, we see "warm-core cell" in which the depth of constant pressure levels becomes shallower along the vertical.

§ 3 Errors in the Reporting Upper-air Temperatures.

We are apt to consider that the temperatures observed by radio sonde are accurate so that they can be used in our study without correction; but this is not the case. Meteorologists who have had chances to analyse the practical upper air charts using abundant data, are wondering if the temperatures could be used without being corrected. Because such a case sometimes happens that we cannot draw height contours or isothermal lines after entering the materials received.

In their study "on an Aerological Investigation of the Structure of Typhoons", Y. Masuda and K. Takeuchi(4) have corrected the

temperatures and heights for constant pressure levels in order to eliminate diurnal variation in pressure and temperature. They used the anomalies defined as the difference of observed temperature and height from those of the monthly mean values for each time of observation. The errors coming from the difference between insolations at noon and midnight are eliminated in that way, however, there remain still appreciable errors which should be corrected in order to carry out the further studies.

(I) RANDOM ERROR

In the vicinity of Tokyo we have three sonde stations, Tokyo, Haneda, and Tateno; therefore, it is possible to compare the reporting temperatures. Fortunately, Mt. Fuji Weather Station in the vicinity reports the temperatures at about 640 mb. level, then the writer compared the reports with of those stations in Fig. 57. The temperatures at Fuji are plotted for every 3 hrs, while those from sonde stations for every 6, 12, or 24 hrs. It will be seen that the temperatures at Fuji contain much perturbations, some of which might be caused by the insolation in the daytime. The amplitude of oscillation, except the diurnal variation,

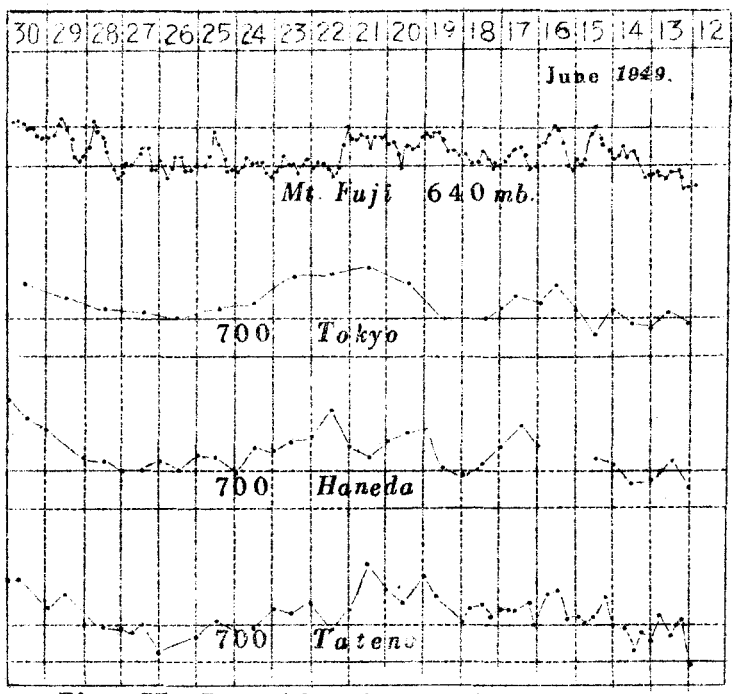

Fig. 57. Reporting temperature from Mt. Fuji and three zonde stations.

is 1 - 2 °C. According to the trace in Fig. 58 showing the detailed variation at Fuji Station for the middle period in Fig. 57, temperature at that level fluctuated at random with higher frequency than those of sonde observations. Another example of temperature measured by thermister attached to the airplane of the Thunderstorm Project (3), is represented in Fig. 59. This is the observation through the thundercloud in earlier dissipating stage. It will be seen that the plotted points are scattered about 2 degrees suggesting that the perturbations of that order are superposed. From these examples, it is natural to conclude that the temperature observed by radio sonde must contain the error of this range. The temperatures observed for every 12 hrs do not always result in the unique curve, since we get different temperature curves by shifting the time of observation. The temperatures at Fuji plotted for every 3 hrs are shown in Fig. 60, together with the curves based upon the two observations a day, namely, (0h 12h) (3h 15h), (6h 18h), and (9h 21h). The four curves, in the ideal case, must coincide, but as will be seen in the figure smaller disturbances

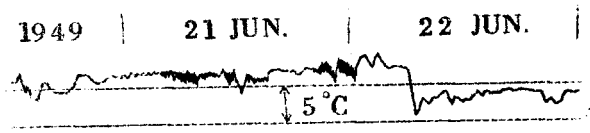

Fig. 58. Variation of temperature at Mt. Fuji Weather Station.

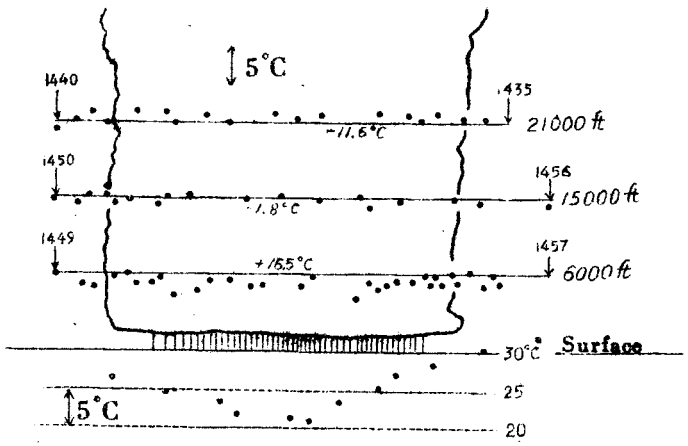

Fig. 59. Temperature of thundercloud measured by the airplane of Thunderstorm Project in U.S.A. 14 August 1947

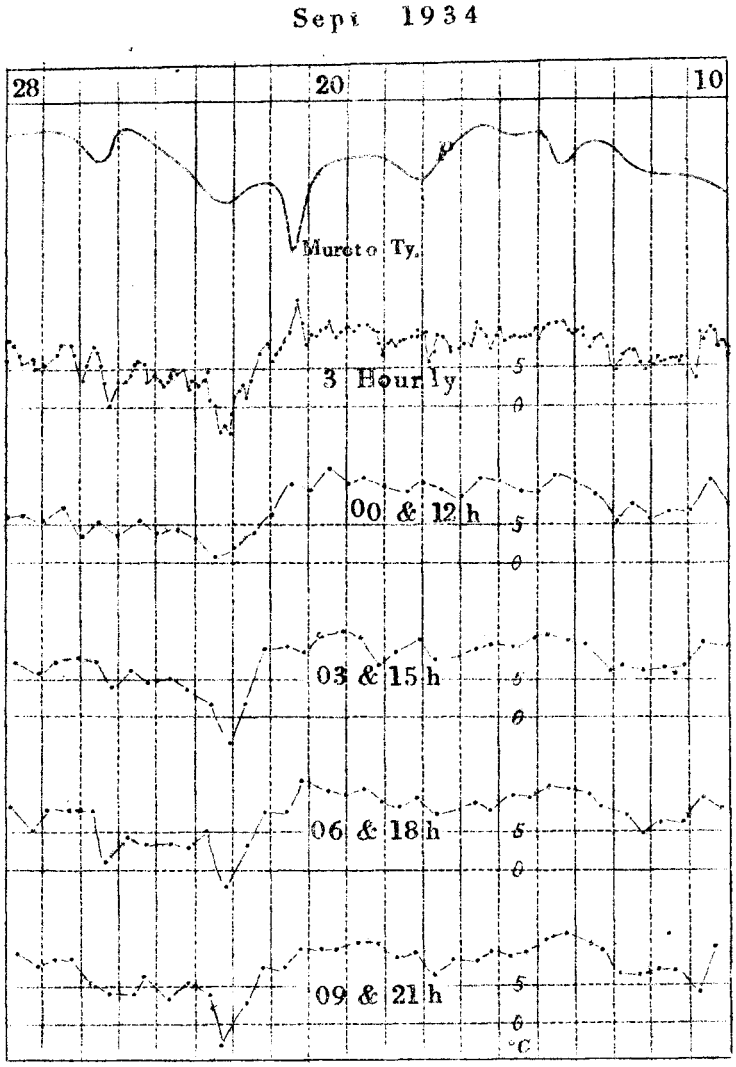

Fig. 60. The temperature at Mt. Fuji Station plotted for every 3 hrs, together with the curves based upon the two observations a day, viz., (0h 12h), (3h 15h), (6h 18h), (9h 21h).

do not give the similar feature, but the long period variations are quite similar. Thus, we must always expect to know the feature of the long period variations only, instead of the short ones.

At any time we should consider that the shape of one wave must be fixed by several observed points endorsing the shape of variation. That is to say, it would require more than 5 reliable observations in order to realize a variation of diurnal amplitude. The connection of the observed points, 1, 2, 3, 4 and etc. using a wavy line in Fig. 61 is not reasonable so long as the existence of the variation is not supported by other independent fact. The expected change in temperature is the line A in the figure. It is because the other observations, which were to be made between the times of present observations, would be located on both sides of the line A at random, as shown by the open circles. There would be no reason why the circles should be arranged just on the wavy line B in question.

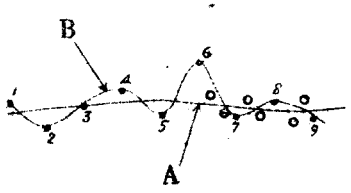

Fig. 61. Bad connection of observed points(B), and better one(A).

(II) EFFECT OF DIURNAL TEMPERATURE VARIATION

Previously, the writer pointed out the fact that there occurs a scattering of the observed temperatures, which are supposed to be measured accurately. The other cause of error due to the solar radiation in the daytime is very important.

Usualy, the temperature for 12h MST is higher than that for 0h. The high temperature at noon may be caused partly by the warming of the air column; but if it absorbs the 20 per cent of the insolation, 2 cal/cm^2·min, after 10 hours the total accumulated heat 200 cal.

would raise the temperature only about 0.8°C. Of course, this is the maximum rise occurring when the heat is all accumulated. In the practical case, on the other hand, the heat must be radiated always. Therefore, the temperature rise will be less than 0.5 degrees.

The difference of the monthly mean temperature at 12h from that at 0h for each Japanese sonde station is plotted in Fig.62. The plotted difference δT is the mean value, but if we examine the individual case, δT more than 2 times larger than the mean value would be seen. The change of δT along the vertical is shown by the thick line, and the possible mean maximum of δT is limited by the broken line. If we consider the case where δT is very large, it will reach about 2°C at 700 mb. level, 4°C at 300 mb., 6°C at 200 mb. and 10°C at 100 mb. An example of very high temperature

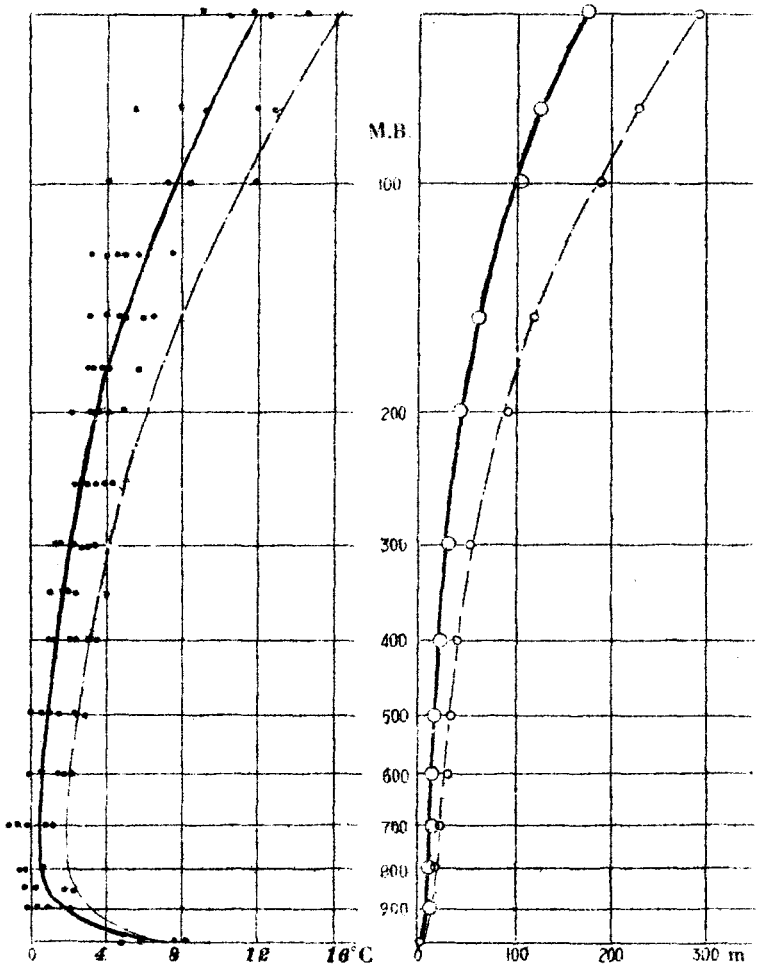

Fig. 62. Vertical distribution of the rise of temperature(left) and the upheaval of constant pressure level(right) due to the expansion of air by insolation.

observed on the weather ship Tare at noon is shown in Fig. 63.

The rise in the constant pressure levels caused by the high temperatures at noon is computed for both mean and maximum values of δT at the reporting sonde stations. As will be seen in Fig. 62, even in the mean conditions, the constant pressure levels rise about 200 - 300 meters in the upper troposphere. Any analyses carried out without consideration of this problem are then not trustworthy.

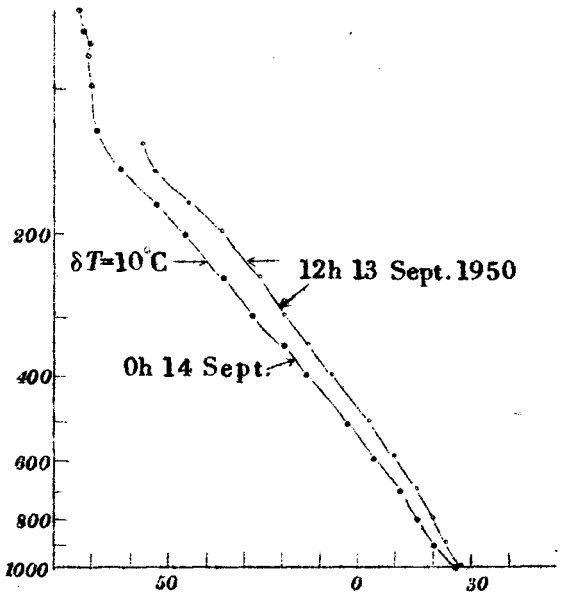

Fig. 63. Errors of δT observed on the weather ship Tare.

(III) INSTRUMENTAL ERROR

The error considered not to be caused by the above-mentioned

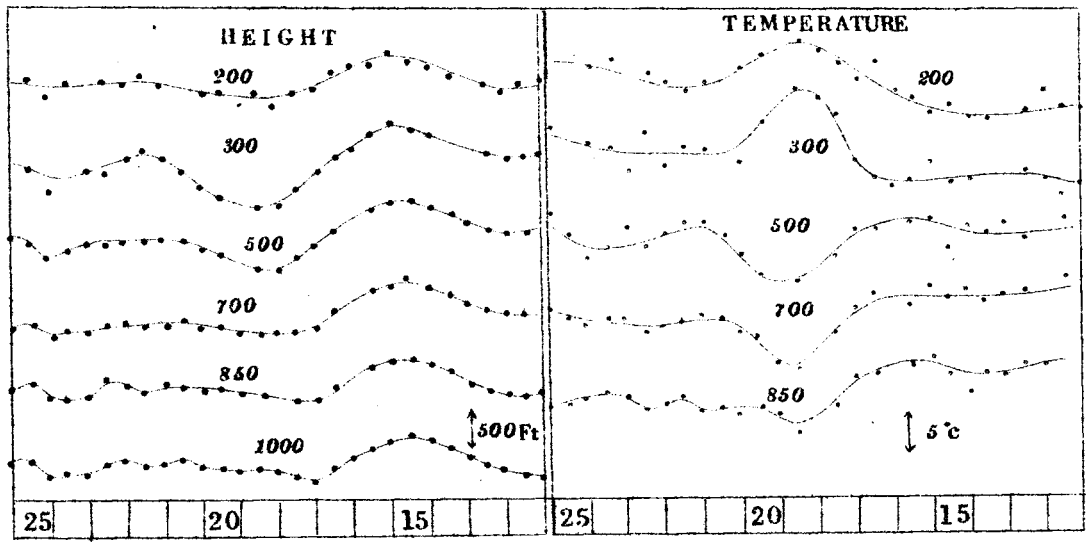

Fig. 64. Temperature and height at Barrow Point in Araska(June 1949)

causes is the instrumental error. This is also very important, but difficult to be taken off. According to the writer's experience, the temperatures from American stations are compensated for the radiation error very well. Examples of heights and temperatures from Barrow Point in Araska, which were read in the microfilm copies(6), are presented in Fig. 64. It will be seen that the errors are mostly of instrumental or accidental origin.

(IV) TECHNIQUE IN CORRECTING THE ERRORS

As has been studied by Masuda and Takeuchi(4), part of the errors from radiation can be corrected by subtracting the amount of δT from the daytime observations. It is rather good, however, the amount of δT we desire to take off ~~are~~ is different from day to day, so that the subtraction of average value from the noon temperature is not always reasonable. The temperatures are presented in Fig. 65. Comparing the temperatures before and after the correction, we know that there still remain the errors which should be eliminated.

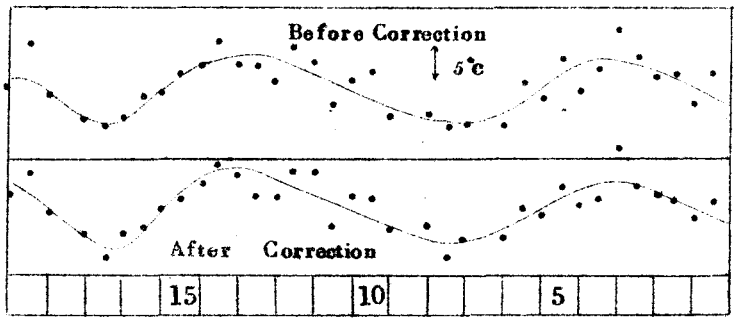

Fig. 65. 200mb temperature at Wajima (Oct. 1950)

The writer's correction is based upon the fact that a large amount of temperature must be subtracted from the noon temperature when it is too high, while if it is not, we need not subtract much. It is rather difficult to pursue such correction using the temperatures each of which contains individual error. As shown in Fig. 66,

however, to plot the middle points of successive temperatures (middle point correction) gives better result than subtracting the average temperature difference (mean value correction). The middle point correction can be done again to the corrected temperatures. This process may be called the 2nd correction, by which the smaller perturbations of unknown origin is reduced.

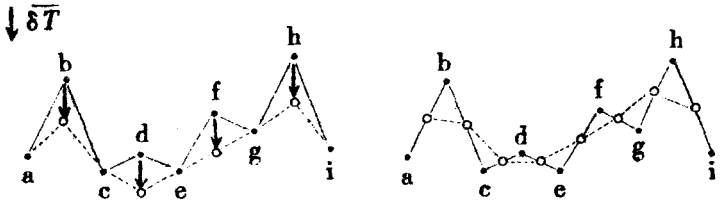

Fig. 66. Mean value correction(left) and middle point correction.

An example of the middle point correction for the same data as in Fig. 65 is presented in Fig. 67. After the 1st correction, the upper data scattered in wide range approach to the curve we desire to obtain. As shown in the lowest distribution, by correcting 3 times, the long period variations do not vanish, while the short ones, the existence of which ~~are~~ is not supported by the original data, decrease in amplitude. In the practical case, it will be better to use the result of 2nd or 3rd correction.

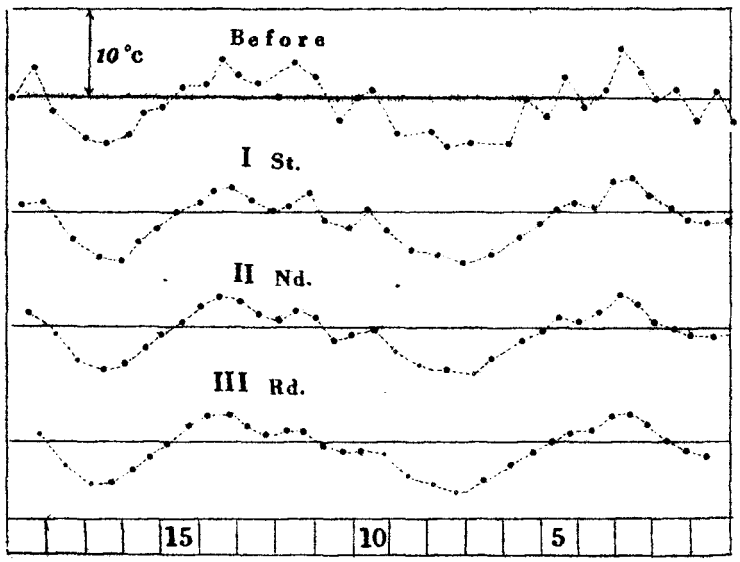

Fig. 67. Middle point correction for the temperature of 200mb level at Wajima(Oct. 1950)

The middle-point correction can be applied not only to the temperature but also to the other elements such as heights, pressures, wind

speeds and etc.

§ 4 ΔH-logP, ΔT-log$P$, and T-log$P$ Diagrams

According to the equation(31d), we know the relation,

$$\frac{g}{R}\overset{*}{\Delta H} = \Delta T$$

namely,

$$\frac{\partial \Delta H}{\partial (logP)} = \frac{R}{g}\Delta T$$

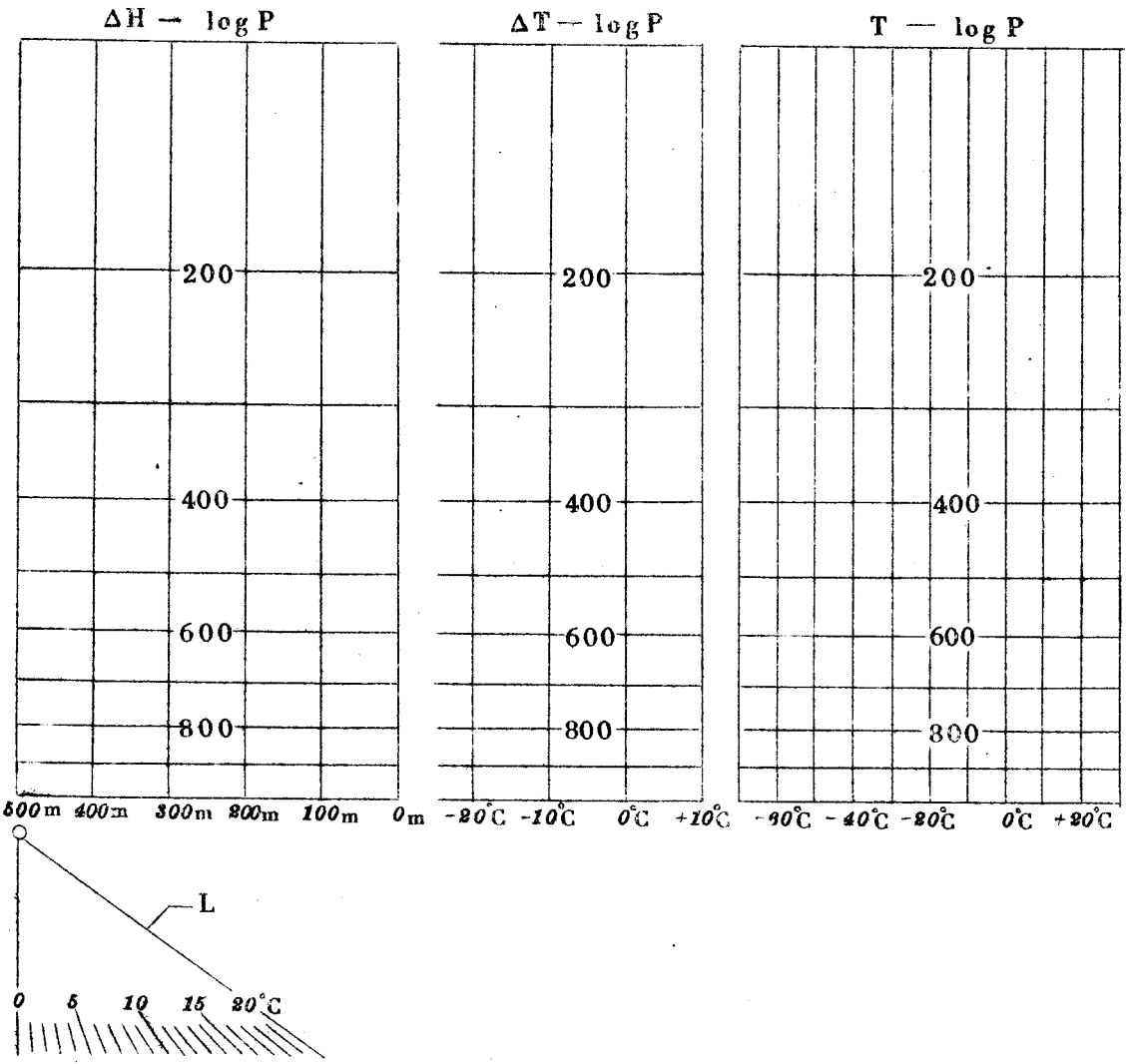

Fig. 68. Three diagrams for cyclone analysis.

which shows that the derivative obtained by differentiating ΔH with respect to the logarithm of pressure is proportional to ΔT, the temperature difference between center and environment. The relations among ΔH, ΔT, and T are well understood by plotting the values in question in the diagrams in Fig. 68, in which the right one is the Emagram. The temperature scale in the lower left is the rate at which the value of ΔH in ΔH-log P diagram increases or decreases in correspondence with the value of ΔT in ΔT-log P diagram. Say, if ΔT is -20 °C, ΔH would change along the line L.

Using the three diagrams in Fig. 68, the relations between the vertical distribution of temperature, ΔH, and ΔT can be studied as follows:

In Fig. 69, vertical distribution of the three elements for a cold cyclone aloft, having no cyclonic feature on the 1000 mb. level, is presented. This cyclone is very simple because the value of ΔH is zero both at the 1000 mb. and 0 mb. levels, viz.,

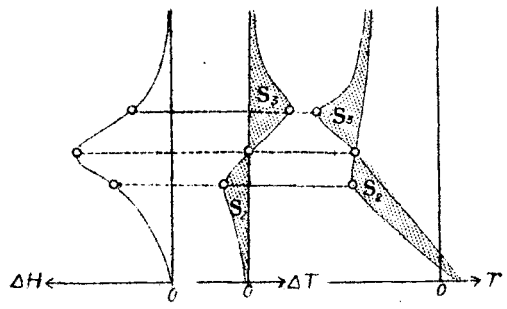

Fig. 69. Showing the change in ΔT, T, and ΔH for the cold cyclone with $\Delta H = 0$ at 1000 mb level.

$$\int_{\text{Surface}}^{\text{Infinity}} d(\Delta H) = 0 \qquad (32a)$$

therefore,

$$\frac{R}{g}\int_{1000\text{mb}}^{0\text{mb}} \Delta T \; d(\log P) = 0 \qquad (32b)$$

This fact is very important, since it shows that the algebraic sum of the areas S_2 and S_3 in the ΔT-log P diagram is zero, namely, there must exist the equal areas on both sides of the $\Delta T = 0$ line. As shown in the figure, the largest ΔH is seen on the level where the temper-

atures at the center and the environment are equal, and at the altitude for the max. or min. values in ΔT, the vertical change rate of ΔH becomes the largest.

In the practical case, however, the definite height depth exists even at the 1000 mb. level, and the integrated value is

$$\int_{1000\,\mathrm{mb}}^{0\,\mathrm{mb}} d(\Delta H) = -\Delta H^{1000}$$

It is desirable to make the algebraic sum of the areas in ΔT-log P diagram just zero. The writer considered the case where the air 20°C lower than the environment is placed below the 1000 mb. level. In such a case, ΔH would decrease along a straight line AE, the direction of which can be decided by the lower left scale in Fig. 68. Therefore, the imaginary area KFGJ would be put below. Thus, the relations,

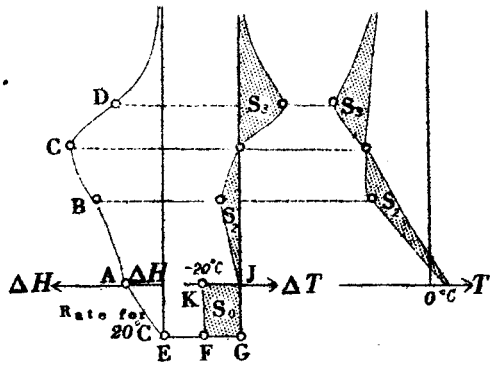

Fig. 70. Vertical distribution of ΔH, ΔT, and T for a cold cyclone with a definite ΔH at the 1000 mb. level.

$$\int_{\mathrm{EFG}}^{0\,\mathrm{mb}} d(\Delta H) = 0\,, \qquad \int_{\mathrm{EFG}}^{0\,\mathrm{mb}} \Delta T\, d(\log P) = 0$$

hold, changing the problem into that discussed before. Now, we have the relation,

$$S_0 + S_2 = S_3$$

The stages of tropical storms can be divided into four: viz.,

Formation, Development, Mature, and Decaying Stages.

The four diagrams for each stage will be discussed here. In the formation stage, the height depth on 1000 mb. level is not too deep yet, and the area S_0 is so small that it could be cancelled by the

positive area in Fig. 71. The height of the storm does not reach the tropopause. A small storm not only in this stage but also in the development stage has the similar temperature distribution.

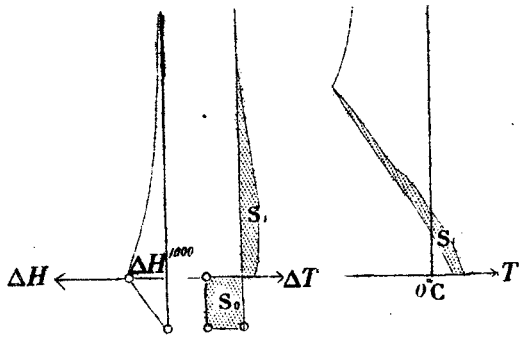

Fig. 71. The case where the area S_0 is compensated inside the troposphere. The vortex does not reach up into the stratosphere. (formation stage)

In the development stage, in which the storm develops rapidly into typhoons of various intensity, the depth of storm becomes deeper and deeper until the top reaches the tropopause, inducing dynamically a tropopause funnel. The area S_0 in Fig. 72, which could not be compensated by the area S_1, is cancelled by the positive area S_3 in the stratosphere. As will be seen in the figure, the funnel depth decreases rapidly inside the stratosphere. Such a warm stratosphere is not observed yet, but in the practical upper-air observations, it is very difficult to raise the Sonde Balloon, reliesed inside the eye, directly up into the funnel aloft, preventing its out-going movement caused by the airs in the eye which entrain successively into the surrounding up-drafts.

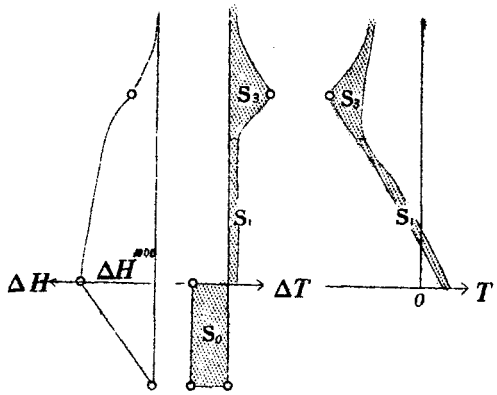

Fig. 72. When ΔH or S_0 is so large, it cannot be compensated inside the troposphere. (devel. st.)

When typhoons reach her mature stage, it is believed, according

to the observations made in U.S.A.(5), that the troposphere in the upper portion of the eye becomes colder than that of the environment. And the so-called warm-core cell in the lower portion lies under the cold-core cell aloft. If this is the case, the distribution can be

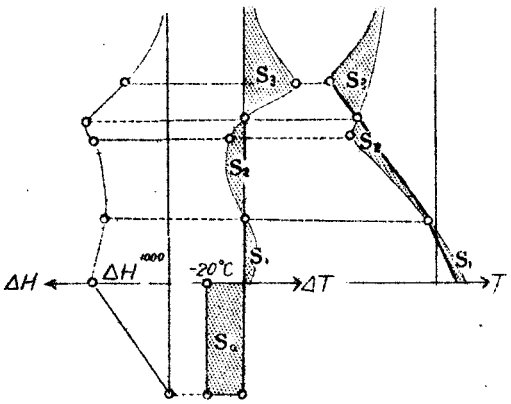

Fig. 73. Typhoon with cold-core cell aloft. (Mature stage)

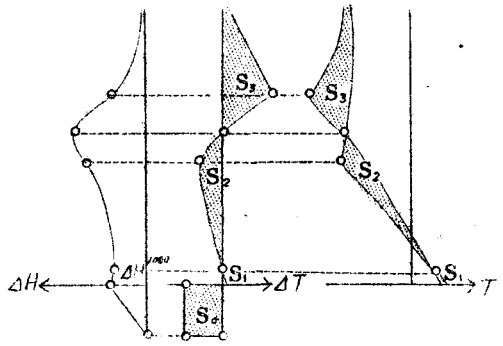

Fig. 74. Typhoon in decaying stage.

drawn as Fig. 73, in which the areas must be balanced, thus:

$$S_0 + S_2 = S_1 + S_3$$

This relation shows that a larger positive area in the stratosphere should exist in order to compensate the negative area in the cold-core cell.

In the decaying stage, most of the eye, except the lowest portion, becomes colder, and the area S_0 in Fig. 74 decreases. We see the largest amount of ΔH on the upper troposphere. In the later decaying stage, the typhoon re-develops into a cold cyclone, reducing the base area S_0 very small. And the appreciable circulation remains only on the upper layers.

The changes in ΔT and ΔH are summarized in Fig. 75. It must be noted here that the disturbances in both temperature and height depth in younger age propagate upward reaching the tropopause when the storm grows old. This fact is very interesting in the life history

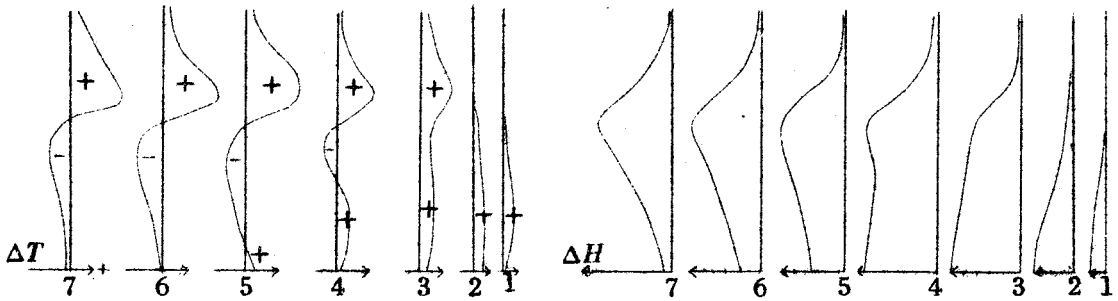

Fig. 75. Showing the change of ΔT and ΔH in the full cycle of typhoon.

of typhoons.

Theoretical distributions with much imagination are presented here in this section, but some day they will be observed in many typhoons.

§ 5 Distribution of Surface Temperatures

Surface temperatures observed at many stations are very helpful in analysing the temperature characteristics. The time section made

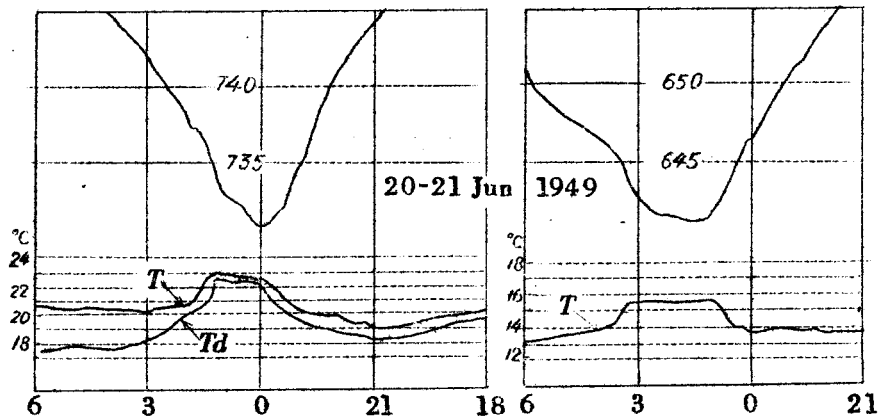

Fig. 76. Showing the traces from Hitoyoshi(left) and Mt. Aso.

by the traces is also useful, however, some conclusions from the sections such as those in Fig. 76, might result in mistakes. According to the figure, one might suppose that the typhoon center consists of warm air forming warm-core cell, however, this is not the case.

To clarify the true characteristic of the temperature distribution, we should make the isothermal chart for each moment of analyses.

In the practical analyses, however, we suffer much from the scarcity of the data. The writer used the method, by which the temperatures observed at each station about one hour before and after the map time are entered on the same chart. The large letters in Fig. 77 are the data at the ± 1 hr, which are followed with small letters at the ± 2 or 3 hrs. The small letters are not reliable because of the fact that typhoons deform even in 1 or 2 hrs. We must be careful in using the unreliable figures at any time, because they sometimes give bad influences upon judging the

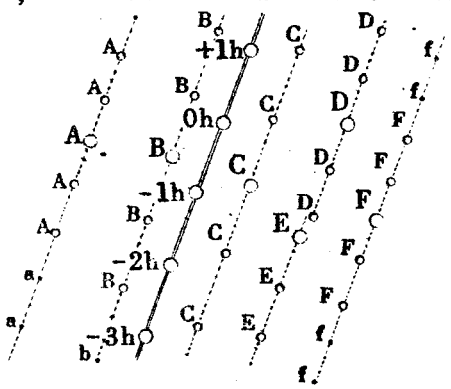

Fig. 77. Auxiliary stations.

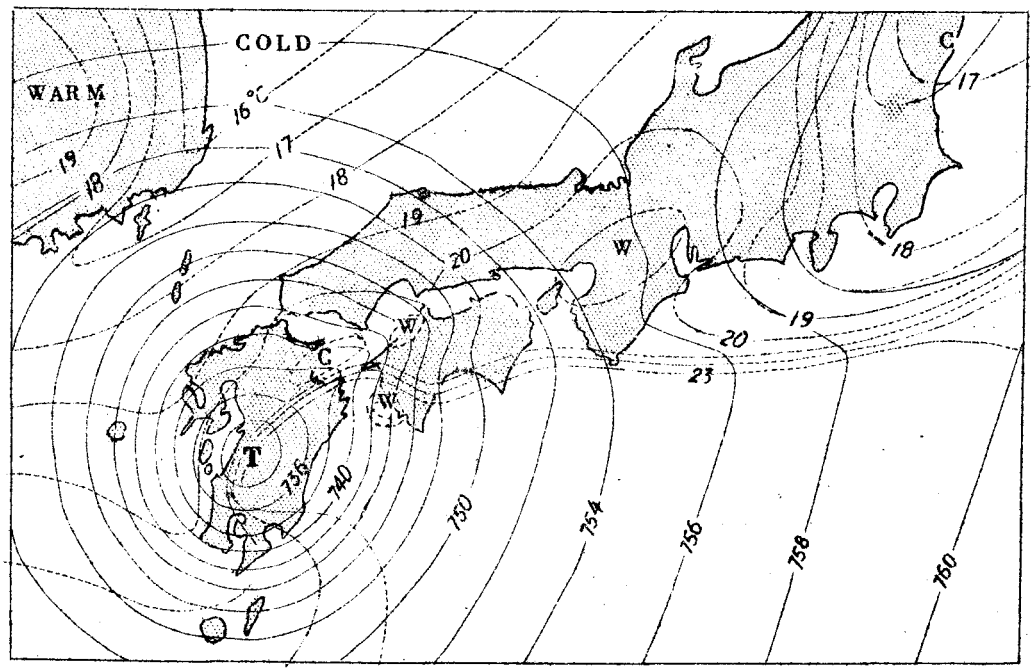

Fig. 78. The isotherms showing the frontal zone within Typhoon Delia 0100 June 21, 1949.

existence of smaller temperature disturbances. An example of surface temperature field is presented in Fig. 78. According to the chart it is evident that the high temperature observed at the time when Typhoon Della passed over Hitoyoshi and Aso was not the appearance of warm eye but it can be explained by the fact that the warm areas in the east had reached as far as central Kyushu. Warm areas in Kinki dis. and north of Shikoku were initiated by topographical föhns which were not related to the nature of typhoon.

DETERMINATION OF PHASE VELOCITY

The velocity at which the typhoon fields propagate is the phase velocity for each weather element. As will be supported by the fact that isotherms do not travel together with the pressure field, the phase velocities are different not only from time to time but also from place to place. We usually see that they draw charts, as shown

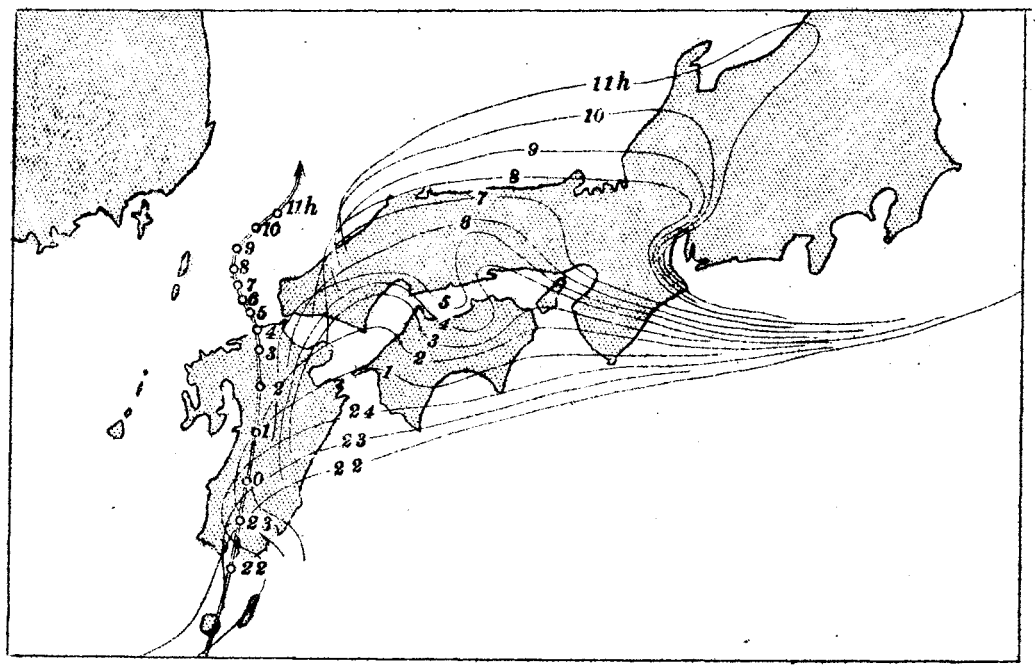

Fig. 79. Showing the movement of isotherms of 22°C accompanied by Typhoon Della of 20-21 June 1949.

in Fig. 77, arranging the auxiliary stations along the same vectors as that of the movement of the typhoon center, however, such method must be revised. As will be seen in Fig. 79 showing the hourly locations of the isotherms for 22 °C, the phase velocity is as much as of the center in the west, but in the east it is very small suggesting that the warm front there would be almost stationary. What will be happen if we arrange the temperature of auxiliary stations on the same interval as of the west ? Perhaps we can not use them. Thus the writer determined the phase velocities for the field in question before entering the temperatures.

Except the special case, the distribution charts for temperature drawn by mixing the data at the stations arranged at the relative locations to typhoon center, is not available. Of course, such charts would be useful if we want to know the average condition of the distribution.

ABSORPTION OF COLD AIR IN TYPHOON CENTER

As the typhoon in tropical area travels northwards it reaches the area of cold air masses. The schematical deformation of iso-

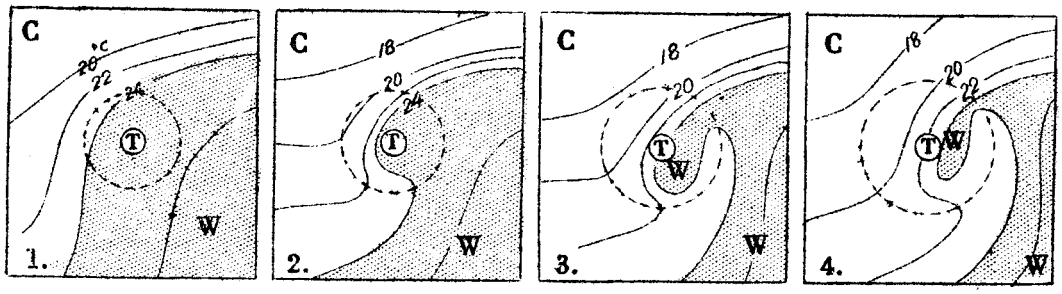

Fig. 80. Showing the isotherms within a typhoon absorbing a cold air in her center.

therms is shown in Fig. 80. It will be seen that typhoons are liable to carry warm tropic air in her center, and she usually pushes the isotherms towards the north or north-west. As soon as the front of

cold air reaches the highest wind area indicated by the dotted circle, the cold air begins to deform quickly advancing along the dotted circle. If the wind speed be 40 m/sec along the dotted circle with its radius 200 km, the isotherms that would be transported by such winds reach the warm front within 4 hrs. Practically, however, the cold air involved outbreaks into the warm sector, meanwhile it mixes with the warm air locating in its way. Thus the isothermal lines move with a speed slower than of the wind. After several hours, which may be determined by the maximum circulation and the steering velocity of the typhoon, the isotherms from the cold front reach the warm front. Thus a small warm air mass is occluded which would still be connected to the warm sector in a high level.

The distribution of dew-point which is more conservative than air temperature shows such occulusion process accurately. Sometimes we see occuluded dew-point temperature while isotherms are still opened.

In the tropical area free from the cold air-mass, however, there are shallow cold airs produced by heavy rains in the storm area. They would be located over the sea surface under the pouring precipitations, and they must be involved around the eye making the temperature of the eye relatively higher at least in the lowermost level than the environment.

It is observed by the airplane observations made through the lower levels of towering cumulo-nimbi around the eye, that the temperature around is colder about several degrees than of the eye. In the upper levels, the temperature inside the towering cloud must be higher.

§ 6 Temperature Associated with Föhn

We observe two föhns in typhoon which are caused by the mountains and the cold dome interacting with typhoon. The former may be called topographical föhn which is usually seen in the leeward side of the currents prevailing over high mountains. Typical example of the isotherms in föhn area caused by typhoon Della is shown in Fig. 81.

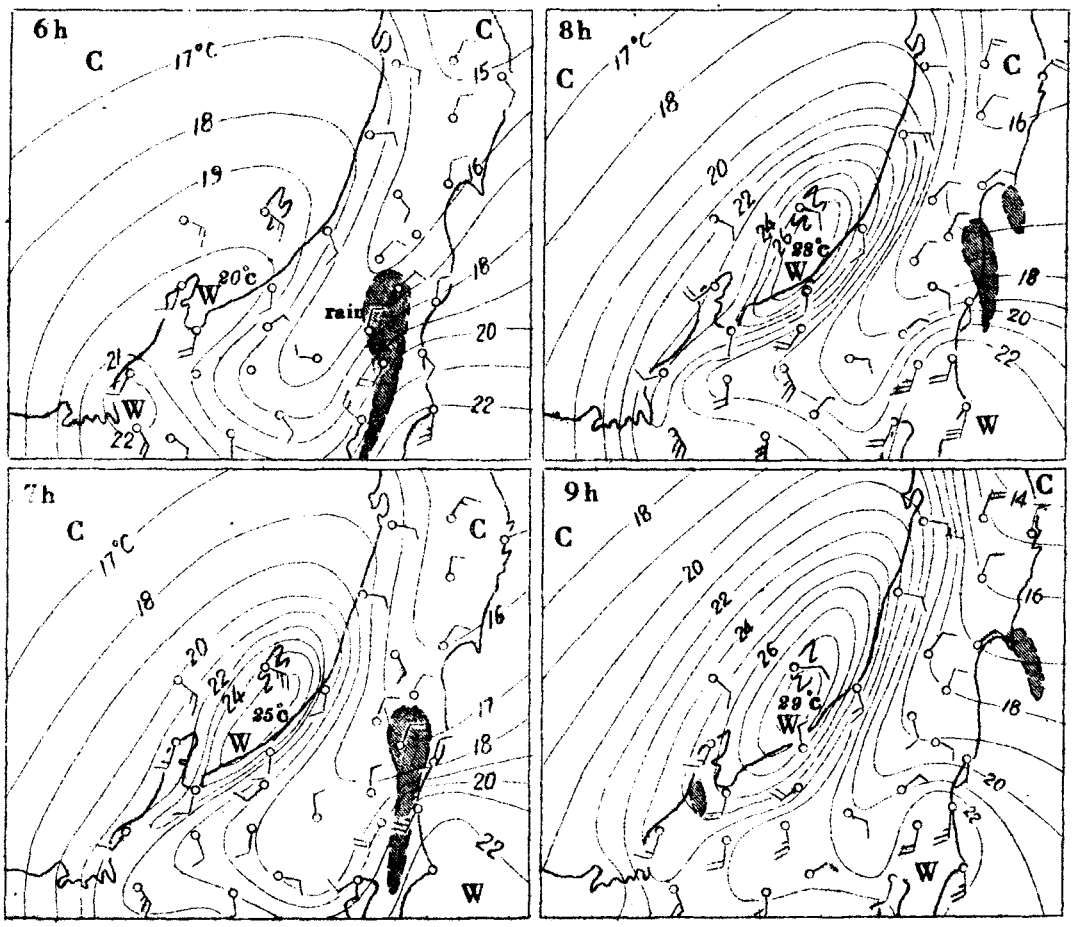

Fig. 81. Showing the isotherms of föhn area. At 6h when the solar radiation was not effective, the surface temperature was about 20°C. After one hour, however, having been warmed by the insolation, the shallow cold airs on the earth's surface were mixed with föhn air aloft. Charts for 06 ⟶ 09 22 June 1949.

Except the shallow layer on the surface, the downward current would be almost const. depending not upon the time of a day. But if we

write the chart using the temperatures observed at the altitude of about 1.5 m. above the surface, the high temperature by föhn does not always appear on the charts at night. But even at night, when the winds are so high that the cold air could be driven away, the rise in temperature occurs with an increasing wind. In the day time, however, a marked föhn are sometimes observed in slow surface winds. The weather change at Takata is shown in Fig. 82. It will be seen that the amount of both high and low clouds decreased from about 3h in the morning, suggesting that the clouds had vanished by the downward motion of the air aloft. Meanwhile the temperature had begun to decrease and did so until it increased again after the sunrise. After that, within one hour, it was heated with the rate that could not be expected on an ordinary day. The winds in föhn are not so strong with the wind force of about 3.

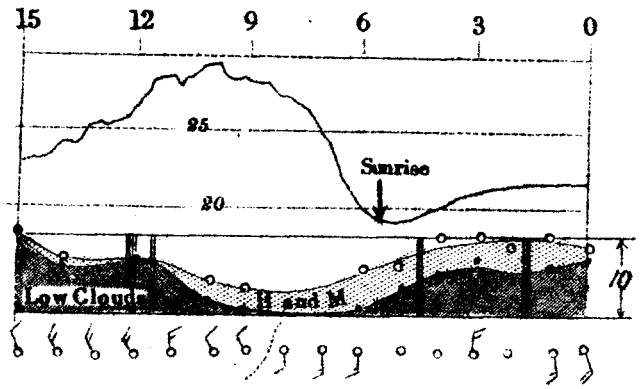

Fig. 82. Rise in temperature due to föhn. (Takata 00-15 22 June 1949)

LITERATURES

(1) Arakawa H. Aerological Observations made in the Kitty Typhoon by the Central Meteorological Observatory of Japan. Papers in Meteorology and Geophysics. 1, 1950.

(2) Arakawa H. Analysis of the tropopause and the Stratospheric Field of Temperature of a Mature Typhoon. Papers in Meteorology and Geophysics, 2, 1951.

(3) Byers H. R. The Thunderstorm.
U.S. Government Printing Office, Washington D.C. 1949

(4) Masuda Y. and Takeuchi T. An Aerological Investigation of the Structure of Typhoon (Jane and Kezia). Papers in Meteorology and Geophysics. Vol. 2 Nos. 3-4 Dec. 1951

(5) U.S. Weather Bureau Training Note No. 1, Hurricane Note, 1948

(6) U.S. Weather Bureau, Microfilm Copy of the Constant Pressure Charts for June and May 1949

(7) Watanabe K. Typhoon Kezia observed by American Weather Planes. Report of Typhoon Kezia of Sept. 1950. C.M.O. of Japan, Oct. 1951.

CHAPTER III

NEW THEORY ON CONVECTION PROBLEMS

CONTENTS

CHAPTER III NEW THEORY ON CONVECTION PROBLEMS

§ 1 Introduction

The studies on horizontal air flow due to the horizontal pressure gradient developed recently. On the other hand, the vertical motions playing an important rôle to produce various meteorological phenomena have not been solved satisfactorily. Especially the dynamics of the air movement capable of solving the nature of smaller disturbances is desired. To this purpose, the theory of buoyancy or vertical acceleration is indispensable.

It is known that the divergence of the three-dimensional motion defined by

$$div\ \mathbf{V} = \frac{\partial u}{\partial x} + \frac{\partial v}{\partial y} + \frac{\partial w}{\partial z}$$

shows the following relation,

$$\frac{\partial u}{\partial x} + \frac{\partial v}{\partial y} = -\frac{\partial w}{\partial z}.$$

Concerning the equation it is possible to give two explanations:

(1) Horizontal convergence pushes the air upward and, as the result, the vertical movements develop. Such convergence in horizontal directions may be produced by temperature effect or solenoid effect, latitude effect, curvature effect, topographical effect, effect of changing pressure system, and etc., and they would produce vertical accelerations.

(2) On the other hand, it is known that an intense horizontal divergence which could be resulted by the change in the vertical velocity is observed in medium scale phenomena in which the effects mentioned above are not to be expected. It may be considered, therefore, that there are the cases where the horizontal divergence could

be produced by a vertical acceleration. In the present chapter, the writer wants to clarify the cause of the horizontal convergence of this type.

§ 2 Equation of Upward Acceleration

Instead of the conventional buoyancy equation, the writer proposes an equation

$$\frac{dw}{dt} = -g - \frac{1}{\rho}\frac{\partial P}{\partial z} = -\frac{1}{\rho}\frac{\partial}{\partial z}\left(P - \int_z^\infty \rho\, g\, dz\right)$$

whence,

$$\frac{1}{\rho}\frac{\partial}{\partial z}\int_z^\infty \rho\, g\, dz = -g$$

Replacing the weight of the air column which may be termed "the weight pressure" by wP, namely,

$$\int_z^\infty \rho\, g\, dz = wP$$

we have

$$\frac{dw}{dt} = -\frac{1}{\rho}\frac{\partial}{\partial z}(P - wP) \qquad (33a)$$

This equation shows that the vertical acceleration is to be caused by the deviation of air pressure from the weight pressure. The difference $(P - wP)$, which would play an important role to initiate vertical motions, may be called "the convection pressure" with the symbol cP.

Thus, the vertical acceleration or buoyancy is given by

$$\frac{dw}{dt} = -\frac{1}{\rho}\frac{\partial}{\partial z}cP \qquad (33b)$$

It might be the question whether the air pressure is different from the weight of air column or not, however, it will become evident in the following discussions.

Dr. L. Prandtl(2) discussed the pressure on the ground exerted by a flying airplane, in the section "Übertragung des Flugzeuggewichts

auf den Erdboden." Under the assumption that the vertical velocity at the surface is zero, he obtained the formula showing the surface pressure,

$$P = \frac{h}{2\pi R^3} W$$

where, W is the weight of the plane, h the altitude, R the distance from the plane. The maximum pressure on the ground,

$$P_{max} = \frac{W}{2\pi h^2}$$

is proportional to the inverse square of the plane altitude. This fact shows that the pressure rise on the ground is negligiblly small if the plane flies over with a considerable altitude.

The most interesting characteristic is that the pressure distribution does not depend upon the speed of the plane nor its direction. Therefore, it can be applied to the case where the plane flies along a very small circle. This shows us also that a helicopter floating at a constant location up in the air would exert the pressure on the surface represented by the same formula as of the airplane case.

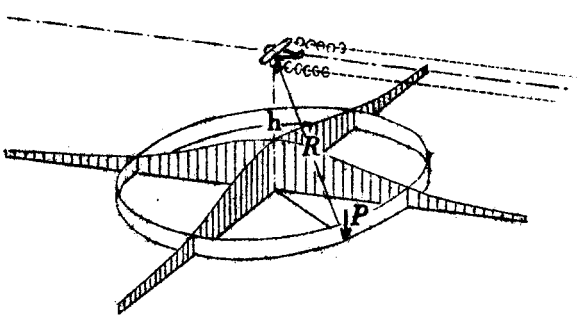

Fig. 83. Distribution of pressure caused by an airplane.

The equation of statical equilibrium is based upon the fact that the weight of the air aloft is transported only downward exerting the pressure just on the surface below the weight. This is, however, not conceivable, if we imagine the transportation of the weight of a helicopter toward the earth's surface. The vertical propeller pushes the airs downward in order to get the reaction from the underlying airs.

The accelerated airs move downward while they are decelerated through the mixing and collision processes which would transform the kinetic energy into heat. By the time when airs reach the dotted circle in Fig. 84, they would exert the force as pressure. Outside the circle, the pressure propagates not only downward but also toward the oblique directions. That is to say, the weight of the helicopter must be supported by the large mass of airs locating in the lower levels.

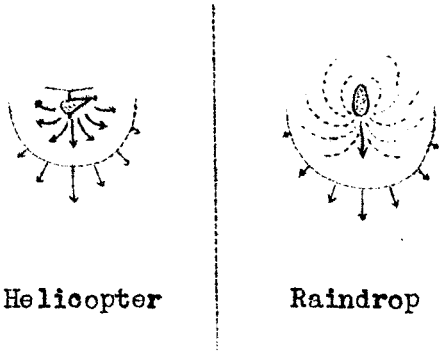

Fig. 84. Pressure exerted by solids in the air.

Using the similar consideration to that of the helicopter, we can imagine the propagation of pressure caused by the rain-drops falling at their terminal velocity. As will be seen in the figure the basic distribution of the pressure will remain unchanged.

§ 3 Proposed Mechanism of Pressure Propagation.

The above-mentioned results lead us to the conclusion that the propagation of air pressure must be explained by using the Huygens' Principle. As shown in Fig. 85, the primary pressure P_o on an area-element $d\sigma$ would produce the secondary pressure propagating downward, with maximum intensity for vertical direction. The intensity of the secondary pressure in

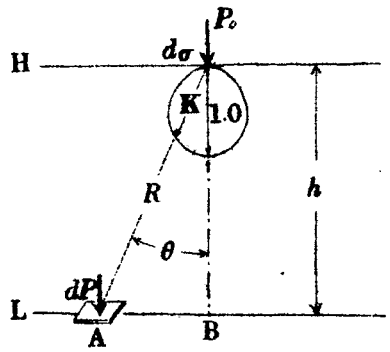

Fig. 85. Showing the propagation of pressure.

oblique direction is multiplied by K, the direction function, which is 1.00 for the direction of gravity and decreases rapidly becoming zero for $\theta = \frac{\pi}{2}$.

We also assume that the pressure weakens proportional to the inverse square of the distance. This assumption is based upon the fact that the area which undergoes the pressure excitation increases proportional to the square of the distance from the primary pressure source, and it can be considered that the pressure may decrease in proportion to the inverse square of the distance that the pressure had been transported. Of course, the pressure we now want to discuss here must not vary so rapidly with time.

From these assumptions, we obtain the pressure on lower surface L, viz.,

$$dP = P_0 \, d\sigma \times K_{(\theta)} \times \frac{C}{R^2}$$

where C is the constant determined by the fact that the integration

$$\iint dP \, dx \, dy$$

must be equal to $P_0 \, d\sigma$, since the same amount of secondary pressure to that of the primary should be transported to the lower level.

The direction function K is still unknown, however, if the pressure formula we now want to obtain hereunder is capable of representing the same distribution as of the airplane, the form of the direction function is unique, that is

$$K_{(\theta)} = \cos\theta$$

which shows that the pressure spreads with the spherical distribution. The shape of the direction function is shown in Fig. 86. Thus we have

$$dP = \frac{C_R}{R^2} \cos\theta \, d\sigma$$

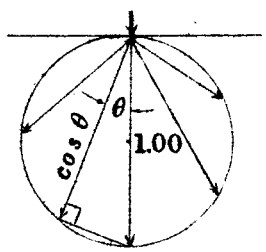

Fig. 86. Showing direction function.

If the height difference between upper and lower levels be h, we integrate the pressure after replacing $\cos\theta$ by h/R, thus:

$$P_0\, d\sigma = \int\int dP\, dx\, dy = \int \frac{C P_0 h}{R^3}\, 2\pi r\, dr\, d\sigma$$

where r is the distance from A to B in Fig. 85. Therefore, we have

$$1 = 2\pi C h \int_0^\infty \frac{r\, dr}{(\sqrt{h^2 + r^2})^3} = 2\pi C \int_0^{\frac{\pi}{2}} \sin\theta\, d\theta = 2\pi C$$

And the constant must be

$$C = \frac{1}{2\pi}$$

Thus, the pressure received on the lower level is known to be

$$dP = \frac{C P_0}{R^2} \cos\theta\, d\sigma = \frac{1}{2\pi} \frac{P_0\, d\sigma}{R^2} \frac{h}{R}$$

$$dP = \frac{h P_0\, d\sigma}{2\pi R^3} \qquad \text{(34a)}$$

It will be seen that the result is just the same as that of the airplane.

Now we consider the resultant pressure caused by the primary pressure shown in Fig. 87. Of course, the pressure at M is written as the summation

$$P = \frac{h P_1 \Delta\sigma_1}{2\pi R_1^3} + \frac{h P_2 \Delta\sigma_2}{2\pi R_2^3} + \frac{h P_3 \Delta\sigma_3}{2\pi R_3^3} + \cdots\cdots$$

$$= \frac{h}{2\pi} \sum_1^n \frac{P_n \Delta\sigma_n}{R_n^3} \qquad \text{(34b)}$$

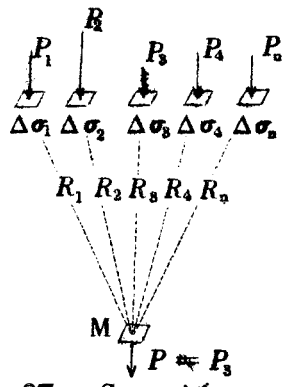

Fig. 87. Summation of the pressure to get the value of P, which is not equal to P_3.

It is clear that the pressure at the point in question is very much different from the weight of the air column aloft. And if there be a heavy mass which is gradually subsiding over the vicinity of a point, the pressure at that point must be larger than the weight pressure.

Such a summation is usually used in quantum theory or physical optics, when we obtain the intensity of material wave or light. And it is believed that even the excitation which is not directed toward a point induces a considerable excitation to the point.

When we compute the air pressure at the location $M(X,Y,Z)$, it is convenient to utilize the formula,

$$P = \frac{1}{2\pi}\int_Z^\infty\int_{-\infty}^{\infty}\int \frac{\rho\, g\, (z-Z)\, dx\, dy\, dz}{\{(x-X)^2+(y-Y)^2+(z-Z)^2\}^{\frac{3}{2}}} \qquad (34c)$$

where, x, y, z are the coordinates of air element with density ρ and volume $dx\,dy\,dz$.

§ 4 Convection Pressure and Excessive Pressure

We knew the method to compute the air pressure accurately, then we try to get the convection pressure, $cP = P - wP$, namely,

$$cP = \frac{1}{2\pi}\int_Z^\infty\int_{-\infty}^{\infty}\int \frac{\rho\, g\, (z-Z)\, dx\, dy\, dz}{\{(x-X)^2+(y-Y)^2+(z-Z)^2\}^{\frac{3}{2}}} - \int_Z^\infty \rho\, g\, dz \qquad (35a)$$

where, ρ is the density of the air given as the function of x, y, and z. If the atmosphere is uniform in horizontal direction and the density is written thus: $\rho_0 = f(z)$, we know,

$$\frac{1}{2\pi}\int_Z^\infty\int_{-\infty}^{\infty}\int \frac{\rho_0\, g\, (z-Z)\, dx\, dy\, dz}{\{(x-X)^2+(y-Y)^2+(z-Z)^2\}^{\frac{3}{2}}} - \frac{2}{\pi}\int_Z^\infty\int_{-\infty}^{\infty} \frac{\rho_0\, g\, (z-Z)\, dy\, dz}{(y-Y)^2+(z-Z)^2} = \int_Z^\infty \rho_0\, g\, dz \qquad (35b)$$

Therefore, in such a case convection pressure must vanish. This fact shows us that, as long as the air density is homogeneous in horizontal directions, the pressure is just the same as the weight pressure. Subtracting the formula,

$$\frac{1}{2\pi}\int_Z^\infty\int_{-\infty}^{\infty}\int \frac{\rho_0\, g\, (z-Z)\, dx\, dy\, dz}{\{(x-X)^2+(y-Y)^2+(z-Z)^2\}^{\frac{3}{2}}} - \int_Z^\infty \rho_0\, g\, dz = 0 \qquad (35c)$$

from the formula (35a), we have

$$cP = \frac{1}{2\pi}\int_Z^\infty\int_{-\infty}^{\infty}\int \frac{(\rho-\rho_0)\, g\, (z-Z)\, dx\, dy\, dz}{\{(x-X)^2+(y-Y)^2+(z-Z)^2\}^{\frac{3}{2}}} - \int_Z^\infty (\rho-\rho_0)\, g\, dz \qquad (36a)$$

In the practical computation, therefore, it is very convenient to carry out the integration after subtracting the density ρ_0 from the practical density ρ. We usually choose the density of warm air mass as ρ_0, so that the value $(\rho - \rho_0)$ is positive. We term $(\rho - \rho_0)$

"excessive density". And the pressure caused by the excessive density,

$$eP = \frac{1}{2\pi}\int_Z^\infty \iint_{-\infty}^{\infty} \frac{(\rho-\rho_0)\,g\,(z-Z)\,dx\,dy\,dz}{\left\{(x-X)^2+(y-Y)^2+(z-Z)^2\right\}^{3/2}} \qquad (36b)$$

can be called "the excessive pressure" with the symbol " eP". In the same way, the weight pressure caused by the excessive density,

$$ewP = \int_Z^\infty (\rho-\rho_0)\,g\,dz$$

may be called "the excessive weight pressure" with the symbol "ewP".

Now the following relations

$$cP = P - wP$$

$$cP = eP - ewP$$

show that the computation of the convection pressure can be done by using the excessive pressure instead of the ordinary air pressure.

The vertical acceleration is given by

$$\frac{dw}{dt} = -\frac{1}{\rho'}\frac{\partial\, cP}{\partial z}$$

where, ρ' is the density of the air, whose acceleration is in question. In the following discussion we obtain the accelerations upon the dry air at 0°C, 1000 mb. with the density,

$$\rho_0 = 1.276\times10^{-3}\ \mathrm{g/cm^3}$$

The word of "acceleration" used in the following sections means the acceleration upon this air, and the practical acceleration in higher altitude must be obtained multiplying the ratio, ρ_0 to the density of the air in question.

Thus the vertical acceleration

$$\frac{dw^0}{dt} = -\frac{1}{\rho_0}\frac{\partial}{\partial z}\,cP,$$

and the horizontal acceleration,

$$\frac{du^0}{dt} = -\frac{1}{\rho_0}\frac{\partial P}{\partial x} = -\frac{1}{\rho_0}\frac{\partial}{\partial x}(cP+wP) = -\frac{1}{\rho_0}\frac{\partial}{\partial x}(eP-ewP+wP)$$

$$= -\frac{1}{\rho_0}\frac{\partial eP}{\partial x} \qquad \left(\because\ wP-ewP=\int_Z^\infty \rho_0\,g\,dz\right)$$

are obtained. Summarizing the result we write, thus:

$$\left.\begin{aligned} \alpha^{\circ} &= \frac{du^{\circ}}{dt} = -\frac{1}{\rho_{\circ}}\frac{\partial\, eP}{\partial x} \\ \beta^{\circ} &= \frac{dv^{\circ}}{dt} = -\frac{1}{\rho_{\circ}}\frac{\partial\, eP}{\partial y} \\ \gamma^{\circ} &= \frac{dw^{\circ}}{dt} = -\frac{1}{\rho_{\circ}}\frac{\partial\, cP}{\partial z} \end{aligned}\right\} \qquad (37)$$

where, α, β, and γ are the accelerations in x, y, and z direction respectively. It must be noticed here again that both vertical and horizontal accelerations vanish when the density is equal horizontally, therefore, we cannot expect to find any acceleration inside a homogeneous air-mass. Thus, an appreciable buoyancy could only be found in the so-called frontal zone or in the vicinity of convective clouds which are warmer or colder than their environments.

Principle of Superposition

We consider the pressure at M caused by the density inside the stippled area in Fig. 88. It can be obtained integrating throughout the volume, thus:

$$P = \frac{1}{2\pi}\oint \frac{\rho g h}{R^3}\, dV$$

It is possible to obtain the integration after dividing the space by EF, and we have

$$\begin{aligned} P &= \frac{1}{2\pi}\int_C \frac{\rho g h}{R^3}\, dV - \frac{1}{2\pi}\int_{C'} \frac{\rho g h}{R^3}\, dV \\ &= \frac{1}{2\pi}\int_C \frac{\rho g h}{R^3}\, dV + \frac{1}{2\pi}\int_{C'} \frac{(-\rho) g h}{R^3}\, dV \end{aligned} \qquad (38)$$

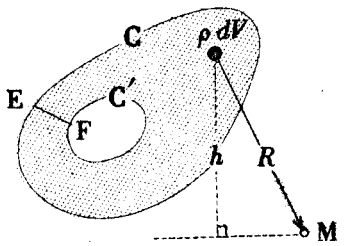

Fig. 88 To obtain the integration using the principle of superposition

This is the formula showing that the pressure can be obtained by superposing the two pressures in (38).

This property is very important and it is used in the computation not only of pressure but also of the accelerations of various kinds.

§ 5 Convection and Excessive Pressure in Frontal Zone

As shown in Fig. 89, if the cold air-mass, extending from $+\infty$ to $-\infty$ in y-direction, is located with its edge represented by the function of the altitude, the excessive pressure at the point M (X,Y,Z) is computed by the equation (36b). We have

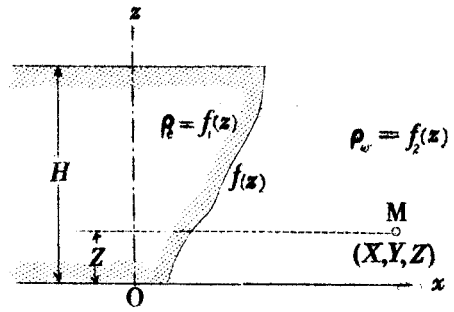

Fig. 89 To obtain the convection pressure in a frontal zone.

$$eP = \frac{1}{2\pi}\int_{Z}^{H}\int_{-\infty}^{f(z)}\int_{-\infty}^{+\infty}\frac{(\rho_c-\rho_w)\,g\,(z-Z)\,dy\,dx\,dz}{\{(x-X)^2+(y-Y)^2+(z-Z)^2\}^{3/2}}$$

where, ρ_w and ρ_c are the density of the warm and the cold air-mass, respectively. In the case where $(\rho_c-\rho_w)$ is constant everywhere, we integrate at first with respect to y.

$$eP = \frac{(\rho_c-\rho_w)g}{\pi}\int_{Z}^{H}\int_{-\infty}^{f(z)}\frac{(z-Z)\,dx\,dz}{(x-X)^2+(z-Z)^2}$$

Integrating again with respect to x, we have

$$eP = \frac{(\rho_c-\rho_w)\,g}{\pi}\int_{Z}^{H}\cot^{-1}\frac{X-f(z)}{z-Z}\,dz \qquad (39a)$$

The convection pressure is, therefore,

$$cP = \frac{(\rho_c-\rho_w)\,g}{\pi}\int_{Z}^{H}\cot^{-1}\frac{X-f(z)}{z-Z}\,dz - \int_{Z}^{H}(\rho_c-\rho_a)\,g\,dz \qquad (39b)$$

where, the second term in the right side, the excessive weight pressure (ewP) must be subtracted only when M is located inside or beneath the cold air of density ρ_c.

INCLINED FRONT

We examine the case in Fig. 90, where the frontal surface extending from $y=-\infty$ to $y=+\infty$ is the plane represented by $x = kz$

The excessive pressure at M(X,Y,Z) is

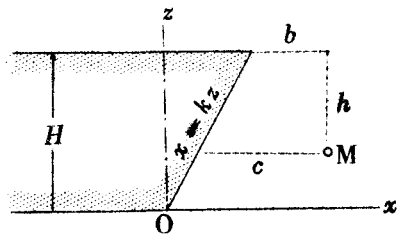

Fig. 90. Definition of h, b, c. When we measure b or c leftward from the frontal surface, they are negative.

$$eP = \frac{(\rho_c - \rho_w)g}{\pi} \int_Z^H \cot^{-1} \frac{X - kz}{z - Z}\, dz$$

We integrate after replacing

$$\frac{X - kz}{z - Z} \quad \text{by} \quad t - k$$

We obtain the excessive pressure

$$eP = \frac{(\rho_c - \rho_w)g}{\pi} \left[(cZ - X) \left\{ \left(\frac{k}{1+k^2} - \frac{1}{t} \right) \tan^{-1}(k-t) + \frac{1}{2(1+k^2)} \log \frac{1+(k-t)^2}{t^2} \right\}_{t_1}^{t_2} + \frac{\pi}{2}(H - Z) \right]$$

where, if we use the values h, b, and c in the figure, $t_1 = \infty$, and $t = c/h$. Thus, we get the excessive pressure

$$eP = \frac{(\rho_c - \rho_w)g}{\pi} \left\{ \left(h - \frac{kc}{1+k^2} \right) \tan^{-1} \frac{h}{b} - \frac{c}{2(1+k^2)} \log \frac{h^2 + b^2}{c^2} \right\}$$

The problem occurring here is the determination of the arctangent in the formula, because, as shown in Fig. 91, it is two-valued function even in the domain of $-\pi \cdots +\pi$. In the discussion herein, we use the positive branch when c is positive. But when c is negative we use the negative branch extending -0 to $-\pi$. Using the different branches according to the sign of c, we have the excessive pressure,

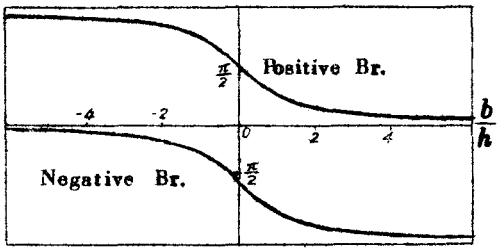

Fig. 91. Showing the arctangent branches for the computation.

$$eP = \frac{(\rho_c - \rho_w)g}{\pi} \left\{ \left(h - \frac{kc}{1+k^2} \right) \tan^{-1} \frac{h}{b} - \frac{c}{1+k^2} \log \sqrt{\frac{h^2 + b^2}{c^2}} \right\} + (\rho_c - \rho_w)\, g\, h \qquad \text{(40a)}$$

where, the last term is used only when the point M is located inside the cold air. The convection pressure is obtained subtracting the value,

$$\int_Z^H (\rho_c - \rho_w)\, g\, dz = \begin{cases} (\rho_c - \rho_w)\, g\, h & \text{(inside cold air)} \\ -(\rho_c - \rho_w)\, g\, \dfrac{b}{k} & \text{(beneath cold air slope)} \end{cases}$$

from the excessive pressure. Thus we have

$$cP = \frac{(\rho_c - \rho_w)g}{\pi} \left\{ \left(h - \frac{kc}{1+k^2} \right) \tan^{-1} \frac{c}{b} - \frac{c}{1+k^2} \log \sqrt{\frac{h^2 + b^2}{c^2}} \right\} + (\rho_c - \rho_w)\, g\, \frac{b}{k}. \qquad \text{(40b)}$$

According to the conventional treatment, the air pressures were computed by the formula of static equilibrium. The distribution of the excessive pressure, the pressure caused by the excessive density of the cold air-mass, is shown in Fig. 92. As the figures are drawn

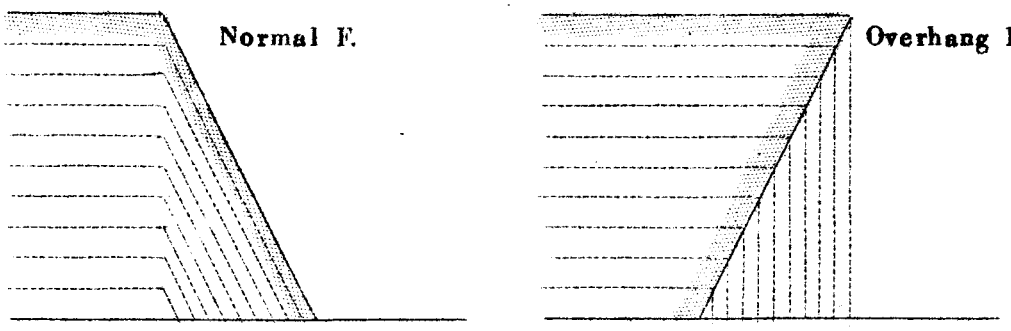

Fig. 92. Distribution of excessive pressure by conventional idea.

after the conventional idea, the isobaric surface is parallel to the frontal surface or the direction of gravity. Looking at such figures we must consider that the cold air will subside by its weight until it spreads over the earth's surface as a shallow cushion, and that the overhang front in the right is quite unstable, since it must fall down into the underlying warm air.

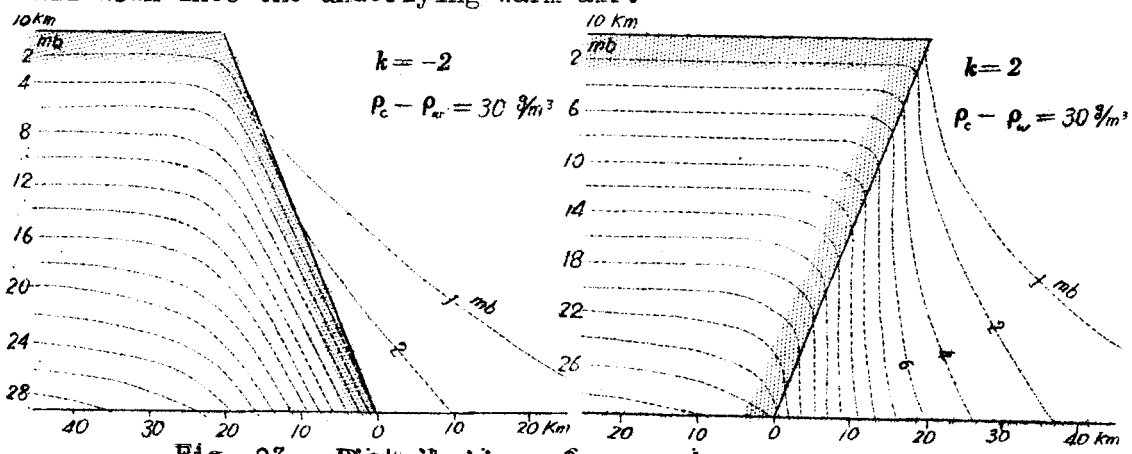

Fig. 93. Distribution of excessive pressure by new theory.

Next we examine the pressure distribution represented by the new formula. Fig. 93 is computed for the frontal zone with the inclination of $\frac{1}{2}$, and the density difference, $(\rho_c - \rho_w) = 30$ g/ m³ which will be produced by the temperature difference of about 10°C. The most interesting feature of the isobaric surface is that the height of constant pressure decreases even under the flat surface of cold air and that the pressure surface extends far into the warm sector showing that the weight of cold air exerts upon the warm air.

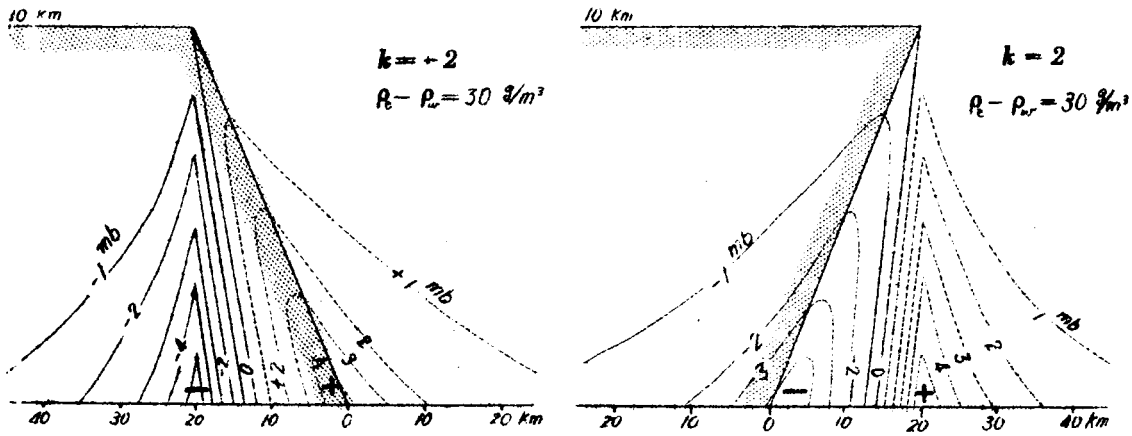

Fig. 94. Distribution of convection pressure.

Distribution of convection pressure in Fig. 94 is also computed by the formula(40b). In this case, there exists large positive convection pressure inside the warm sector, while the negative convection pressure is seen inside the cold air-mass. In the frontal zone, the equation of static equilibrium can be applied no more, and the deviation from that equation, which has long been neglected, must be closed up here in order to explain the meteorological phenomena.

As will be expected, the convection pressure becomes very small when the inclination of the front is small. Cases of the normal and overhang fronts with the inclination of 1/100 are shown in Fig. 95. It will be seen that the convection pressure is no more than 0.5 mb.,

which seems to be very small. This amount, however, is capable of

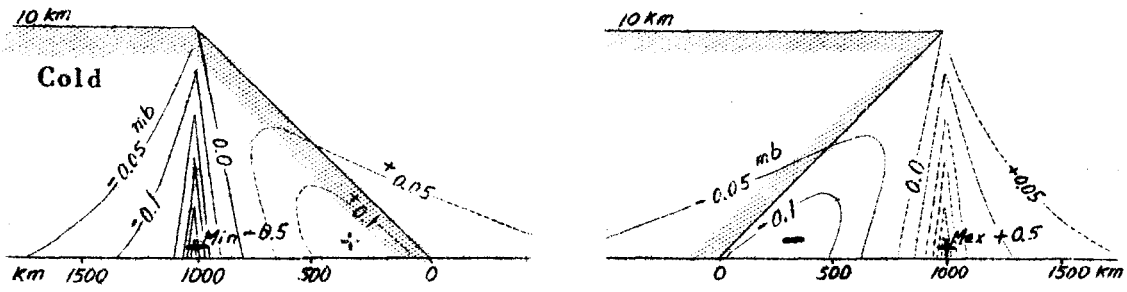

Fig. 95. Distribution of convection pressure.

producing the vertical speed of about 10 m/sec, and if we expect to produce such a speed of the warm air gliding upward the frontal surface in discussion, it would require the speed of 1 km/sec, which is impossible to be expected.

§ 6 Vertical and Horizontal Acceleration.

The acceleration upon the air of density ρ_0 is given by (37). Therefore, utilizing the formulas (40a) and (40b), we obtain the vertical acceleration in the frontal zone,

$$\gamma^0 = -\frac{1}{\rho_0}\frac{\partial cP}{\partial z} = \frac{(\rho_c-\rho_i)g}{\rho_0\pi}\left(\frac{1}{1+k^2}\tan^{-1}\frac{h}{b} - \frac{k}{1+k^2}\log\sqrt{\frac{h^2+b^2}{c^2}}\right) \quad (41a)$$

and the acceleration in x-direction,

$$\alpha^0 = -\frac{1}{\rho_0}\frac{\partial eP}{\partial x} = \frac{(\rho_c-\rho_w)g}{\rho_0\pi}\left(\frac{k}{1+k^2}\tan^{-1}\frac{h}{b} + \frac{1}{1+k^2}\log\sqrt{\frac{h^2+b^2}{c^2}}\right) \quad (41b)$$

These formulas show that the acceleration at any point is to be determined as the function of the inclination of the front and the direction of the point looked from the upper edge of the frontal surface.

In this section we desire to discuss the acceleration upon the imaginary air with the density ρ_0. Because it depends only upon the characteristic of the field of acceleration. While the practical

acceleration upon the air is not so simple, because as shown by

$$\frac{dw}{dt} = \frac{\rho_\circ}{\rho'} \frac{dw^\circ}{dt}$$

it contains the density ρ' which varies in horizontal and vertical directions.

Using the formulas (41a) and (41b), the acceleration in the frontal zone are computed. The fronts studied herein are classified according to the value of k characterizing the inclination, thus:

$k < 0$	$k = 0$	$k > 0$
Normal Front	Vertical Front	Overhang Front

The accelerations for the normal front of $k = -2$ are plotted in Fig. 96. It will be seen in the upper figure that the buoyancy force, acting upon the air inside the warm sector, reaches long distance. While the acceleration increases up to infinity at the frontal surface. This is, of course, not conceivable, however, the infinity in question is originated by the fact that we have admitted the discontinuous density jump at the frontal surface. Therefore, if we solve the problem for the frontal surface at which the density increases gradually into that of the cold air, a finite acceleration could be expected. Such a case is discussed later.

The horizontal acceleration shown in the middle figure is appreciable only under the inclined frontal surface. In the warm sector or under the flat surface of the cold air mass, the acceleration is always negligible. The resultant accelerations are, therefore, almost vertical in the sectors far from the frontal surface.

This fact can be proved computing the tangent of the direction angle of the acceleration,

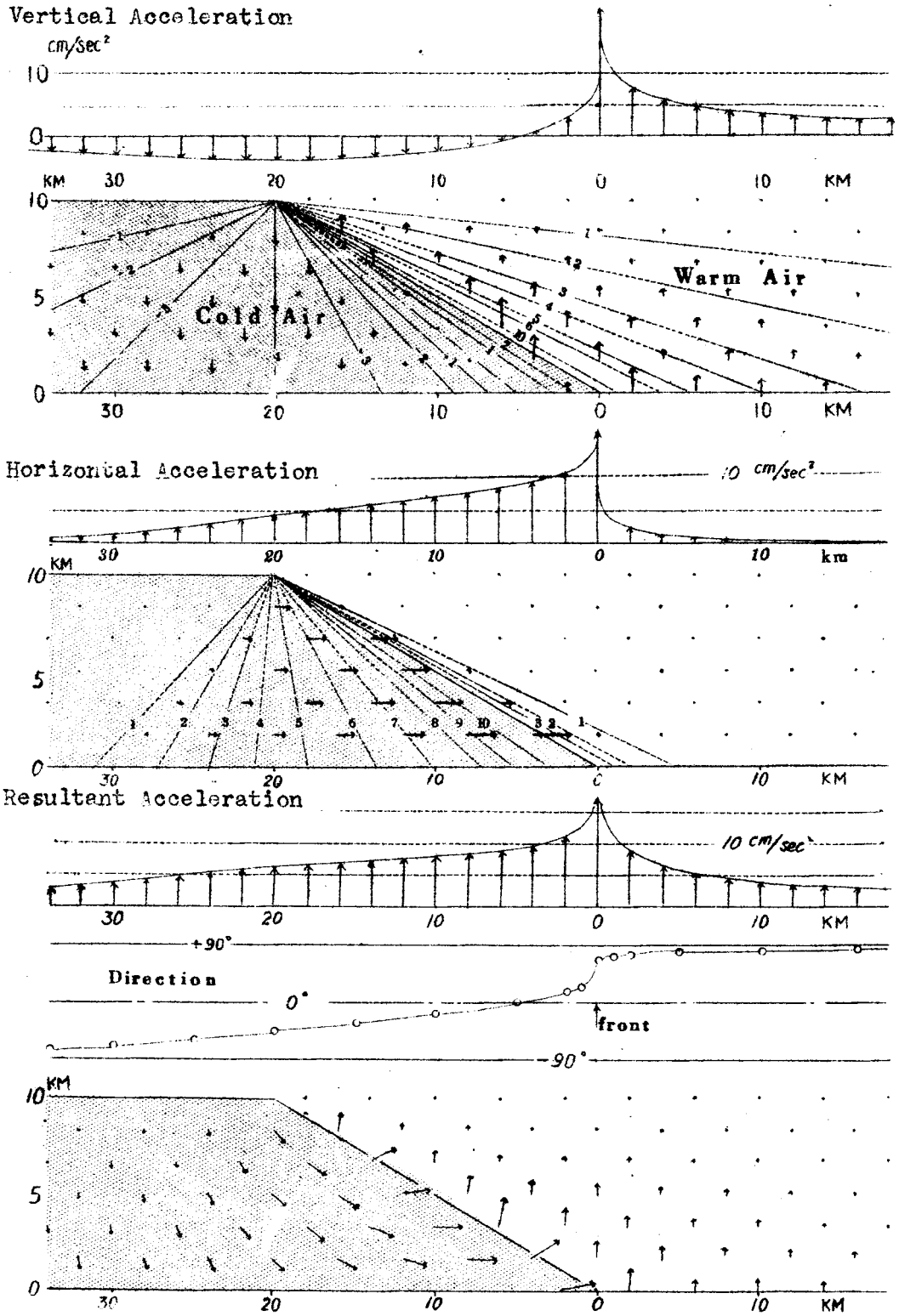

Fig. 96 Accelerations in the vicinity of the normal front extending from $y = -\infty$ to $+\infty$. Constants are $K = -2$, $\rho_1 - \rho_2 = 3 \times 10^{-5}$ g/cm³, and the height of the cold air-mass = 10 km.

$$\tan \mathcal{U}(A) = \frac{\tan^{-1}\frac{h}{b} - k \log\sqrt{\frac{h^2+b^2}{c^2}}}{k\tan^{-1}\frac{h}{b} + \log\sqrt{\frac{h^2+b^2}{c^2}}} \qquad (42a)$$

when we limit the value of b and c to infinity, thus:

$$\left.\begin{aligned} \lim_{\substack{b\to\infty \\ c\to\infty}} \tan \mathcal{U}(A) &= \lim_{b\to\infty} \frac{hb\,(1+k^2)}{h^2\,(1+k^2)} \to \infty \\ \lim_{h\to 0} \tan \mathcal{U}(A) &= \lim_{h\to c} \frac{b^2\,(1+k^2)}{hb\,(1+k^2)} \to \infty \end{aligned}\right\} \qquad (42b)$$

It will be seen that the accelerations are directed up or downward when b is very large or h is very small.

On the other hand, at the frontal surface where the value of c tends to zero, the direction of acceleration is perpendicular to the surface, since the value of $\log c$ decreases to $-\infty$, Thus we have

$$\lim_{c\to 0} \tan \mathcal{U}(A) = -k \qquad (42c)$$

It is evident that the acceleration at the surface is directed toward the warm air side perpendicularly to the surface. These characteristics should be kept in mind when we plot the accelerations in the frontal zone.

The accelerations for the overhang front of $k = +2$ are shown in Fig. 97. According to our direct consideration, such a overhang cold air is considered to be very unstable. The result of the computation shows us that, so long as the accelerations are concerned, there is no fundamental difference from the normal front.

As will be seen in the figure of vertical acceleration, the downward force to pull down the wedge of the cold air is similar in amount to the force by which the cold air under a normal frontal surface subsides downward. The conventional idea, that the heavy overrunning mass is liable to fall down quickly, must be revised, and we must remember that it is the gradient of the convection pressure

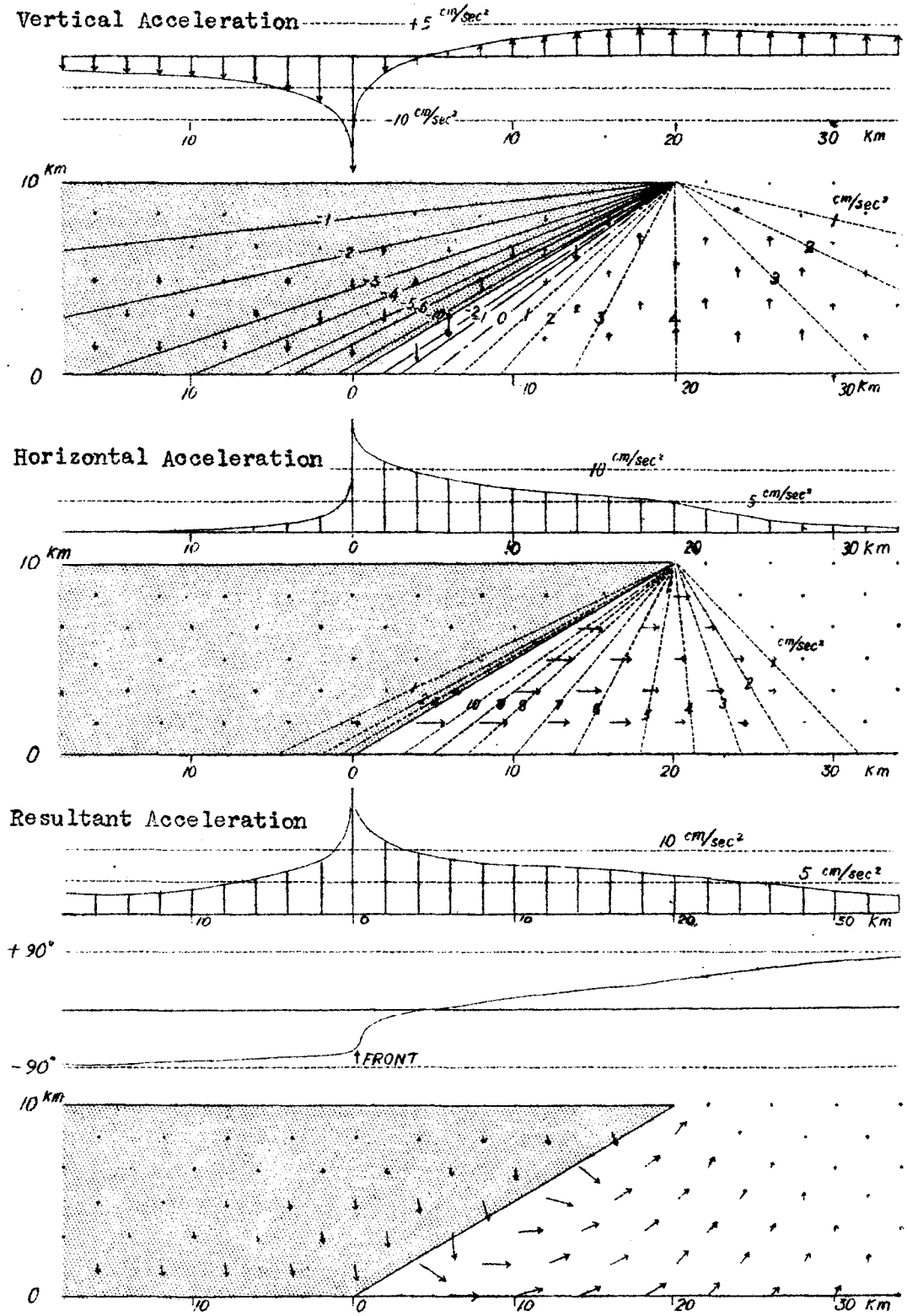

Fig. 97 Accelerations in the vicinity of the overhang front extending from $y = -\infty$ to $+\infty$. Constants are $K = +2$, $\rho_c - \rho_w = 3 \times 10^{-5}$ g/cm³, and the height of the cold air-mass = 10 km.

which accelerates the air in vertical direction. The force from the cold air wedge acts mainly upon the underlying warm air, as the result the airs are accelerated downward just under the surface and upward in the distant sector.

The dynamics of the overrunning cold air, which has not been evident according to the conventional idea, became very clear. The computation of the vertical and horizontal accelerations can easily be carried out by using the principle of superposition. Namely, we at first compute the case of normal or overhang front, after that we subtract the amount of acceleration for the warm air which must be replaced in order to eliminate the lower portion of the cold air-mass.

The schematical accelerations in the vicinity of overrunning overhang front are shown in Fig. 98. This is the pattern for $k = 2$. It will be seen that the accelerations decrease as the altitude decreases. Comparing the pattern with that of the overrunning normal front in Fig. 99, it will be seen that they are quite similar each other.

The most important problem occurring here is the stability of the overrunning front far from the frontal surface where the value of $-b$ is very large. There we cannot expect to find any force accelerating the cold air downward showing that the stratification is very stable. Thus, the conventional stability problems should be re-examined in the following section.

ROTATION OF THE ACCELERATION FIELD

It is the question that the field of acceleration is rotational or irrotational, it is, however, easily seen by subtracting

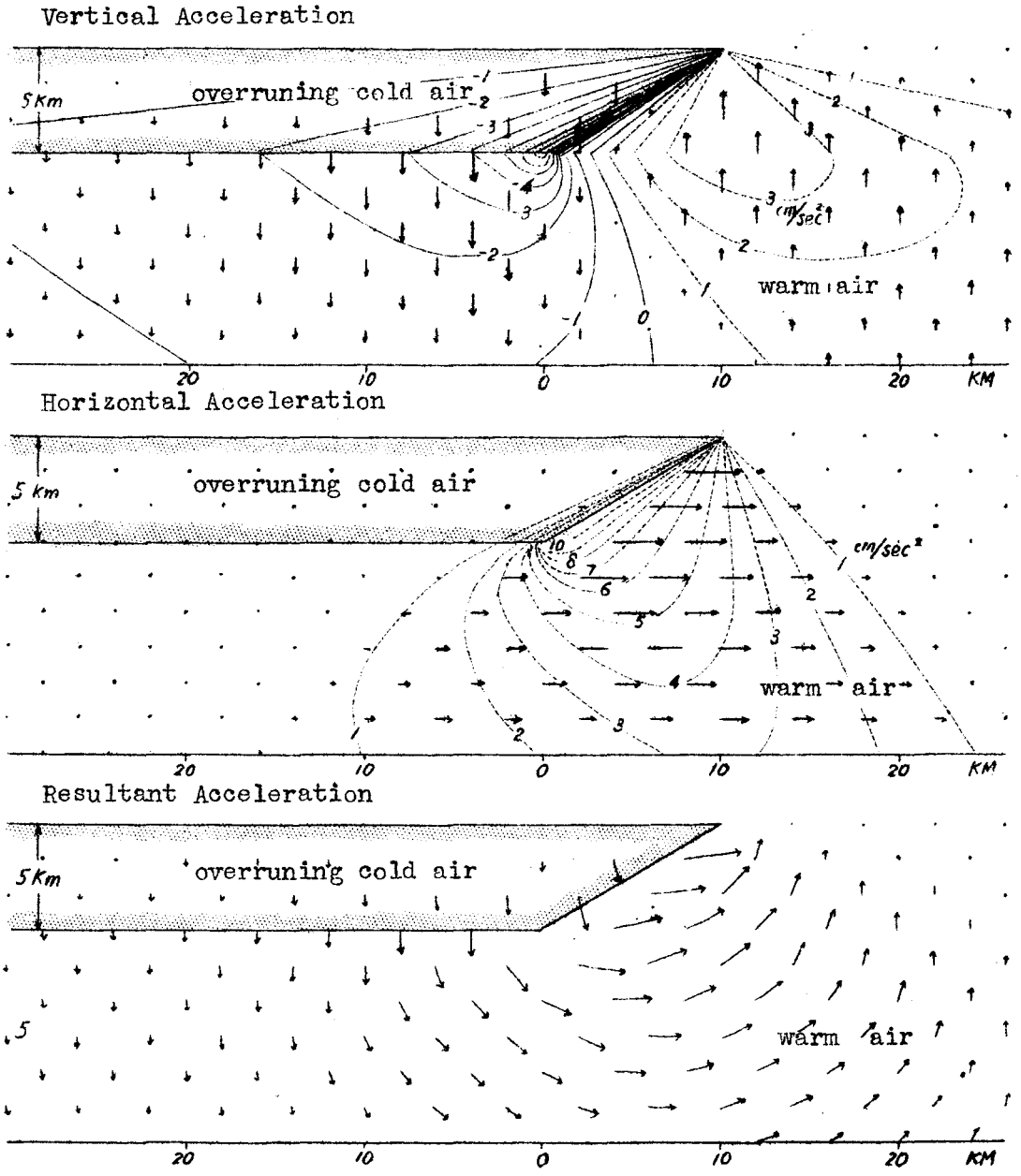

Fig. 98. Acceleration patterns for an overruning cold front with overhang frontal surface. The constants are: thickness of cold air, 5 km., beta c = beta 30 g/m³, inclination, 1/2.

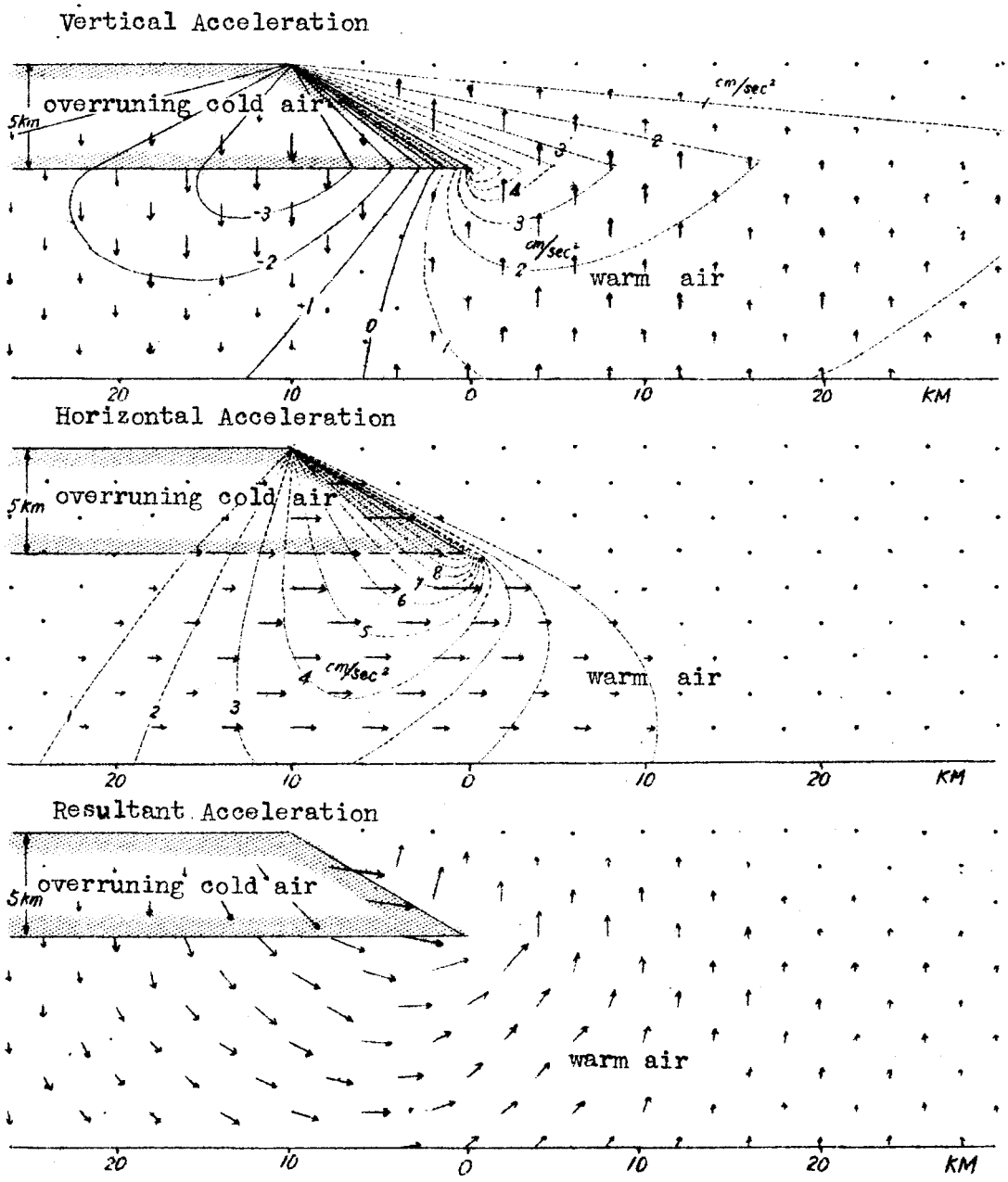

Fig. 99. Acceleration patterns for an overruning normal cold front with the constants: thickness of cold air, 5 km.; $\rho_c - \rho_w = 30$ g/m³; inclination of 1/2.

$$\frac{\partial}{\partial x}(\gamma^{\circ}) = \frac{(\rho_c - \rho_w)g}{\rho_{\circ}\pi(h^2+b^2)} \times \frac{kh^2 + kb^2 - kbc - hc}{c(1+k^2)}$$

from

$$\frac{\partial}{\partial z}(\alpha^{\circ}) = \frac{(\rho_c - \rho_w)g}{\rho_{\circ}\pi(h^2+b^2)} \times \frac{-kbc - hc + kh^2 + kb^2}{c(1+k^2)}$$

As the result we know the fact that the rotation of the vector field is zero, viz.,

$$\frac{\partial}{\partial z}(\alpha^{\circ}) - \frac{\partial}{\partial x}(\gamma^{\circ}) = 0 \qquad (43)$$

Thus we know the acceleration field is irrotational and the acceleration must have the potential,

$$\frac{(\rho_c - \rho_w)g}{\rho_{\circ}\pi}\left\{\left(h - \frac{kc}{1+k^2}\right)\tan^{-1}\frac{h}{b} - \frac{c}{1+k^2}\log\sqrt{\frac{h^2+b^2}{c^2}}\right\} \qquad (44)$$

DIVERGENCE OF THE ACCELERATION FIELD

Next we compute the divergence of the field of acceleration. Taking the relations,

$$\frac{\partial h}{\partial z} = -1, \quad \frac{\partial b}{\partial z} = 0, \quad \frac{\partial c}{\partial z} = -k$$

into consideration, we compute the partial derivative with respect to z, and we have

$$\frac{\partial}{\partial z}(\gamma^{\circ}) = \frac{(\rho_c - \rho_w)g(khc - bc - k^2h^2 - k^2b^2)}{\rho_{\circ}\pi(1+k^2)c(h^2+b^2)}$$

Next we obtain the other one,

$$\frac{\partial}{\partial x}(\alpha^{\circ}) = \frac{(\rho_c - \rho_w)g(bc - khc - h^2 - b^2)}{\rho_{\circ}\pi(1+k^2)c(h^2+b^2)}$$

using the relations

$$\frac{\partial h}{\partial x} = 0, \quad \frac{\partial b}{\partial x} = 1, \quad \frac{\partial c}{\partial x} = 1$$

The sum of them,

$$\frac{\partial}{\partial z}(\gamma^{\circ}) + \frac{\partial}{\partial x}(\alpha^{\circ}) = \frac{-(\rho_c - \rho_w)g}{\rho_{\circ}\pi}\,\frac{1}{c} \qquad (45)$$

shows that the divergence is not zero but it is inversely proportional to the negative value of c, the horizontal distance from the frontal surface. Of course, the divergence must be positive infinity on the cold air side of the frontal surface, and negative infinity on

the warm air side. When the density does not jump at the surface, we would have a finite divergence even at the surface.

The conclusion is very important, which shows that the accelerations are newly initiated inside the cold air, meanwhile they vanish inside the warm air. It is also clear that, in case of any overrunning front, there exists no divergence below the bottom of the cold air where the positive and negative divergences are cancelled.

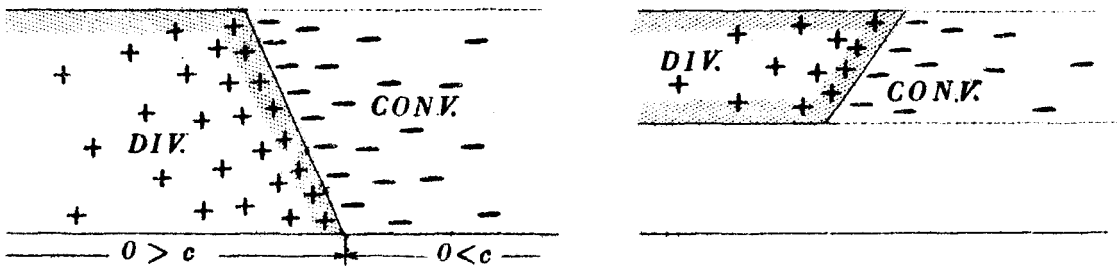

Fig. 100. Distribution of divergence of acceleration.

The distribution will be seen also in Fig. 100, in which the schematical distribution is illustrated.

MODEL OF PRACTICAL FRONTAL SURFACE

As a model of inclined frontal surface, the distribution of accelerations for the system with a finite density jump separated by an inclined surface with large absolute value of k is computed.

The acceleration pattern for $k = -100$ is presented in Fig. 101. Comparing with Fig. 102, it will be understood that the horizontal accelerations exist only beneath the frontal surface, and that the downward accelerations concentrate under the edge of the top of the frontal surface. On the other hand, when the cold air overhangs with $k = +100$, appreciable upward accelerations develop just under the edge, suggesting that the pre-frontal squall-line might be initiated there. This fact will be seen in the lowest figure showing the resultant

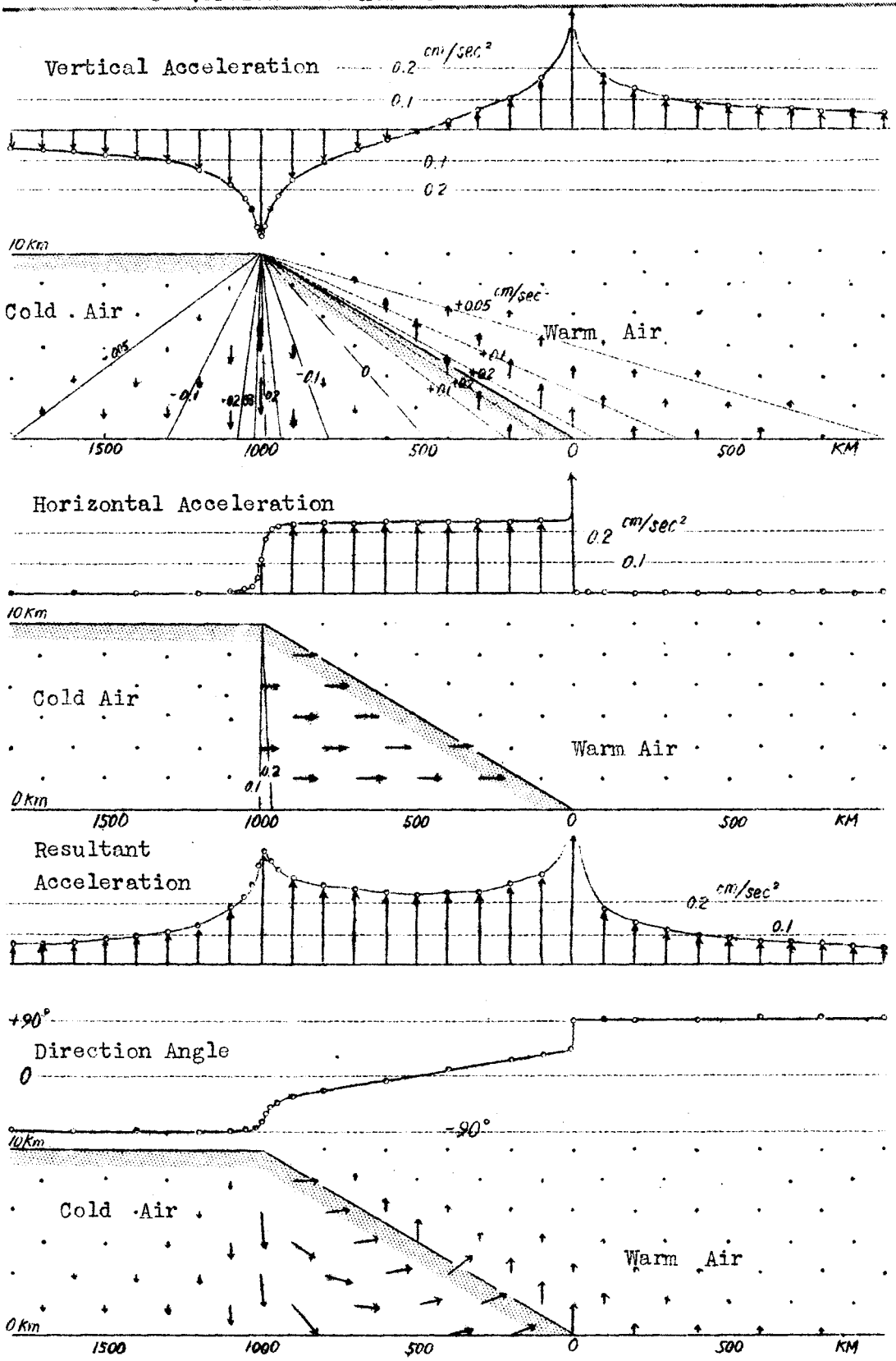

Fig. 101 Accelerations in the vicinity of the normal front extending from $y=-\infty$ to $+\infty$. $k = -100$, $\rho_c - \rho_w = 30$ g/m³, $h = 10$ km.

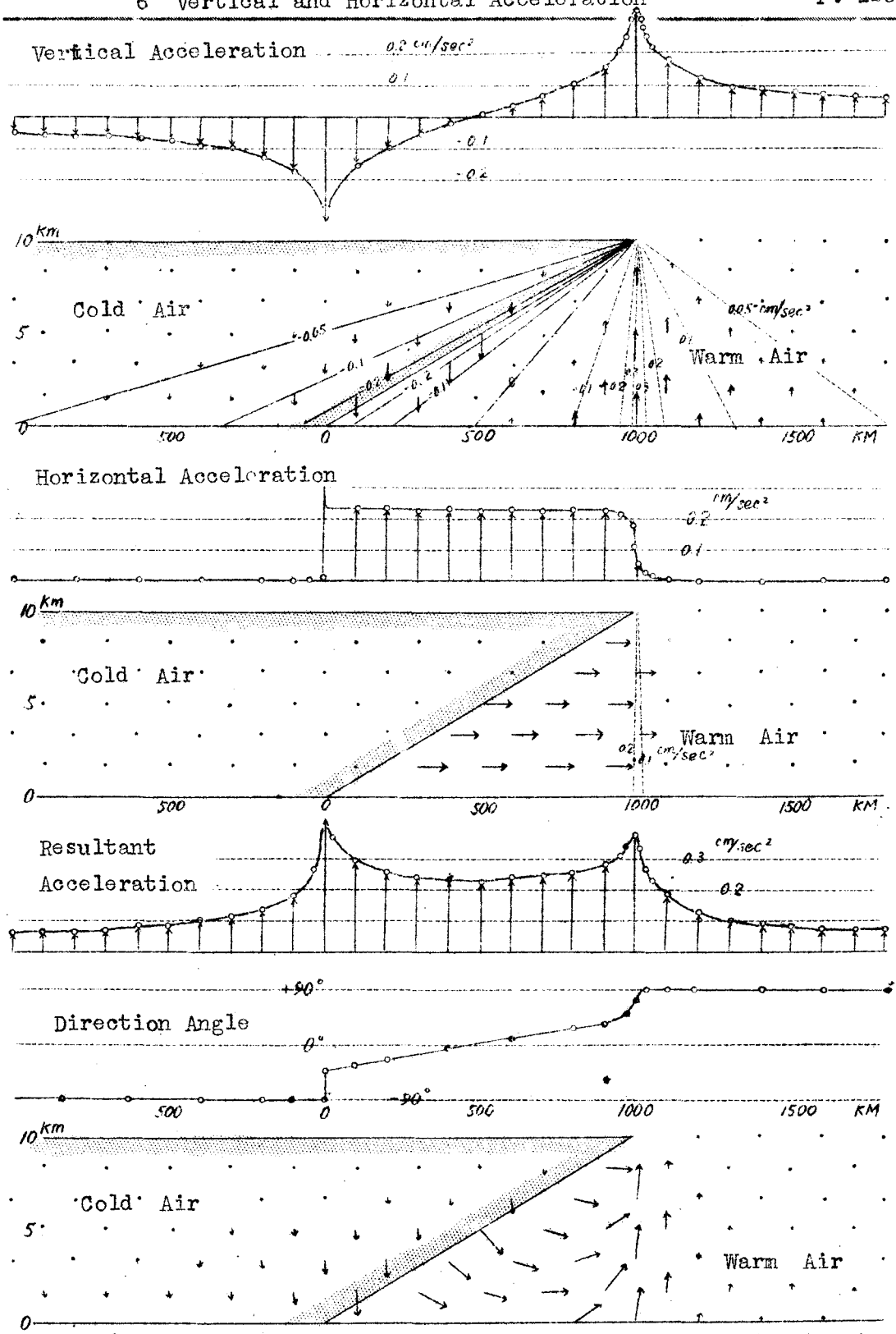

Fig. 102 Accelerations in the vicinity of the overhang front extending from $y = -\infty$ to $+\infty$. $k = +100$, $\rho_c - \rho_w = 30$ g/m³, $h = 10$ km.

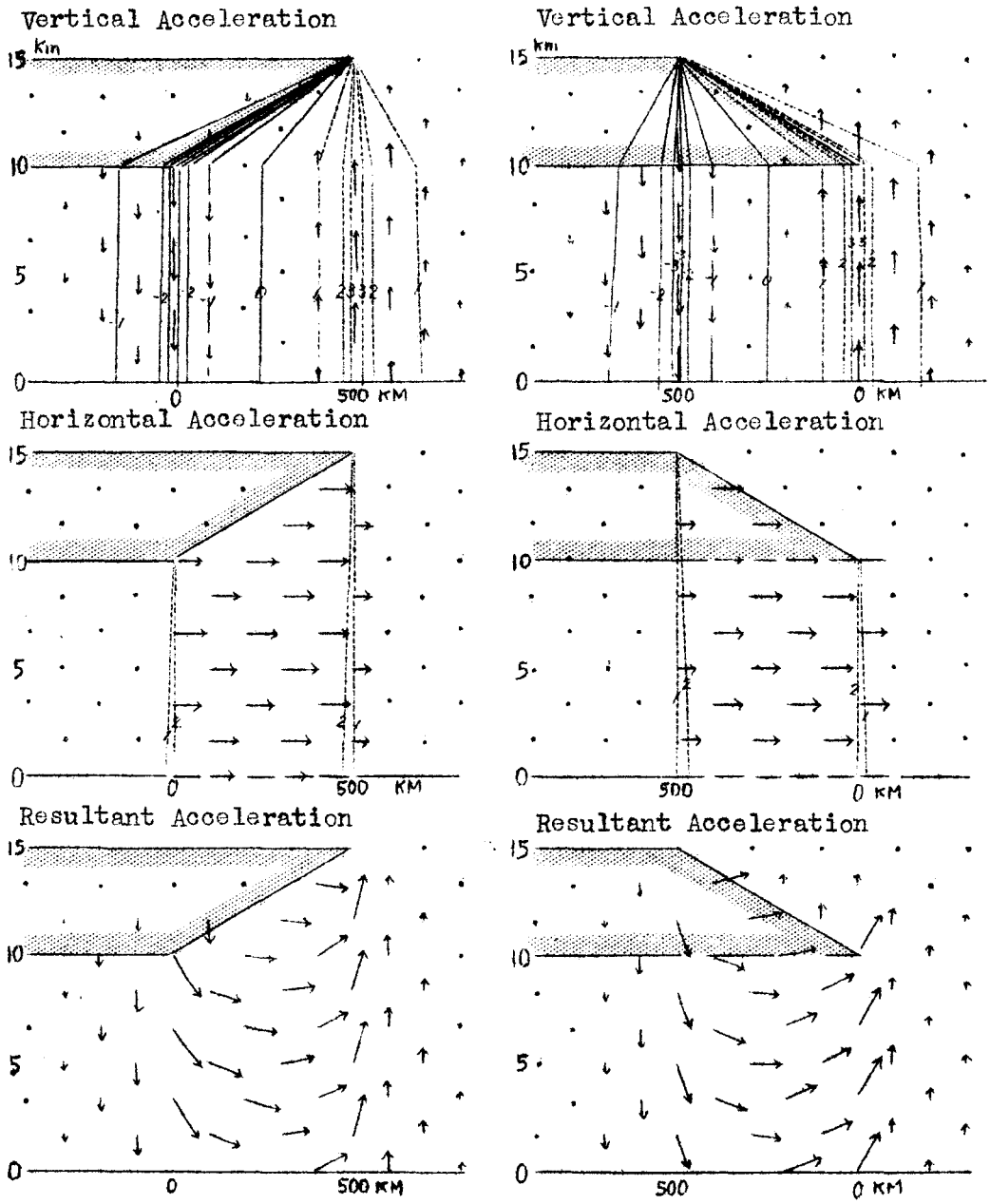

Fig. 103 Acceleration Patterns for overruning normal and overhang fronts. The height of the cold air base is 10 km, the thickness 5 km and the other constants are just the same as those of Figs. 101 and 102. Computed by (41a) and (41b).

accelerations.

Similar distributions for overrunning fronts are given in Fig. 103. The patterns are computed by using the accurate formulas (41a) and (41b).

§ 7 Movement of the Air in the Field of Accelerations.

When the air undergoes vertical accelerations in the field free from the horizontal acceleration, it does not move toward the direction of acceleration, according to the rotation of the earth. The velocity components for such a wind can be solved by the equations of motion,

$$\left.\begin{aligned} \dot{u} + 2\omega(w\cos\phi - v\sin\phi) &= 0 \\ \dot{v} + 2\omega u \sin\phi &= 0 \\ \dot{w} - 2\omega u\cos\phi &= -\frac{1}{\rho}\frac{\partial cP}{\partial z} \end{aligned}\right\} \quad \cdots\cdots (46)$$

where the positive directions of x, y and z axes are chosen toward the east, north and vertical direction, respectively.

Differentiating the first equation with respect to time, we get

$$\ddot{u} + 2\omega\dot{w}\cos\phi - 2\omega\dot{v}\sin\phi = 0$$

Then we replace $\dot{w}$ and $\dot{v}$ by these in the second and third equations, so we obtain the differential equation,

$$\frac{d^2u}{dt^2} + 4\omega^2 u = 2\omega\cos\phi\,\frac{1}{\rho}\frac{\partial cP}{\partial z}$$

The velocity components for the boundary condition that the air starts to move at t=0 are obtained thus:

$$\left.\begin{aligned} u &= (1 - \cos 2\omega t)\cos\phi\,\frac{1}{2\omega\rho}\frac{\partial cP}{\partial z} \\ v &= (\sin 2\omega t - 2\omega t)\sin\phi\cos\phi\,\frac{1}{2\omega\rho}\frac{\partial cP}{\partial z} \\ w &= -(2\omega t\sin^2\phi + \cos^2\phi\sin 2\omega t)\,\frac{1}{2\omega\rho}\frac{\partial cP}{\partial z} \end{aligned}\right\} \quad \cdots\cdots (47a)$$

The displacement components, obtained by integrating each velocity

component from t=0 to t, are

$$\left.\begin{aligned} x &= (2\omega t - \sin 2\omega t)\cos\phi \frac{1}{4\omega^2\rho}\frac{\partial cP}{\partial z} \\ y &= (1 - 2\omega^2 t^2 - \cos 2\omega t)\sin\phi\cos\phi \frac{1}{4\omega^2\rho}\frac{\partial cP}{\partial z} \\ z &= (\cos^2\phi \cos 2\omega t - 2\omega^2 t^2 \sin^2\phi - \cos^2\phi)\frac{1}{4\omega^2\rho}\frac{\partial cP}{\partial z} \end{aligned}\right\} \quad (47b)$$

The wind represented by (47) is the new wind deviating from the gradient wind which is zero in this case.

When this wind develops in the field of gradient wind represented by the equations of motion,

$$\left.\begin{aligned} 2\omega w'\cos\phi - v'\sin\phi &= -\frac{1}{\rho}\frac{\partial P'}{\partial x} \\ 2\omega u'\sin\phi &= -\frac{1}{\rho}\frac{\partial P'}{\partial y} \\ -2\omega u'\cos\phi &= -\frac{1}{\rho}\frac{\partial P'}{\partial z} - g \end{aligned}\right\} \quad (48)$$

where P' is the pressure in order to develop the gradient wind with the velocity components u', v', and w'.

Adding the equations of motion in (48) to those in (46), we get,

$$\left.\begin{aligned} (\dot{u} + \dot{u}') + 2\omega(w + w')\cos\phi - 2\omega(v + v')\sin\phi &= -\frac{1}{\rho}\frac{\partial P'}{\partial x} \\ (\dot{v} + \dot{v}') + 2\omega(u + u')\sin\phi &= -\frac{1}{\rho}\frac{\partial P'}{\partial y} \\ (\dot{w} + \dot{w}') - 2\omega(u + u')\cos\phi &= -\frac{1}{\rho}\frac{\partial cP}{\partial z} - \frac{1}{\rho}\frac{\partial P'}{\partial z} - g \end{aligned}\right\} \quad (49)$$

where $\dot{u}' = \dot{v}' = \dot{w}' = 0$, and we consider the wind by (48) far exceeds. The solution of the equations (49) is, therefore, given by the vector,

$$\begin{aligned} \mathbf{V} &= \mathbf{i}(u + u') + \mathbf{j}(v + v') + \mathbf{k}(w + w') \\ &= (\mathbf{i}u + \mathbf{j}v + \mathbf{k}w) + (\mathbf{i}u' + \mathbf{j}v' + \mathbf{k}w') \end{aligned} \quad (50)$$

It is evident that the second term is the gradient wind balancing to the horizontal accelerations, and that the first term is the wind caused by the vertical acceleration. Here, the wind initiated by the vertical acceleration may be termed "the convection wind".

CONVECTION WIND

As has been seen before, the convection wind represented by (47)

superposes upon the geostrophic or gradient wind field. This wind is, of course, accelerational showing that the speed might increase up to infinity toward the vertical and northward directions. As shown in Fig. 104, the air of such a wind moves spirally around the curve of parabola drawn on the surface inclined toward the pole-star. It will

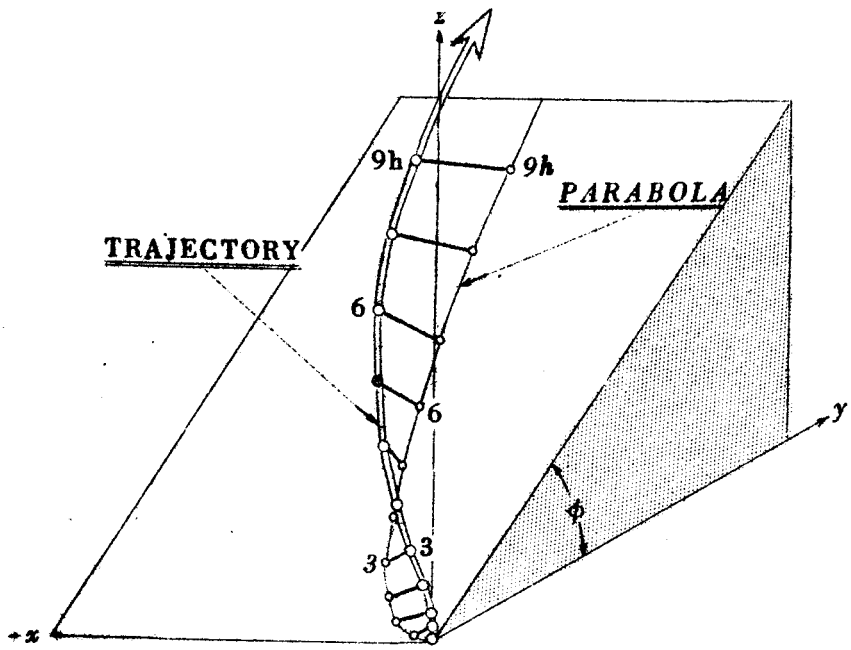

Fig. 104. Showing the trajectory of the convection wind, computed for the latitude of 45 degrees N and the acceleration field directed upward.

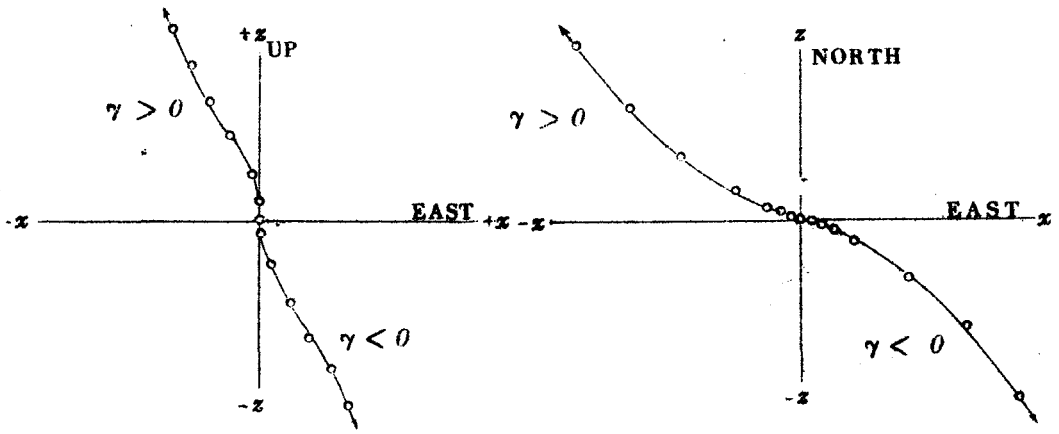

Fig. 105. Left: vertical component of the trajectory. Right: horizontal component of the trajectory.

be seen in the figure that the air moves upward, gradually changing its direction of movement westward while the northerly speed increases proportional to the time lapsed. The trajectories projected on the vertical and horizontal surfaces are shown in Fig. 105.

THE RESISTANCE UPON THE CONVECTION WIND

If the convection winds develop, according to the vertical acceleration; the horizontal convergence must be followed with. Or else, in the portion from which the airs have risen, there must start a low pressure which would pull back the ascending airs downward. On the other hand, the air converging into that portion should be resisted by the earth's surface, showing that the resistances of the earth's surface which act upon the converging airs are the force to prevent the development of the convection wind. Thus, the convection wind is accelerational no more, but it reaches the terminal velocity.

The time by which the convection wind reaches the terminal velocity is not known but it will depend upon the roughness of the earth's surface just as in the case where the horizontal winds are resisted.

If we assume that the convection wind balances to the resistance directed toward the opposite direction to the wind speed represented by (47a), the tangent of the direction of the horizontal wind vector must be

$$\frac{v}{u} = -\sin\phi \left(\frac{2\omega t - \sin 2\omega t}{1 - \cos \omega t} \right), \qquad (51)$$

where the value in the parentheses depends upon the time by which the convection wind reaches its terminal velocity. From this, it can be said, when $-\frac{1}{\rho}\frac{\partial cP}{\partial z}$ is positive,

(1) the convection wind is directed westward on the equator, and

(2) as the latitude increases, the direction changes as follows:

$$W \rightarrow WNW \rightarrow NW,$$

(3) while the air rises upward.

But when $-\frac{1}{\rho}\frac{\partial cP}{\partial z}$ is negative,

(4) the convection wind is directed eastward on the equator, and

(5) as the latitude increases, the direction changes as follows:

$$E \rightarrow ESE \rightarrow SE,$$

(6) while the air subsides.

Each component of the convection wind velocity is proportional to the vertical acceleration, therefore, as shown in Fig. 106, the

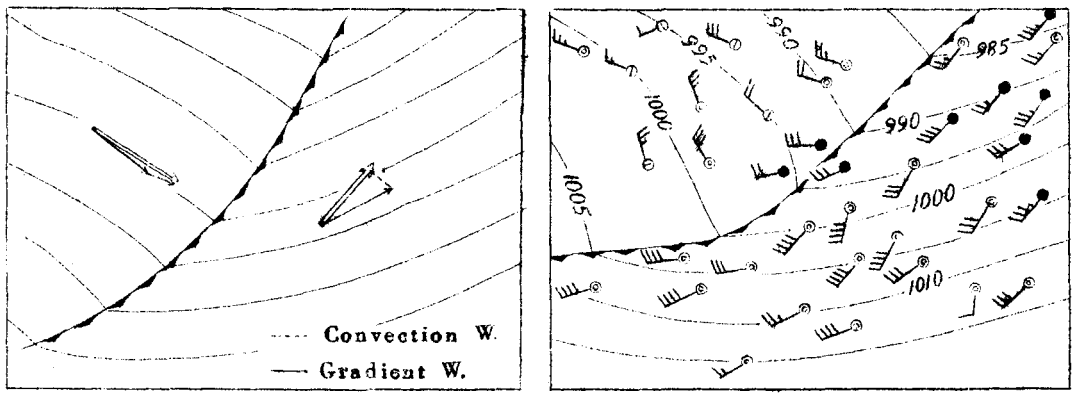

Fig. 106. Convection winds in both sectors of a cold front.

directions of the wind in both sectors of a cold front have quite different feature. In the warm sector, where the accelerations are usually upward, the prevailing winds shift north-westward resulting in the larger deviation angle than expected.

In the cold sector, the downward accelerations shift the gradient winds south-eastward. A great number of examples are seen in our dayly weather analyses.

§ 8 Vertical Front with Infinite Straight Edge.

Replacing the value of k in (40a) & (40b) by zero, we have the excessive pressure,

$$eP = \frac{(\rho_c - \rho_w)g}{\pi}\left\{ h\tan^{-1}\frac{h}{c} - c\log\sqrt{\frac{h^2+c^2}{c^2}}\right\} + (\rho_c - \rho_w)\,g\,h \qquad (52a)$$

where the last term is used only when c is negative.

The convection pressure is

$$cP = \frac{(\rho_c - \rho_w)g}{\pi}\left\{ h\tan^{-1}\frac{h}{c} - c\log\sqrt{\frac{h^2+c^2}{c^2}}\right\} \qquad (52b)$$

At the boundary surface, according to the conventional idea, the pressure must be considered to be discontinuous. In the new treatment, however, if we approach the surface from the warm air side, we have the limiting value.

$$\lim_{c\to+0} eP = \frac{(\rho_c - \rho_w)g}{\pi}\,\frac{\pi h}{2} = \frac{1}{2}(\rho_c - \rho_w)\,g\,h \qquad (53a)$$

while that for the cold air side is

$$\lim_{c\to-0} eP = \frac{(\rho_c - \rho_w)g}{\pi}\,\frac{-\pi h}{2} = -(\rho_c - \rho_w)\,g\,h = \frac{1}{2}(\rho_c - \rho_w)\,g\,h \qquad (53b)$$

It is evident that the excessive pressure is continuous even at the boundary surface, with the air pressure of

$$P = eP + \int_Z^\infty \rho_w\, g\, dz = \frac{1}{2}\int_Z^\infty (\rho_c - \rho_w)\,g\,dz + \int_Z^\infty \rho_w\, g\, dz$$

$$= \frac{1}{2}\int_Z^\infty \rho_c\, g\, dz + \frac{1}{2}\int_Z^\infty \rho_w\, g\, dz \qquad (54)$$

This is the mean value of the pressures inside the warm and cold air-

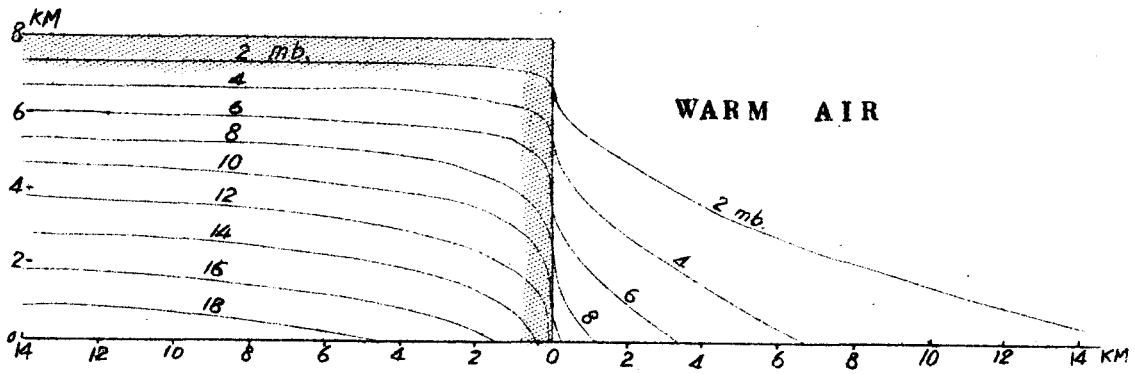

Fig. 107. Distribution of pressure across a frontal surface.

masses. The pressure distribution through the frontal surface is shown in Fig. 107.

The vertical and horizontal accelerations are known from the formulas (41a) and (41b). They are

$$\gamma^{\circ} = \frac{B^{\circ}}{\pi} \tan^{-1}\frac{h}{c}, \qquad \alpha^{\circ} = \frac{B^{\circ}}{\pi} \log \sqrt{\frac{h^2 + c^2}{c^2}} \qquad \text{.....(55)}$$

where $B^{\circ} = \frac{\rho_c - \rho_w}{\rho_0} g$. The acceleration pattern is presented in Fig.108.

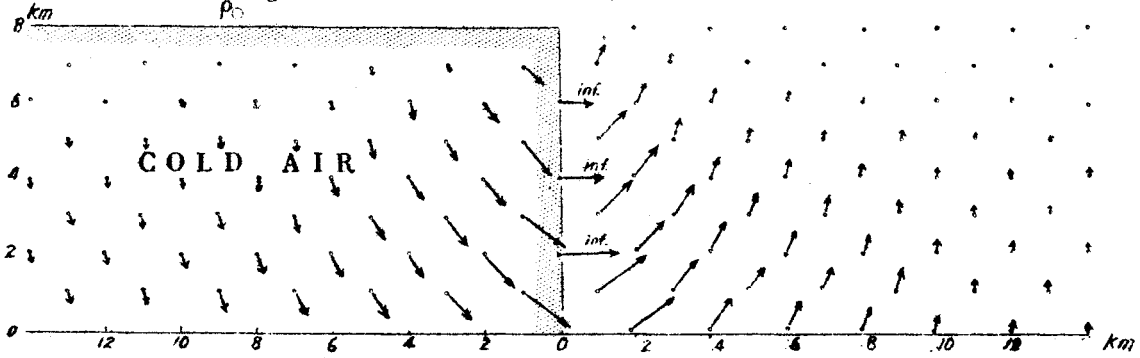

Fig. 108. Acceleration pattern.

It will be seen that the resultant accelerations are vertical at the frontal surface with infinite amount. In order to avoid the occurrence of such unreasonable value, we solve the problem of vertical front with gradually changing density distribution.

According to the infinite acceleration at the boundary, the vertical front must have the density distribution changing continuously in the frontal zone. Now we consider the front shown in Fig. 109.

To compute the acceleration caused by such a front, we make the sammation of the accelerations caused by the imaginary vertical front with the finite density jump for every Δc interval. Thus the

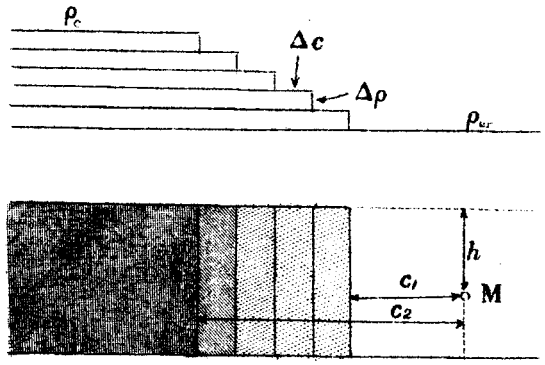

Fig. 109. To get the acceleration at M.

vertical acceleration at M is given by

$$\gamma^{\circ} = \frac{\Delta\rho}{\rho_{\circ}\pi}\left(tan^{-1}\frac{h}{c_1} + tan^{-1}\frac{h}{c_1+\Delta c} + tan^{-1}\frac{h}{c_1+2\Delta c} + \cdots\cdots + tan^{-1}\frac{h}{c_2}\right)$$

If the density gradient be $G\frac{g}{cm^3}/cm$, we substitute the relation

$$G = -\frac{\Delta\rho}{\Delta c} = -\frac{d\rho}{dc} = +\frac{d\rho}{dx}$$

into the above formula changing the sammation into integration, thus:

$$\gamma^{\circ} = -\frac{gG}{\rho_{\circ}\pi}\int_{c_1}^{c_2} tan^{-1}\frac{h}{c}\,dc$$

$$= \frac{gGh}{\rho_{\circ}\pi}\left(-\frac{c_2}{h}tan^{-1}\frac{h}{c_2} + \frac{c_1}{h}tan^{-1}\frac{h}{c_1} - log\sqrt{\frac{h^2+c_2^2}{h^2+c_1^2}}\right) \cdots\cdots (56a)$$

In the same way, the horizontal acceleration is known to be

$$\alpha^{\circ} = -\frac{gG}{2\rho_{\circ}\pi}\int_{c_1}^{c_2} log\,\frac{h^2+c^2}{c^2}\,dc$$

$$= \frac{gG}{\rho_{\circ}\pi}\left(h\,tan^{-1}\frac{c_1}{h} - h\,tan^{-1}\frac{c_2}{h} + c_2 log\sqrt{\frac{h^2+c_2^2}{c_2^2}} - c_1 log\sqrt{\frac{h^2+c_1^2}{c_1^2}}\right) \cdots\cdots (56b)$$

Using these formulas the vertical accelerations are drawn in Fig.110.

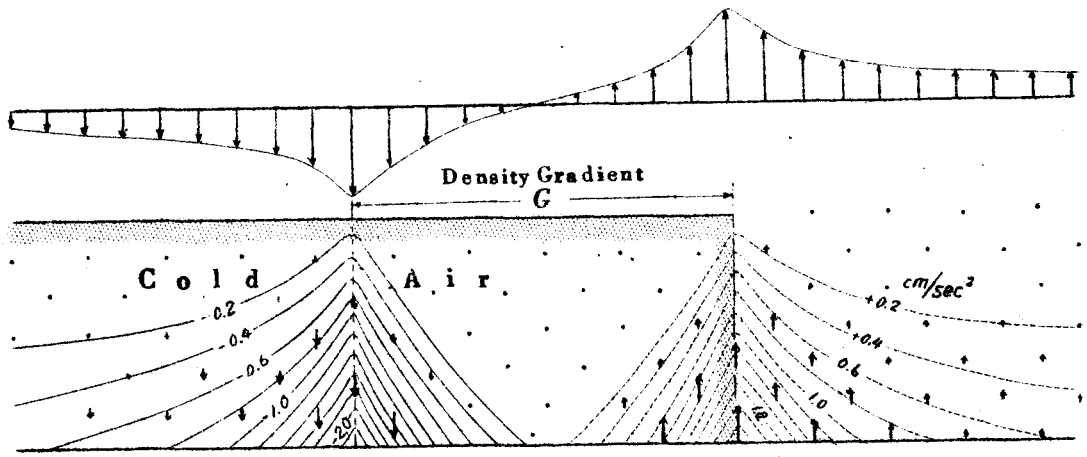

Fig. 110. Vertical accelerations around the vertical cold front with continuously changing density.

It is evident that the accelerations at the boundary are no more infinite. The most interesting features of the buoyancy pattern are that the largest values appear at the location where the density gradient changes abruptly, and that any appreciable acceleration is not

expected in the zone of constant density gradient.

§ 8 Approximation of the Formulas for Large Scale Phenomena.

If we want to compute the vertical accelerations for the dayly synoptic situation, the density jump separated by a surface would not be expected. Usually, as shown in Fig. 111, the density for a warm air-mass increases up to that for the cold air-mass continuously. It is necessary, therefore, to set up the formula capable of computing the acceleration field for an arbitrary distribution. As the height of the atmosphere is very small comparing with the horizontal extension, the absolute values of b and c in the formulas are, in many cases, more than 10 times larger than h, namely

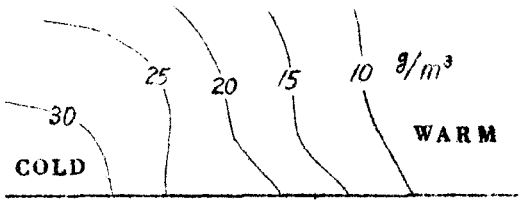

Fig. 111. Schematical distribution of density anomaly.

$$\left|\frac{h}{c}\right| < \frac{1}{10} \quad , \quad \left|\frac{h}{b}\right| < \frac{1}{10}$$

This fact shows us that the formulas (56a) & (56b) can be reduced to

$$\gamma^{\circ} = \frac{g\,G\,h}{\rho_0 \pi} \log\left|\frac{c_1}{c_2}\right| \qquad \text{(57a)}$$

$$\alpha^{\circ} = -\frac{g\,G\,h}{\rho_0} \quad \text{(in the zone of changing density)} \qquad \text{(57b)}$$

$$= 0 \quad \text{(in the other zones)} \qquad \text{(57c)}$$

respectively.

Using the principle of superposition, the acceleration at the surface caused by a density gradient aloft can be computed. If we use the notations in Fig. 112, the vertical acceleration at M computed by (57a) is

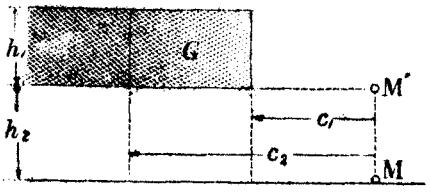

Fig. 112. To compute the accelerations at M and M'.

$$\frac{g\,G(h_1+h_2)}{\rho_0\,\pi}\log\left|\frac{c_1}{c_2}\right| - \frac{g\,G\,h_2}{\rho_0\,\pi}\log\left|\frac{c_1}{c_2}\right| = \frac{g\,G\,h_1}{\rho_0\,\pi}\log\left|\frac{c_1}{c_2}\right| \quad \text{(58a)}$$

According to (57), this is the vertical acceleration at M′ just above the point M in the figure. It is obvious, therefore, that the acceleration is the same at any point on the line M M′. In the similar manner it can be proved that the formulas (25b) & (25c) can be applied in the same way.

HORIZONTAL ACCELERATION IN LARGE SCALE PHENOMENA

Differentiating the relation,

$$P = wP + cP$$

with respect to x, we obtain

$$\frac{\partial P}{\partial x} = \frac{\partial wP}{\partial x} + \frac{\partial cP}{\partial x}$$

$$\fallingdotseq \frac{\partial wP}{\partial x} = g\,h\,\frac{\partial \rho}{\partial x} = g\,h\,G \quad \text{(58b)}$$

Namely, in the practical case, change in air pressure is caused only by the density gradient within the layer of the thickness h. The formula(57b) can be transcribed into

$$\alpha^{\circ} = -\frac{gGh}{\rho_0} = -\frac{1}{\rho_0}\frac{\partial P}{\partial x}. \quad \text{(58c)}$$

This fact shows that the conventional formula,

$$\frac{du}{dt} = -\frac{1}{\rho}\frac{\partial P}{\partial x}$$

holds good for the case of horizontal accelerations.

VERTICAL ACCELERATION IN LARGE SCALE PHENOMENA

If the density is homogeneous in y-direction, the vertical acceleration can be computed. As shown in Fig. 113, we divide the zone where the density is different in x-direction into uniform distances of Δx that is larger than about 300 km so as to make $\frac{1}{2}\Delta x$ more than 10 times larger than the height of the zone. After numbering the vertical segments from the bottom, thus:

$$n = 1, 2, 3, 4, 5, 6, \ldots\ldots \text{ etc.}$$

and the horizontal segments, thus:

$$m = \ldots\ldots -3, -2, -1, 0, +1, +2, +3, \ldots\ldots \text{ etc.}$$

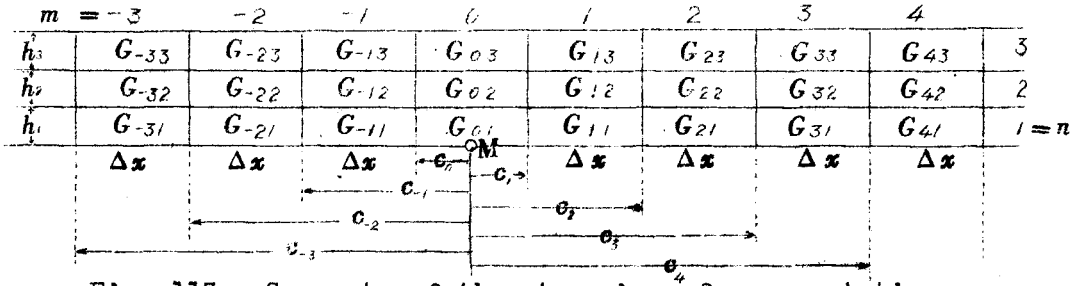

Fig. 113. Segments of the atmosphere for computation of the acceleration.

we compute the vertical acceleration at M, the middle point of the bottom of the segment G_{01}. Applying the formula(57a) for the segments in Fig. 113, we obtain the vertical acceleration at M,

$$\gamma^{\circ} = \frac{g}{\rho_{\circ}\pi} \sum_{-m}^{+m} \log \left| \frac{c_{m+1}}{c_m} \right| \sum_{1}^{n} G_{mn}\, h_n$$

$$= \frac{1}{\rho_{\circ}\pi} \sum_{-m}^{+m} \left(\frac{\Delta P}{\Delta x}\right)_m \log \left| \frac{c_{m+1}}{c_m} \right| \qquad \text{(59a)}$$

whence, from (58b), we know

$$\left(\frac{\Delta P}{\Delta x}\right)_m \doteq g \left(G_{m1} h_1 + G_{m2} h_2 + G_{m3} h_3 + \cdots \right)$$

The practical acceleration is, therefore,

$$\gamma = \frac{1}{\rho\pi} \sum_{-m}^{+m} \left(\frac{\Delta P}{\Delta x}\right)_m \log \left| \frac{c_{m+1}}{c_m} \right| \qquad \text{(59b)}$$

This formula is very convenient since it gives the method by which the vertical acceleration is to be computed using our ordinary synoptic charts.

Using the approximate relation,

$$\frac{1}{\rho} \frac{\Delta P}{\Delta x} \doteq g \frac{\Delta H}{\Delta x}$$

we transcribe the formula(59a) into

$$\gamma = \frac{g}{\pi} \sum_{-m}^{+m} \left(\frac{\Delta H}{\Delta x}\right)_m \log \left| \frac{c_{m+1}}{c_m} \right| \qquad \text{(59c)}$$

where H is the height of constant pressure level. Because of the fact that the height gradient not on a constant altitude must be used for the present computation, the results computed by this formula are not so accurate but the distribution of the vertical accelerations on high level chart can be known approximately.

To make the computation of the formula easier, the values of $\log\left|\frac{C_{m+1}}{C_m}\right|$ are tabulated in Table 5, which is available as long as we divide the zone into uniform horizontal segments Δx.

m	-20	-19	-18	-17	-16	-15	-14	-13
log	-0.050	-0.052	-0.054	-0.058	-0.061	-0.066	-0.071	-0.077
m	-12	-11	-10	- 9	- 8	- 7	- 6	- 5
log	-0.083	-0.091	-0.100	-0.110	-0.126	-0.143	-0.167	-0.200
m	- 4	- 3	- 2	- 1	0	1	2	3
log	+0.251	-0.333	-0.511	-1.100	0.000	+1.100	+0.511	+0.333
m	4	5	6	7	8	9	10	11
log	+0.251	+0.200	+0.167	+0.143	+0.126	+0.110	+0.100	+0.091
m	12	13	14	15	16	17	18	19
log	+0.083	+0.077	+0.071	+0.066	+0.061	+0.058	+0.054	+0.052

Table 5. The value of $\log\left|\frac{C_{m+1}}{C_m}\right|$ as the function of m.

§ 9 Proposed Mechanism of Typhoon Initiation.

The accelerations upon the air of density ρ° in the intertropic zone with the pressure distribution represented by the top curve in Fig. 114 are computed by using (59a). The computations are carried out after assuming that the pressure gradient vanishes at the altitude of 10 km. As will be seen in the figure, this is the case where the pressure distribution is symmetrical with respect to the front, however, when the southern part of the zone is filled with the cold air-mass from the southern hemisphere, the distribution varies appre-

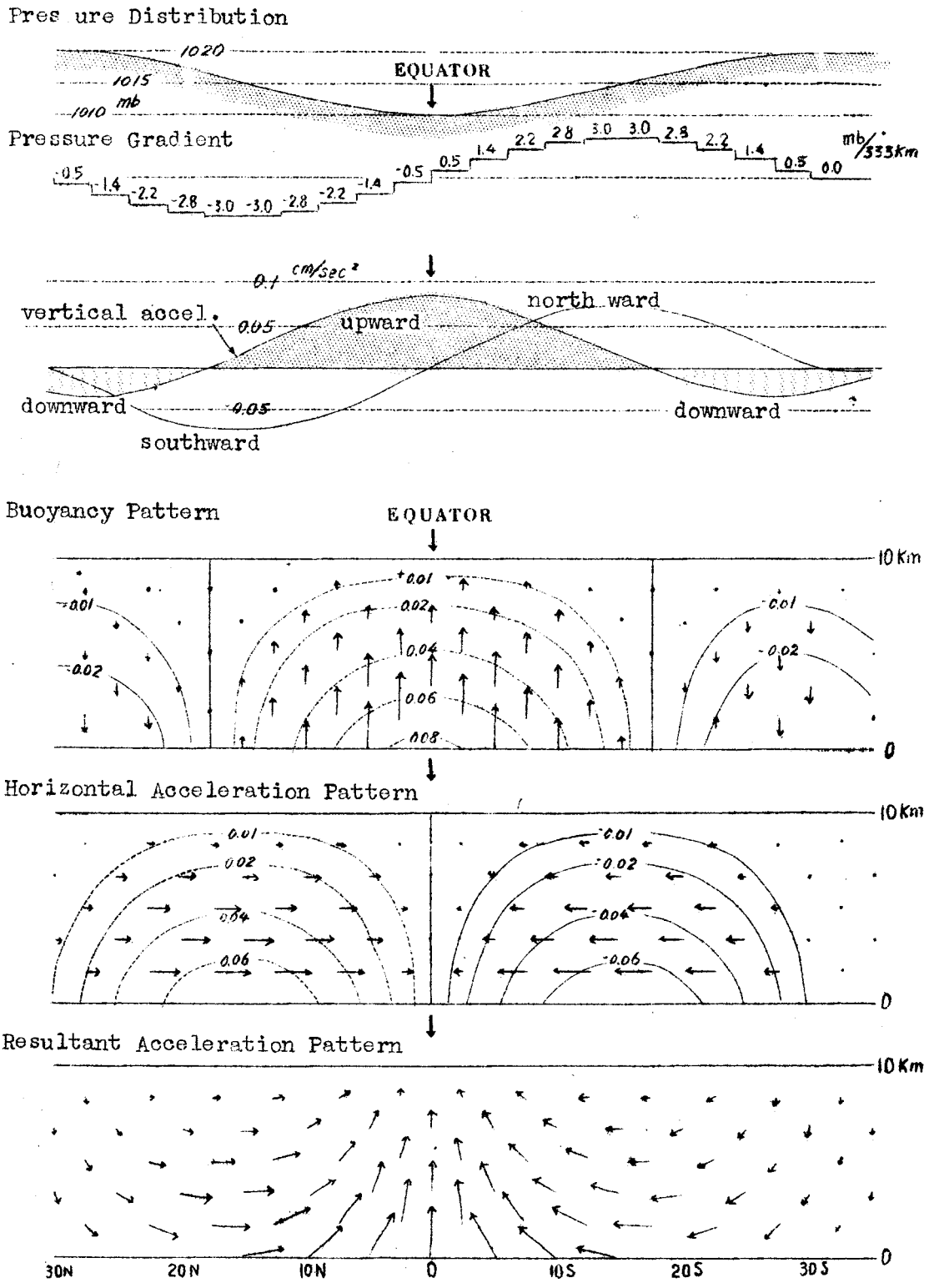

Fig. 114. Acceleration Pattern in the intertropic zone. The accelerations are computed for the pressure distribution of annual mean condition.

ciablly.

The vertical accelerations for such a case are presented in Fig. 115. The top curve shows the surface pressure distribution and the

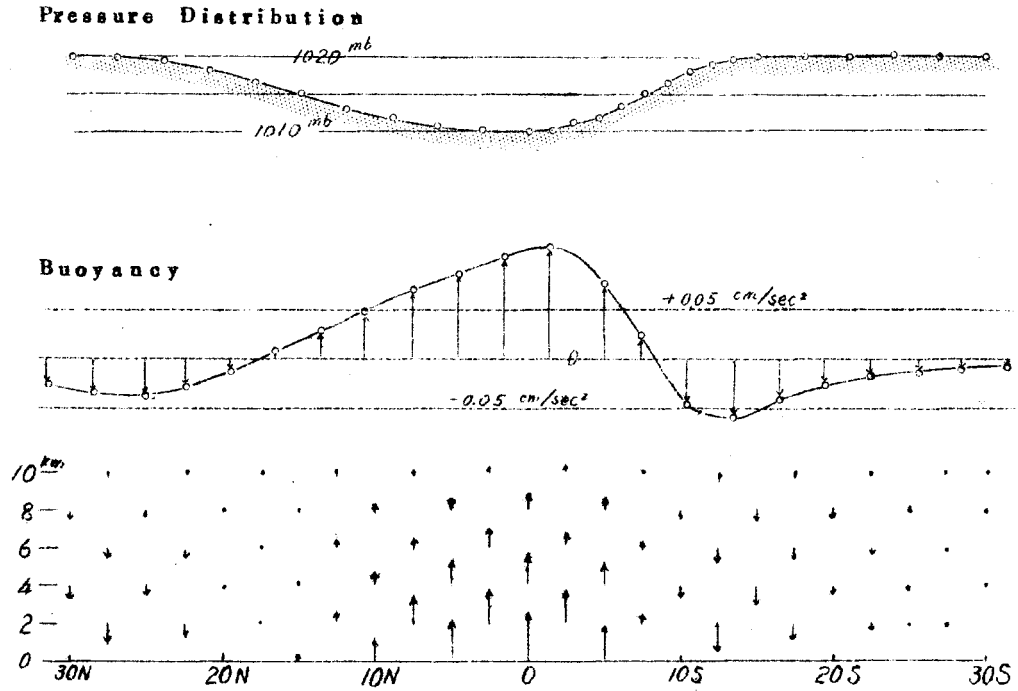

Fig. 115. Distribution of vertical acceleration in the intertropic frontal zone when its southern half is occupied by cold air from the southern hemisphere.

middle one the vertical acceleration. It will be seen that the cold air from the south results in a very large buoyancy in the frontal zone and downward acceleration south of the front.

INITIATION OF TROPICAL STORM

Using the fact that the buoyancy force in the intertropic frontal zone increases, it is possible to explain the initiation of a typhoon. As has been pointed out by Dr. Syono(5), decrease in pressure, especially in the lower levels, caused by heavy presipitation inside the cumulonimbi would develop into the tropical circulation. The cause of heavy showers can be explained by the present theory.

As shown in Fig. 116-a, the maximum buoyancy inside the intertropic frontal zone is no more than 0.1 cm/sec^2. This amount is, however, not enough since, according to the formula,

$$V = \sqrt{2ah}$$

where a is the acceleration, h the altitude through which air is accelerated by a, V the terminal velocity; if the air on sea level were to be accelerated, without friction, up to 5 km level, the terminal velocity would be about 3 m/sec. It is known that, on an ordinary day when such amount of the buoyancy is expected, there develop intermittent squalls which pour in short duration with high intensity.

When the air pressure south of the intertropic front increases, the pattern of the vertical acceleration changes appreciablly, and as will be seen in Figs.113-b-c-d, the buoyancy inside the low pressure area increases up to several times, say 0.3 cm/sec^2. On the other hand, a marked subsidence zone develops along the south of the front. The cumulonimbi which would presipitate heavy shower continuously, that would make the pressure lower, will develop and the processes of typhoon initiation presented by Dr. Syono will begin.

It should be pointed out here that, though we require the existence of the cold air outbreaking from the southern hemisphere, the mechanism of the shower initiation is quite different from the idea of frontal theory which was established to explain the typhoon initiation by using the frontal wave. In the present explanation, the high density masses from the south play a role to increase the convection pressure, namely its vertical gradient. Thus we do not need the contact of warm and cold air-masses at the intertropic frontal surface which is very difficult to imagine.

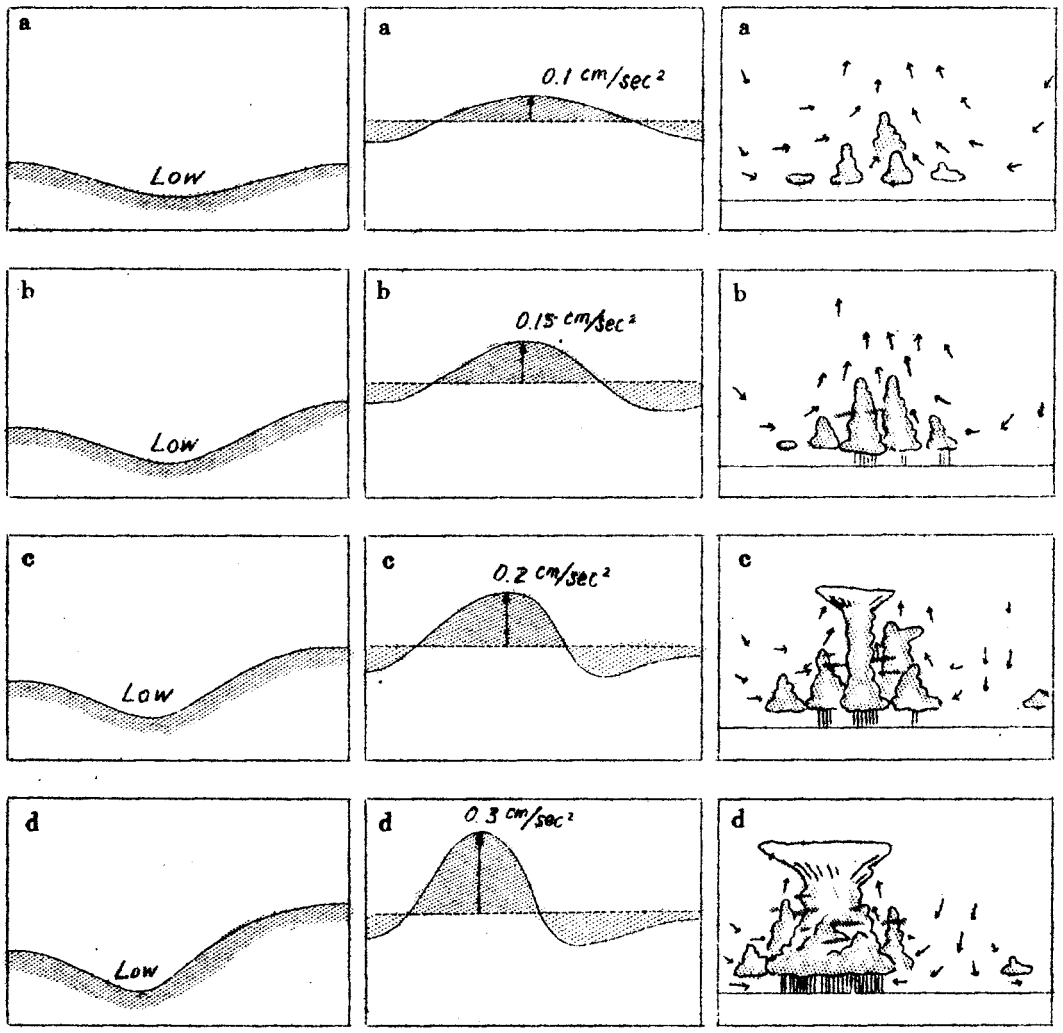

Fig. 116. Showing the initiation of heavy showers which would develop into a tropical storm.

(a) Ordinary day free from the cold air from the southern hemisphere.
(b) As the cold air south of the equator develops, the buoyancy force in the intertropic zone increases.
(c) If the cold air which might change into warm air enter the south of the intertropic front, the pressure unbalance results in the large buoyancy.
(d) The stage in which heavy showers develop.

The most interesting and important result which must be emphasized here is the fact that the airs from the south, which might be virtually colder, undergo buoyancy as well as the warm air locating before. It is evident that the heavy showers develop inside the airs reaching the frontal zone from the south, and that the cause is not the lifting effect of the cold air-mass that produces upward motion but the pressure or density distribution itself inside a large area in the vicinity.

Schematical chart showing the horizontal distribution of the vertical accelerations is presented in Fig. 117. The intensity of the accelerations is represented by the density of the negative and positive signs.

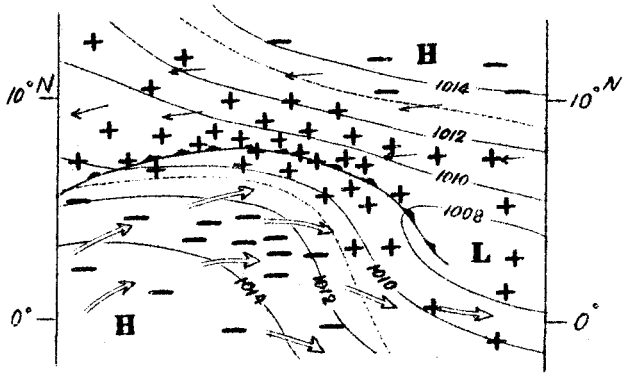

Fig. 117. Schematical figure showing the distribution of upward(+) and downward(-) accelerations.

§ 10 Buoyancy Caused by Arbitrary Warm or Cold Area.

We compute the excessive pressure in the field with warm area surrounded by cold one. Let ρ_w be the density of the warm air-mass, and ρ_c be that of the cold, the excessive pressure can be computed using (36b) after changing it into that for the cylindrical coordinates.

In the following computation, when the point whose pressure or the acceleration is in question is located inside a warm area, we use the subscript 1, while the point is located inside a cold area, we use the subscript 2.

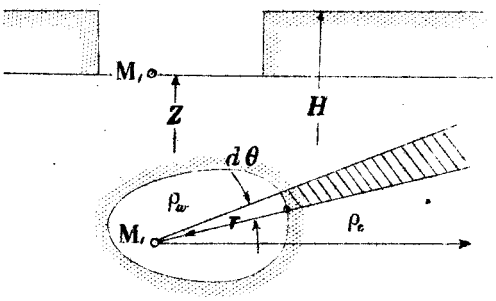

Fig.118. Computation of excessive pressure at M, inside a warm area.

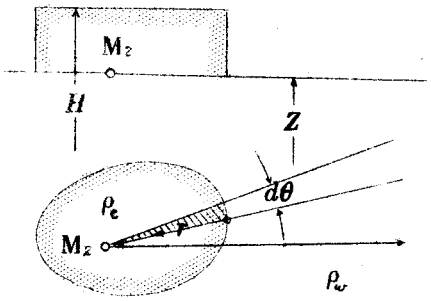

Fig.119. Computation of excessive pressure at M_2 inside a cold area.

The excessive pressures for M_1 and M_2 are, therefore,

$$eP_1 = \frac{1}{2\pi}\int_0^{2\pi}\int_Z^H\int_r^\infty \frac{(\rho_c-\rho_w)\,g\,(z-Z)\,r\,dr\,dz\,d\theta}{\{r^2+(z-Z)^2\}^{\frac{3}{2}}} \qquad (60a)$$

$$eP_2 = \frac{1}{2\pi}\int_0^{2\pi}\int_Z^H\int_0^r \frac{(\rho_c-\rho_w)\,g\,(z-Z)\,r\,dr\,dz\,d\theta}{\{r^2+(z-Z)^2\}^{\frac{3}{2}}} \qquad (60b)$$

where r is the distance of the point M from the boundary. Integrating the formulas, under the assumption that $(\rho_c-\rho_w)$ is constant, we obtain

$$eP_1 = \frac{(\rho_c-\rho_w)g}{2\pi}\int_0^{2\pi}\int_Z^H \frac{z-Z}{\sqrt{r^2+(z-Z)^2}}\,dz\,d\theta$$

$$= \frac{(\rho_c-\rho_w)g}{2\pi}\int_0^{2\pi}\left(\sqrt{r^2+h^2}-r\right)d\theta \qquad (61a)$$

$$eP_2 = \frac{(\rho_c-\rho_w)g}{2\pi}\int_0^{2\pi}\int_Z^H\left(1-\frac{(z-Z)}{\sqrt{r^2+(z-Z)^2}}\right)dz\,d\theta$$

$$= (\rho_c-\rho_w)\,gh - eP_1 \qquad (61b)$$

where $h = H - Z$. Next we compute the convection pressures, by using the relations,

$$cP = eP - ewP\,, \qquad ewP_2 = (\rho_c-\rho_w)\,gh\,.$$

The convection pressures are, therefore, written thus:

$$cP_1 = eP_1 \qquad (\because\ ewP_1 = 0) \qquad (61c)$$

$$cP_2 = eP_2 - (\rho_c-\rho_w)\,gh = -eP_1 \qquad (61d)$$

VERTICAL ACCELERATION

The vertical acceleration is given by differentiating the convection pressure with respect to z, namely,

$$\gamma_1^{\circ} = -\frac{1}{\rho_{\circ}}\frac{\partial cP_1}{\partial z} = \frac{B^{\circ}}{2\pi}\int_0^{2\pi}\frac{h}{\sqrt{r^2+h^2}}\,d\theta$$

$$= \frac{B^{\circ}}{2\pi}\int_0^{2\pi}\frac{1}{\sqrt{1+x^2}}\,d\theta$$

$$= \frac{B^{\circ}}{2\pi}\int_0^{2\pi}\psi\,d\theta \quad , \qquad (62a)$$

where $h = H - Z$, $x = r/h$, $B^{\circ} = \frac{\rho_c - \rho_w}{\rho_{\circ}}g$, and ψ the cyclone function for $a = 1$. We have also the vertical acceleration for the point M',

$$\gamma_2^{\circ} = -\frac{1}{\rho_{\circ}}\frac{\partial cP_2}{\partial z} = -\left(-\frac{1}{\rho_{\circ}}\frac{\partial eP_1}{\partial z}\right) = -\left(-\frac{1}{\rho_{\circ}}\frac{\partial cP_1}{\partial z}\right) = -\gamma_1^{\circ} \quad . \qquad (62b)$$

HORIZONTAL ACCELERATION

To compute the horizontal accelerations at M_1 locating inside a warm air-mass of ρ_w, surrounded by ρ_c, we obtain first the excessive pressure at M_1 caused by the area element ABCD in Fig. 120. Using the formula(61a) we obtain

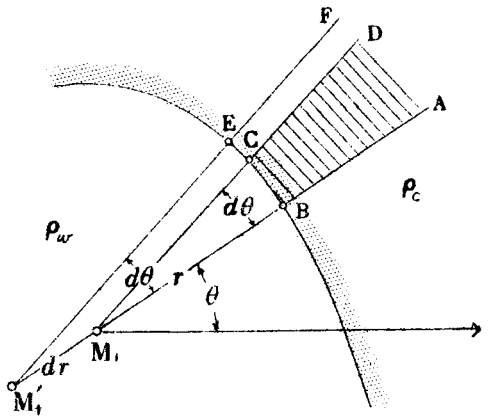

Fig. 120. To obtain the horizontal acceleration caused by ABCD.

$$eP_1' = (\rho_c - \rho_w)\frac{g}{2\pi}\left(\sqrt{r^2+h^2} - r\right)d\theta$$

$$eP_1' + de P_1' = (\rho_c - \rho_w)\frac{g}{2\pi}\left[\left\{\sqrt{(r+dr)^2+h^2} - (r+dr)\right\}d\theta - log\,\frac{r+\sqrt{r^2+h^2}}{2r}\,dl\right],$$

where the second term in the right side is the excessive pressure caused by the area DCEF, and $dl = dr\,d\theta$. Dividing the difference of these two formulas by dr, we obtain

$$\frac{\partial e R'}{\partial r} = (\rho_c - \rho_w)\frac{g}{2\pi}\left\{\frac{\partial}{\partial r}\left(\sqrt{r^2+h^2}-r\right) - log\frac{r+\sqrt{r^2+h^2}}{2r}\right\} d\theta$$

Replacing r/h by x, and $1/\sqrt{1+x^2}$ by ψ, we have

$$-\frac{1}{\rho_0}\frac{\partial eR'}{\partial r} = \frac{B^\circ}{2\pi}\left\{1 - x\psi + log\frac{1}{2}\left(1+\frac{1}{x\psi}\right)\right\} d\theta$$

$$= \frac{B^\circ}{2\pi}\varphi\, d\theta \qquad (63a)$$

where φ is the quantity in the braces. Thus we obtained the similar formula to (62a) used for the computation of vertical acceleration.

On the other hand, when the point is located inside the cold air using the relation(61), we have

$$-\frac{1}{\rho_0}\frac{\partial eP_2}{\partial r} = -\left(-\frac{1}{\rho_0}\frac{\partial eR}{\partial r}\right) \qquad (63b)$$

The x-ward acceleration can be obtained by integrating the x-component of the acceleration element given by (63a), thus:

$$\alpha_1^\circ = -\frac{1}{\rho_0}\frac{\partial eP_1}{\partial x} = \frac{B^\circ}{2\pi}\int_0^{2\pi}\varphi\,(-\cos\theta)\,d\theta = \frac{B^\circ}{2\pi}\int_0^{2\pi}\varphi\, d(-\sin\theta) \qquad (64a)$$

In the same way, we integrate the y-component

$$\beta_1^\circ = -\frac{1}{\rho_0}\frac{\partial eP_1}{\partial y} = \frac{B^\circ}{2\pi}\int_0^{2\pi}\varphi\,(-\sin\theta)\,d\theta = -\frac{B^\circ}{2\pi}\int_0^{2\pi}\varphi\, d(\cos\theta) \qquad (64b)$$

The horizontal accelerations obtained here are the case where the point in question is located inside the warm air, but if it is inside the cold, we obtain them from (63b) which can be transcribed as:

$$\alpha_2^\circ = +\alpha_1^\circ \quad , \quad \beta_2^\circ = -\beta_1^\circ \qquad (64c)$$

DIAGRAMS TO COMPUTE α, β, AND γ.

The formulas (62a), (64a) and (64b) show the fact that the accelerations can be integrated using the acceleration diagrams in Fig. 118. To obtain the accelerations, it is convenient to carry out in the following way.

(A) If the point M is located in the warm-air side of the tangent

(A) Acceleration Diagram for " γ ", the Buoyancy.

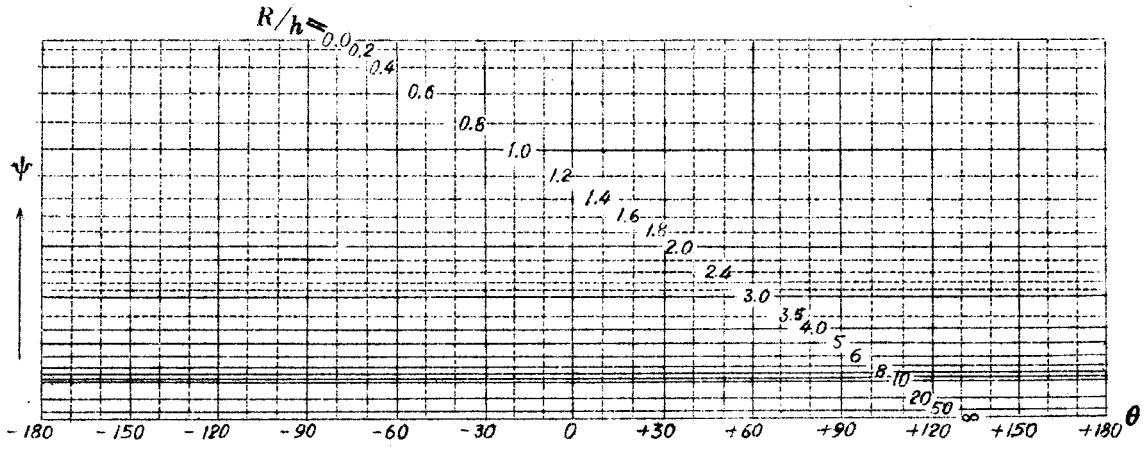

(B) Acceleration Diagram for α. (C) Acceleration Diagram for β.

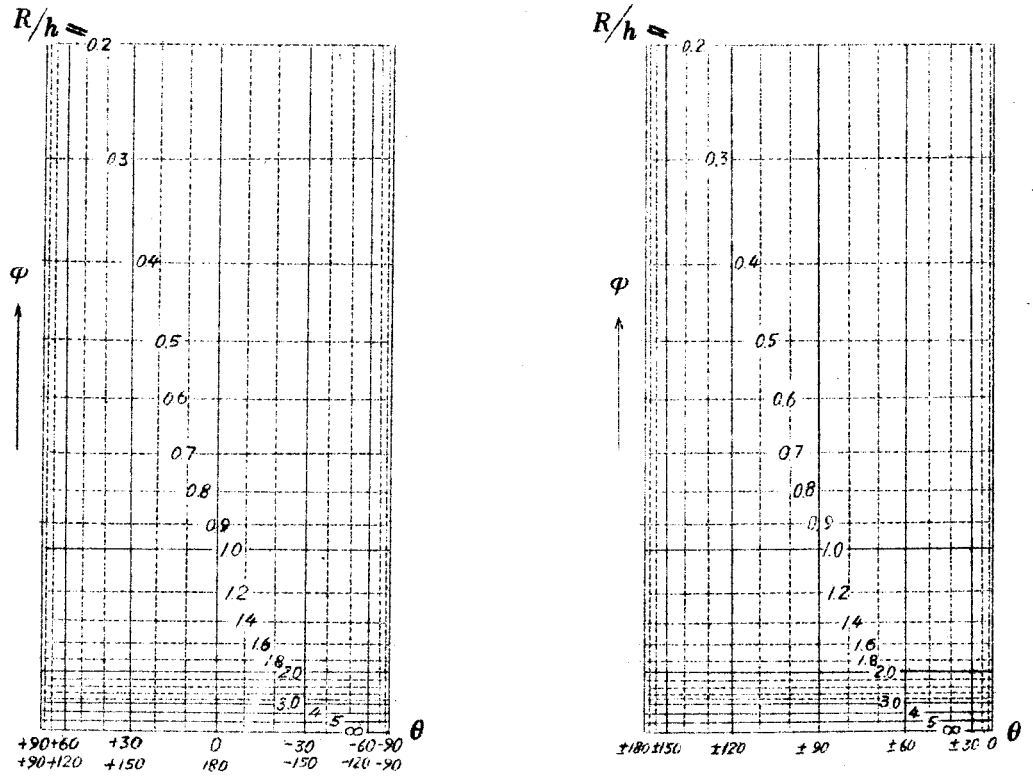

Fig. 121. Acceleration Diagrams for α, β, and γ. These diagrams are used when we want to compute the accelerations caused by an area having a temperature higher or colder than its environments.

To compute the horizontal acceleration pattern, it is convenient to utilize the excessive pressure diagram in Fig. 133.

at the boundary, we plot the curve so that θ increases, however, if the point is located in the cold air side, we do it as θ decreases.

(B) We put the arrow along the curves on the diagram in order to represent the plotted direction.

(C) It is evident, from (64a) (64b) and (64c), that the area under the curve directed rightward shows the positive acceleration. In the opposite case, the sign reverses.

(D) Usually the curves on the diagrams are closed, therefore, the area enclosed is proportional to the acceleration.

(E) When the point is located on the boundary, horizontal acceleration is infinite, and it is directed from cold to warm area.

The accelerations at M. inside the warm area are shown in Fig. 122. As was noticed above, the directions are always entered in the

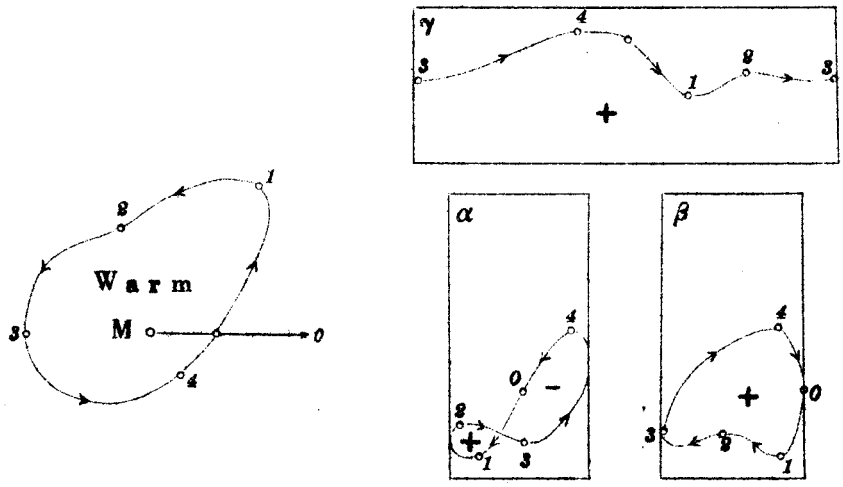

Fig. 122. Representation of the accelerations on the diagrams when the point is located inside a warm area.

figure, so that the acceleration directions can be determined easily.

When the point is located outside the enclosed warm area, the curve on the vertical acceleration diagram closes, and the direction

reverses. It will be understood, comparing the buoyancies inside and outside the warm area, that the downward acceleration is very small.

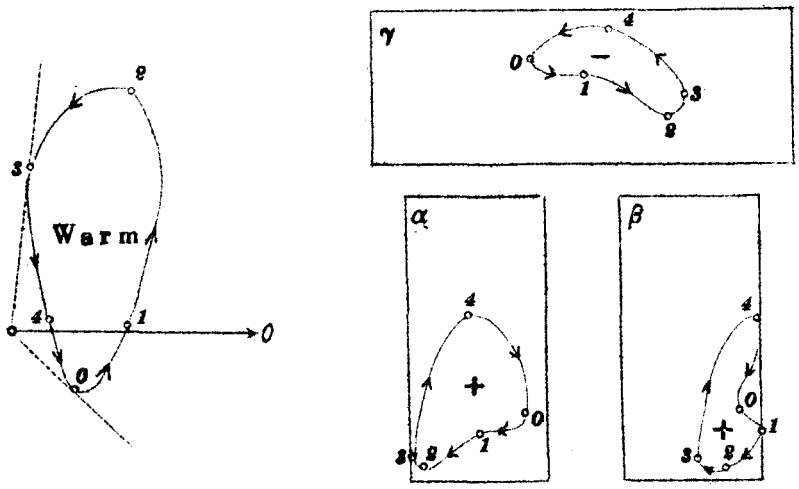

Fig. 123. Showing the curves on the acceleration diagrams when the point is located outside the enclosed warm area.

This is the reason why the airs surrounding a cloud do not descend rapidly to compensate the ascending current. By using the diagram, it is not possible to obtain the resultant acceleration in horizontal direction directly, however, it can be obtained by adding the x- and y-components.

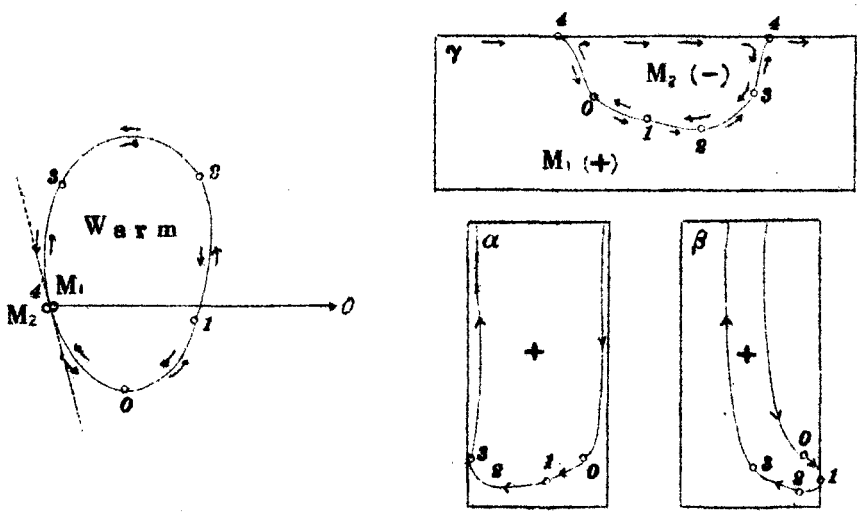

Fig. 124. Showing the acceleration at the boundary.

It might be peculiar to get the infinite acceleration at the boundary. This is true since we have assumed a density jump there. The curve on the vertical acceleration diagram in Fig. 124 shows that vertical accelerations at M_1 and M_2 are quite different in amount and direction. That is to say, the amount on the enclosed side is larger than that on the other, but the sum of the absolute values is just the same as the conventional buoyancy force.

ACCELERATION FAR FROM THE BOUNDARY

(1) Straight Boundary.

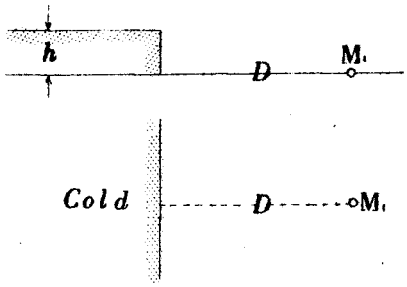

Fig. 125. To obtain the accelerations far from a straight edge.

D	$\pi\alpha^\circ$	$\pi\gamma^\circ$
5	0.o20000	0.200000
10	0.oo5000	0.100000
20	0.oo1250	0.o50000
30	0.ooo555	0.o33333
40	0.ooo312	0.o25000
50	0.ooo200	0.o20000
60	0.ooo139	0.o16666
70	0.ooo102	0.o14286
80	0.oooo78	0.o12500
90	0.oooo62	0.o11111
100	0.oooo50	0.o10000
200	0.oooo12	0.oo5000
300	0.oooooo5	0.oo3333
400	0.oooooo3	0.oo2500
500	0.oooooo2	0.oo2000
km	cm/sec	

Table 6. Decrease in acceleration far from a straight boundary.

The acceleration at M_1 in Fig. 125 is given by (55). When the distance is very large, comparing with the height of the air-mass of different density, they are reduced to

$$\alpha^\circ = \frac{B^\circ}{\pi} \log \sqrt{1+\frac{h^2}{D^2}} \fallingdotseq \frac{B^\circ}{2\pi}\left(\frac{h}{D}\right)^2 \qquad (65a)$$

$$\gamma^\circ = \frac{B^\circ}{\pi} \tan^{-1}\frac{h}{D} \fallingdotseq \frac{B^\circ}{\pi}\left(\frac{h}{D}\right) \qquad (65b)$$

It is obvious that the buoyancy γ° decreases inversely proportional to the distance from the boundary, while that of x-direction decreases more rapidly or proportional to the inverse square of the distance. In the case where the height of the cold air-mass with straight frontal boundary is 10 km, at the distance of 1000 km from the boundary, there still exists the vertical acceleration of 1/300 B. The horizontal acceleration is, however, only

5/300000 B which is about 1/200 smaller than the vertical one.

(2) Circular Boundary. We consider the accelerations at M with distance D from the center of a circular warm or cold area. As the distance D is very large, the values of ψ and φ are reduced to

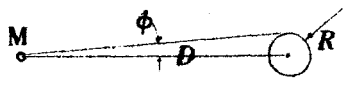

Fig. 126. To obtain the accelerations far from a circular boundary.

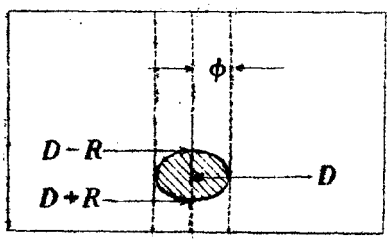

Fig. 127. Showing the curve on the vertical acceleration diagram for the point far from the circular area.

$$\psi \fallingdotseq \frac{1}{x} \quad , \quad \varphi \fallingdotseq \frac{3}{4}\frac{1}{x^2} .$$

The area on the vertical acceleration diagram corresponding to the given circular area is to be obtained, by assuming the elliptic shape. Therefore, the vertical and horizontal accelerations are obtained approximately, thus:

$$\gamma^{\circ} \fallingdotseq \frac{B^{\circ}}{2\pi} \pi \times \phi \times \frac{\partial \psi}{\partial x}\frac{R}{h} \fallingdotseq \frac{B^{\circ}}{2}\frac{hR^2}{D^3} \qquad (66a)$$

$$\alpha^{\circ} \fallingdotseq \frac{B^{\circ}}{2\pi} \pi \times \frac{R}{D} \cdot \frac{3\cdot 2}{4}\frac{h^3}{D^3}\frac{R}{h} = \frac{3}{4} B^{\circ}\frac{h^2R^2}{D^4} \qquad (66b)$$

As the result, it will be seen that the vertical acceleration decreases in proportion to the negative 3rd power of the distance, and that the horizontal acceleration to the negative 4th power. Comparing this result with that of the straight edge case, it will be understood that the effect of the pressure unbalance caused by a enclosed system vanishes so rapidly that we cannot detect it at a considerable distance.

§11 Application to Thunderstorm Convection

It was known, according to the Thunderstorm Project in U.S.A. (1), that there exist warm (up-draft) and cold (down-draft) areas

inside a thundercloud. The temperature corresponding to the density of the air which would produce atmospheric pressure must be T_{vw}, the temperature presented by the writer(4). That is

$$T_{vw} = (1 - w) T_v$$

where w is the mass(gr.) of water droplets imbedded within a gram of air. Cunningham and Miller(3) reported the water amount as much as 6.5 g/m' at the 700 mb level which would lower the temperature about 2 degrees. It is valuable to clarify the acceleration pattern within such systems as develop on thunderstorm day.

VERTICAL ACCELERATION

Distribution of buoyancy inside and outside a circular cloud

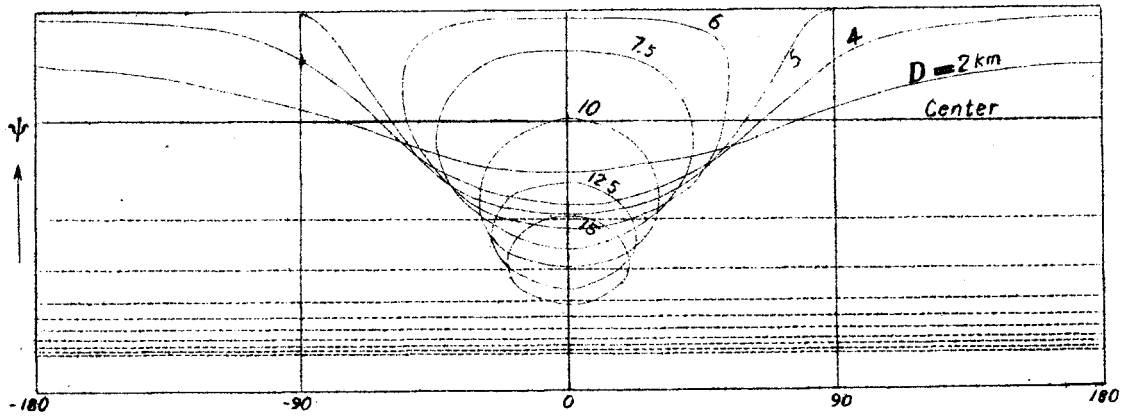

Fig. 128. Computation of buoyancy for 5 km level.

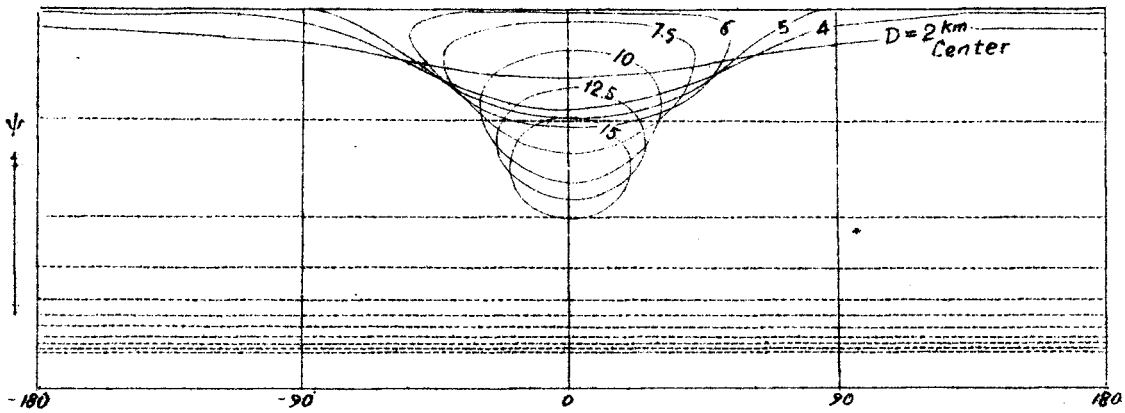

Fig. 129. Computation of buoyancy for the bottom of cloud.

with smaller density than of the environments was computed by the vertical acceleration diagrams in Figs. 128 & 129. Constants for the clouds are: $h = 10$ km, $R = 5$ km, $\rho_c - \rho_{\nu} = 3$ g/m³ (temp. diff. of about 1°C), $\rho_{5\,km} = 710$ g/m³, $\rho_{bottom} = 1160$ g/m³.

* * * * * * *

UNIT OF ACCELERATION

To carry out the practical evaluation of the accelerations it is desirable to use a suitable unit. The gravity is too large for the present case. The writer, therefore, want to put forward the acceleration unit comparable to the acceleration caused by the pressure gradient of 1 mb/1° latitude. The acceleration given to the unit mass of surface air is

$$\text{Acceleration} \fallingdotseq \frac{1}{\rho_{surface}} \cdot \frac{1\,mb}{111\,km}$$

The density of the surface air is different from place to place and from time to time; however, if we assume $\rho_{surface} = 1.2 \times 10^{-3}$ g/cm³, we have

$$\text{Acceleration} \fallingdotseq \frac{10^3 \times 1000}{1.2 \times 11100000} = 0.075 \text{ cm/sec}^2$$

It is convenient, therefore, to introduce the unit of

$$0.1 \text{ cm/sec}^2 = 1 \text{ A.U.}$$

and it may be termed "the acceleration unit"(abbreviated as A.U.).

* * * * * * *

D	Cloud Bottom	5 km Level	D	Cloud Bottom	5 km Level
0	22.8	32.3	20	-0.35	-0.33
2	22.9	32.9	30	-0.11	-0.10
4	23.0	35.9	40	-0.05	-0.06
5	23.3	37.4	50	-0.03	-0.02
5	-2.1	-7.9	60	-0.02	-0.01
6	-1.8	-6.3	70	-0.01	-0.01
8	-1.5	-3.9	80	-0.01	-0.00
10	-1.1	-2.3	90	-0.00	-0.00
15	-0.64	-0.76	100	-0.00	-0.00

Table 7. Buoyancy(A.U.) in and outside of a circular cloud.

The computed results are tabulated in Table 7. As will be seen in the table, within the cloud warmer 1°C than of the environments, there exists the acceleration of about 3 cm/sec² which would accelerate the air

to the speed

$$V = \sqrt{2 \div 3 \times H} \quad \text{cm/sec}$$

where, if H be 5 km = 500000 cm, the final speed would be 17 m/sec.

It will be understood that there is the gradient of convection pressure reaching as much as 30 A.U. which would be expected on the surface weather maps where the pressure gradient of 20 mb/1° latitude exists.

Outside the cloud, however, the downward acceleration is very small, and even at the boundary it is not more than 10 A.U. The dis-

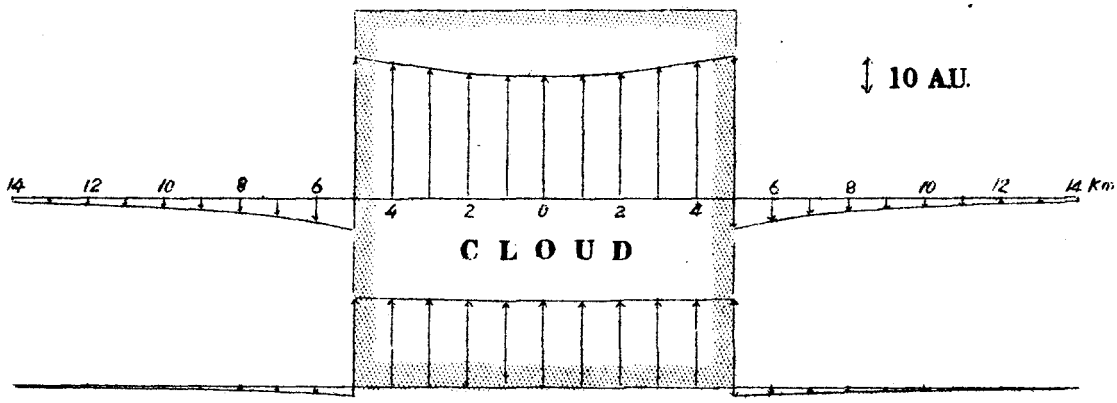

Fig. 130. Distribution of buoyancy in and outside the circular cloud.

tribution of buoyancy is shown in Fig. 130. As we go away from the cloud the downward acceleration decreases rapidly, and at the place 5 km from the cloud edge, it is about 1 to 2 A.U. Therefore, it can be considered that the downward current to compensate the up-draft develops only in the vicinity of a thundercloud.

HORIZONTAL ACCELERATION (ENTRAINMENT AND DETRAINMENT)

The horizontal inflow of the surrounding air has been discovered by the Thunderstorm Project, however, the reasons are remained unsolved yet. So long as we believe the conventional idea that the air

pressure propagates only downward, the horizontal force by which the surrounding airs entrain into a thundercloud is very difficult to be studied.

According to the new theory, the horizontal acceleration can be computed by using the horizontal acceleration diagrams in Fig. 118. And the entrainment process is the natural result which comes from the distribution of excessive pressure field formed by the extraordinary density distribution of thunderstorm.

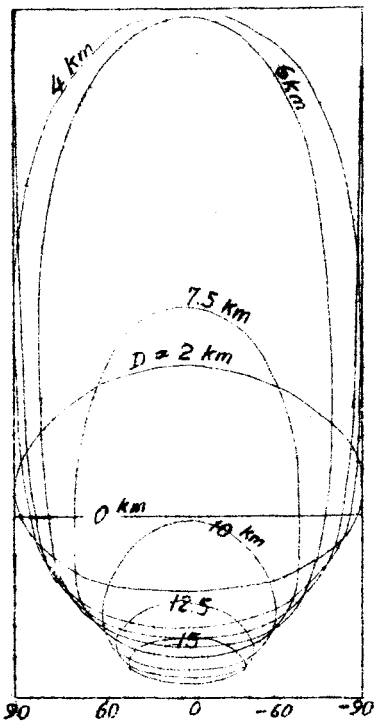

D	5 km Level
0	0.oo
2	6.24
4	18.4
5	} infinity
5	
6	16.0
8	4.50
10	2.10
15	0.39
20	0.12
30	0.o2
40	0.oo6
50	0.ooo3
60	0.oool
70	0.ooooo7
80	0.ooooo4
90	0.ooooo2
100	0.ooooo1
km	A.U.

Fig. 131. Computation of the entrainment force.

As an example, the entrainment accelerations for the circular cloud mentioned before are computed by the diagram in Fig. 131. In contrast with the buoyancy force, it is known that the entrainment acceleration decreases almost to zero at the distance of about 10 km from the cloud. At the center of the cloud, where the distance from the cloud edge is equal in every direction, the entrainment force is, of course, zero.

DETRAINMENT

If there be a cold cell, the direction of the horizontal acceleration reverses. Therefore, it is evident that a force to detrain the cold airs from the down-draft appears not only inside the cell

but also in its environments. Such a process may be termed "detrainment"

The detrainment will be observed whenever a cold portion is located within a warmer environment. The detraining air from the top of a developed thundercloud is a good example of the detrainment. If we want an example in the large scale phenomena, we can see a large mass of cold air locating over the equatorial zone, which diverges gradually toward the poles.

In the similar reason, we must expect a detrainment process for a cold down-draft. This process will, however, be revealed by observations in future.

Next we consider the entrainment field within the system of cold and warm areas. Fig. 132, showing the acceleration patterns, is computed by the acceleration diagram. It will be seen the airs are given a force to get out from the cold area and enter the warm one. The patterns are, however, somewhat different from those we see in the electric or magnetic lines of force; it is because, the entrainment force decreases proportional to the negative 4th power while the electric or magnetic force to the negative 2nd power.

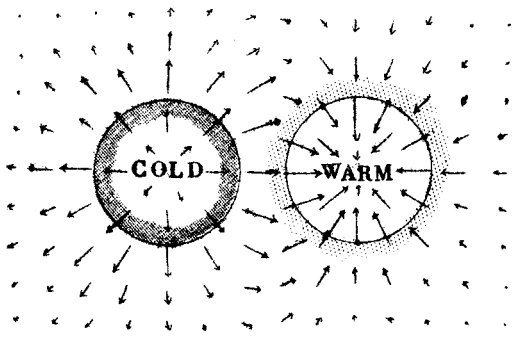

Fig. 132. Entrainment and detrainment within the system of cold and warm areas..

Excessive Pressure Diagram.

When we compute the horizontal acceleration pattern of arbitrary system, it is rather troublesome to obtain it as vector field. Therefore, it is more convenient to draw the isobar for excessive

pressure by using the formulas (61a) and (61b), which show that the excessive pressure can be obtained by graphical integration.

Changing (61a), we write

$$e P_1 = \frac{(\rho_c - \rho_{ur}) g h}{2\pi} \int_0^{2\pi} \left(\sqrt{x^2 + 1} - x\right) d\theta \qquad (67a)$$

where $x = r/h$. We also write eP_2 as

$$e P_2 = (\rho_c - \rho_{ur}) g h - e P_1$$

$$= \frac{(\rho_c - \rho_{ur}) g h}{2\pi} \int_0^{2\pi} \left\{1 - \left(\sqrt{x^2 + 1} - x\right)\right\} d\theta \qquad (67b)$$

Instead of ψ or φ used in acceleration diagrams, as shown in Fig. 133,

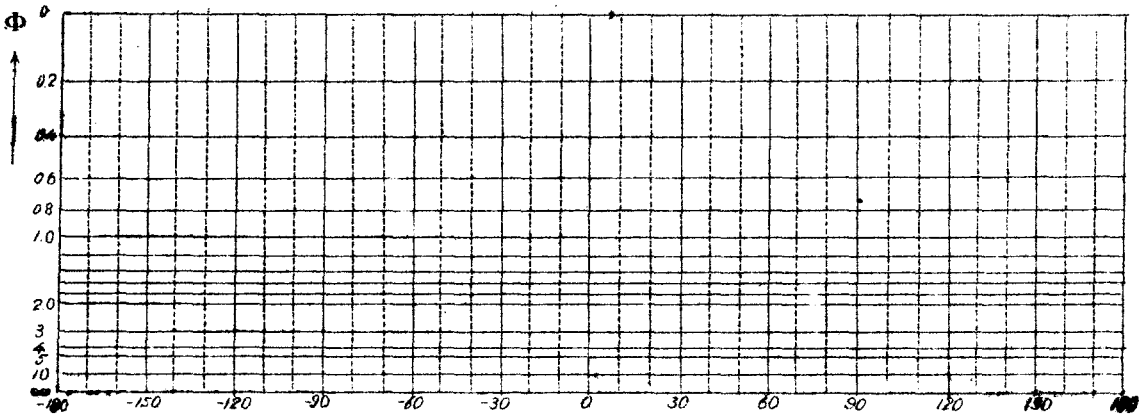

Fig. 133. Excessive pressure diagram.

excessive pressure diagram has the scale of

$$\Phi = \sqrt{x^2 + 1} - x$$

We utilize the excessive pressure diagram as shown in Fig. 134, in which the examples of representation are illustrated.

The pressure distribution beneath a thundercloud warmer than the environment is obtained by the diagram in Fig. 135.

According to the conventional idea, it was only known that the pressure inside the cloud under discussion is lower 1.47 mb, however, as shown in Fig. 136, the pressure computed by the new theory is lower only 0.86 mb than the environments. This is because the pressure

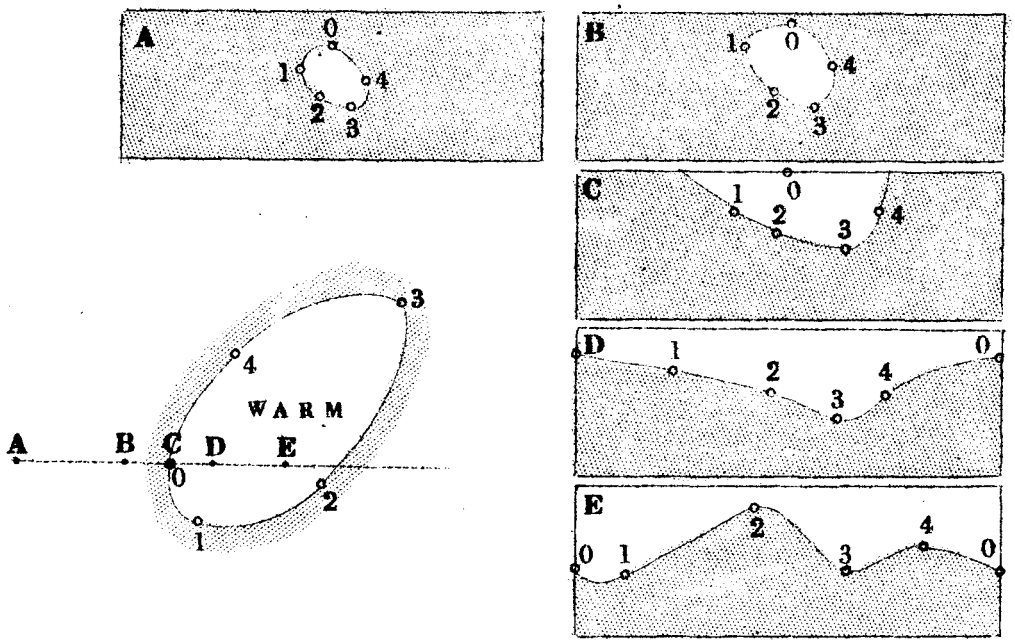

Fig. 134 Representation of excessive pressures for the points A,B,C,D, and E. From (67a) and (67b) it is known that the areas on the diagram which correspond to the cold area on the density chart show the excessive pressure.

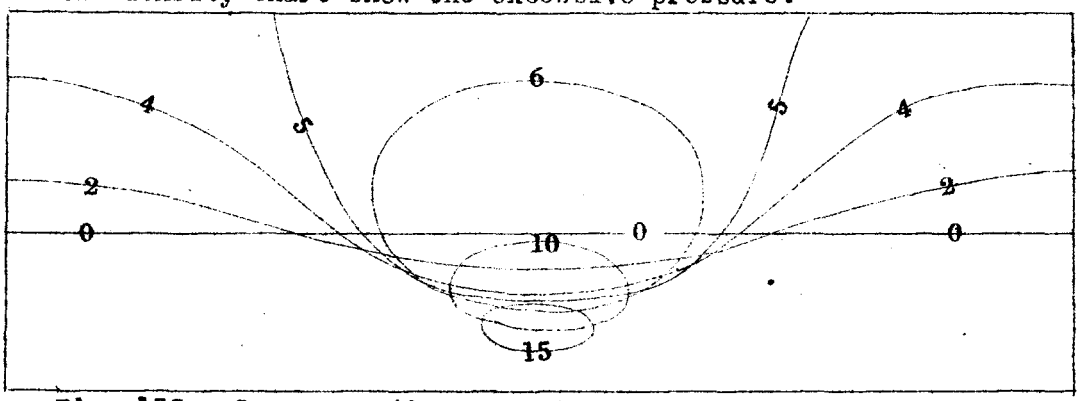

Fig. 135. Curves on the excessive pressure diagram. Numbers in km unit on the diagram represent the distance from the center of the cloud with diameter of 10 km and the height of 5 km.

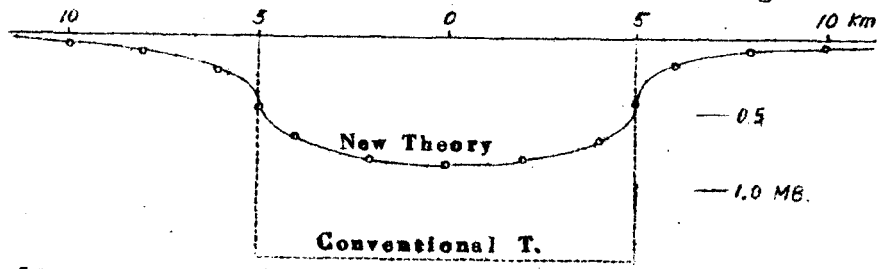

Fig. 136. Pressure distribution on the 5 km level.

caused by the heavy surrounding airs exerts pressure into the cloud through its boundary.

Thus, the structure and the process taking place within thundercloud can be clarified by using the new convection theory.

LITERATURES

(1) Byers H.R. The Thunderstorm.
U.S. Government Printing Office, Washington D.C. 1949

(2) Prandtl-Tietjens Hydro-und Aeromechanik IIter Band 1931
Julius Springer, Berlin

(3) Cunningham, R.M., and Miller, R.W., Five Weather Rader Flights: Measurement and Analysis, Technical Report No. 7, Weather Rader Reaearch, Massachusetts Institute of Technology. 1948.

(4) Fujita T. Micro-analytical Study of Thunder-nose. Geophysical Magazine, Vol. 22 No. 3.

(5) Syono S. On the Theory of Formation of Tropical Cyclones. (not yet published)

CHAPTER IV

EXAMPLES OF ANALYSES

EXAMPLE I

PRESSURE PROFILES OF TYPHOONS

(A) Typhoon Muroto of 21 Sept. 1934

	06	07	08	09	10	11	12	13	14	
P_∞	1018	1018	1018	1018	1018	1018	1018	1018	1018	mb
ΔP	89.2	78.7	66.7	56.0	48.0	46.0	44.7	44.0	42.7	mb
a	0.06	0.05	0.06	0.16	0.32	0.36	0.48	0.65	0.85	dimensionless
r_0	126	172	222	245	245	248	251	243	236	km

(B) Typhoon Della of 20-21 June 1949

	21	22	23	00	01	02	03	04
P_∞	1018	1018	1018	1018	1018	1018	1018	1018
ΔP	56.0	50.6	49.3	46.7	44.0	42.7	40.0	38.6
a	0.50	0.70	0.95	1.2	1.1	0.90	0.90	0.80
r_0	136	131	126	128	141	166	191	240

(C) Typhoon Jane of 3-4 Sept. 1950

	06	08	10	12	14	16	18	20	22	24	02	04	06
P_∞	1017	1017	1017	1017	1018	1018	1018	1018	1018	1019	1019	1019	1019
ΔP	64.0	61.2	57.3	53.4	47.6	42.8	39.0	36.1	33.3	31.5	29.7	28.9	28.0
a	0.40	0.34	0.27	0.22	0.18	0.19	0.24	0.32	0.44	0.60	0.85	0.95	1.20
r_0	62	68	80	103	128	151	168	182	192	200	200	200	212

(D) Typhoon Kezia of 13-14 Sept. 1950

	12	15	18	21	24	03
P_∞	1014	1014	1014	1014	1014	1014
ΔP	52.0	52.4	47.2	37.0	34.3	31.1
a	0.54	0.46	0.34	0.46	0.38	0.48
r_0	99	108	129	144	174	126

(E) Typhoon Ruth of 14 Oct. 1951

	19	20	21	22	23	24
P_∞	1014	1014	1014	1014	1014	1014
ΔP	70.0	66.1	60.4	54.2	52.1	50.5
a	0.54	0.70	0.90	1.10	0.95	0.80
r_0	144	144	149	162	203	249

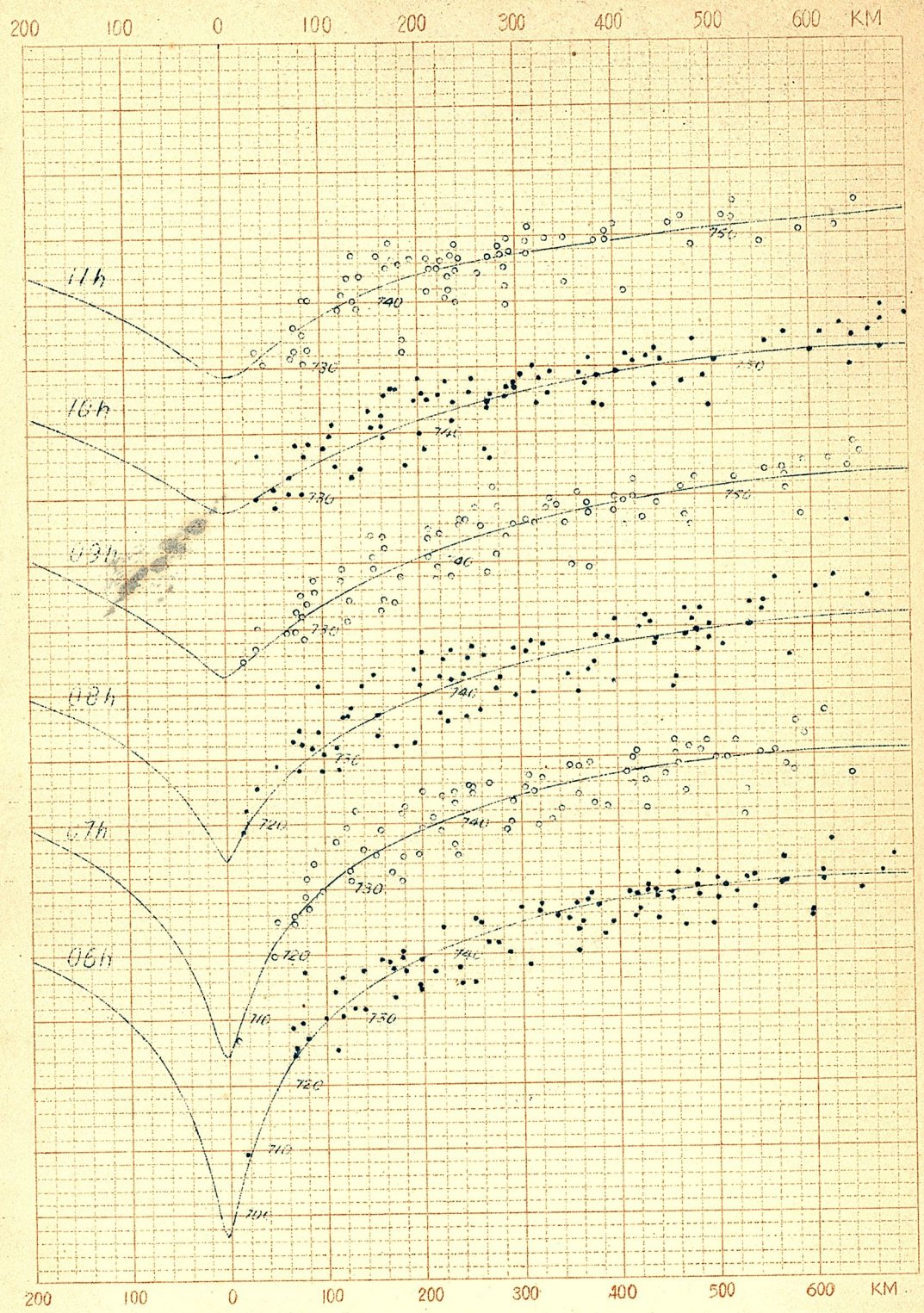

Profiles of Typhoon Muroto

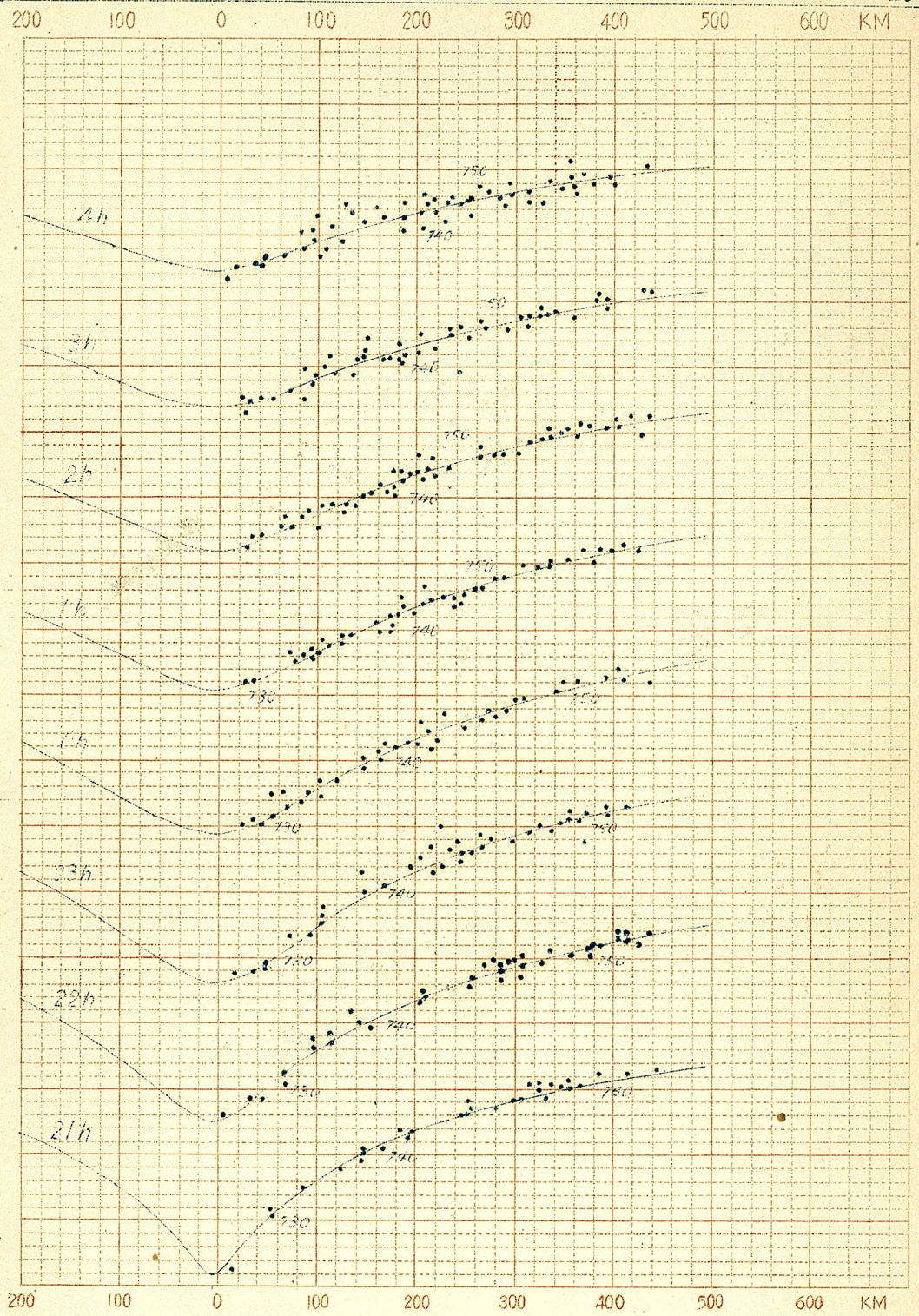

Pressure Profile of Typhoon Della

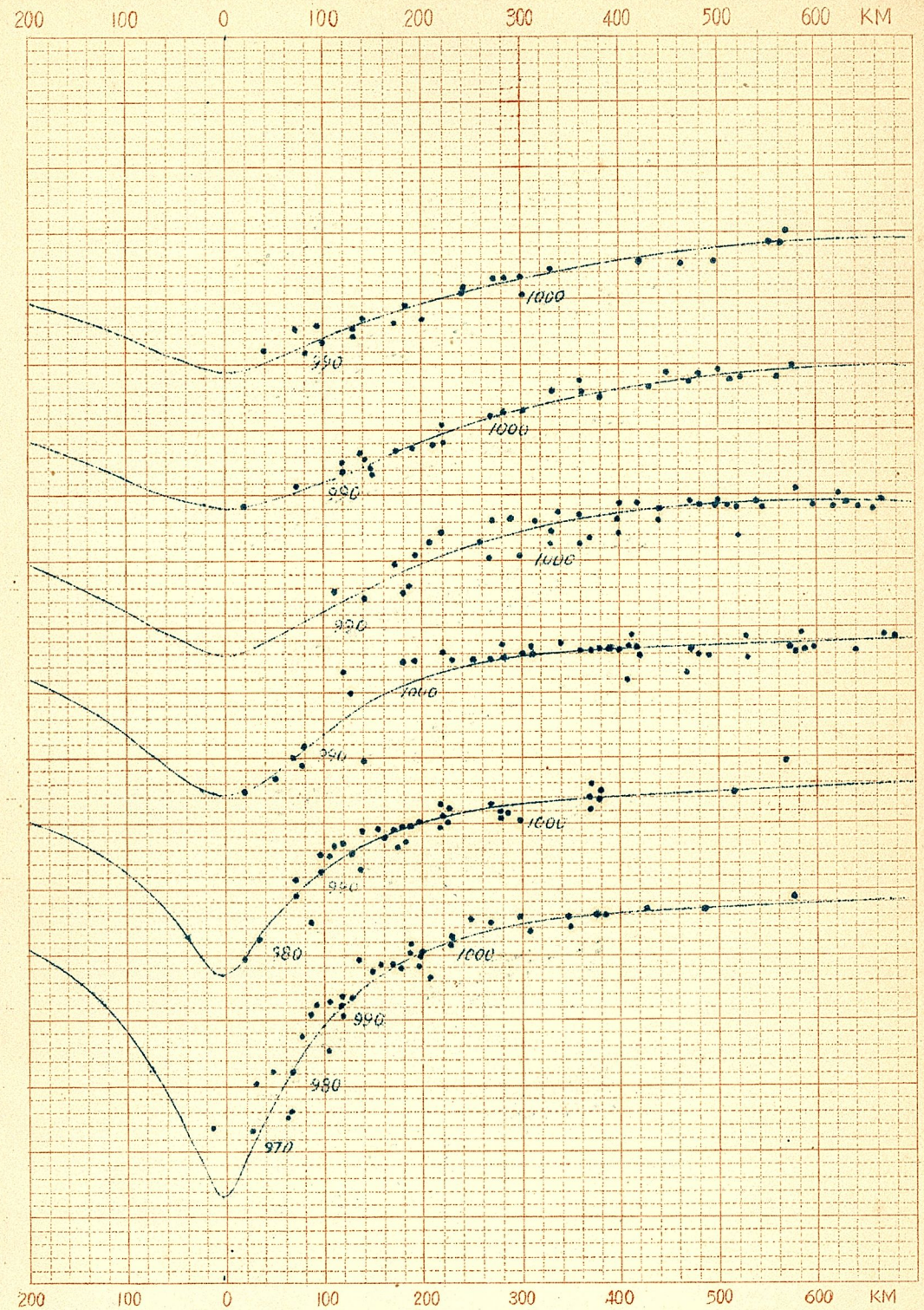

Pressure Profile of Typhoon Jane

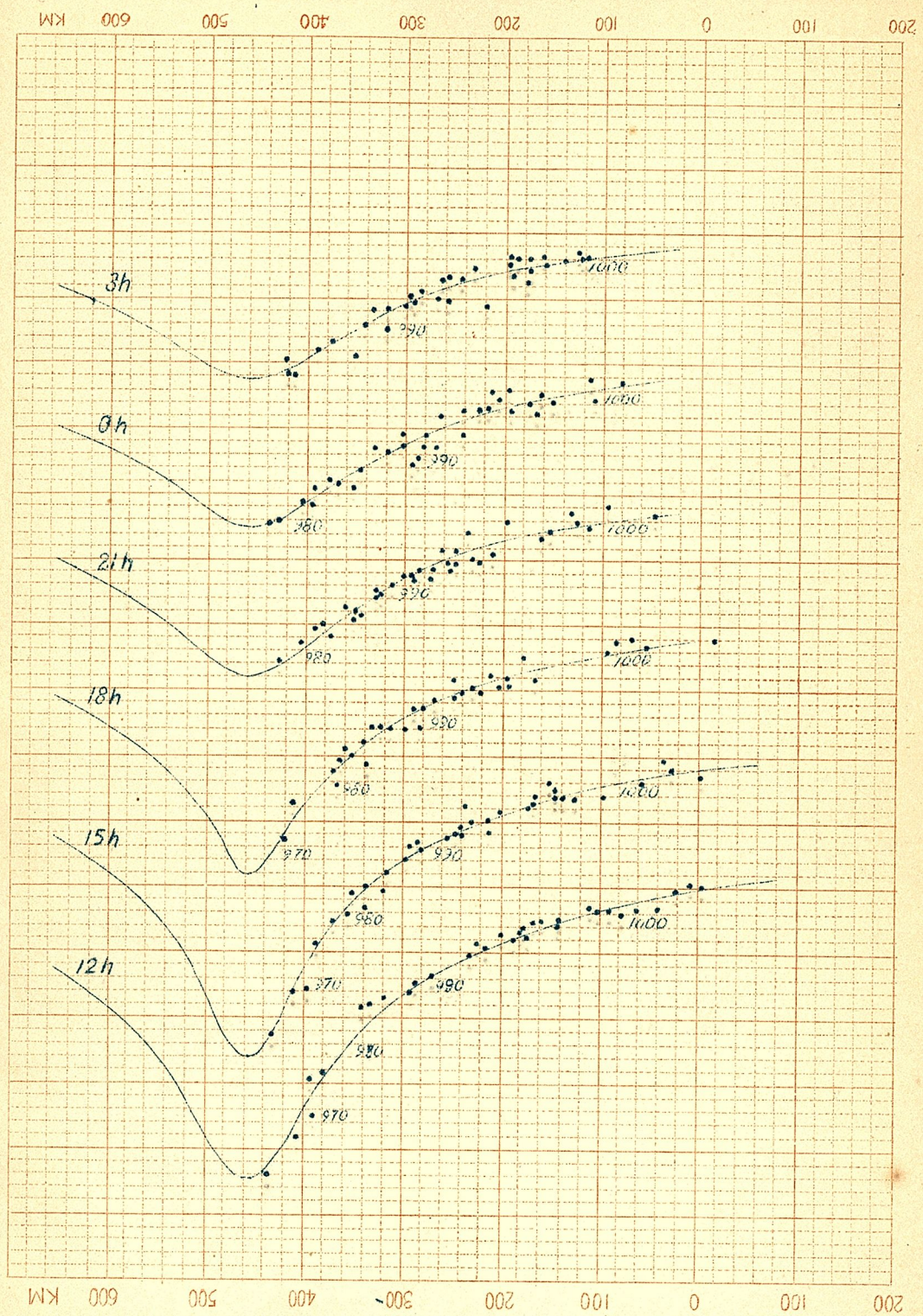

Pressure Profile of Typhoon Kezia

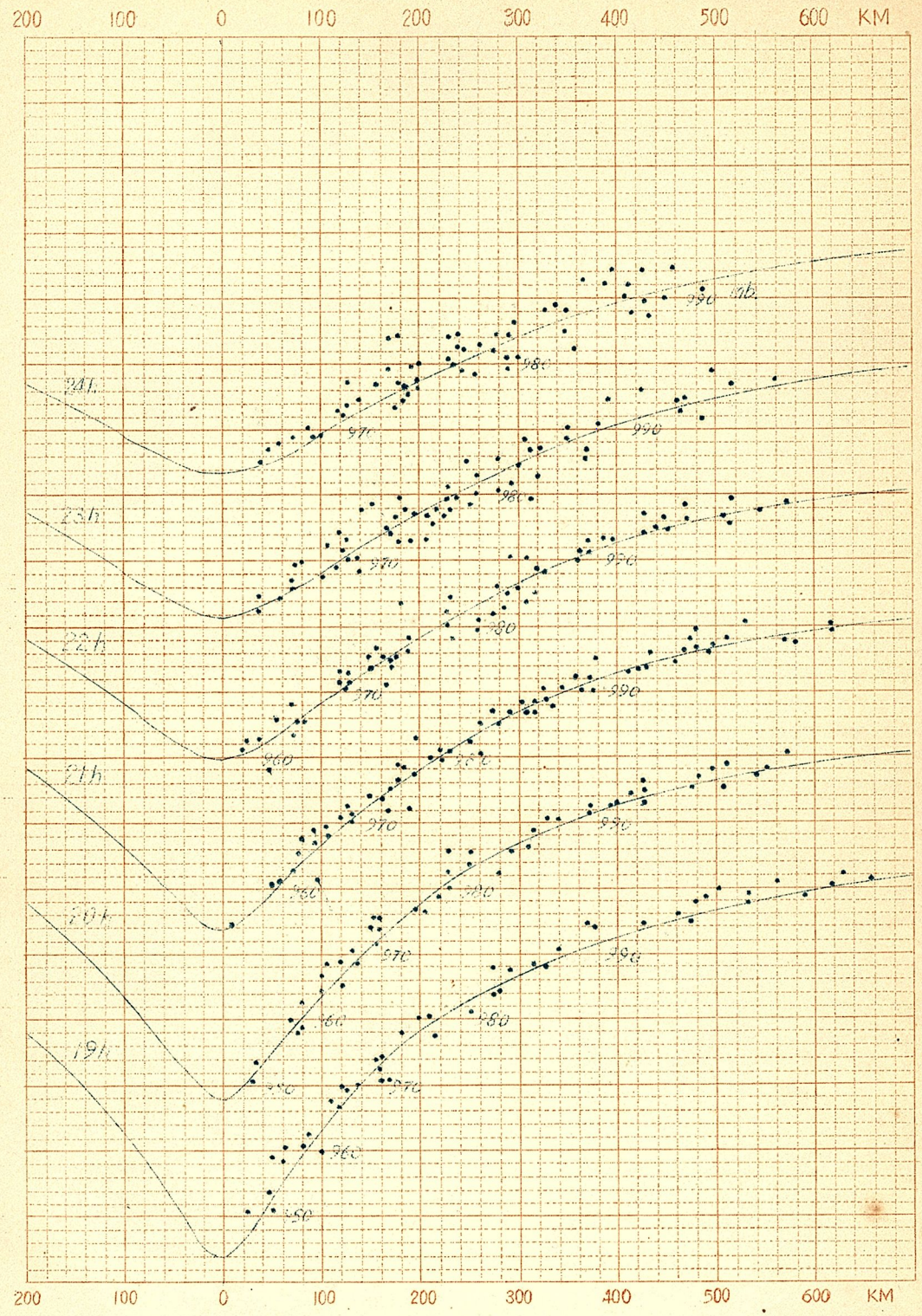

Pressure Profile of Typhoon Ruth

EXAMPLE 2

HOURLY SURFACE CHARTS OF TYPHOON DELLA

From 12h 20th to 08h 22nd

June 1949

"Isobars" are contoured for every 1 mm Hg by black curves. In the central areas of the typhoon where the relation of winds to isobars is not so evident, the isobars are drawn after referring to the pressure traces from each weather station. Especially the areas affected by the dips are contoured by using the traces only, since the angle between wind and isobar is quite different from the one we believed conventionally. Thus, the angles can be studied by the following map sequence.

"Isotherms" are contoured for every 1 degree centigrade. Before drawing the isotherms, the temperatures at those stations locating at the top of a hill or plateau had been corrected to sea level, and the lapse rate was assumed to be 6°C/km.

Before the typhoon reached the frontal zone locating over Japanese Islands, the temperature gradient near the front was not prominent, however, as she advanced northward, a marked warm front appeared along the Pacific side of Japanese Islands. The most interesting feature of the temperature distribution is the development of the warm area which has started to form west of Shikoku at 01h 21 June. The warm area spread over Chugoku and Shikoku Districts with the maximum temperature of about 30°C.

"Rain Intensities" are contoured for the values, 0, 1, 3, 5, 10, 30, 50 mm/hour. In order to make the precipitation pattern, the traces of rain at each station are differentiated carefully, and the values at each map time are entered.

It is found that the moderate rain south of Japan was intensified as the typhoon approached. This is the case for a decaying typhoon, and the precipitation pattern around the typhoon center is not concentric but the heavy rains are seen mainly in the cold sector. In the eastern areas of the typhoon far from the center there were observed heavy showers moving north-eastward.

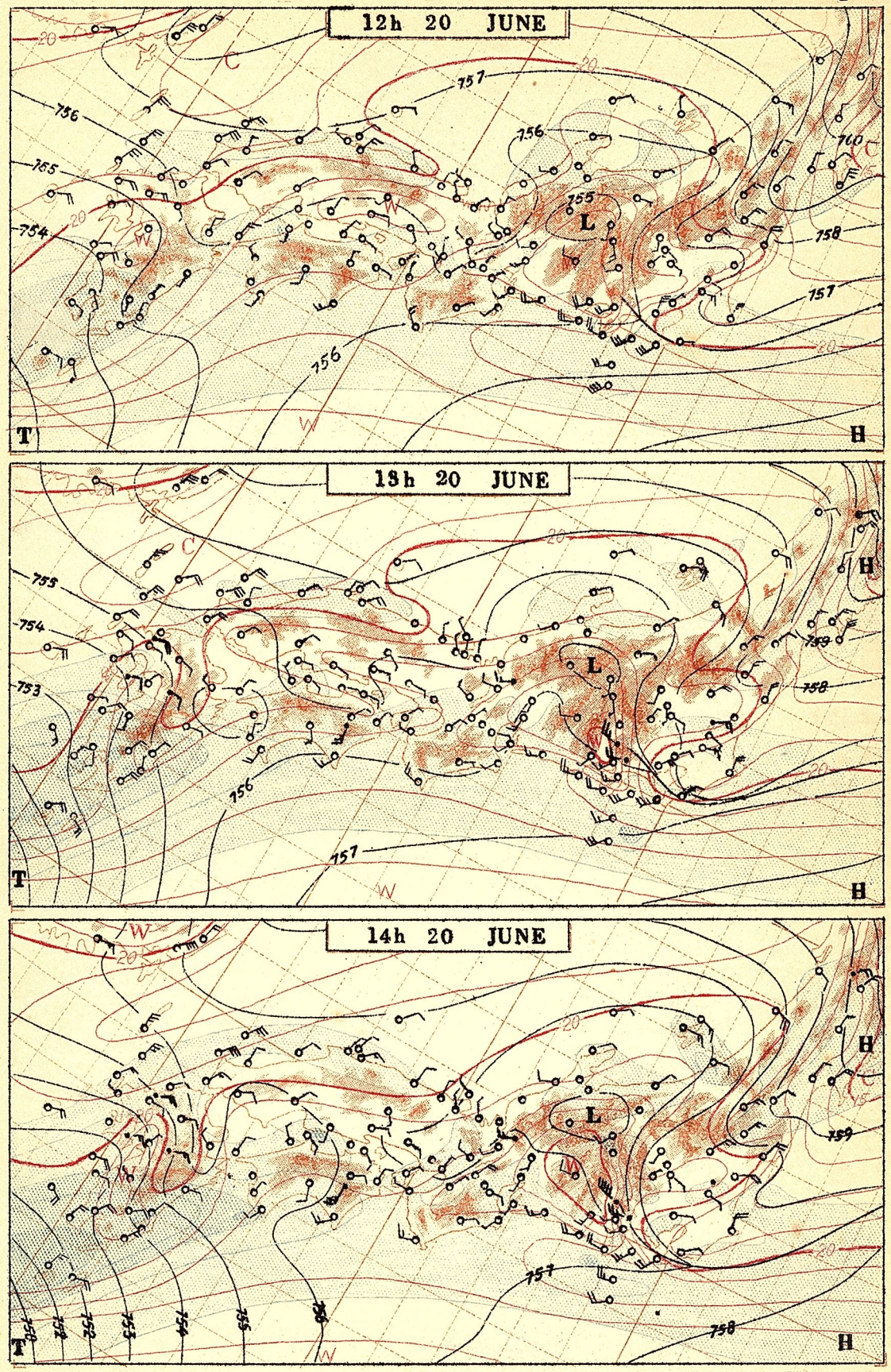

WEATHER MAPS OF TYPHOON DELLA BY T. FUJITA

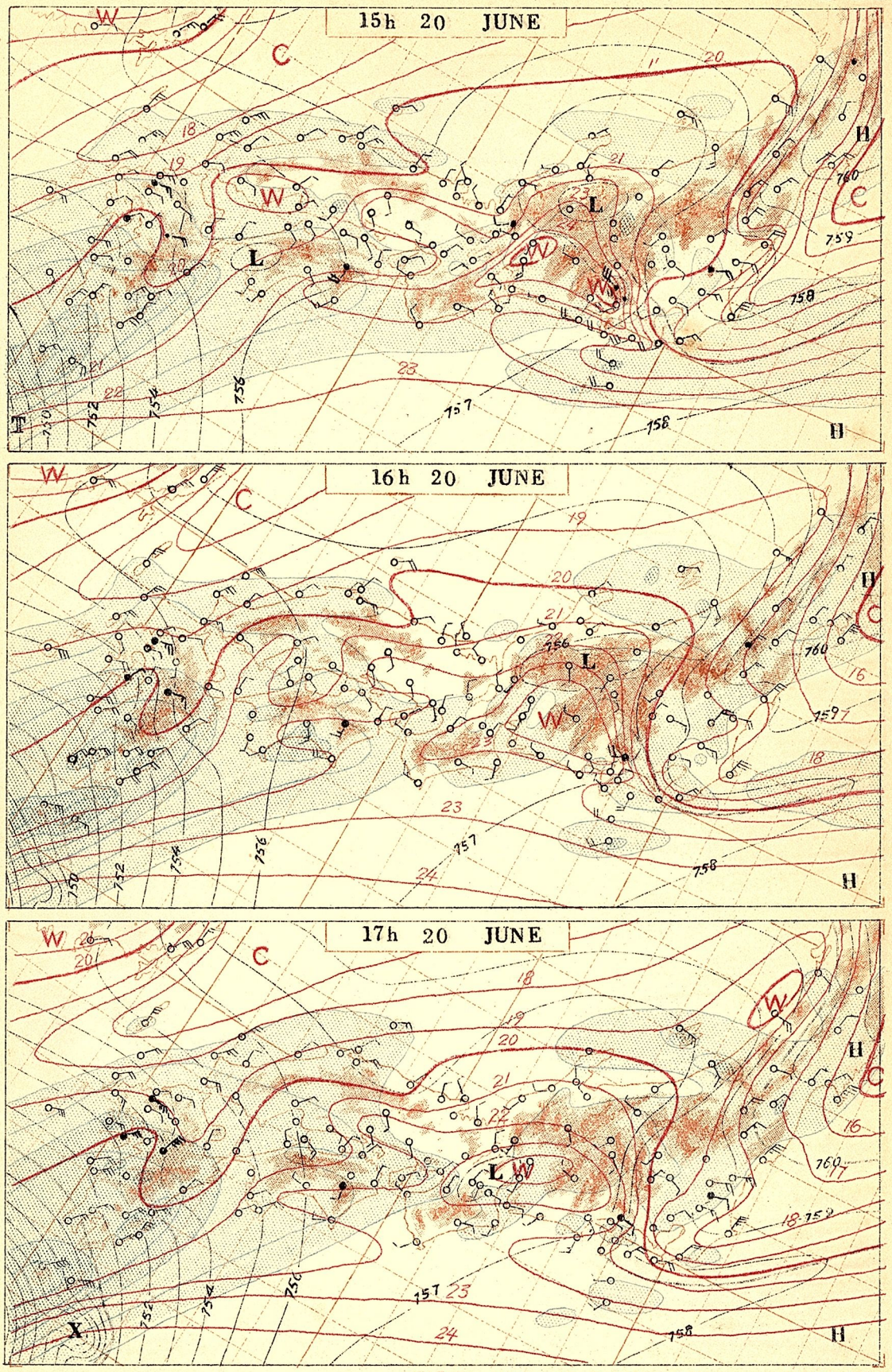

WEATHER MAPS OF TYPHOON DELLA BY T. FUJITA

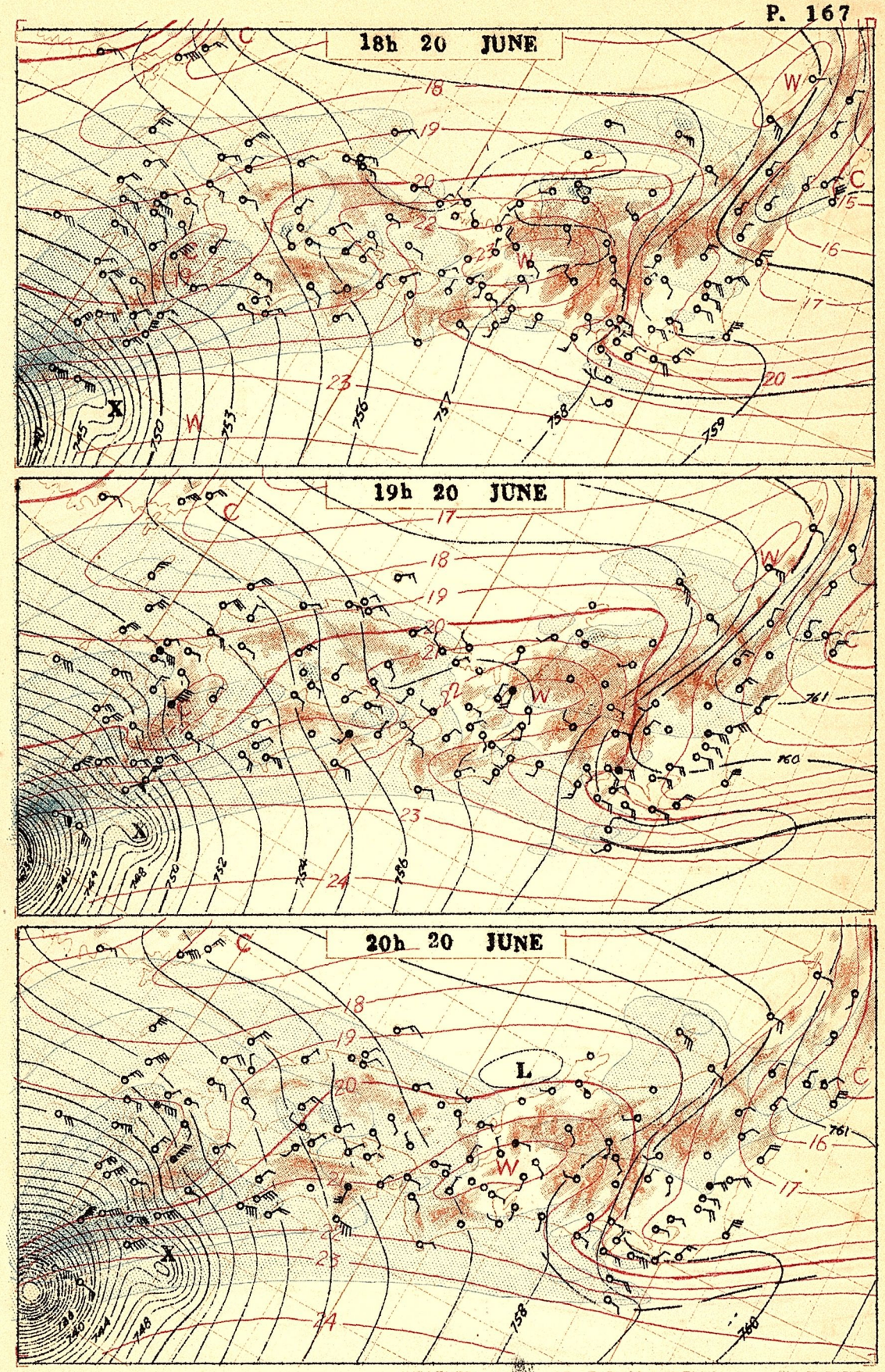

WEATHER MAPS OF TYPHOON DELLA BY T. FUJITA

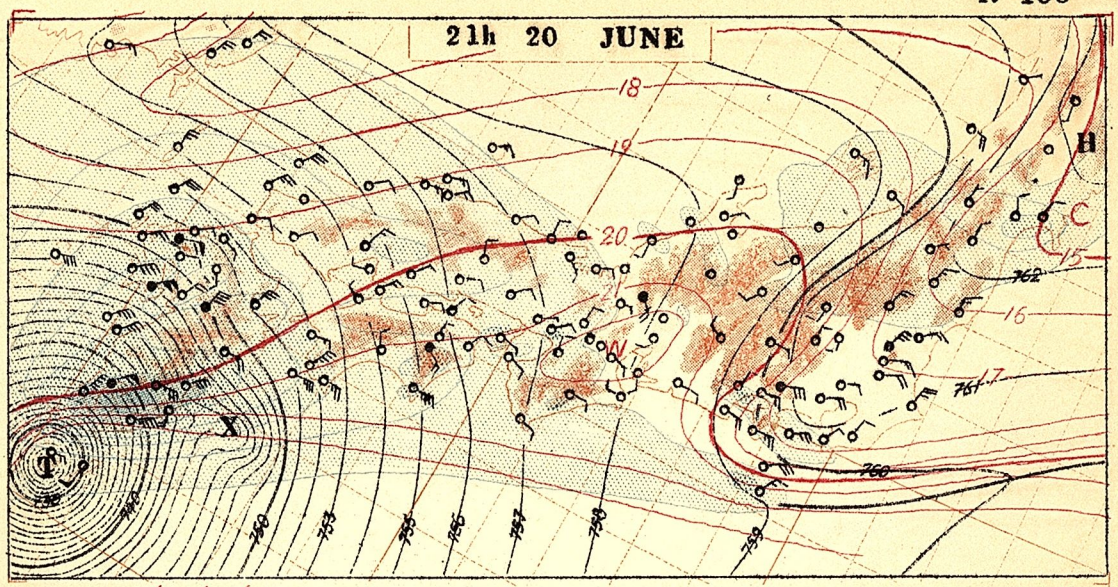

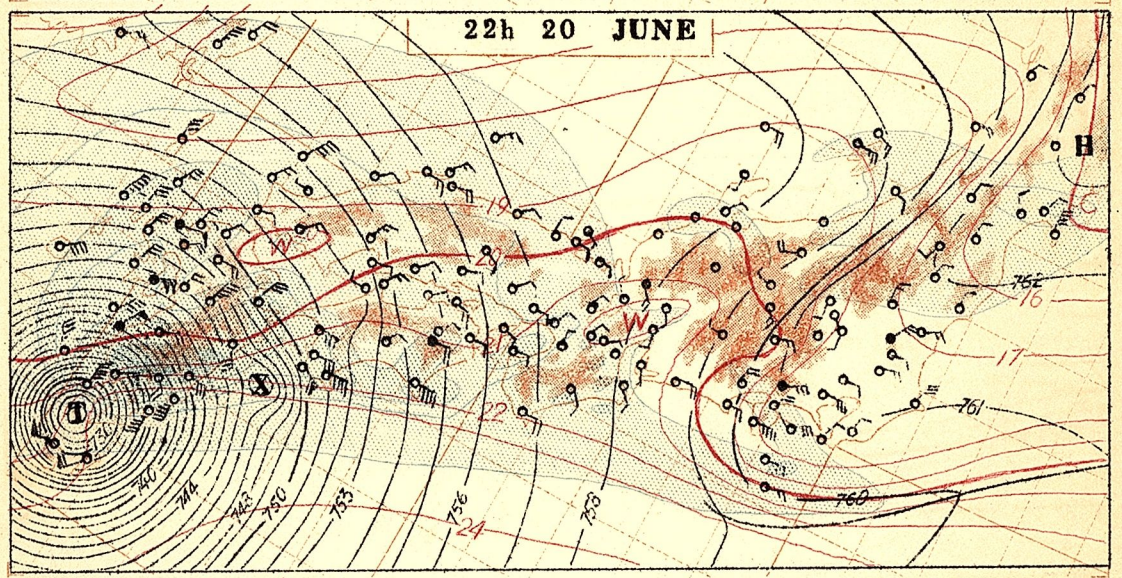

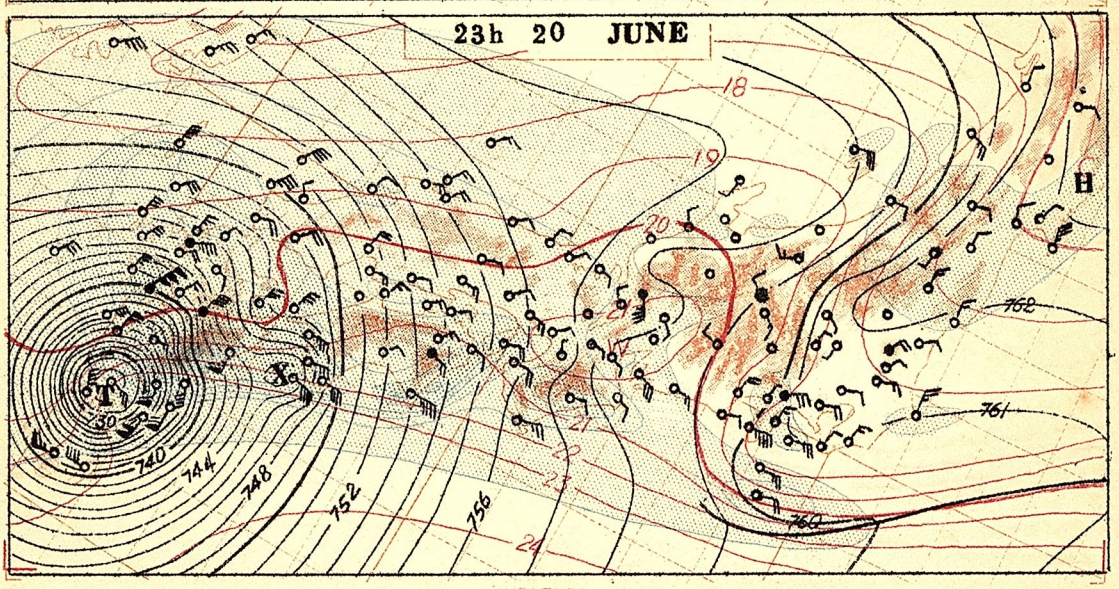

WEATHER MAPS OF TYPHOON DELLA BY T. FUJITA

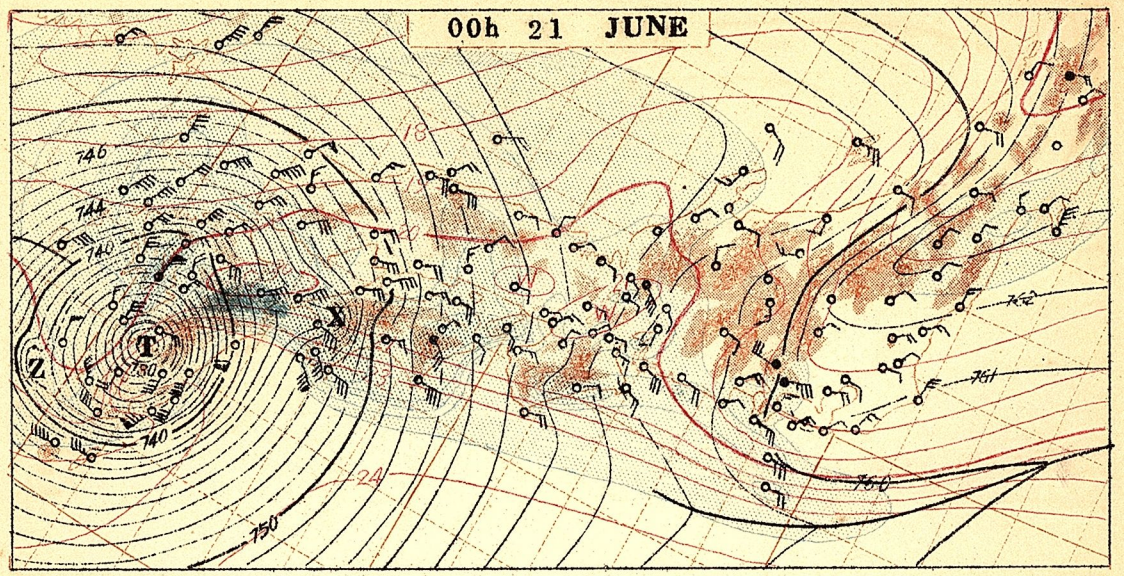

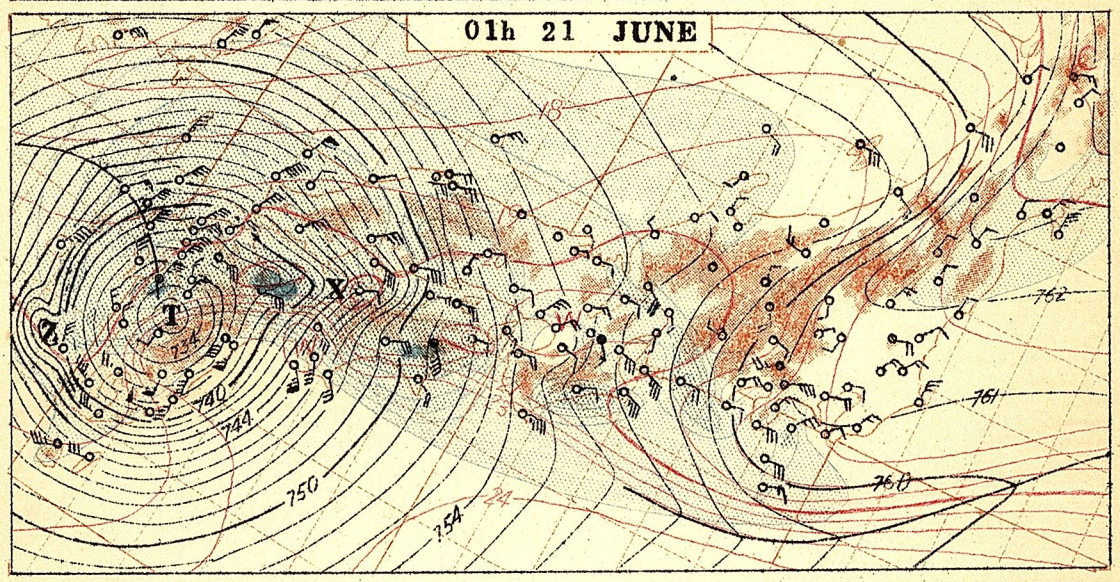

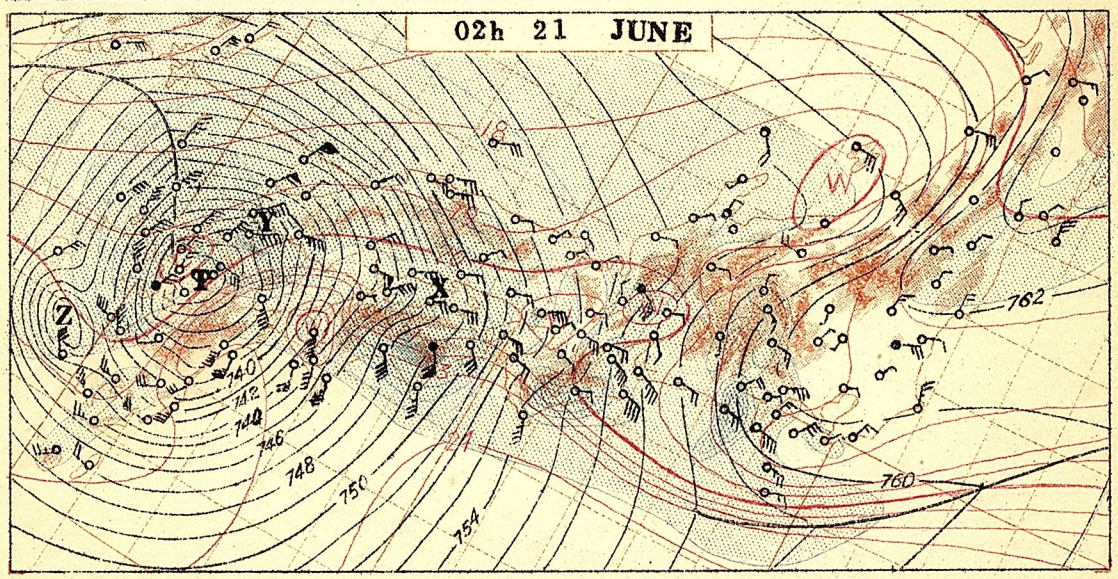

WEATHER MAPS OF TYPHOON DELLA BY T. FUJITA

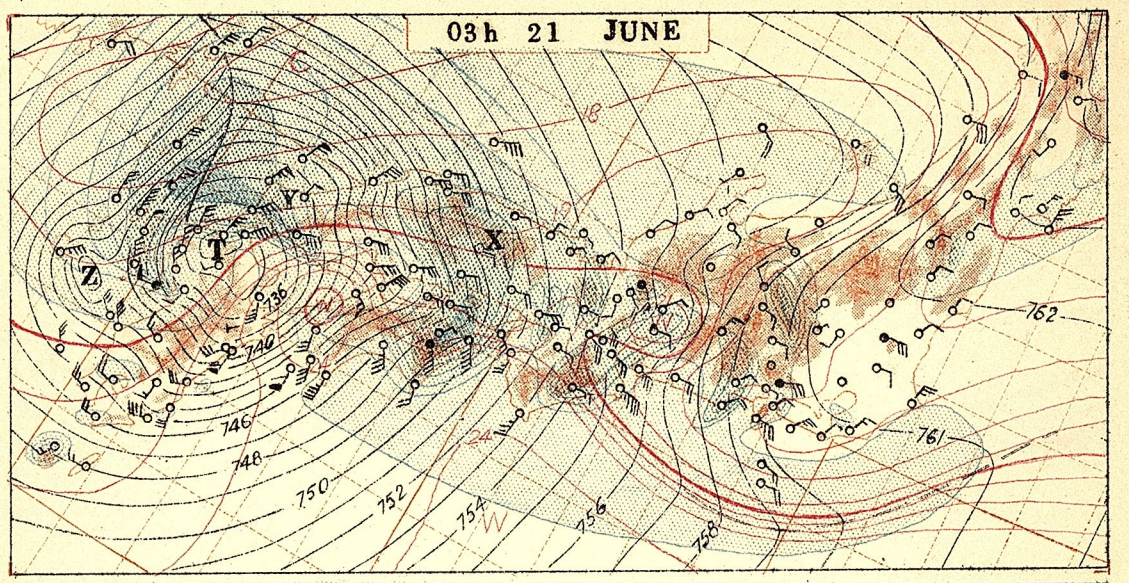

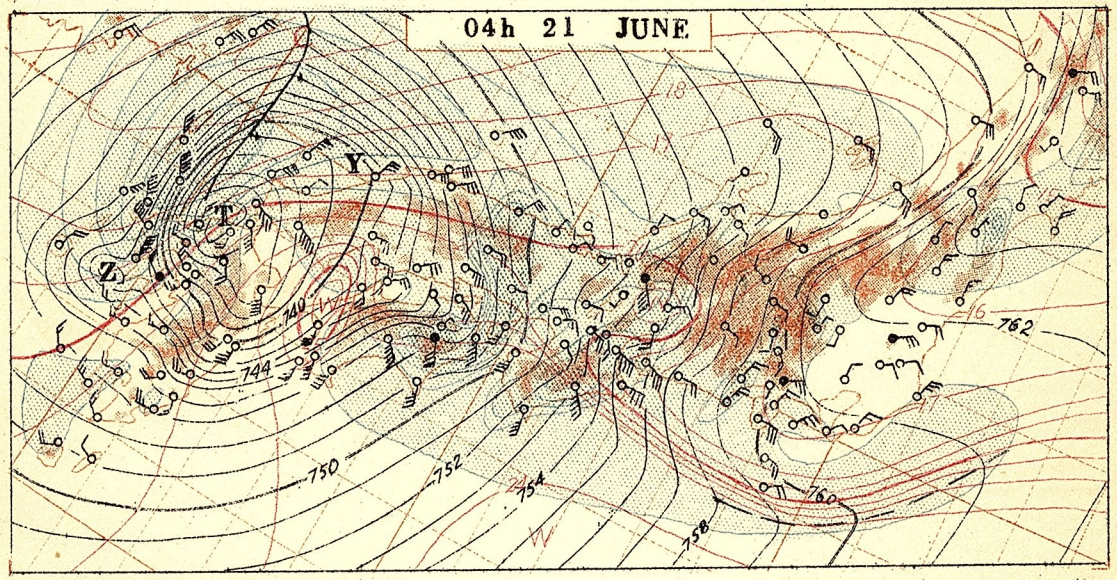

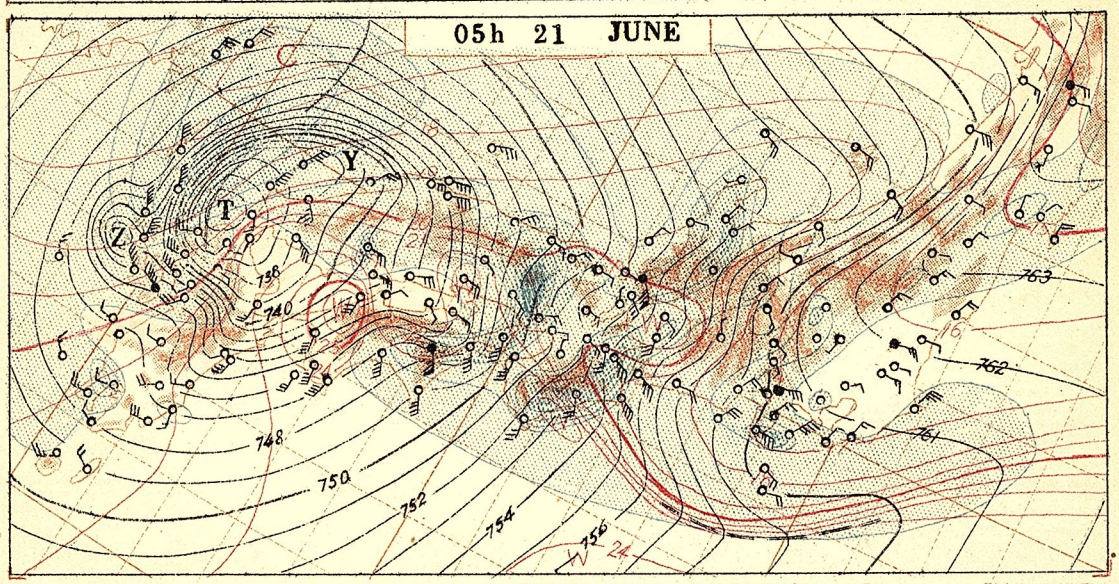

WEATHER MAPS OF TYPHOON DELLA BY T. FUJITA

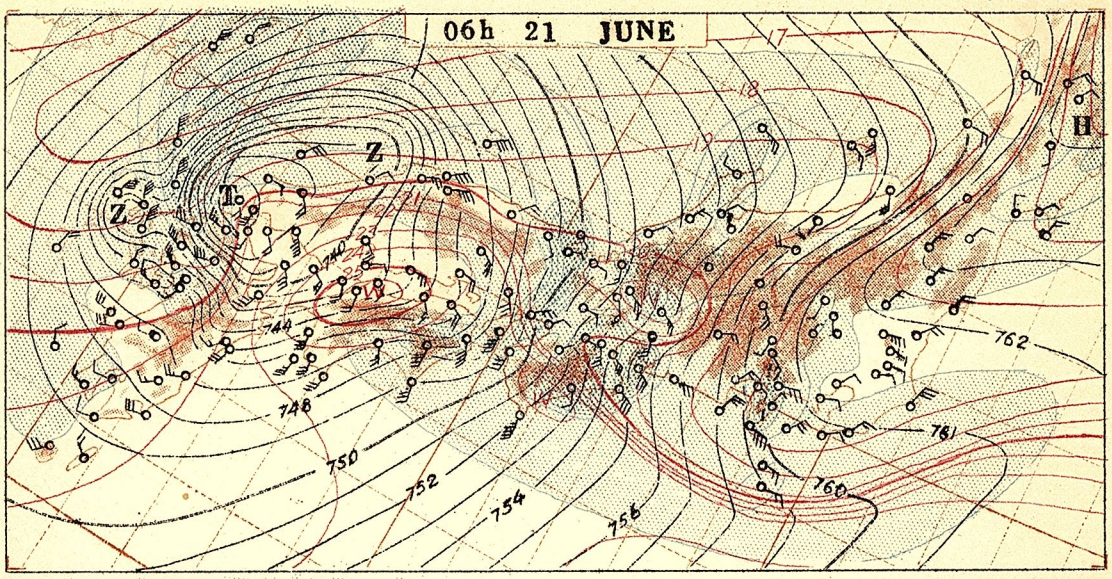

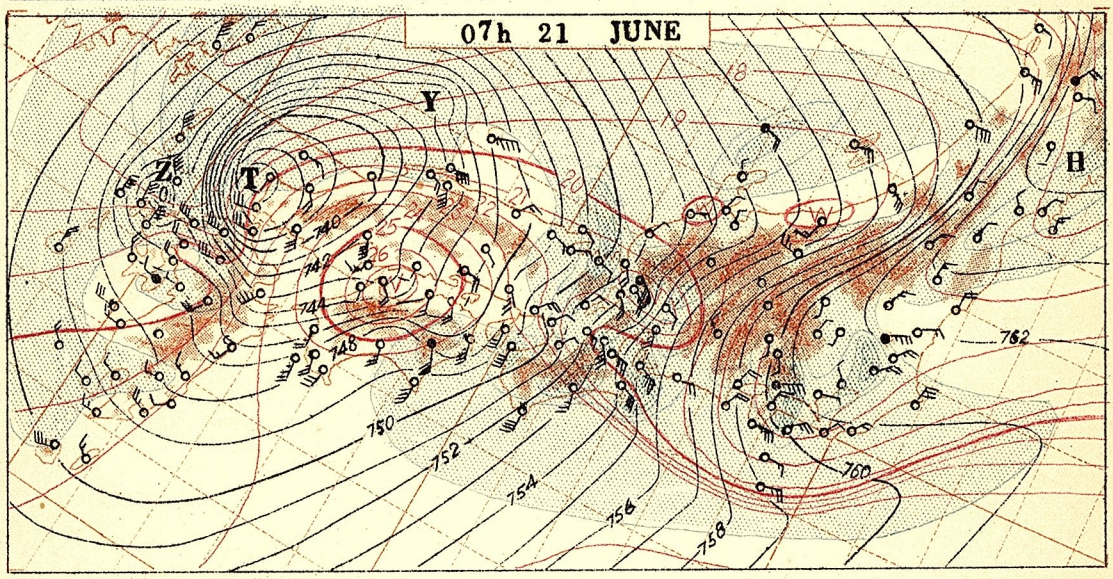

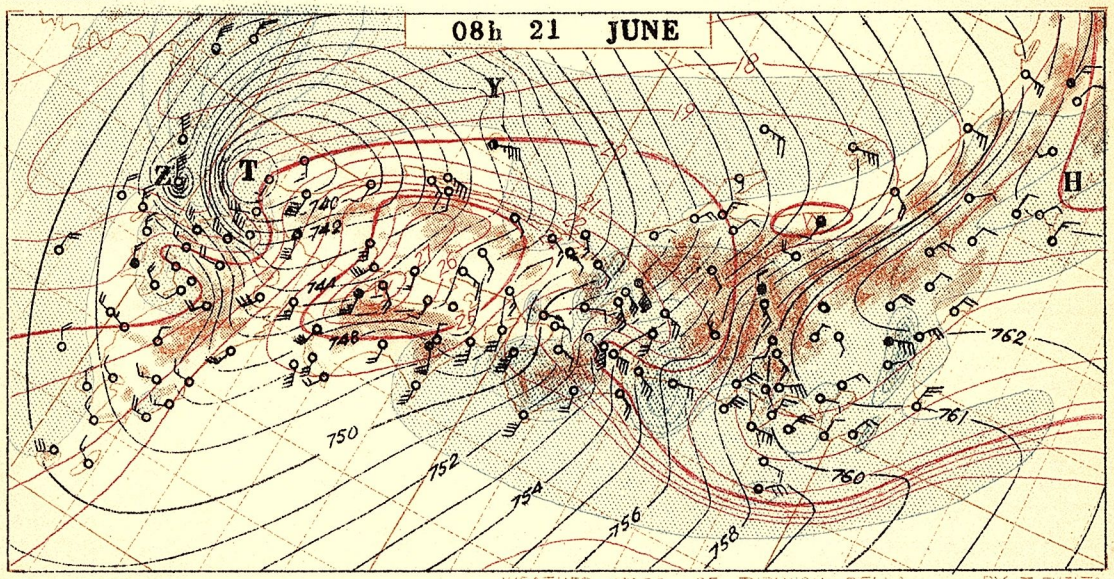

WEATHER MAPS OF TYPHOON DELLA BY T. FUJITA

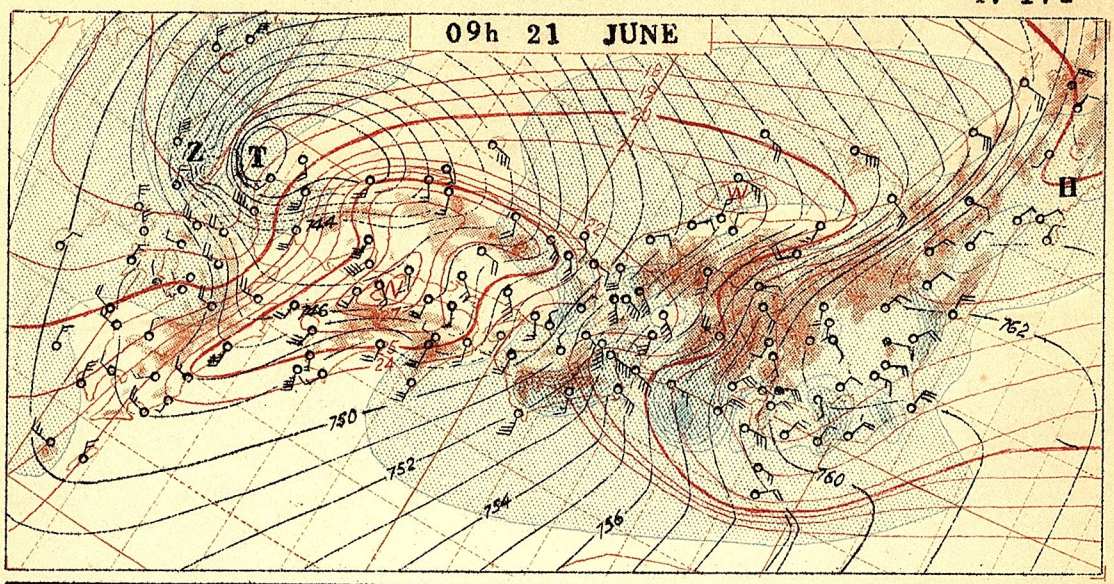
09h 21 JUNE
T
Z
H
744
746
748
750
752
754
756
760
762

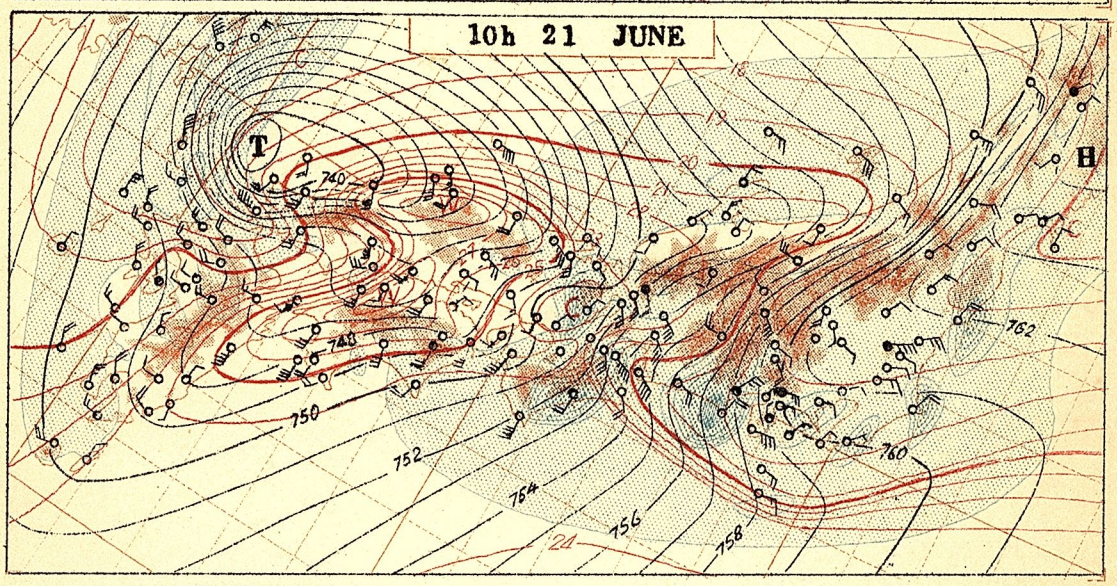
10h 21 JUNE
T
H
740
742
744
746
748
750
752
754
756
758
760
762

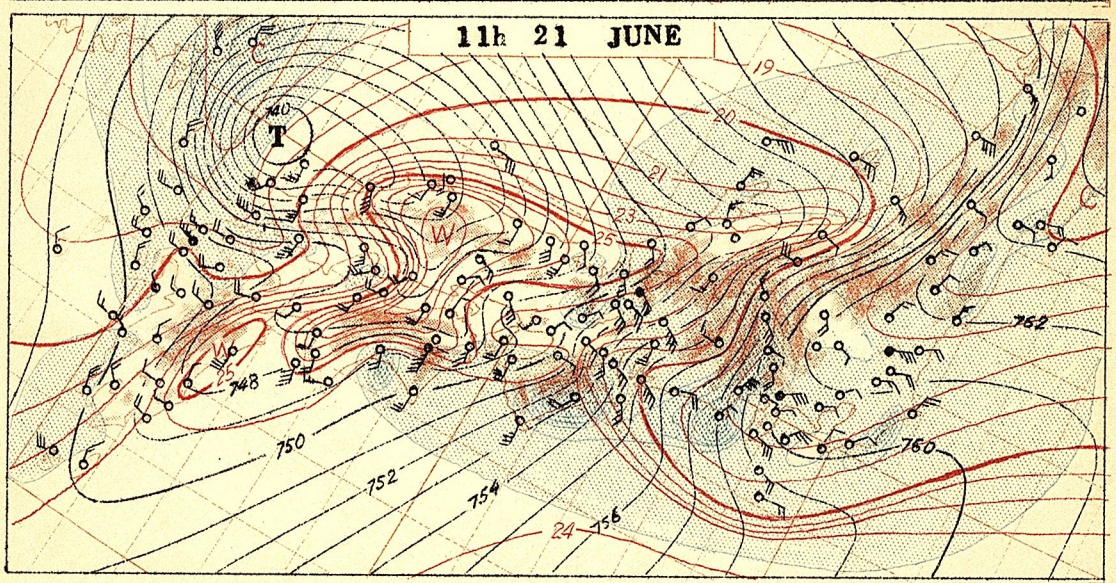
11h 21 JUNE
T
740
748
750
752
754
756
760
762

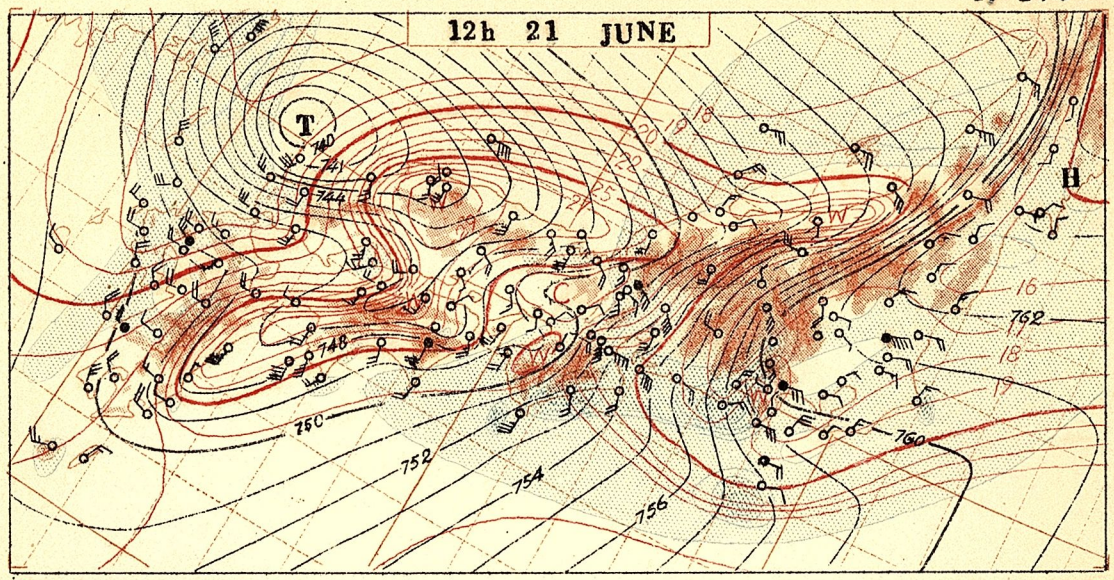

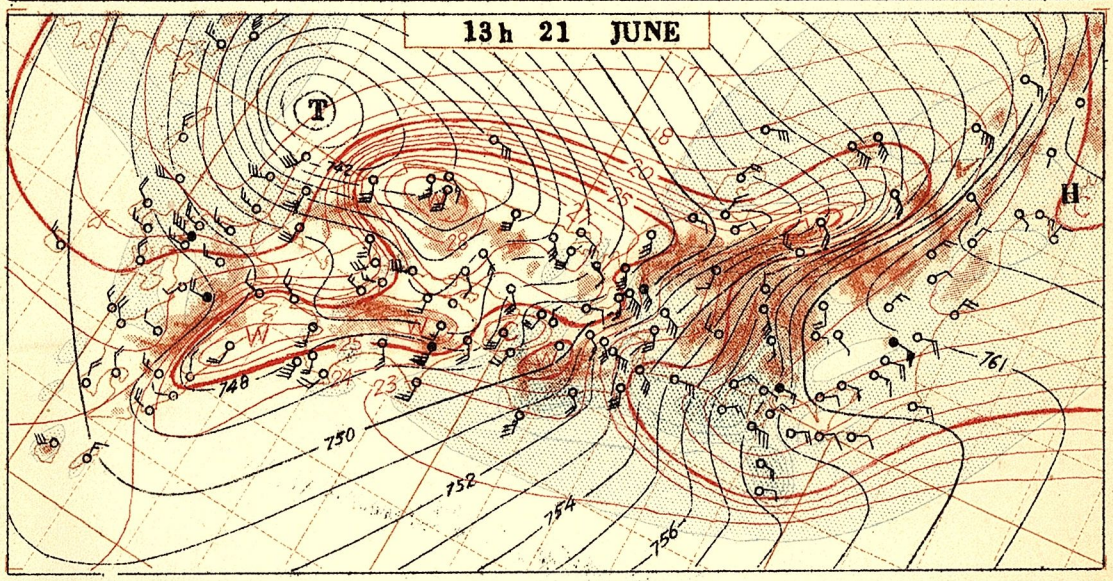

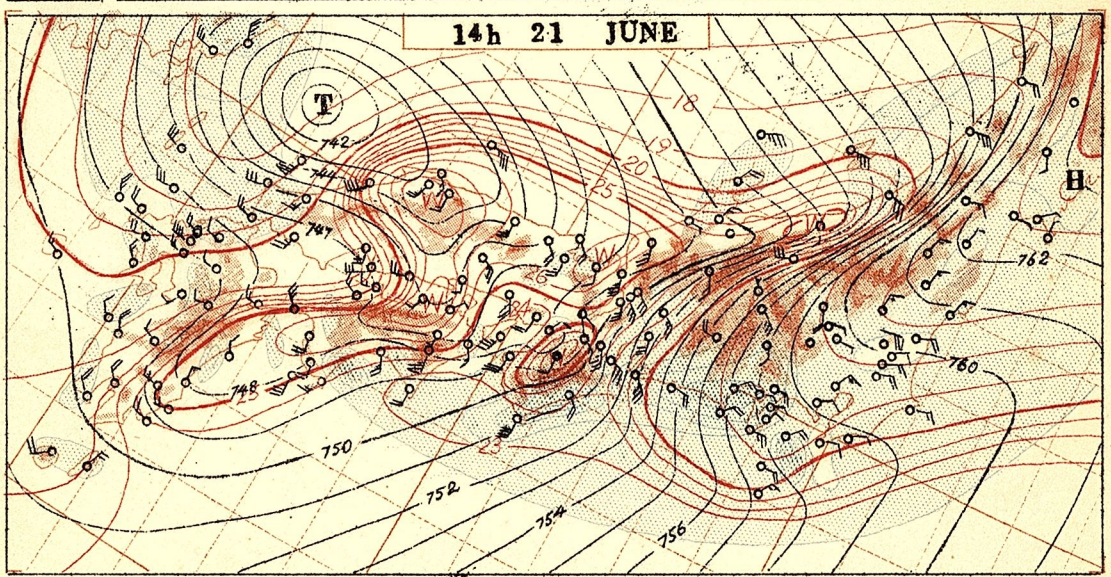

WEATHER MAPS OF TYPHOON DELLA BY T. FUJITA

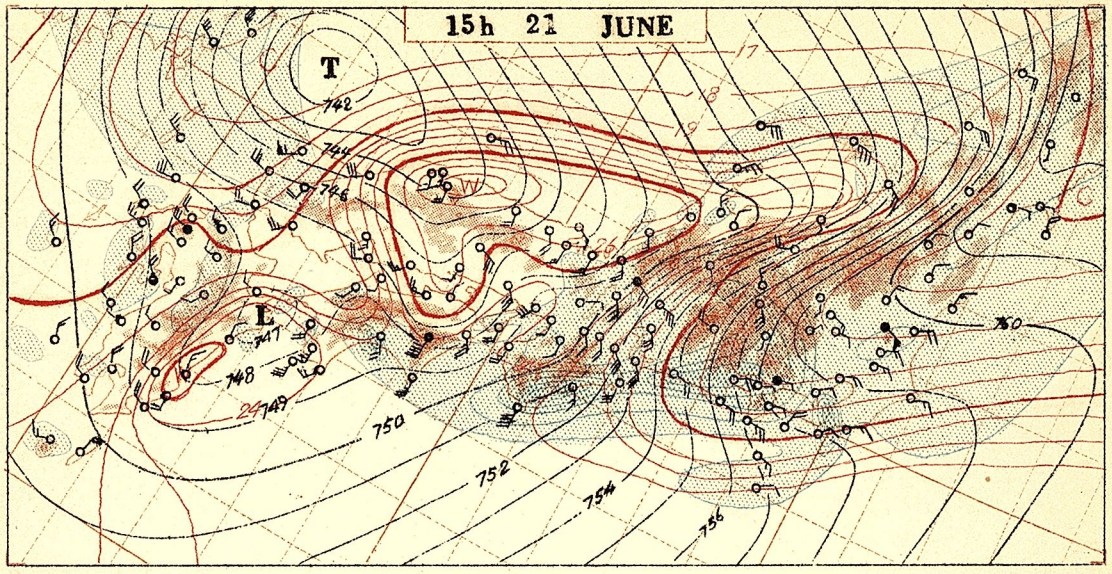
15h 21 JUNE
T
L
742
744
746
747
748
749
750
752
754
756
760

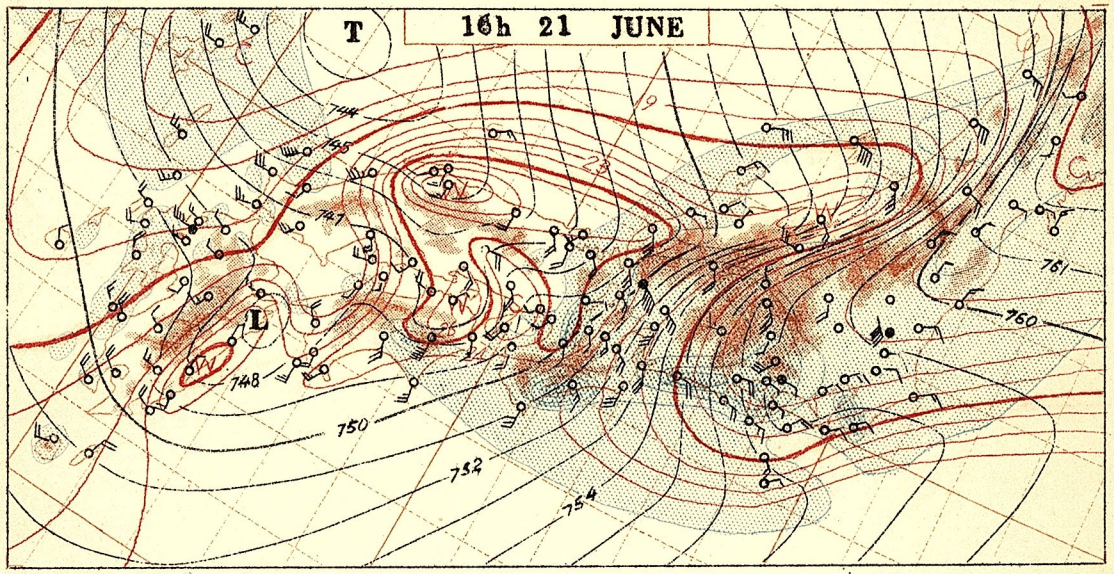
16h 21 JUNE
T
L
744
745
747
748
750
752
754
760
761

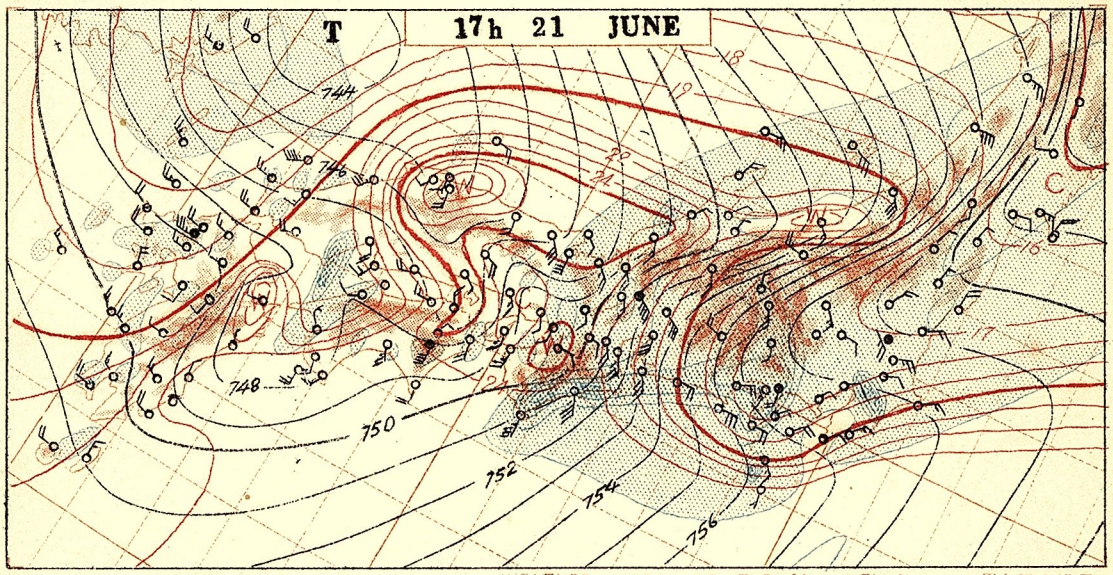
17h 21 JUNE
T
L
744
746
748
750
752
754
756

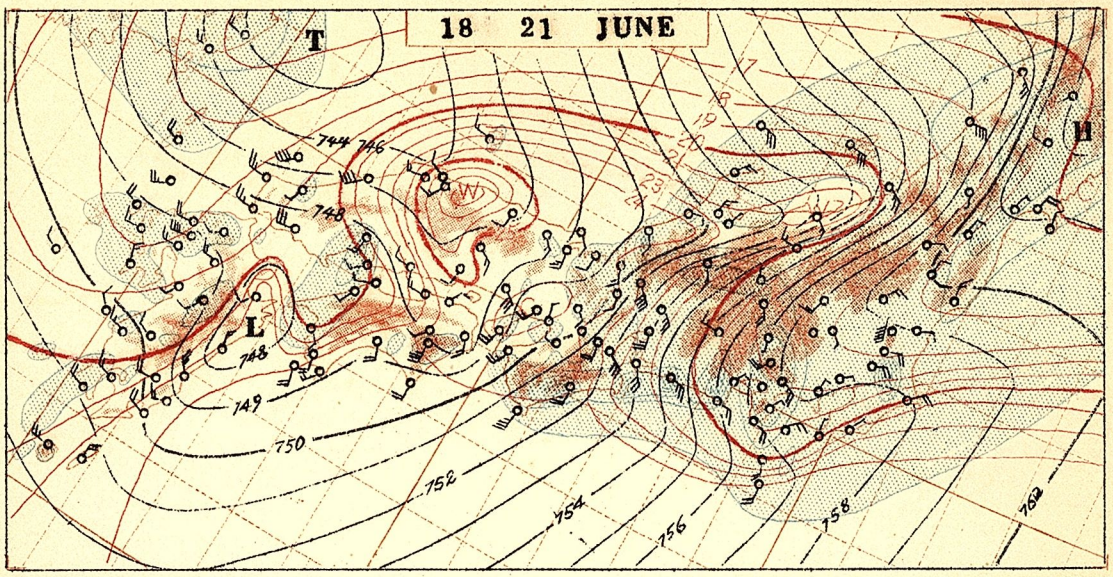

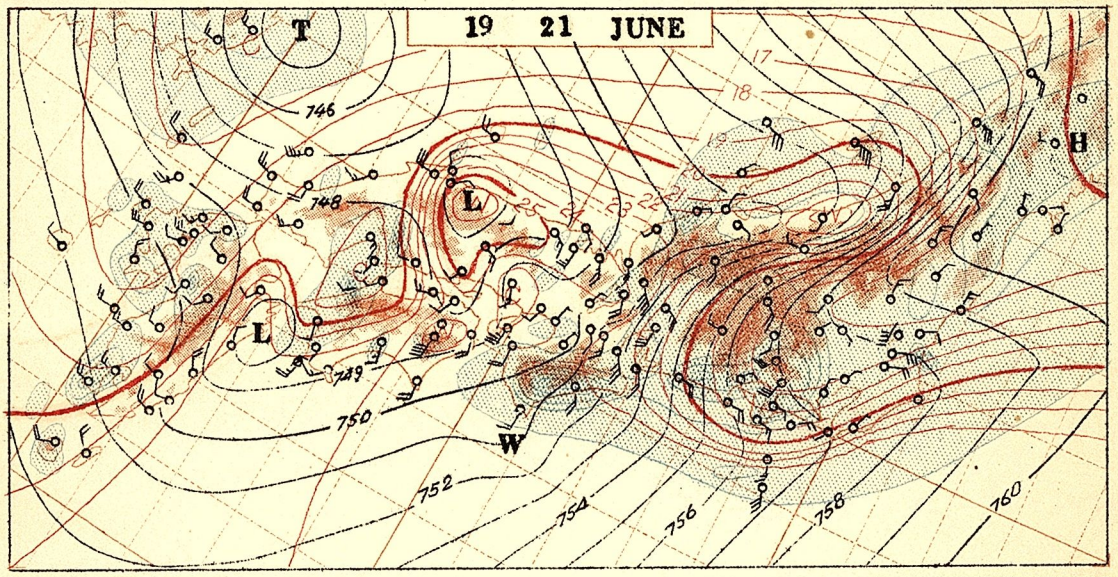

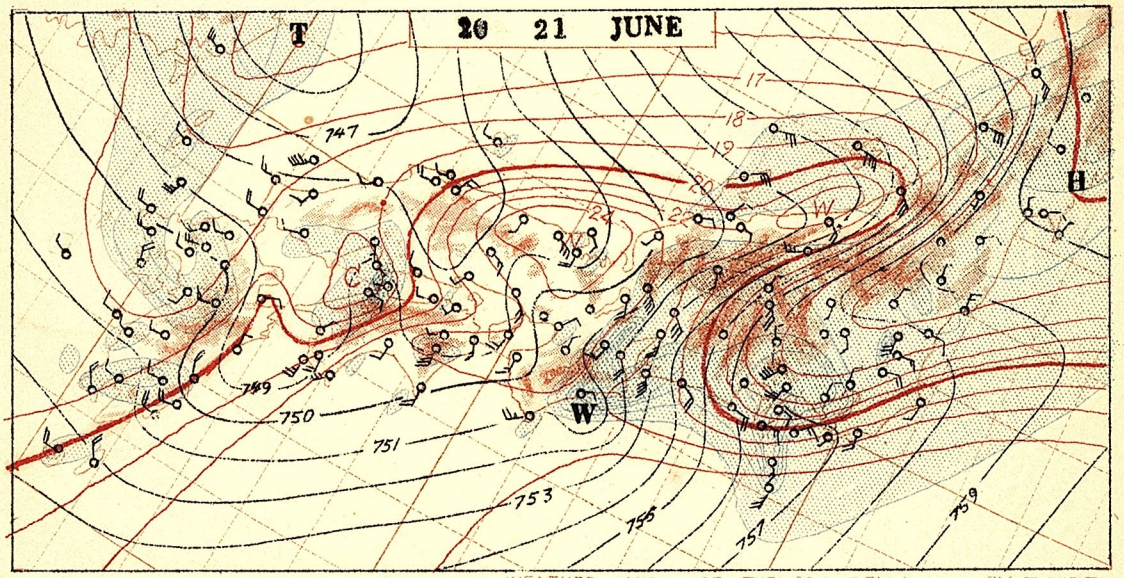

WEATHER MAPS OF TYPHOON DELLA BY T. FUJITA

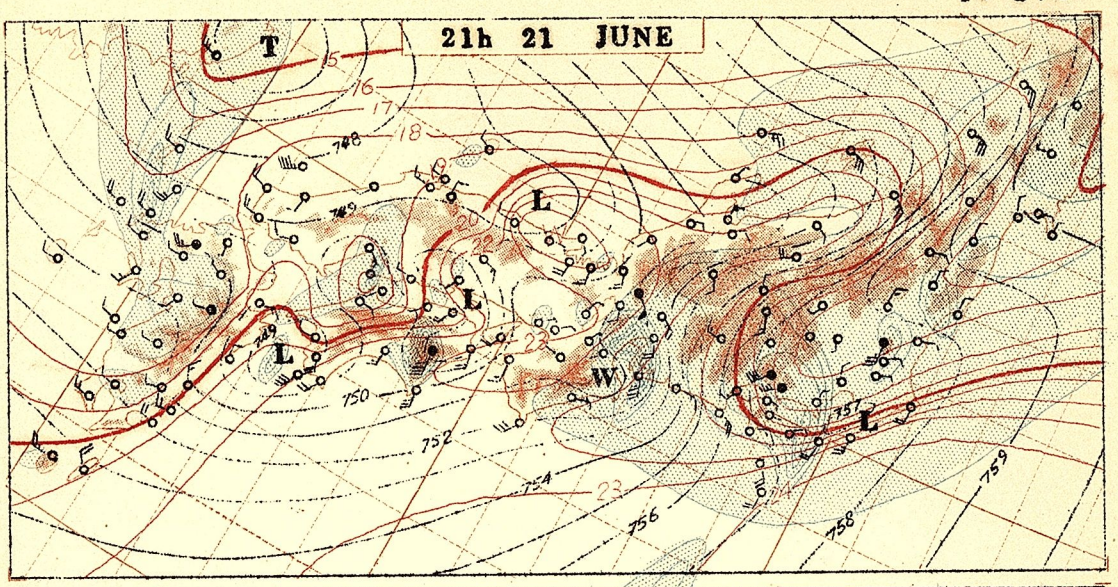

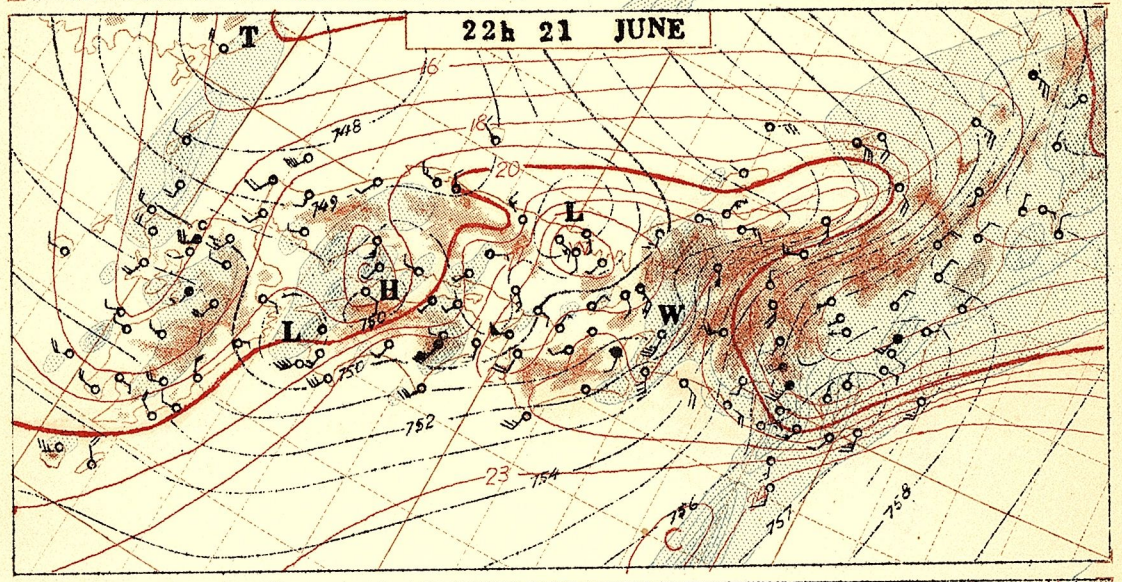

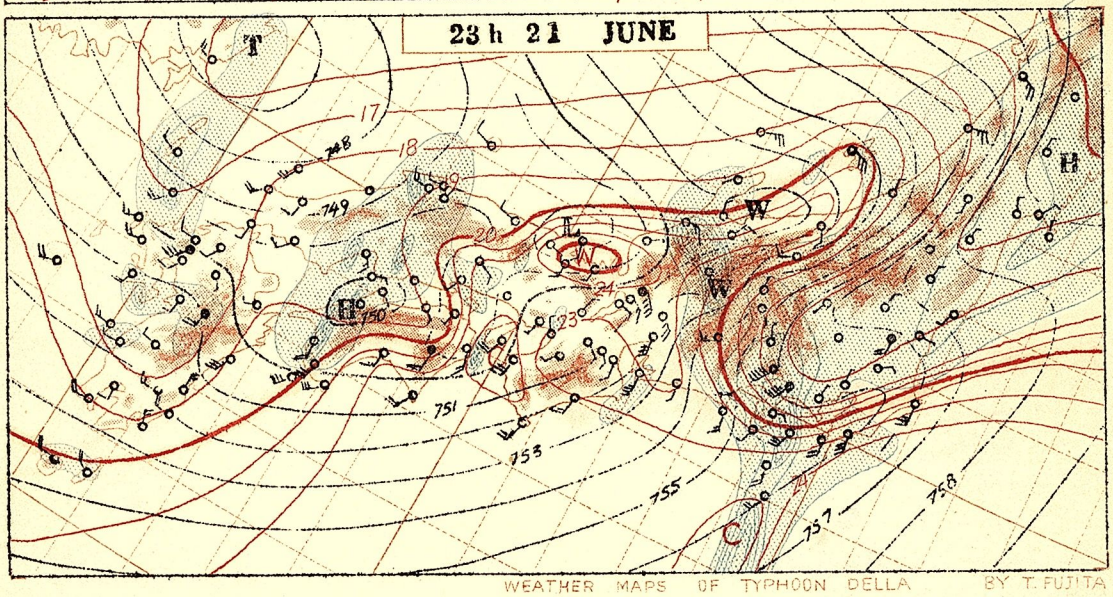

WEATHER MAPS OF TYPHOON DELLA BY T. FUJITA

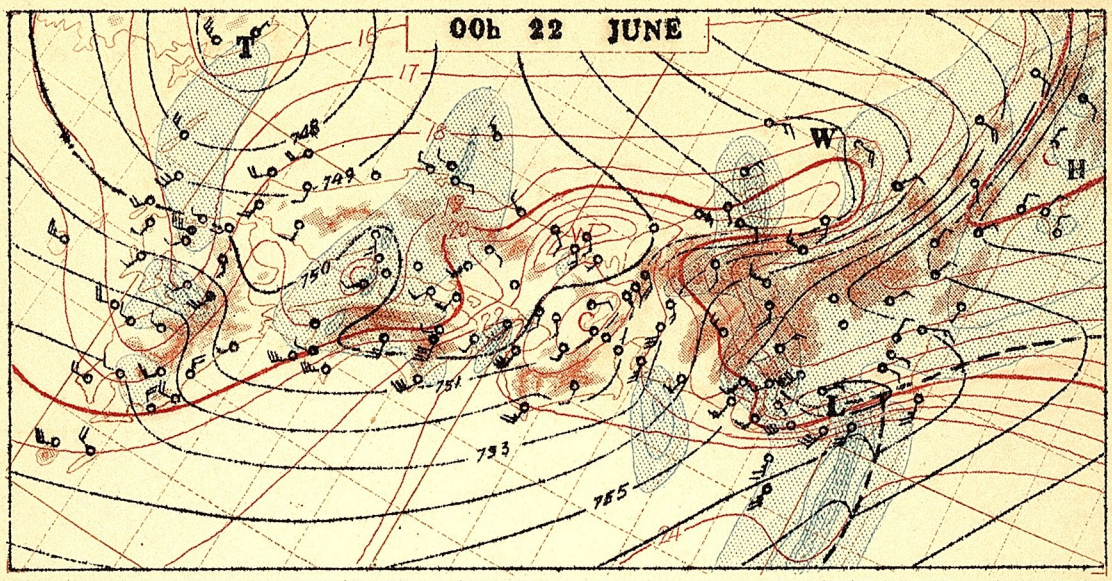
00h 22 JUNE
T
W
H
L
748
749
750
751
753
755

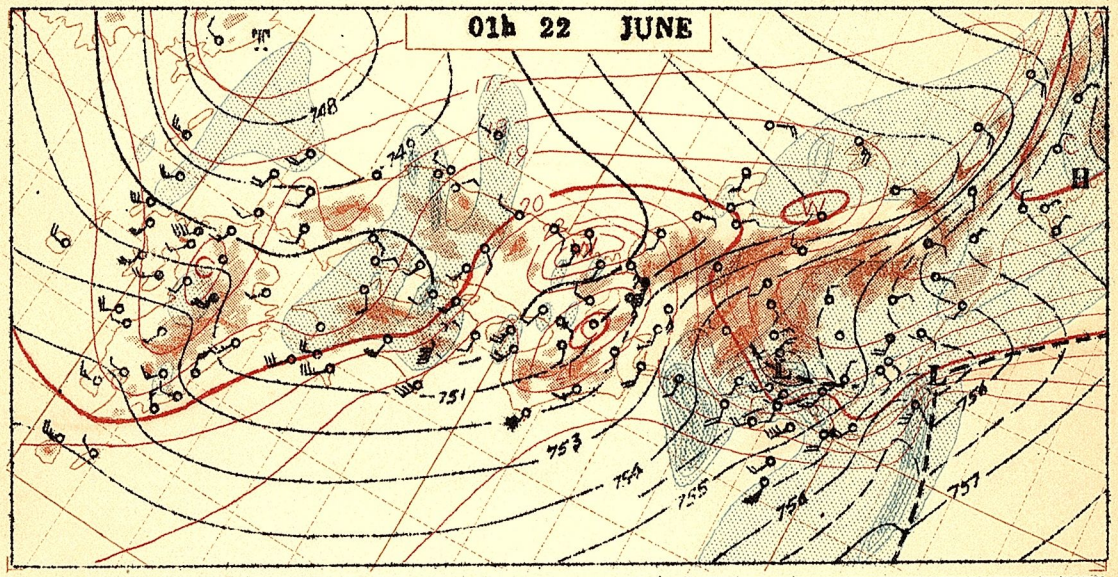
01h 22 JUNE
748
749
751
753
754
755
756
757
H
L

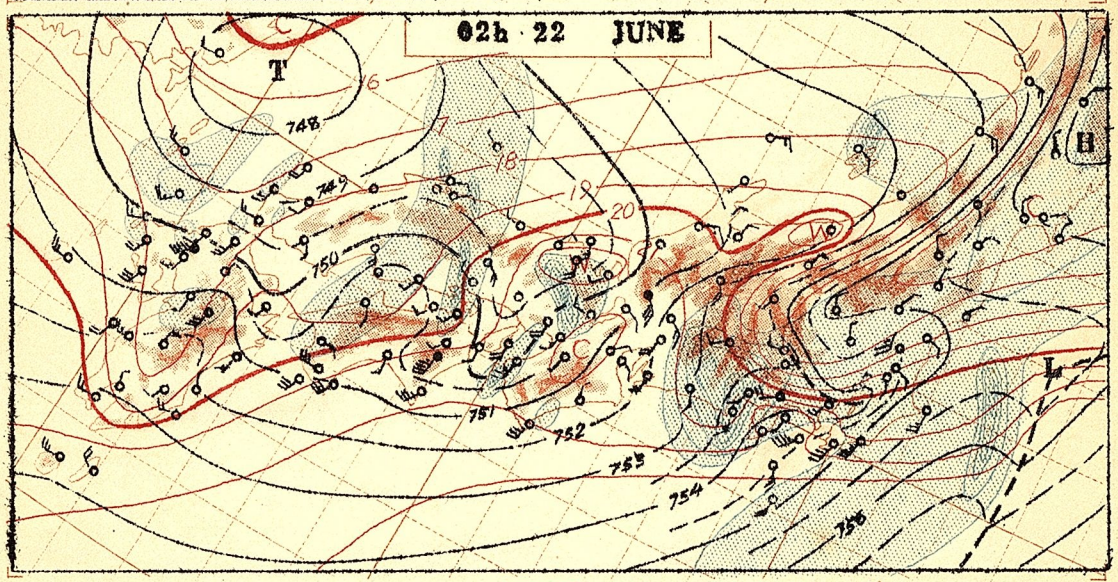
02h 22 JUNE
T
748
749
750
751
752
753
754
756
H
L

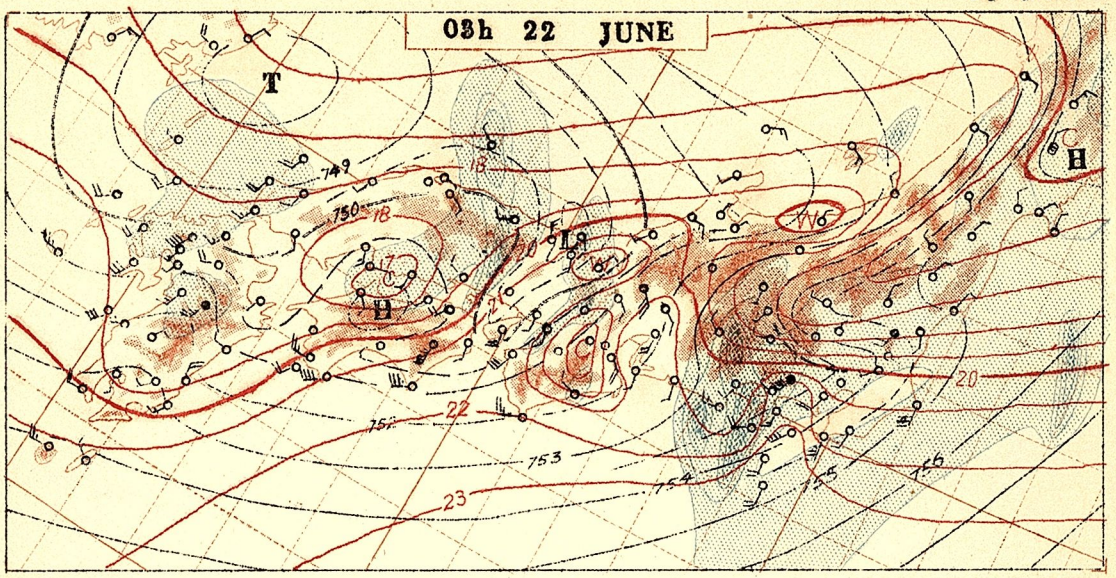

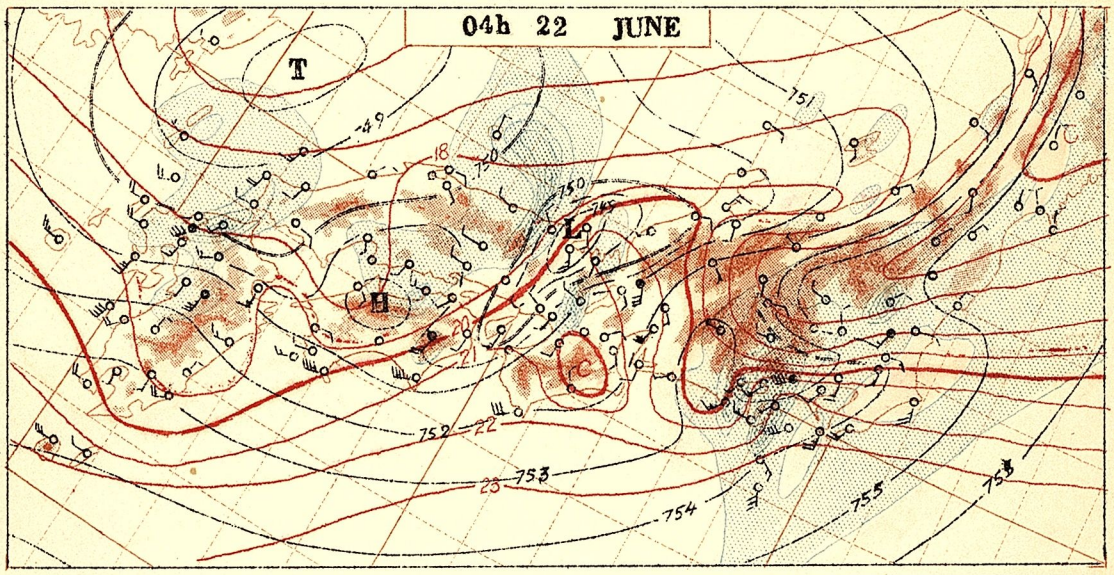

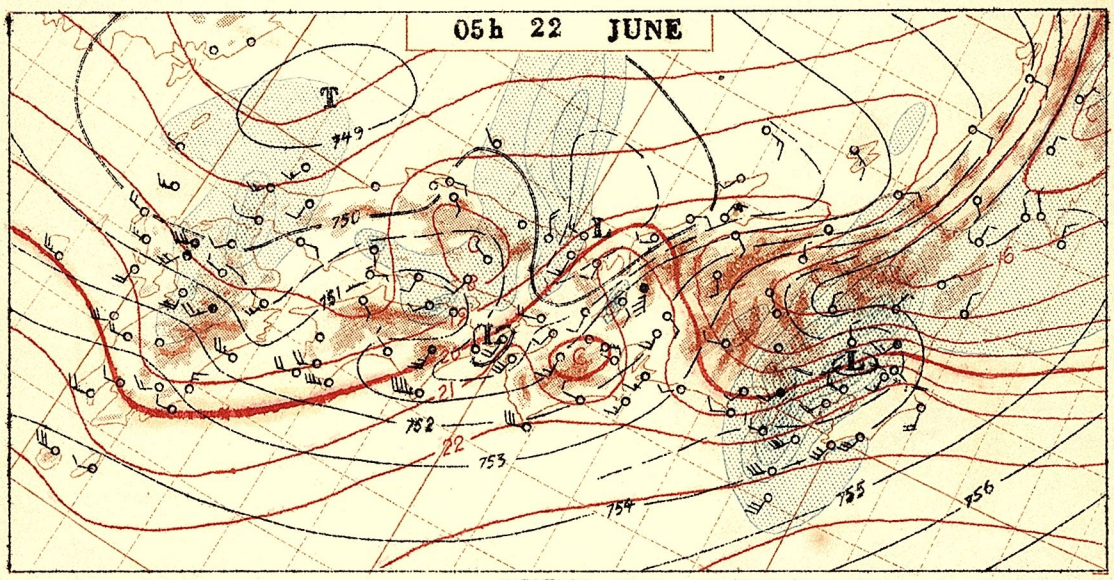

WEATHER MAPS OF TYPHOON DELLA BY T. FUJITA

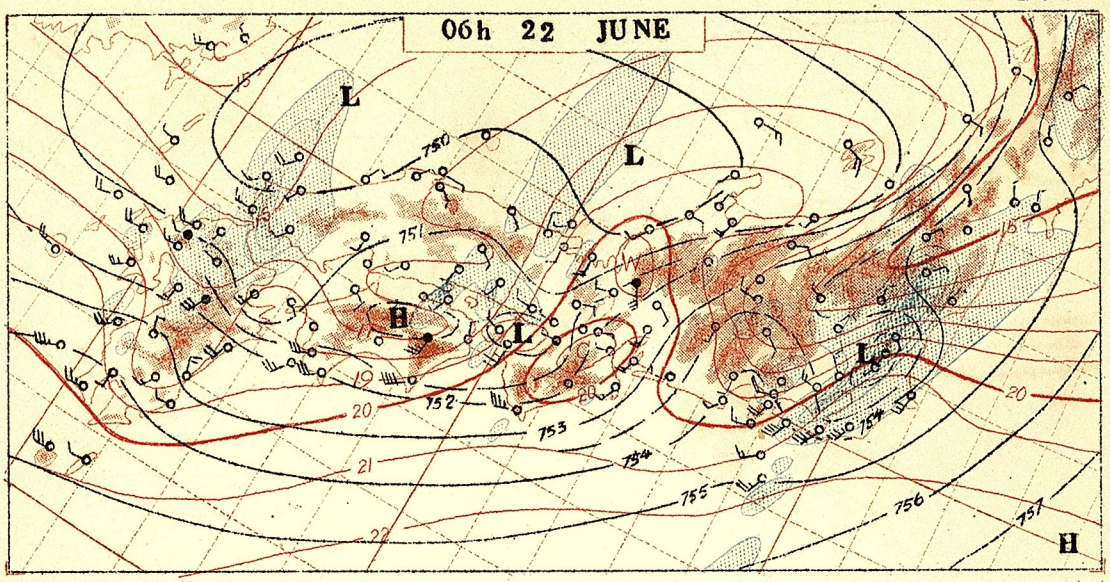

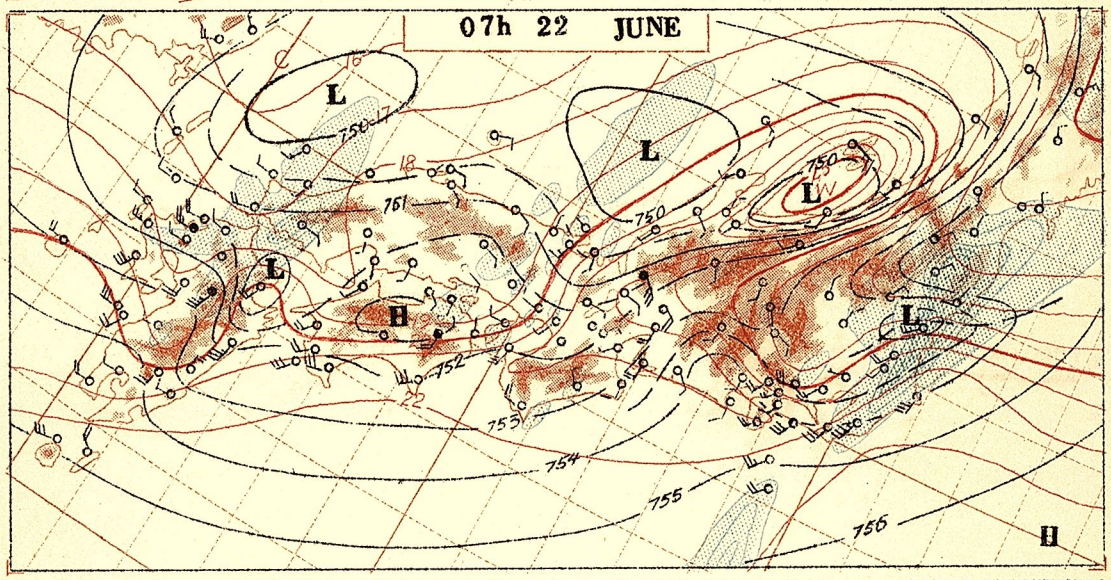

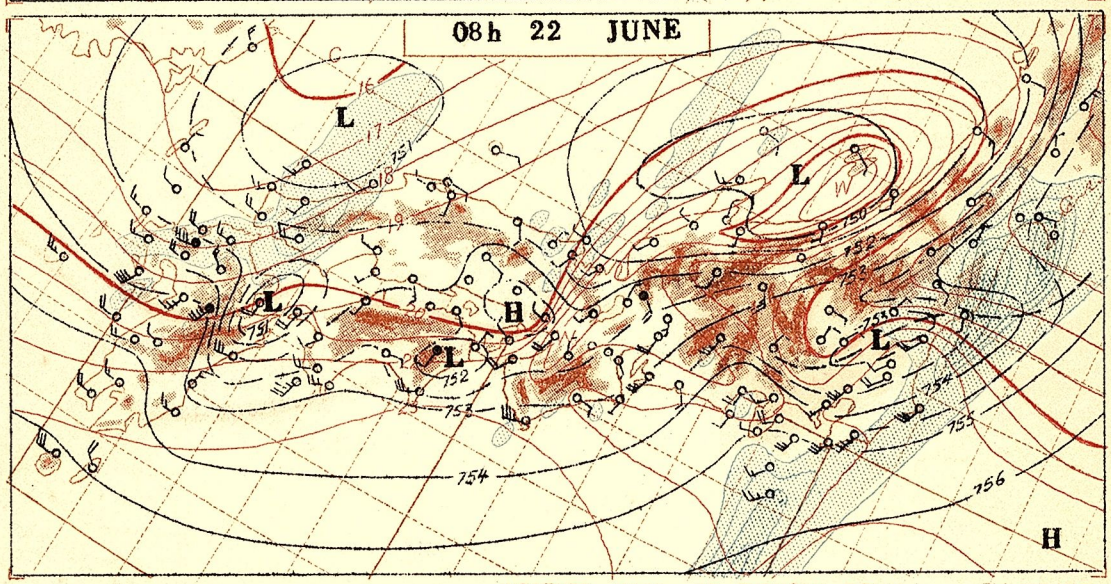

WEATHER MAPS OF TYPHOON DELLA BY T. FUJITA

EXAMPLE 3

DISTRIBUTION OF WIND SPEED WITHIN TYPHOON DELLA

From 21h 20th to 06h 21st

June 1949

In the following charts, the wind speeds are contoured for every 5 knots, and the areas with the speed more than 30 knots are represented by stippled ones.

At 21h, when the typhoon has passed over Yakushima Island, the slow wind area in the center extended north-eastward, but as the time passed on, the direction changed NNE to N. While the strong winds were observed, as expected, in the eastern area.

At 01h, the strong winds surrounded the typhoon center perfectly. This is due to the fact that the wind speeds were not so high on Kyushu Island.

At 05h, the high wind speed is seen over the cold air push entering from the west of typhoon. In many cases the typhoon winds slow down when they enter the area of complicated topography, but in the present case, the cold northery winds were prevailing over north Kyushu without changing their speed, This is because the cold airs tend to subside carrying the large momentum on higher levels down to the ground, and the action would help the maintenance of the high speed.

After all, it can be said that an attempt to draw the wind speed pattern by entering the observed values at different time of observation to the same chart is not reasonable. Since the patterns change so rapidly even within one hour. Of course, in drawing the present charts, the auxiliary data observed 30 minutes before and after the map time are used for helping the main data.

It must always be kept in mind that the reporting wind speed for lighthouse weather station is usually one and half times higher than that for the surface station that is located below the hill, and that the speed at the station in a town is slower than expected, because the wind tower of such a station is sometimes located inside the appreciable turbulent layer caused by trees and buildings.

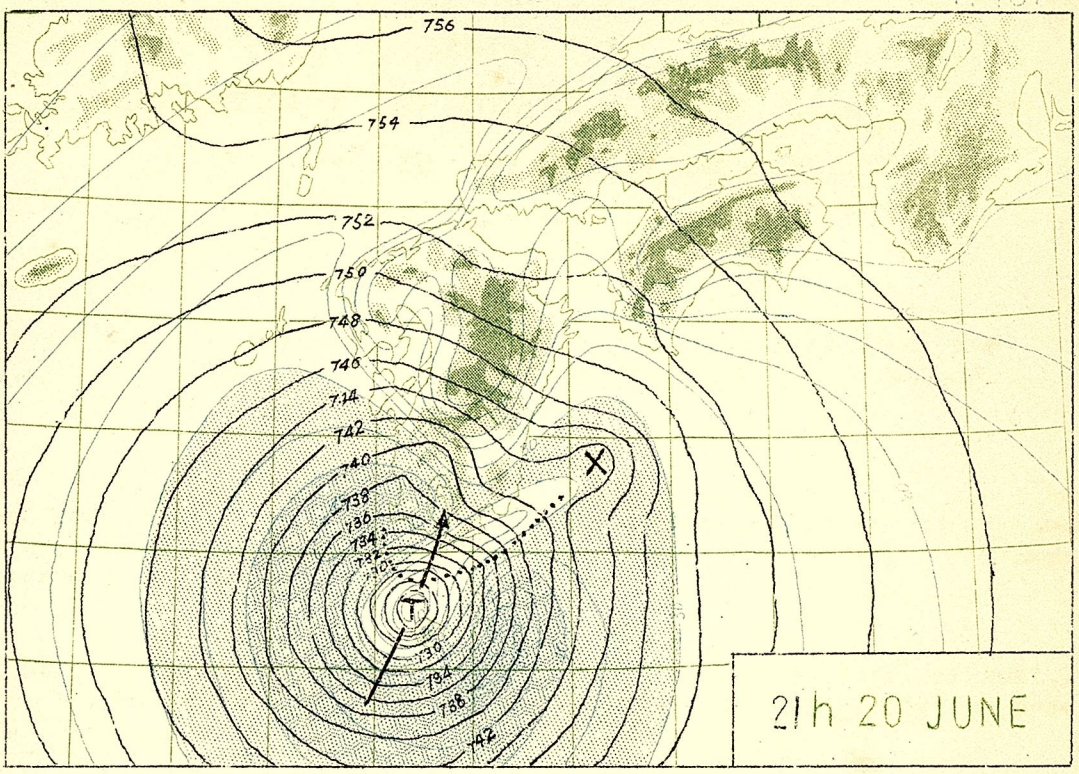
756
754
752
750
748
746
744
742
740
738
736
734
732
730
734
738
742
21h 20 JUNE

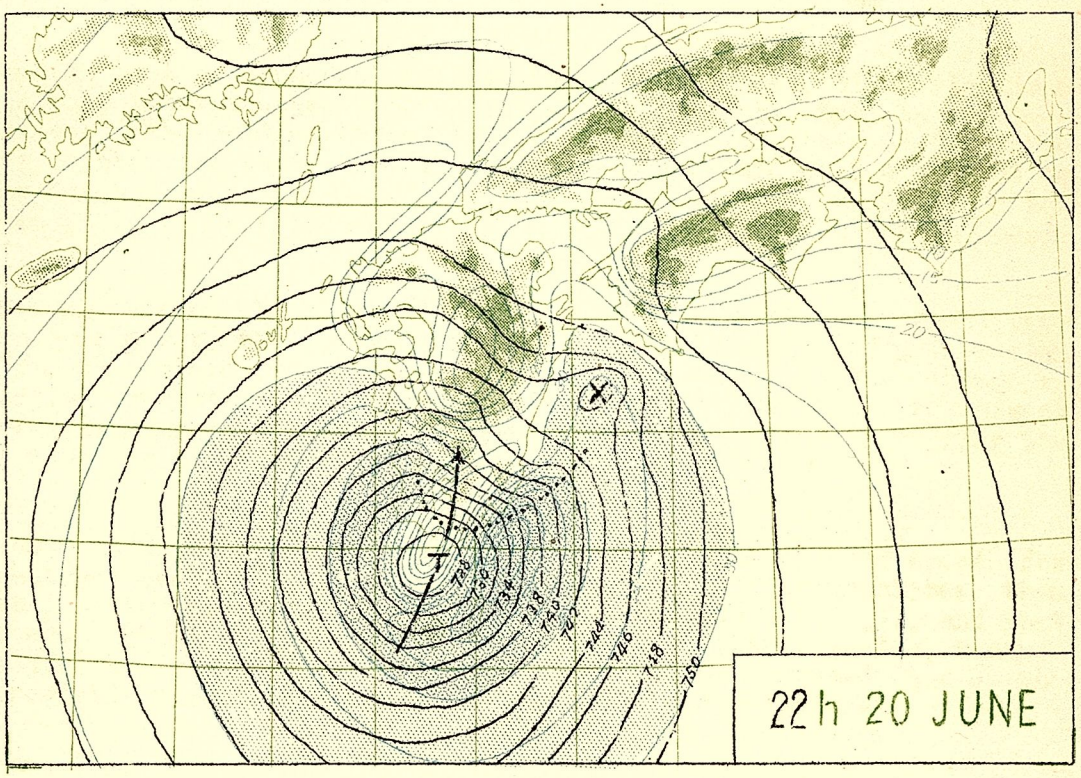
20
728
730
734
738
740
742
744
746
748
750
22h 20 JUNE

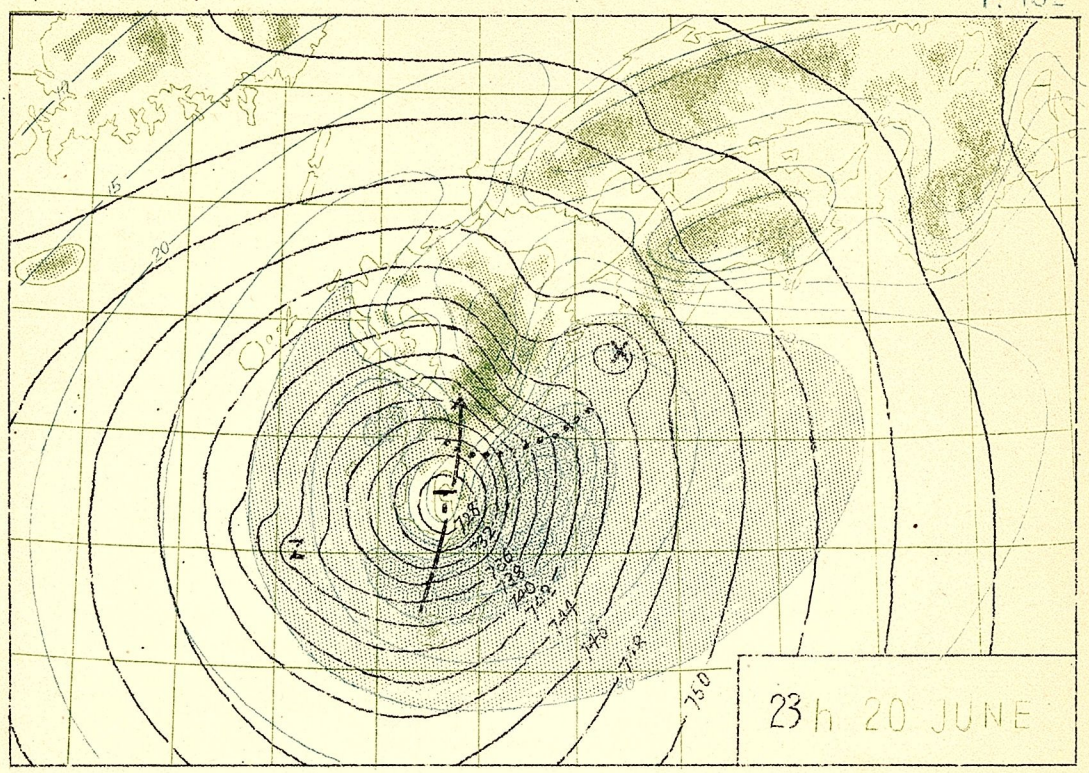
15
20
25
730
732
734
736
738
740
742
744
745
746
748
750
23h 20 JUNE

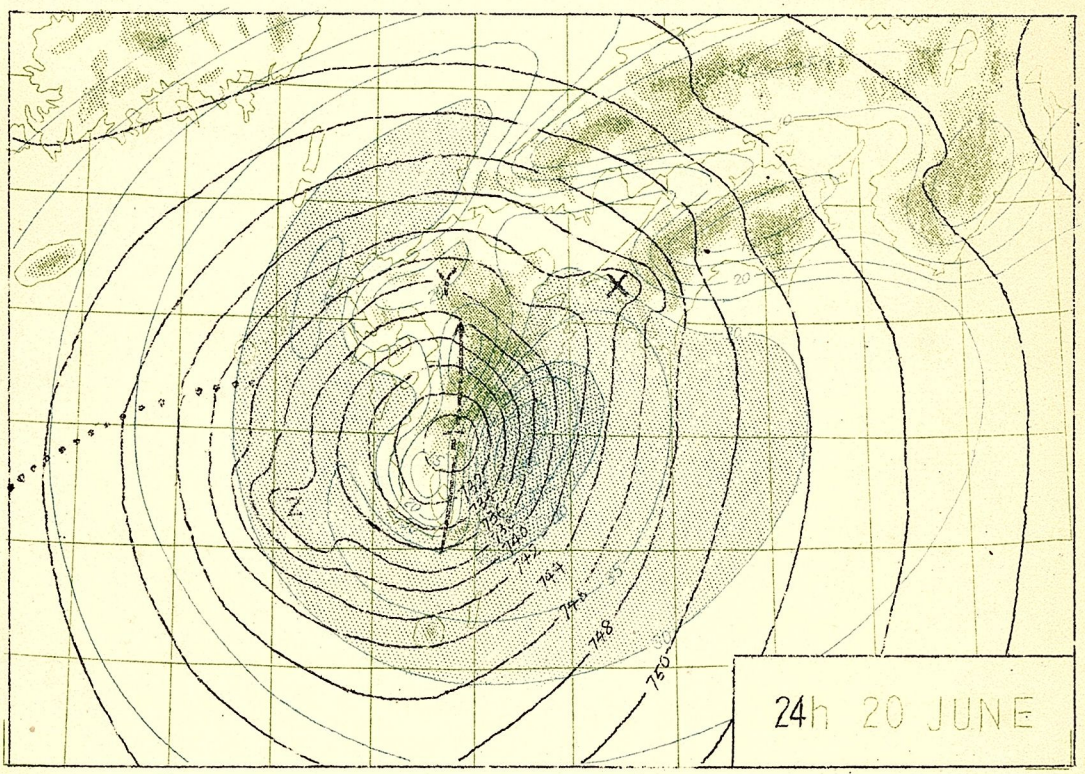
730
732
734
736
738
740
742
744
746
748
750
24h 20 JUNE

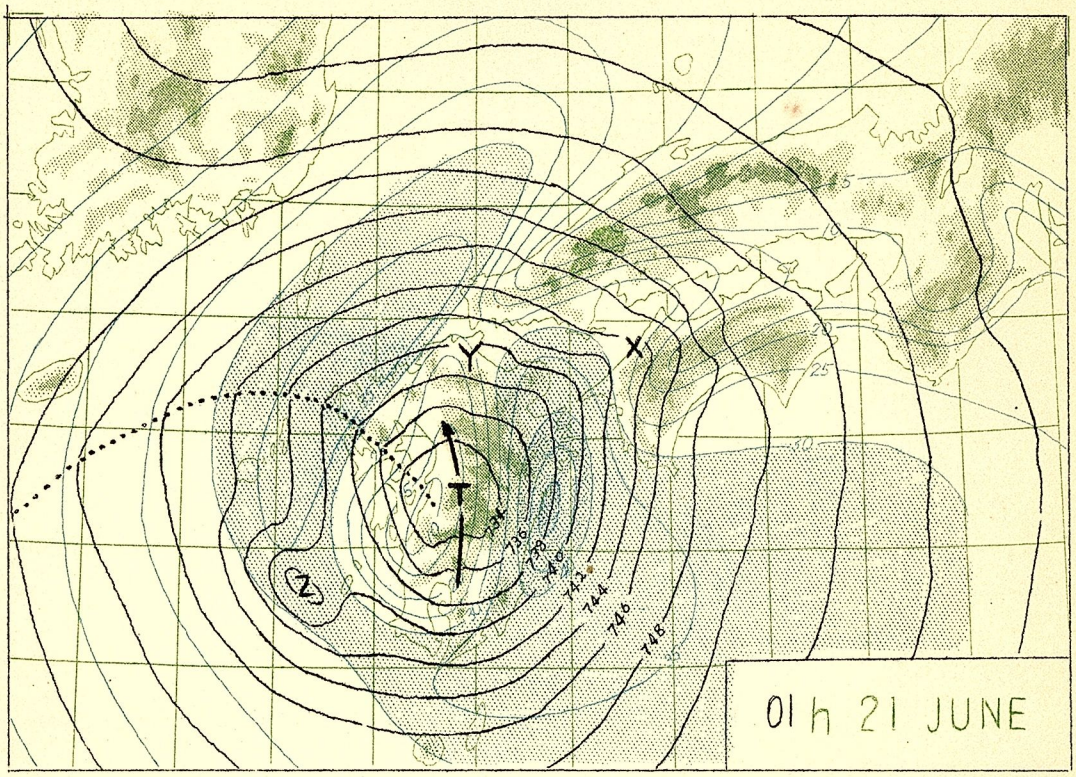
Y
X
T
Z
734
736
738
740
742
744
746
748
01 h 21 JUNE

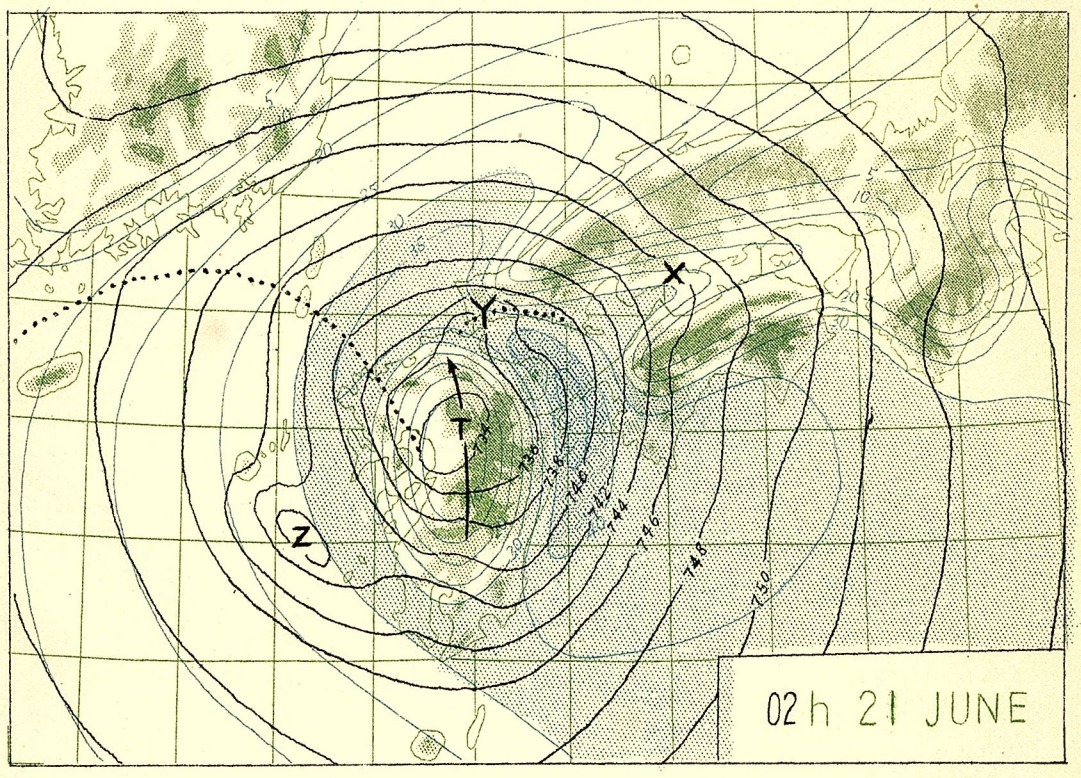
X
Y
T
Z
734
736
738
740
742
744
746
748
750
02 h 21 JUNE

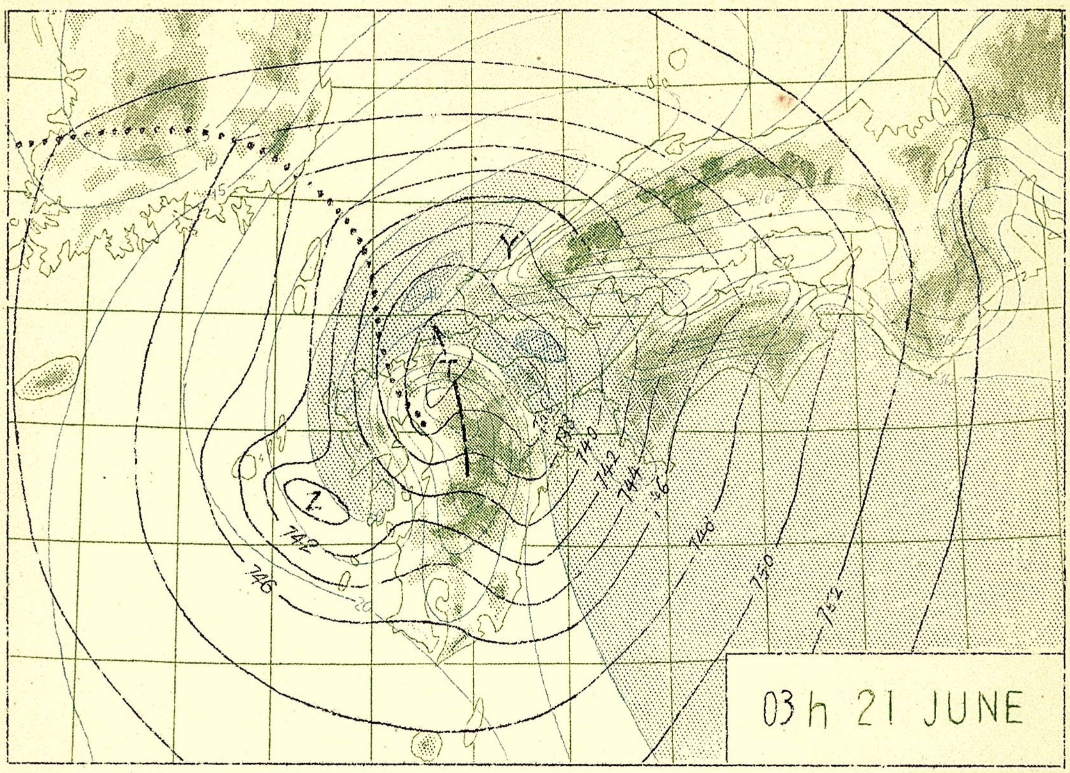

03 h 21 JUNE

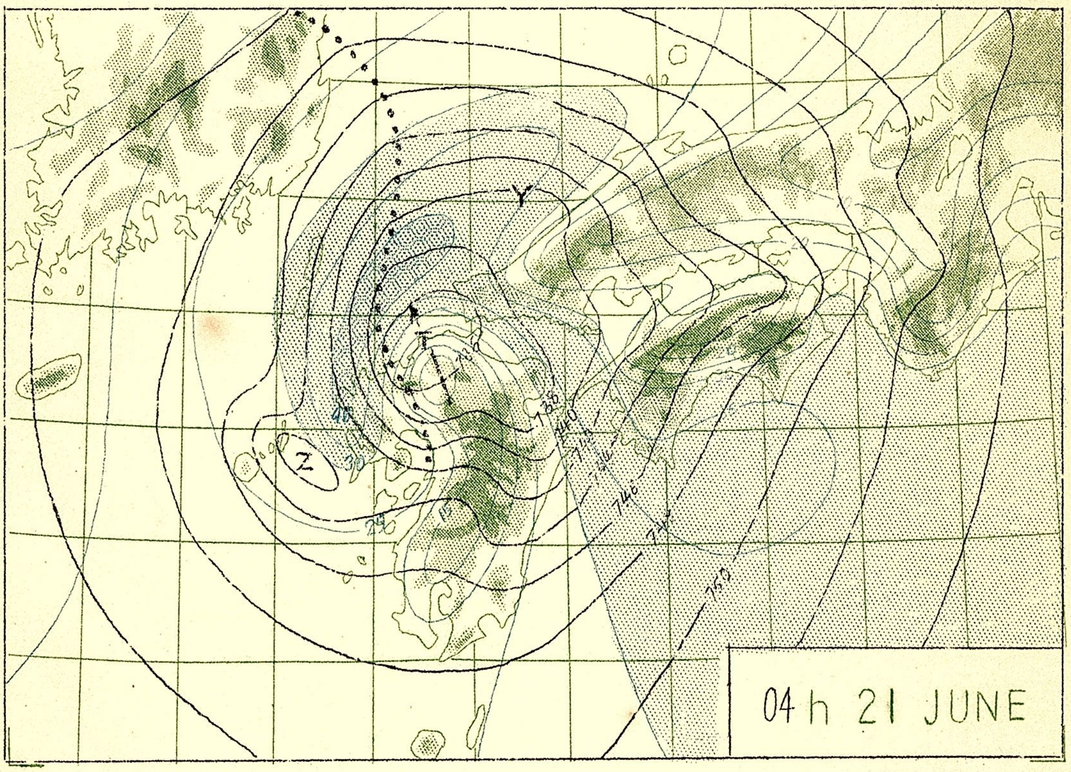

04 h 21 JUNE

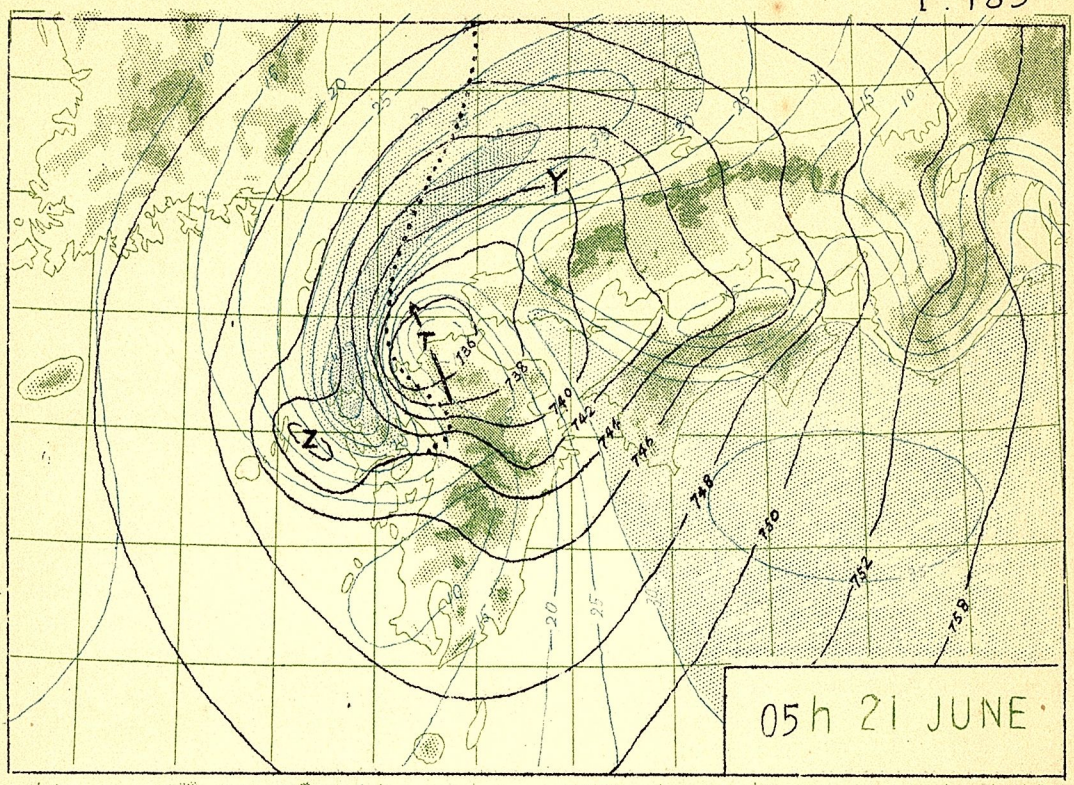
Y
T
Z
736
738
740
742
744
746
748
750
752
758
05h 21 JUNE

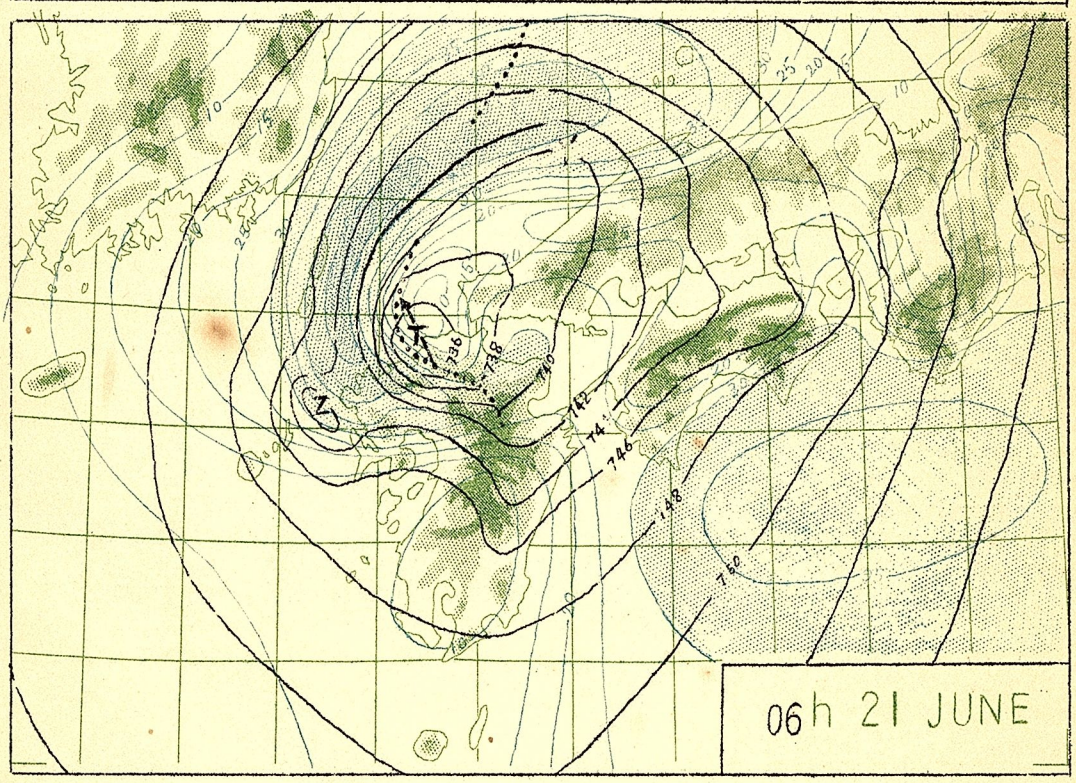
T
Z
736
738
740
742
744
746
748
750
06h 21 JUNE

EXAMPLE 4

ISALLOBARS WITHIN TYPHOON DELLA

From 21h 20th to 06h 21st

June 1949

The following charts show the isallobars contoured for every 1 mm-Hg/hour. The tendencies for the map time were computed by differentiating the pressure traces with respect to time. The areas of positive tendencies are represented by stippled areas.

At 21h, the minimum pressure line extended from WSW to ESE passing through the typhoon center. A marked trough line travelled northward in the western sector resulting in a marked pressure rise south of the trough. As will be seen in the chart for 24h, at first the minimum pressure line bended southward but according to the northward movement of the trough the positive tendency area advanced northward rapidly.

At 02h, the marked trough reached Tsushima Island, meanwhile the isallobars concentrated near the trough line. It is known that the pressure traces at the stations north-west of Kyushu showed a pointed bottom at the time of the trough passage.

At 05h, the greater parts of the typhoon areas showed positive tendency, and especially in the region through which the cold air from the north-west was entering the southern sector of the typhoon, the rate of the pressure rise was very large.

Isallobars are very useful in distinguishing the dip from the topographical low pressure areas which do not move as a dip does. As will be seen in the charts, pressure drops appreciablly when a dip approaches, and sometimes it happens, even when the main storm is closing near, that the pressure rises after the passage of the dip center. On the other hand, there are no special pressure tendencies in the leeward side of a mountain where the pressure is sometimes lower 1 or 2 mbs. than of the undisturbed regions. This is because the topographical low stays almost at the constant location.

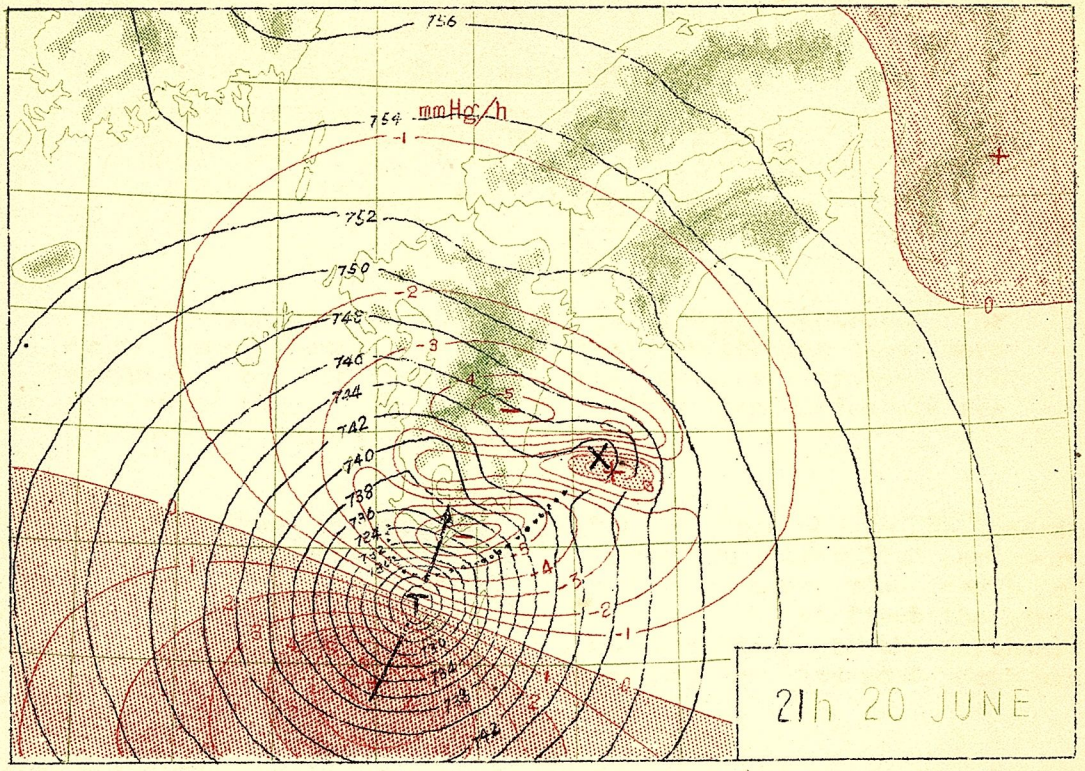
mmHg/h
21h 20 JUNE

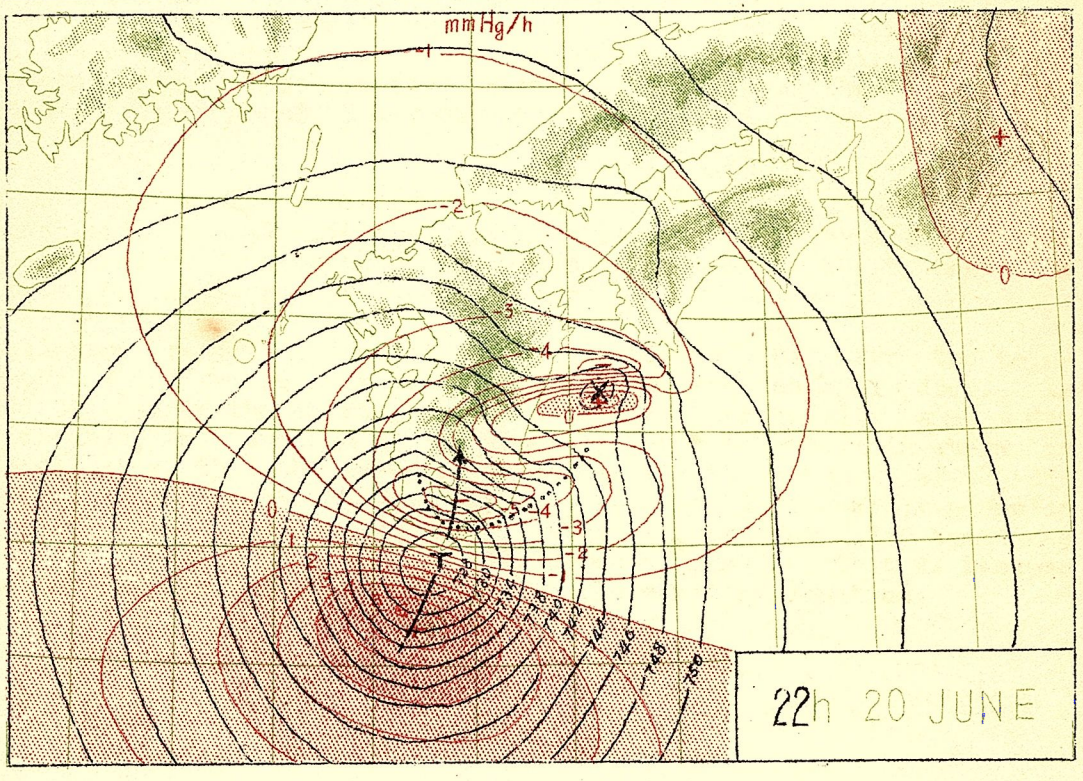
mmHg/h
22h 20 JUNE

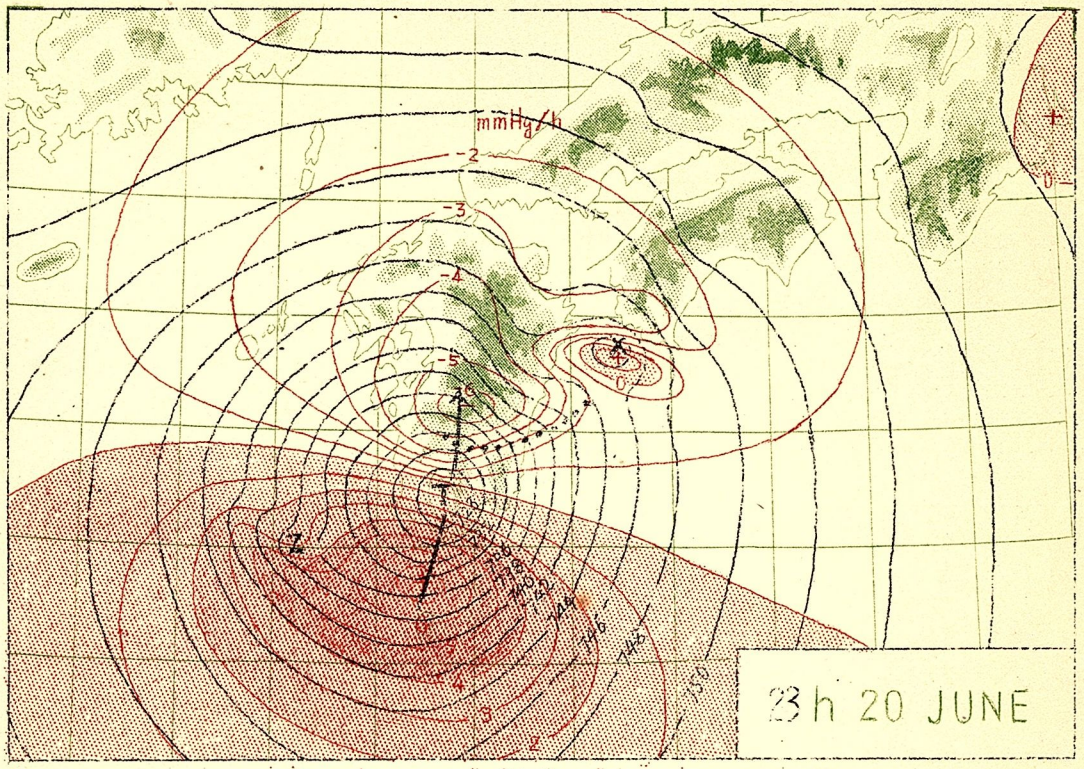
mmHg/h
-2
-3
-4
-5
-6
0
+
0
23 h 20 JUNE

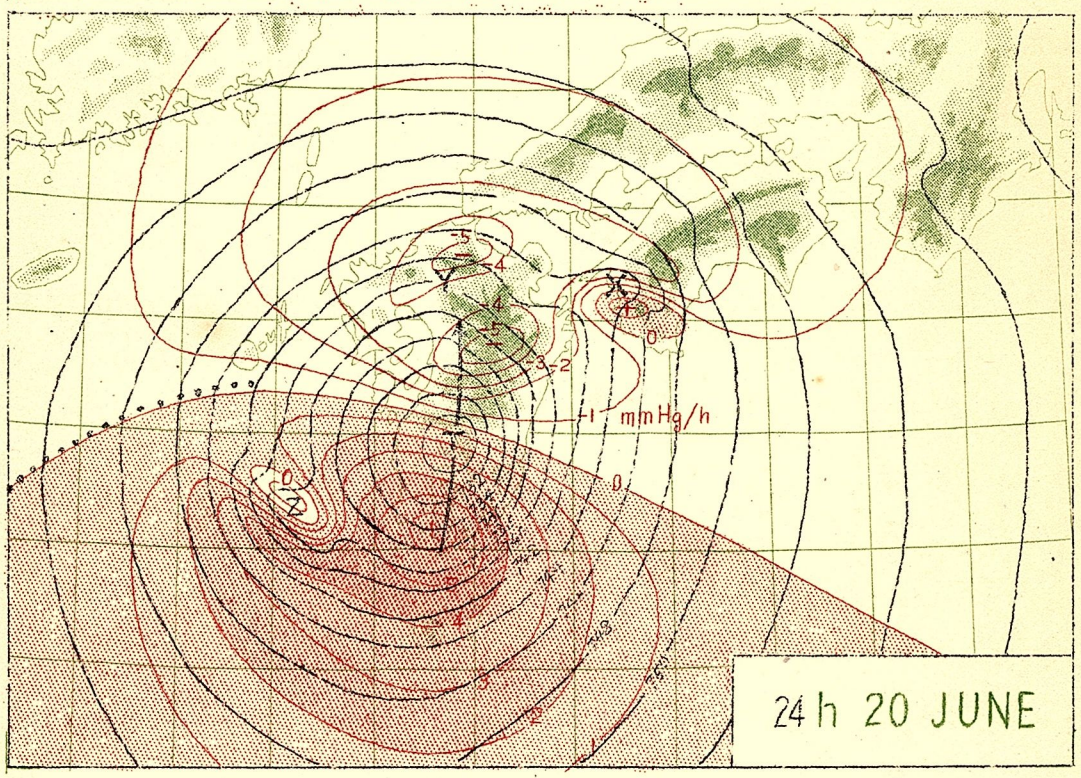
-5
-4
-4
-5
-3
-2
0
-1
mmHg/h
0
0
-2
-3
-4
-5
24 h 20 JUNE

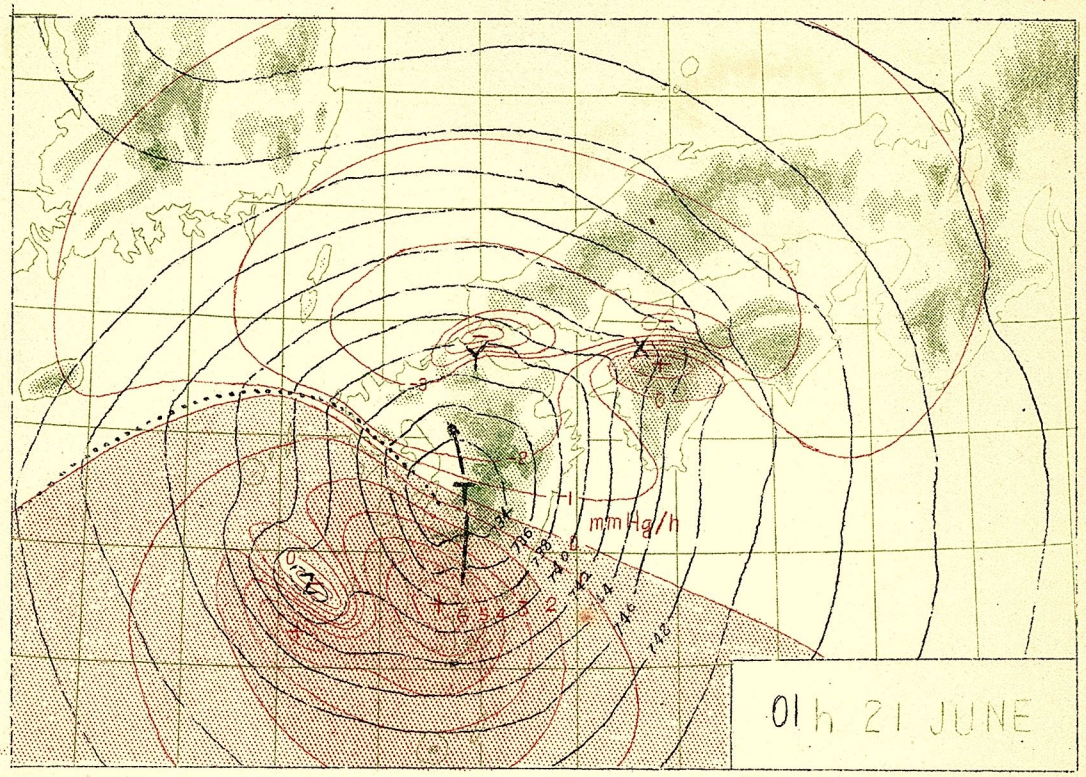
01 h 21 JUNE
mm Hg/h

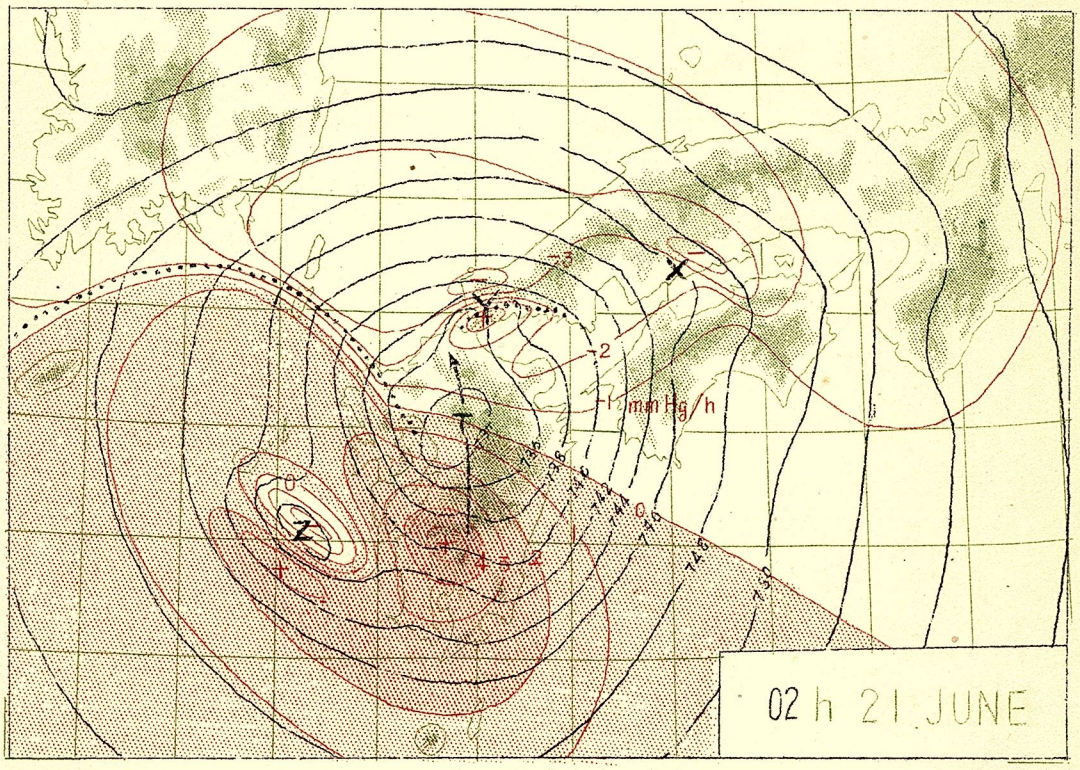
02 h 21 JUNE
mm Hg/h

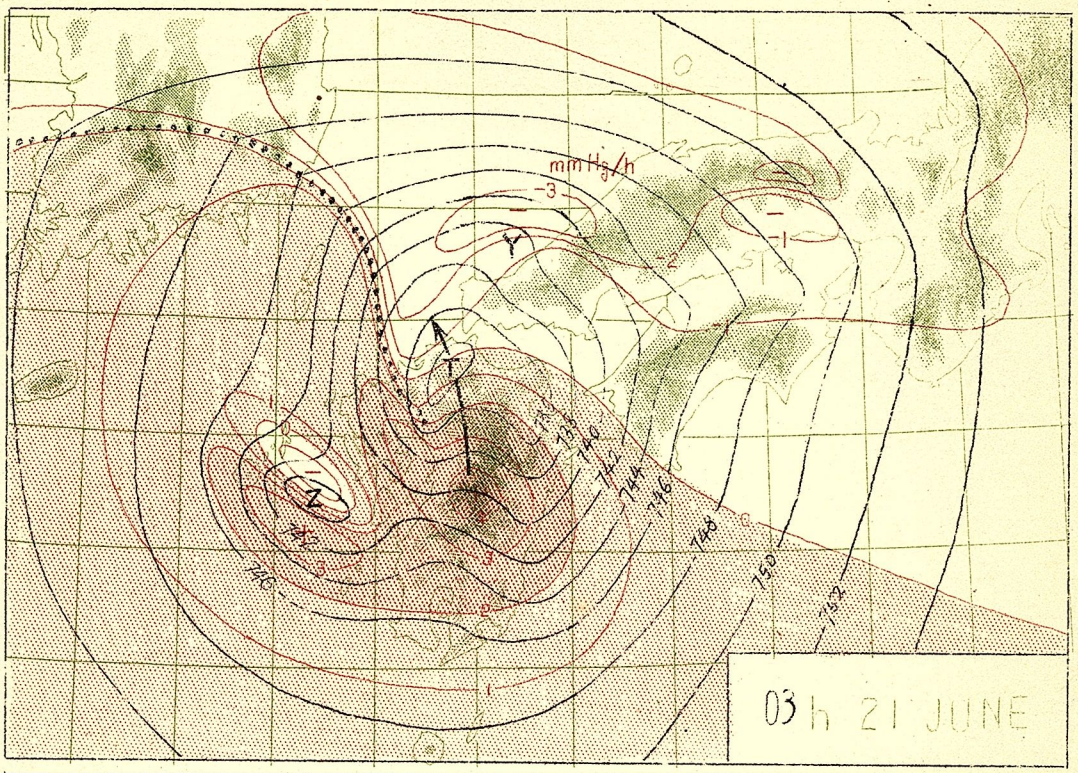
mmHg/h
-3
-1
1
3
740
742
744
746
748
750
752
03 h 21 JUNE

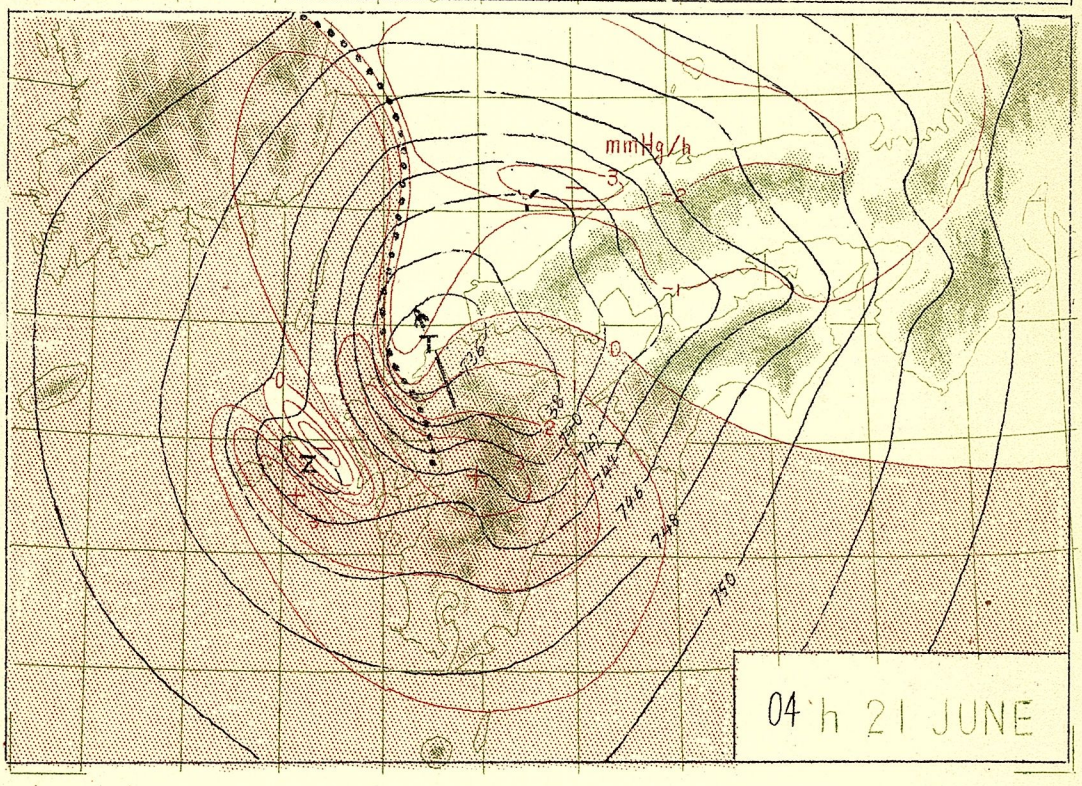
mmHg/h
-3
-2
-1
0
1
2
3
740
742
744
746
748
750
04 h 21 JUNE

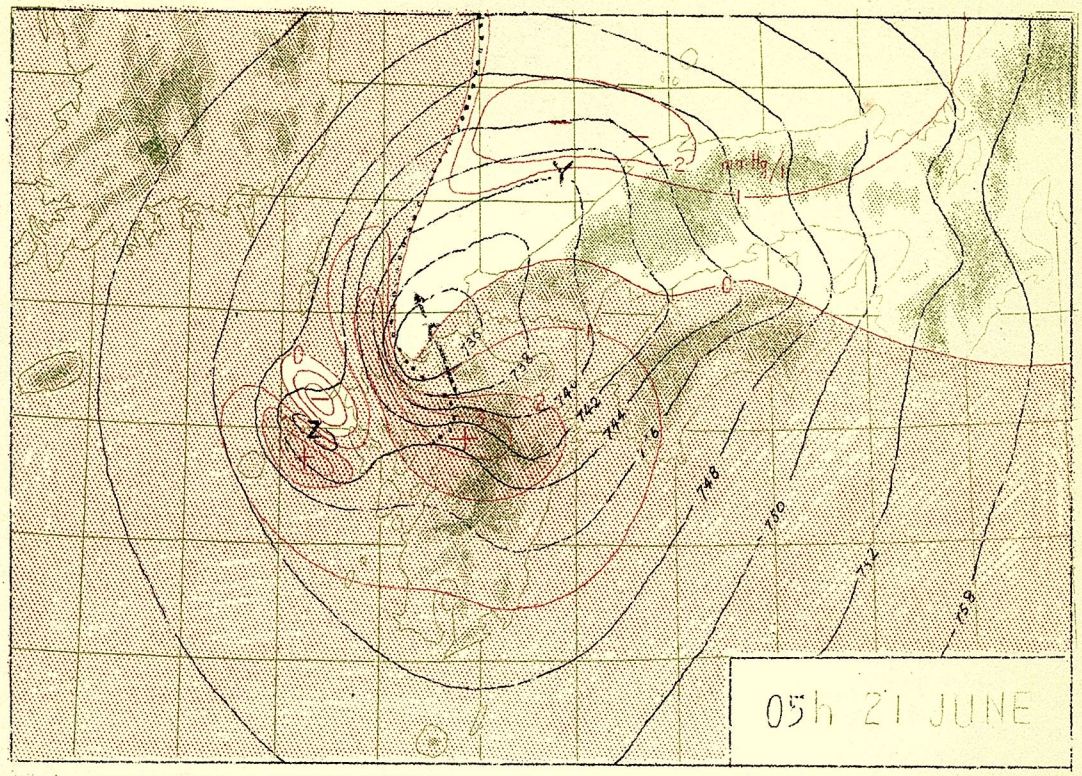
mm Hg/h
2
1
0
-1
-2
730
734
738
742
744
746
748
750
752
758
05h 21 JUNE

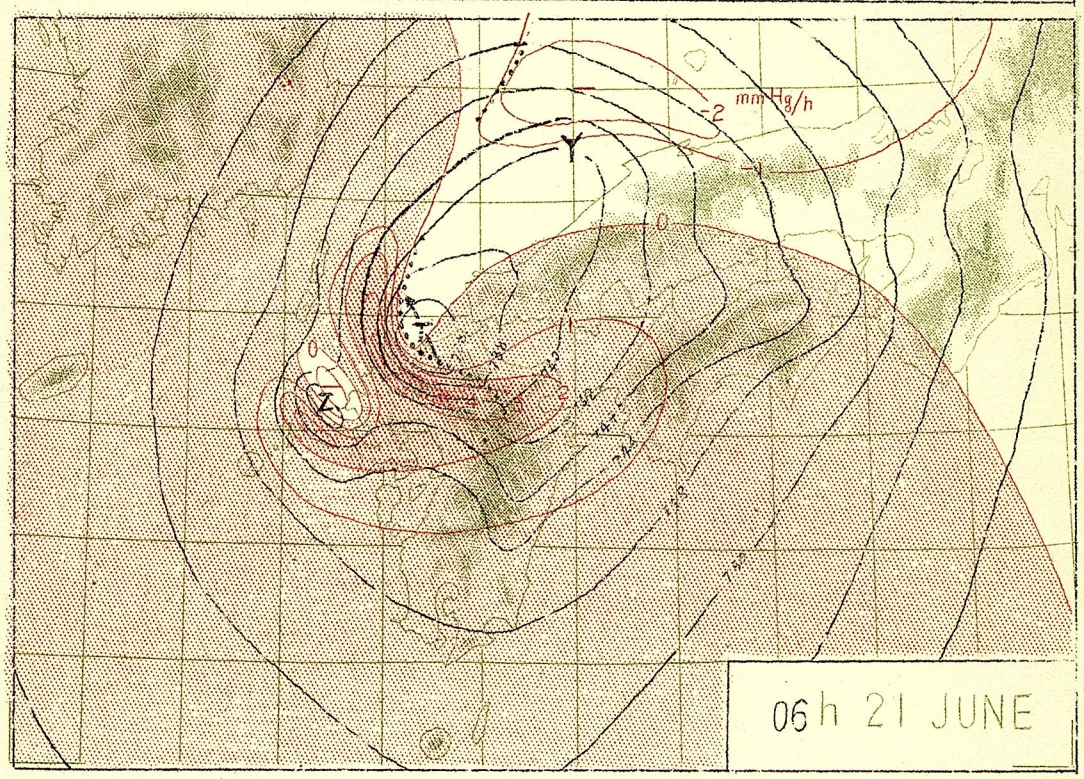
mm Hg/h
-2
0
-1
730
734
738
742
744
746
748
750
752
758
06h 21 JUNE

EXAMPLE 5

MIDDLE POINT CORRECTION FOR THE UPPER-AIR DATA IN TYPHOON KEZIA

From 10 to 18 Sept. 1950

To eliminate the errors in the upper-air data, the middle point correction is very useful. The examples of the corrected results are shown in the following sheets.

The corrections were carried out for the heights and temperatures at the constant pressure levels of 1000, 850, 700, 500, 300, 200, 150, 100 and 80 mbs. The circles in the figure show the middle point of each line segment connecting the successive observed values. When the observation interval is larger than 12 hrs, the segment is represented by broken line.

INDEX OF STATIONS

YONAGO	35 26 N	133 21 E	7.9 m
SHIONOMISAKI	33 27 N	135 46 E	74.9 m
KAGOSHIMA	31 34 N	130 33 E	5.4 m
ITAZUKE	33 35 N	130 27 E	7.0 m
TARE(W.S.)	29 00 N	135 00 E	0.0 m
X-RAY(W.S.)	39 00 N	153 00 E	0.0 m
TATENO	36 03 N	140 08 E	27.2 m
SENDAI	38 16 N	140 54 E	39.8 m
SAPPORO	43 04 N	141 20 E	18.1 m
WAKKANAI	45 25 N	141 41 E	3.2 m
WAJIMA	37 23 N	136 54 E	6.9 m
AKITA	39 43 N	140 06 E	9.9 m

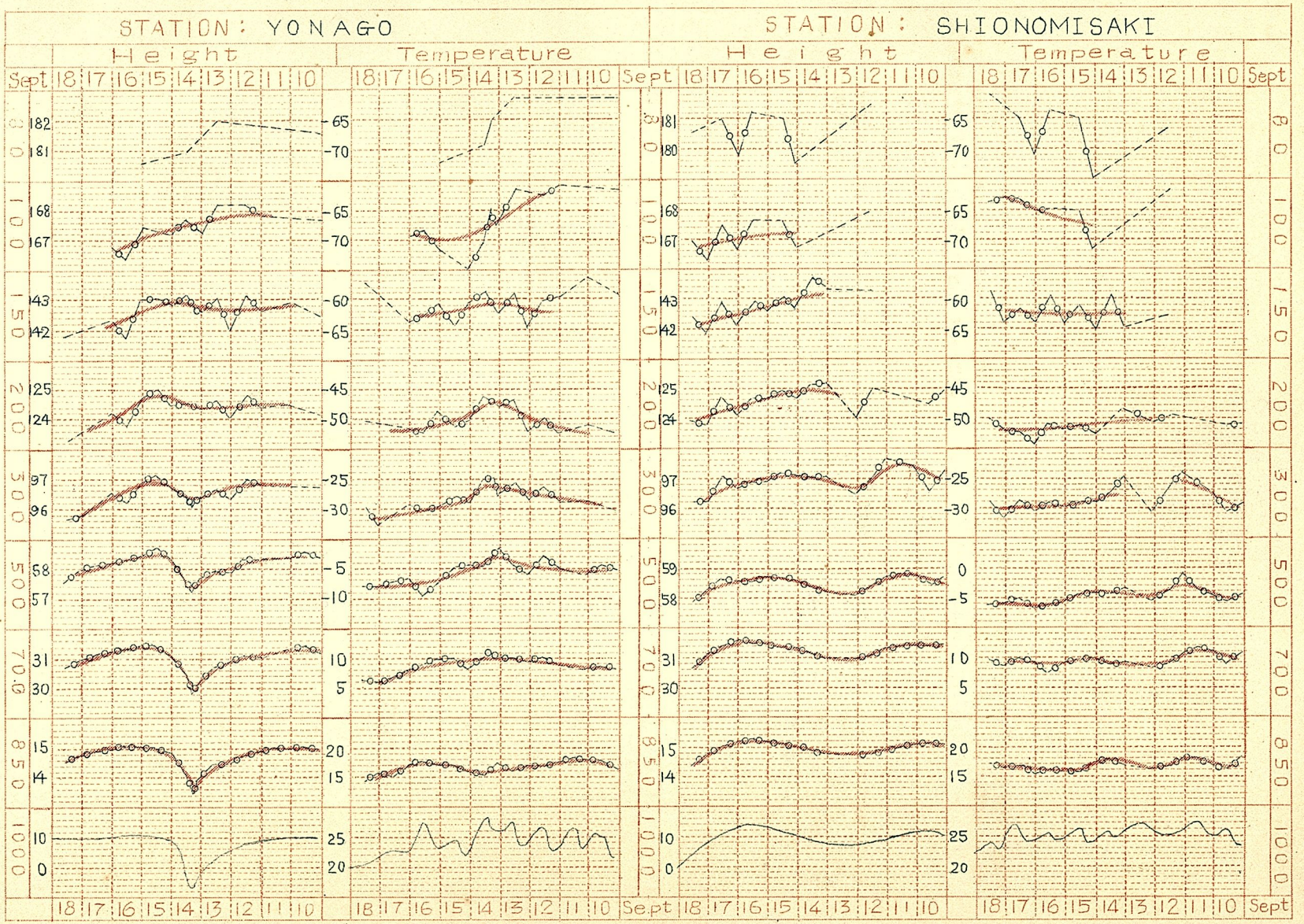

MIDDLE POINT CORRECTION (TYPHOON KEZIA).

P.193

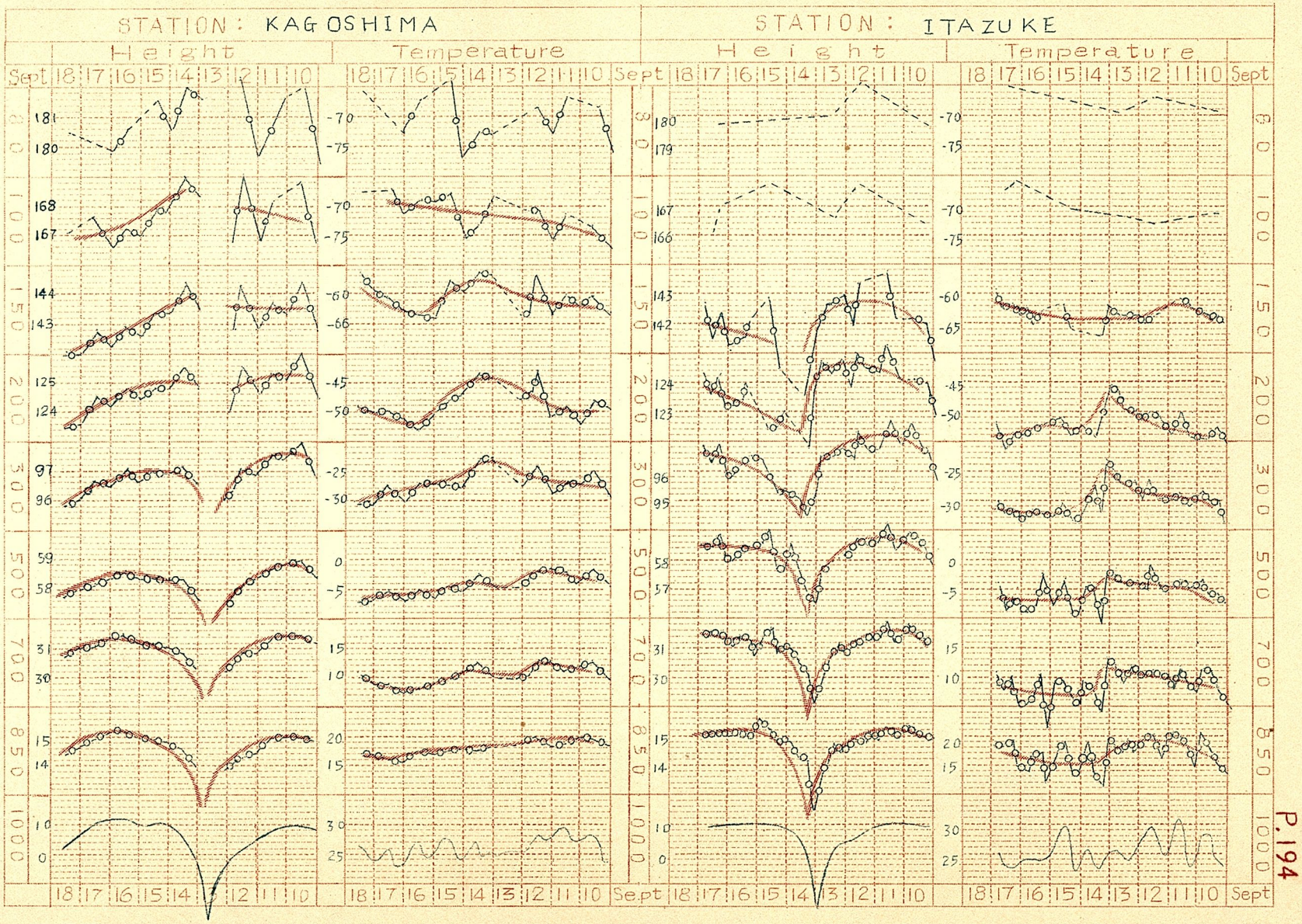
STATION : KAGOSHIMA
Height
Temperature
STATION : ITAZUKE
Height
Temperature
Sept 18 17 16 15 14 13 12 11 10
200 181 180
100 168 167
150 144 143
200 125 124
300 97 96
500 59 58
700 31 30
850 15 14
1000 10 0
-70 -75
-70 -75
-60 -66
-45 -50
-25 -30
0 -5
15 10
20 15
30 25
180 179
167 166
143 142
124 123
96 95
58 57
31 30
15 14
10 0
-70 -75
-70 -75
-60 -65
-45 -50
-25 -30
0 -5
15 10
20 15
30 25
MIDDLE POINT CORRECTION) TYPHOON KEZIA)

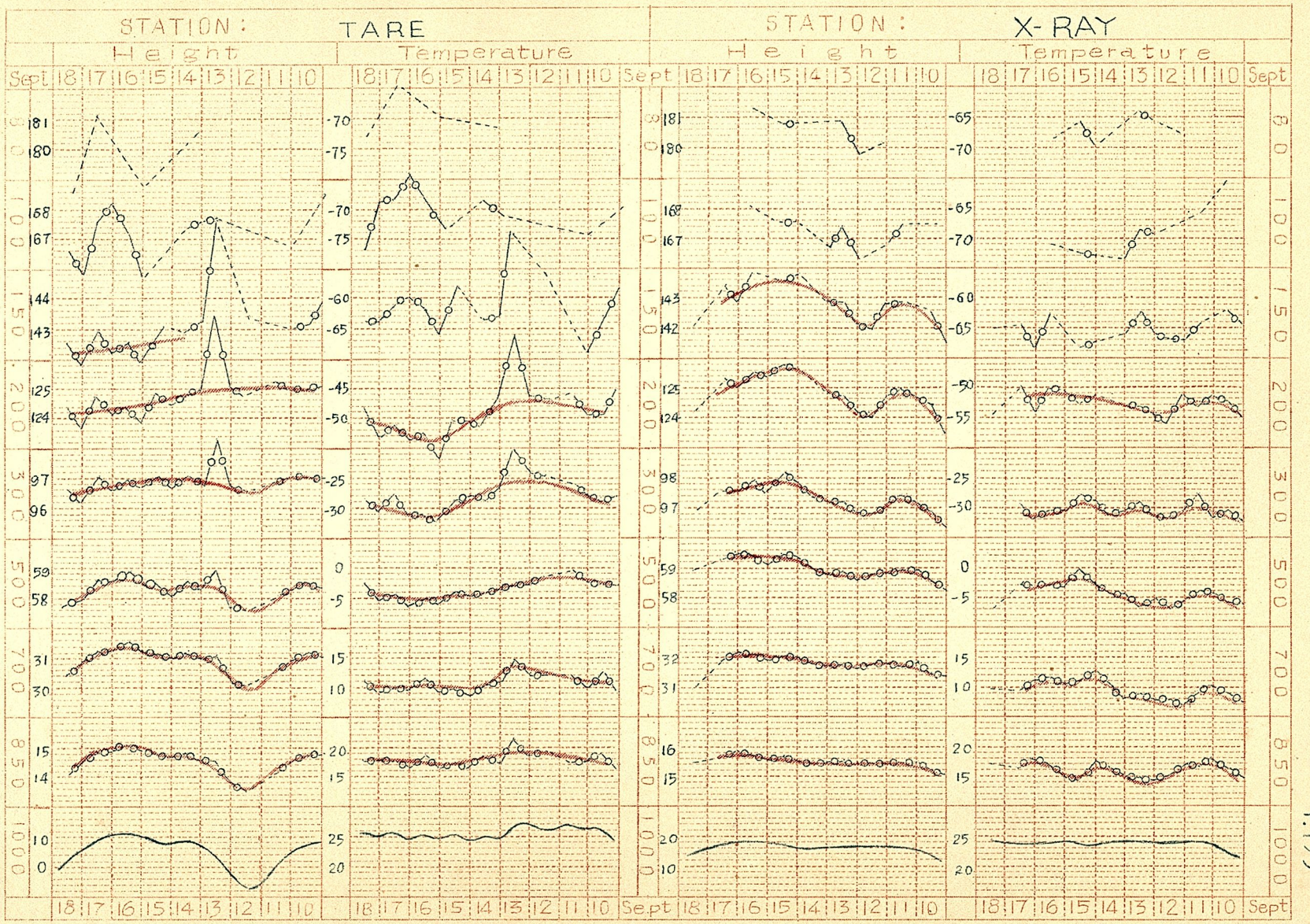
STATION : TARE
Height
Temperature
STATION : X-RAY
Height
Temperature
Sept 18 17 16 15 14 13 12 11 10
MIDDLE POINT CORRECTION (TYPHOON KEZIA) .
P.195

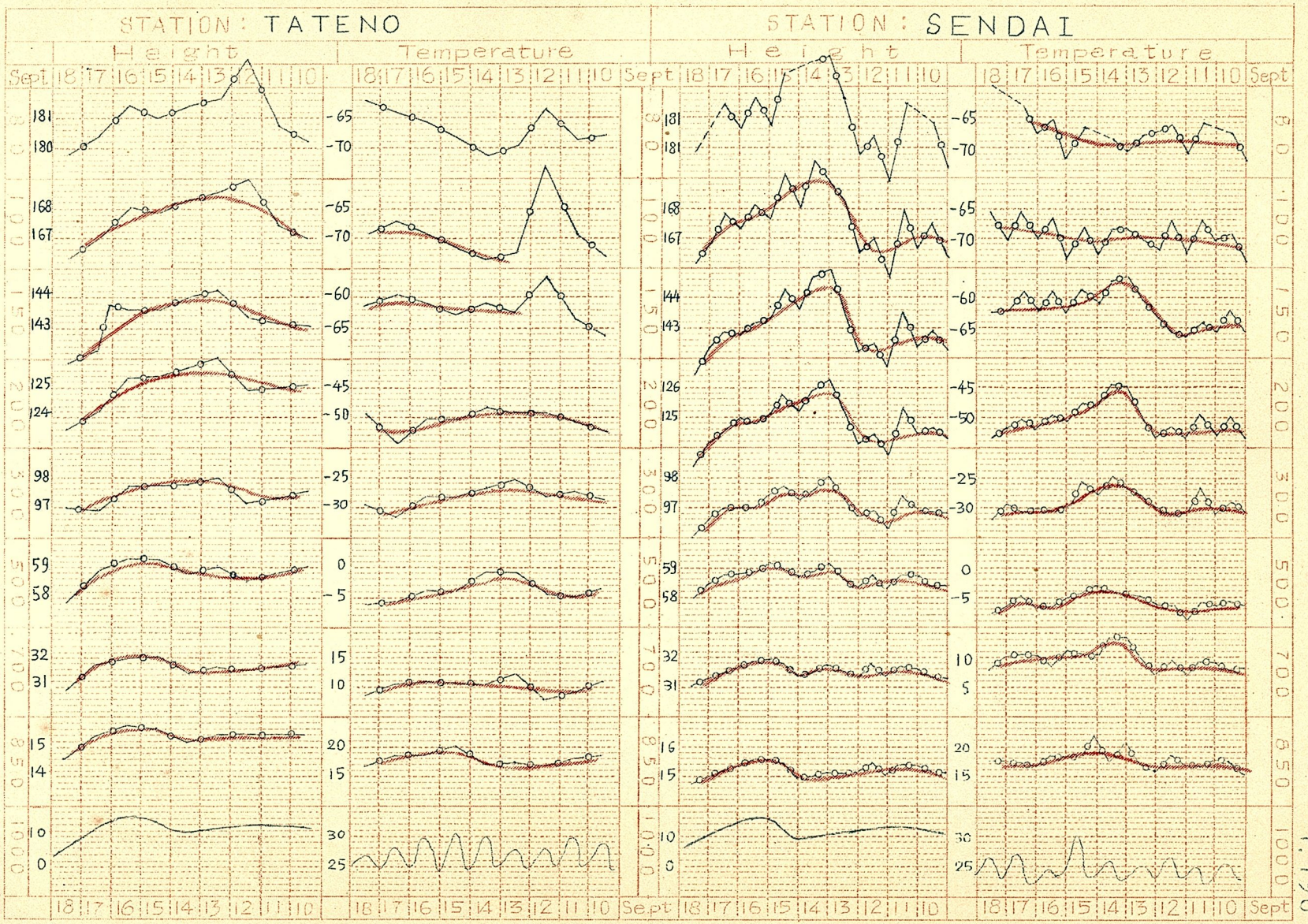
STATION : TATENO
Height
Temperature
STATION : SENDAI
Height
Temperature
Sept 18 17 16 15 14 13 12 11 10
800 181 180 -65 -70
1000 168 167 -65 -70
1500 144 143 -60 -65
2000 125 124 -45 -50
3000 98 97 -25 -30
5000 59 58 0 -5
7000 32 31 15 10
8500 15 14 20 15
10000 10 0 30 25
MIDDLE POINT CORRECTION (TYPHOON KEZIA)
P.196

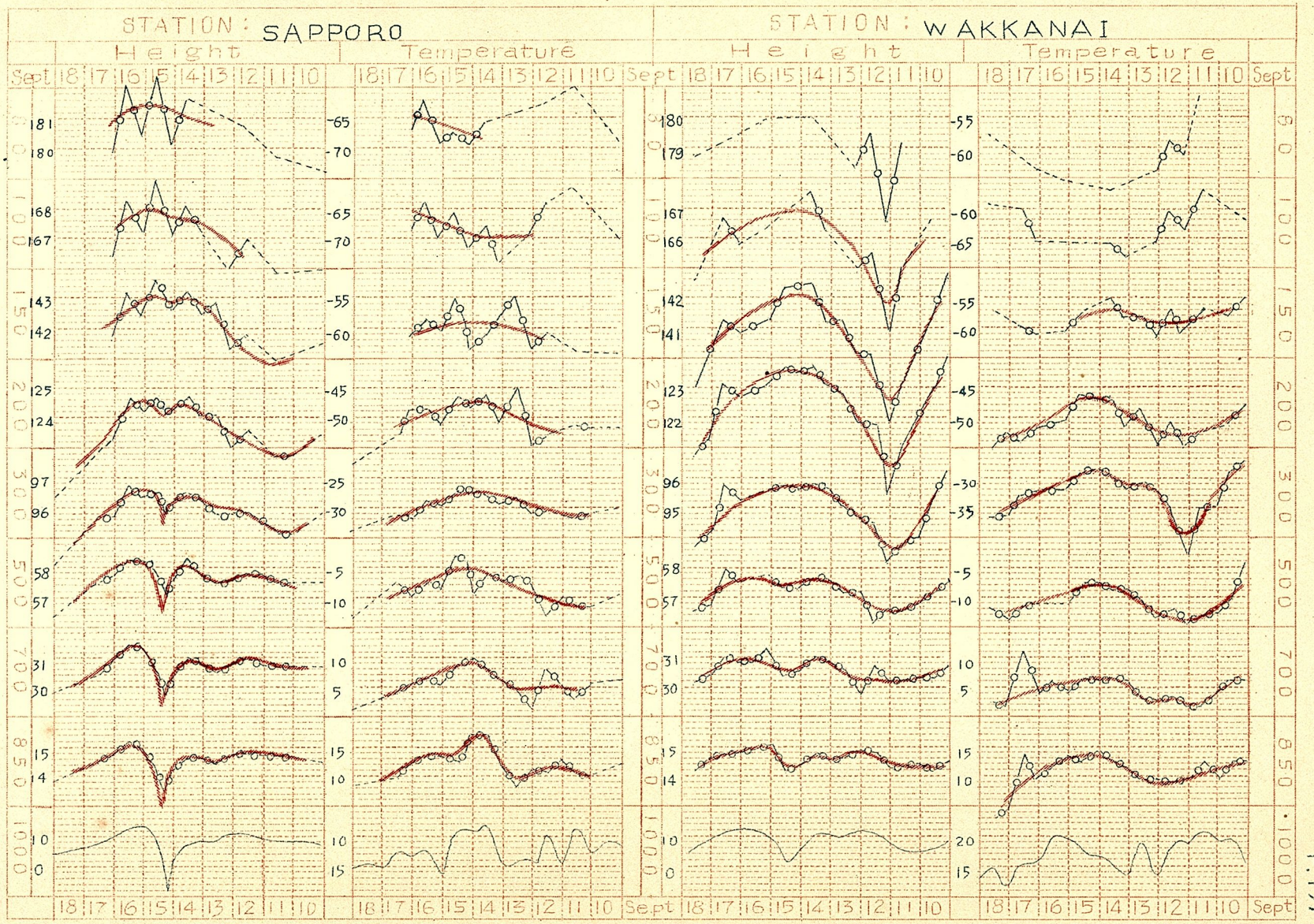
STATION : SAPPORO
Height
Temperature
STATION : WAKKANAI
Height
Temperature
Sept 18 17 16 15 14 13 12 11 10
500 700 850 1000
181 180 168 167 143 142 125 124 97 96 58 57 31 30 15 14 10 0
-65 -70 -65 -70 -55 -60 -45 -50 -25 -30 -5 -10 10 5 15 10 10 15
180 179 167 166 142 141 123 122 96 95 58 57 31 30 15 14 10 0
-55 -60 -60 -65 -55 -60 -45 -50 -30 -35 -5 -10 10 5 15 10 20 15
MIDDLE POINT CORRECTION (TYPHOON KEZIA)
P.197

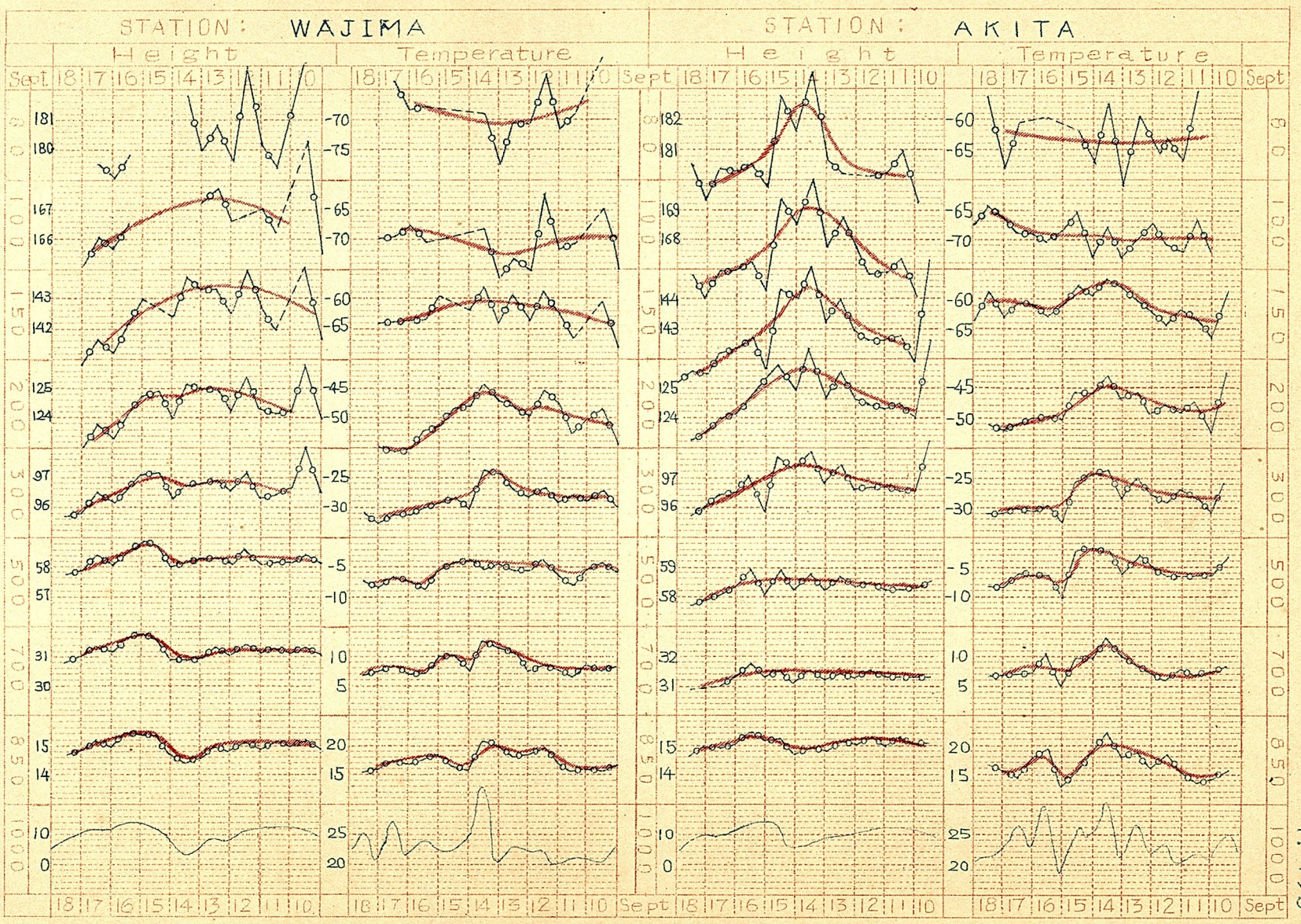
STATION : WAJIMA
Height
Temperature
STATION : AKITA
Height
Temperature
Sept 18 17 16 15 14 13 12 11 10
800 1000 1500 2000 3000 5000 7000 8500 10000
181 180 167 166 143 142 125 124 97 96 58 57 31 30 15 14 10 0
-70 -75 -65 -70 -60 -65 -45 -50 -25 -30 -5 -10 10 5 20 15 25 20
182 181 169 168 144 143 125 124 97 96 59 58 32 31 15 14 10 0
-60 -65 -65 -70 -60 -65 -45 -50 -25 -30 -5 -10 10 5 20 15 25 20
MIDDLE JOINT CORRECTION (TYPHOON KEZIA)
F. 198

EXAMPLE 6

CONSTANT PRESSURE CHARTS FOR TYPHOON KEZIA
AT 300 mb LEVEL

From 12h 12th to 18h 15th

Sept. 1950

To make the charts at 300 mb level of our area, the number of the available stations is not so large enough. In the present analyses, therefore, the values read from the red curves in the previous middle point corrections are also entered on the chart at the locations 6 hrs before and after the map time. At the same time the arrows showing the tendencies of temperature and height are entered.

In spite of the careful correction of the original data, the values on the charts are not so accurate as we see on the surface maps. The height contours are drawn under such condition, but it is possible to know the approximate patterns.

It must be pointed out here that the time section at a station locating near the typhoon path does not always represent the similar pressure field to what we see on spatial chart. For instance, one might suppose, by looking at the time section at Wajima or Akita, that the constant pressure surface of the 300 mb in the typhoon center is higher than of the environments, however, it is not the case.

As will be seen in the typhoon pattern, in which only the -26°C lines are contoured, warm air surrounding the typhoon over southern ocean advanced northward together with her, until it formed a tongue which changed into an enclosed area. It must be pointed out also that the warm areas in question were accompanied by cold stratosphere in the levels higher than the 150 mb level.

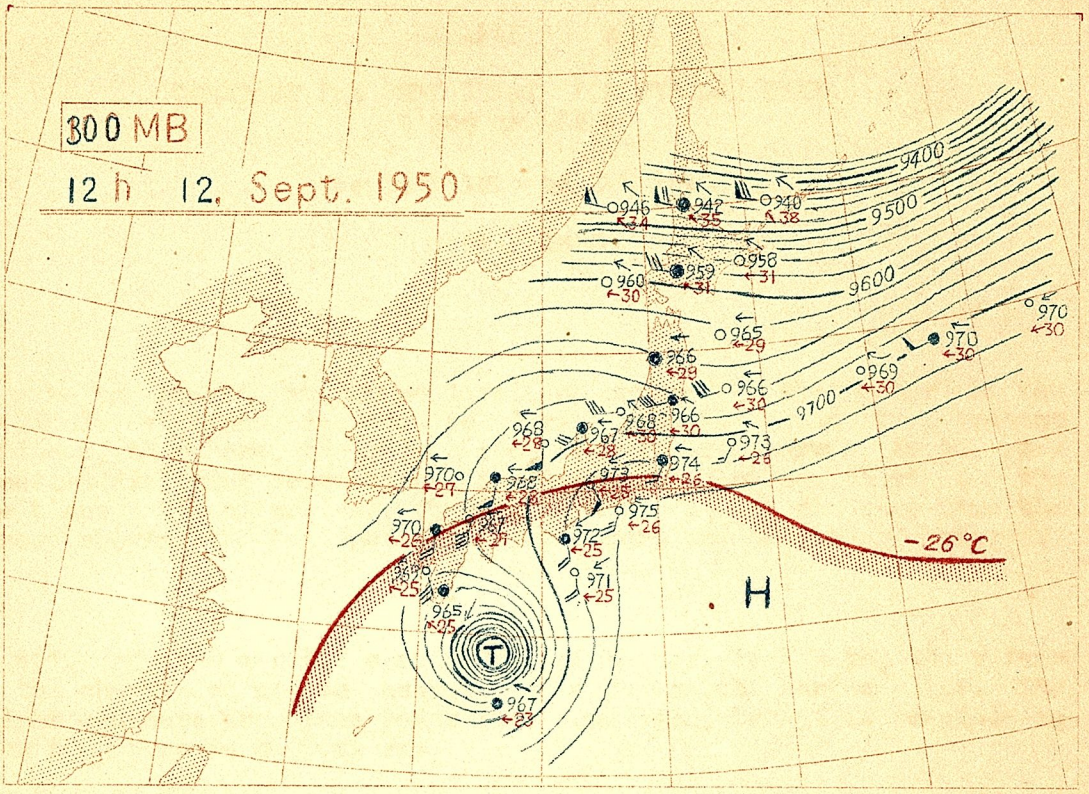
300 MB
12 h 12. Sept. 1950
9400
9500
9600
9700
-26°C
H
L

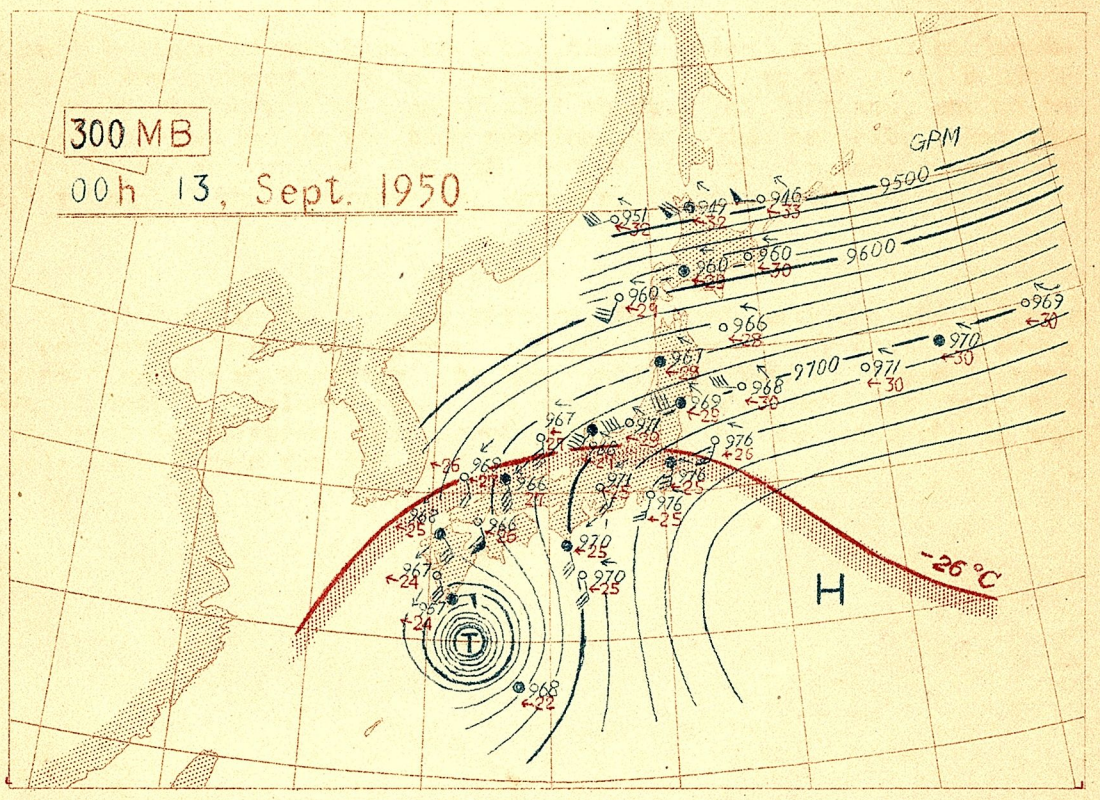
300 MB
00 h 13. Sept. 1950
GPM
9500
9600
9700
-26°C
H

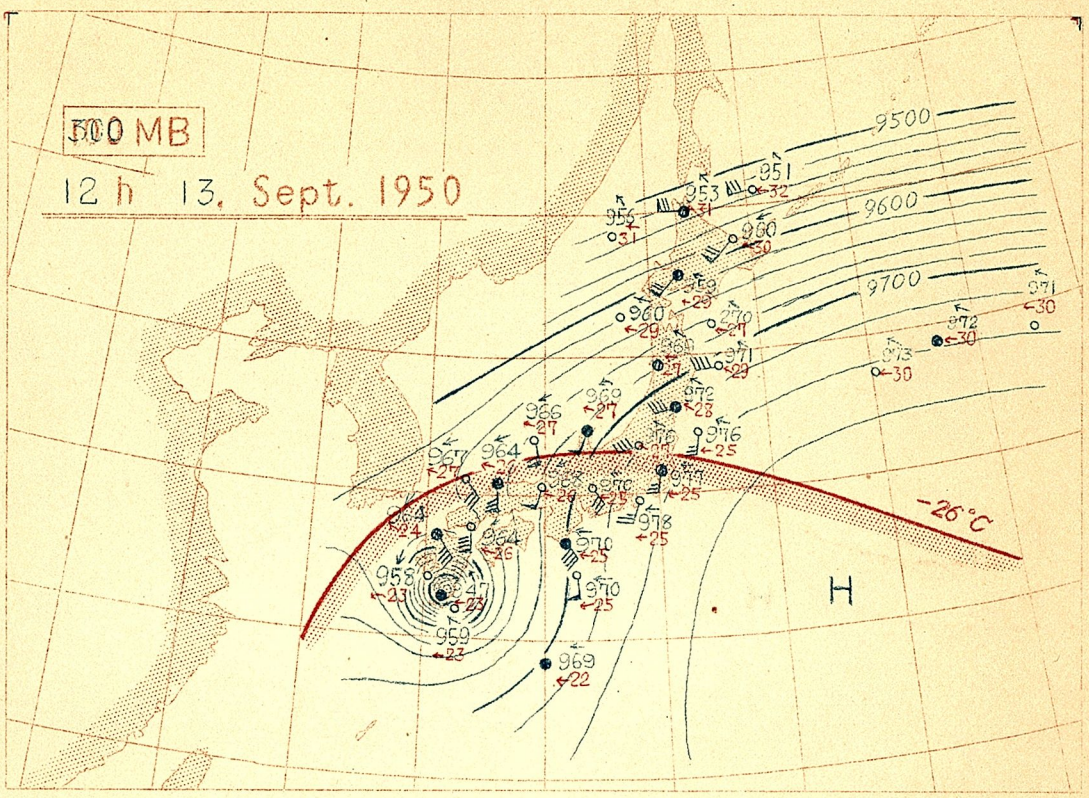
500 MB
12 h 13. Sept. 1950
9500
9600
9700
-26°C
H

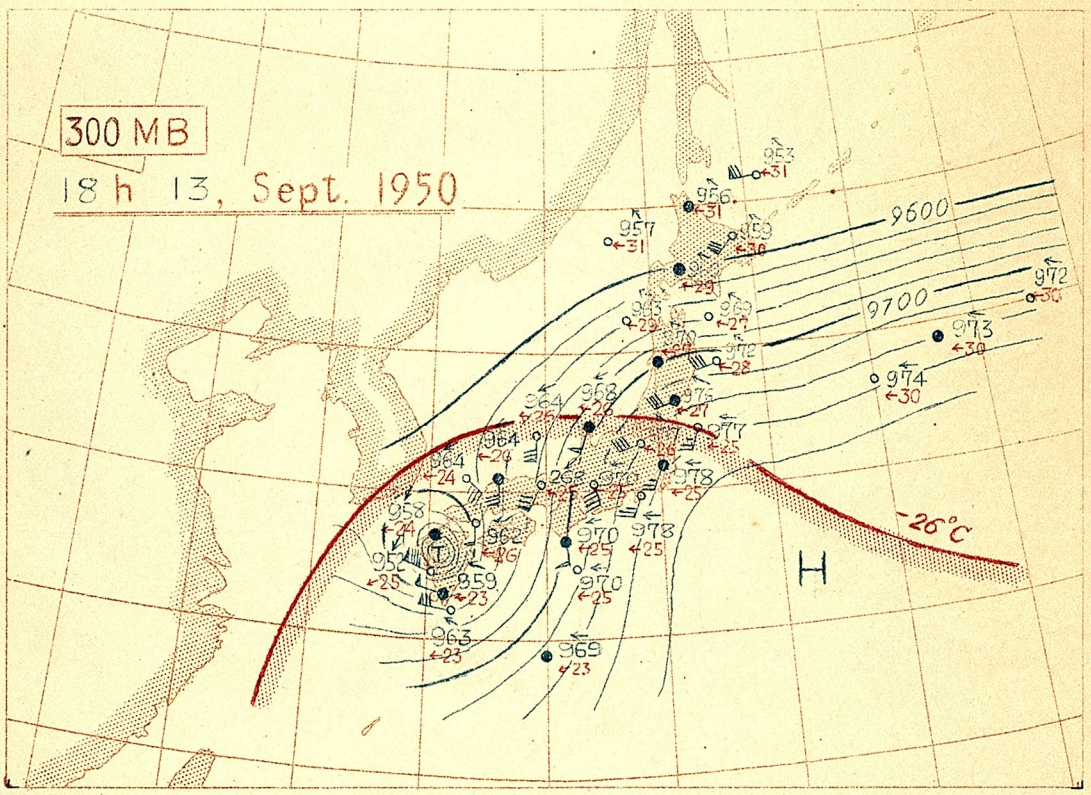
300 MB
18 h 13, Sept. 1950
9600
9700
-26°C
H

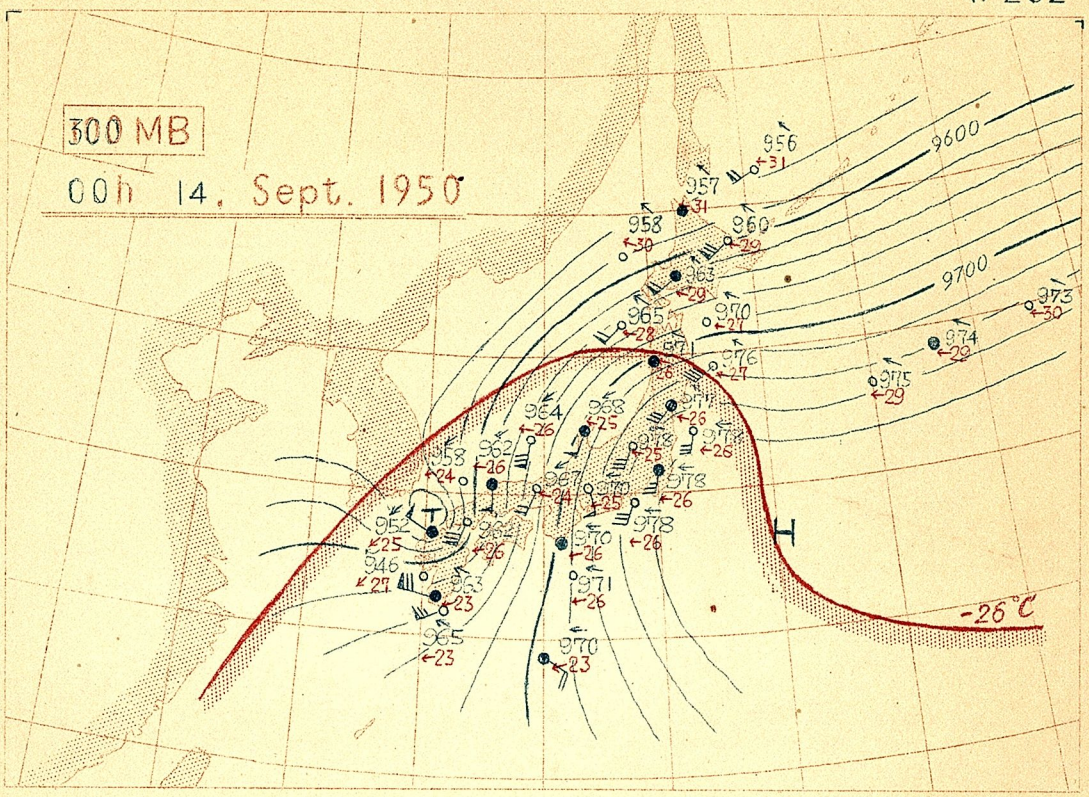
300 MB
00h 14. Sept. 1950
9600
9700
H
-26°C

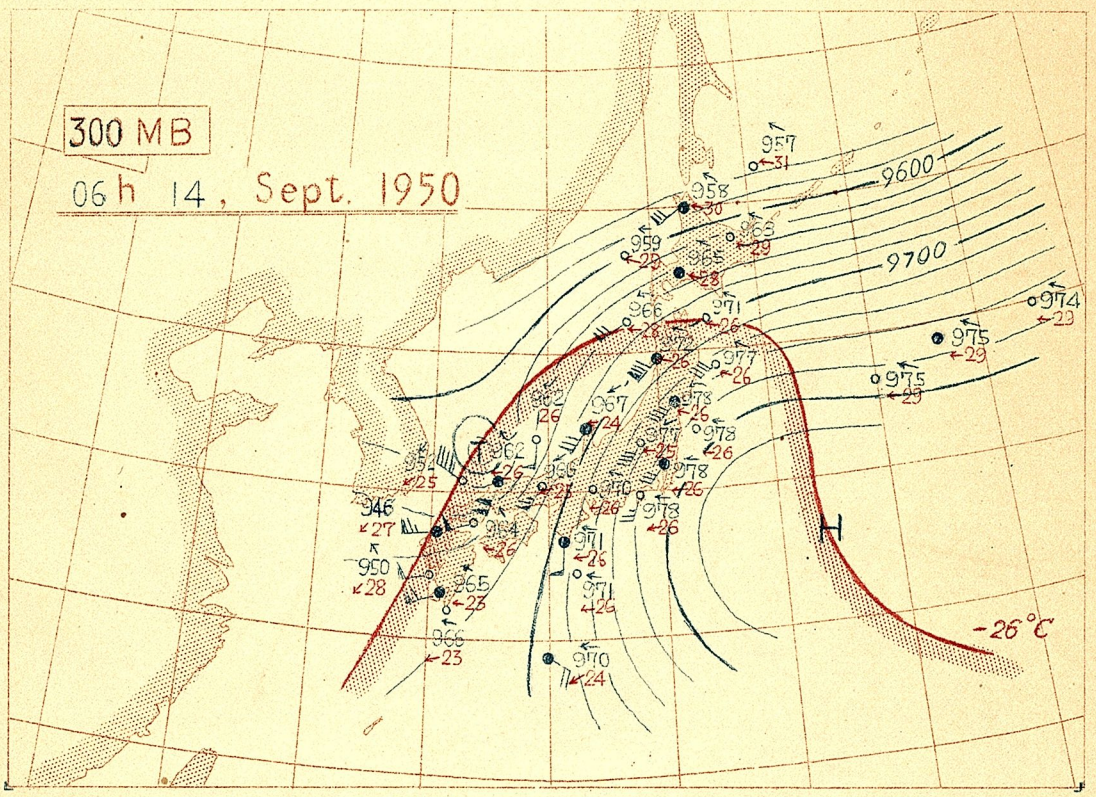
300 MB
06h 14, Sept. 1950
9600
9700
H
-26°C

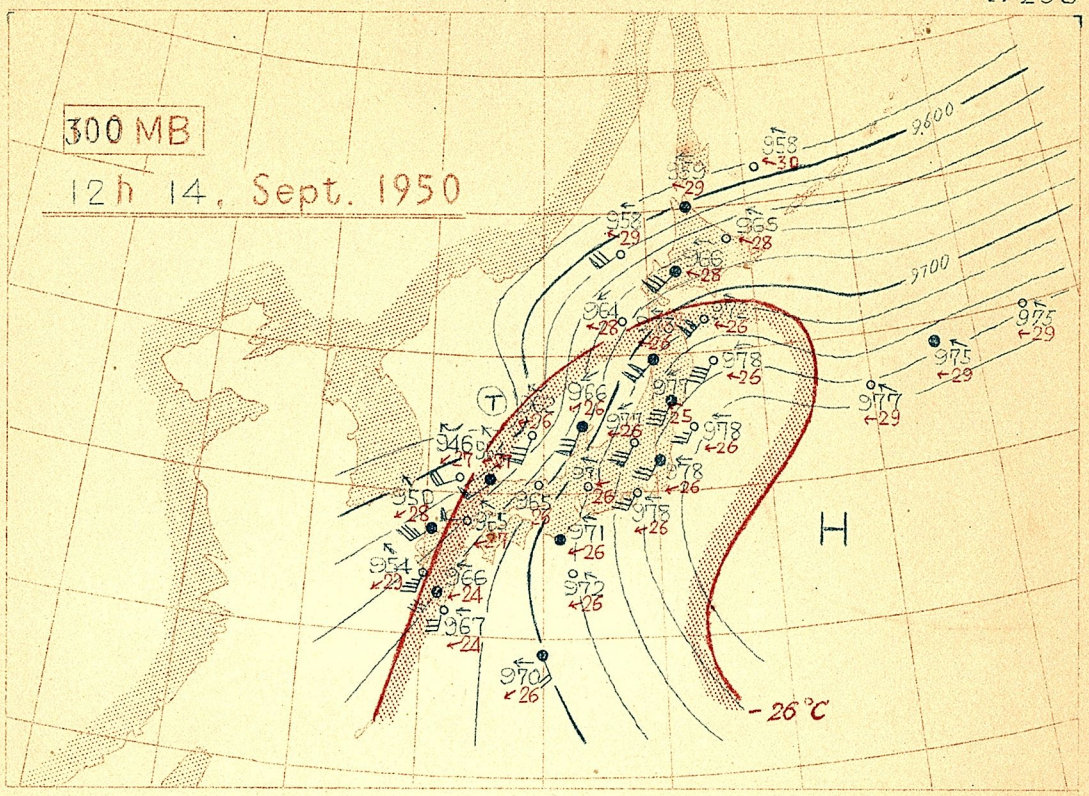
300 MB
12h 14, Sept. 1950
9600
9700
T
H
-26°C

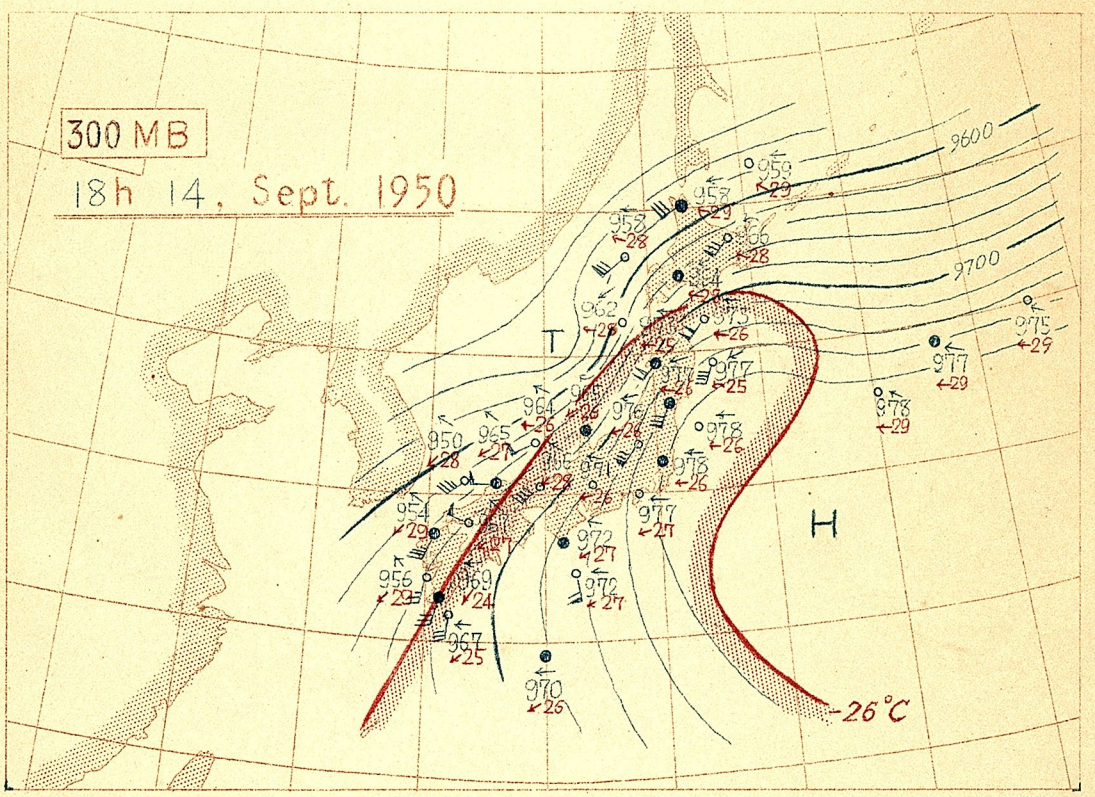
300 MB
18h 14, Sept. 1950
9600
9700
T
H
-26°C

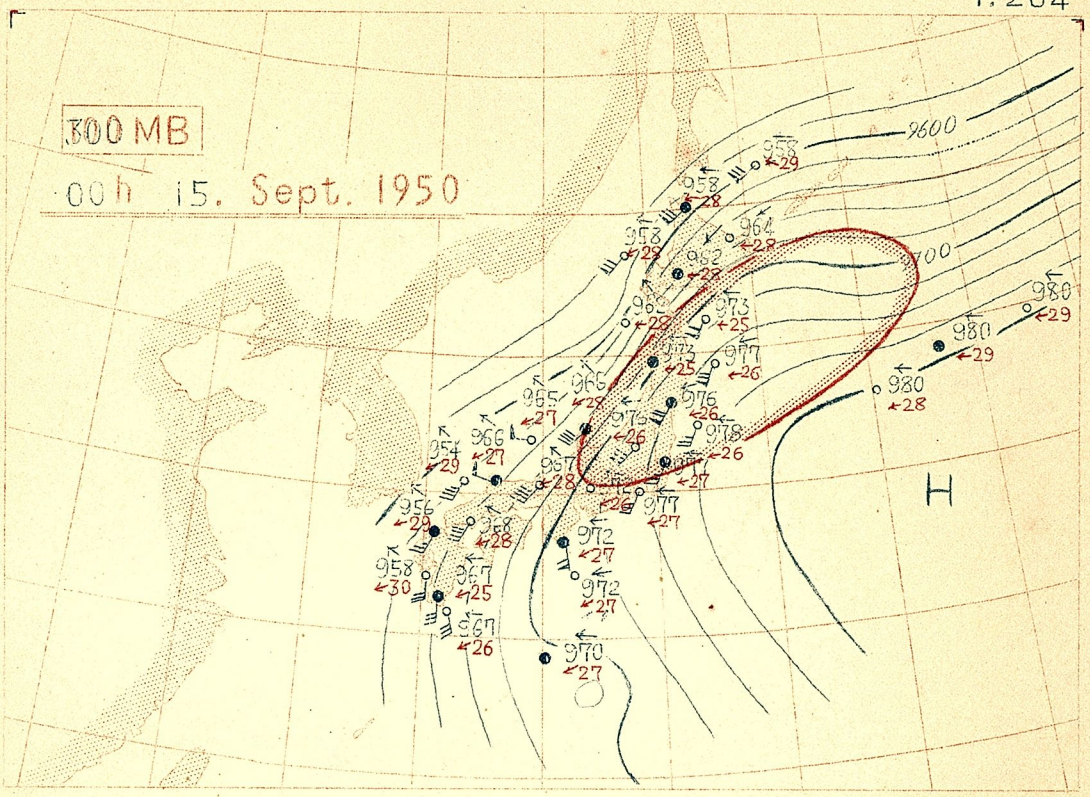
300 MB
00h 15. Sept. 1950
9600
9700
H

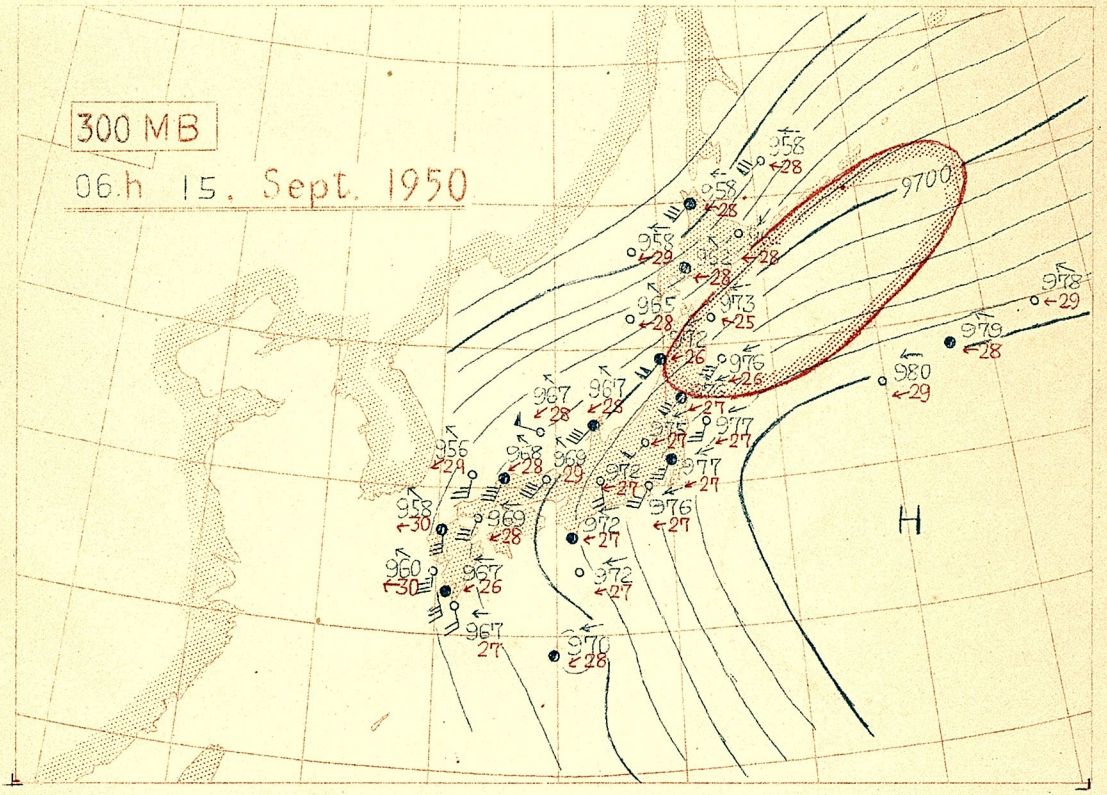
300 MB
06h 15. Sept. 1950
9700
H

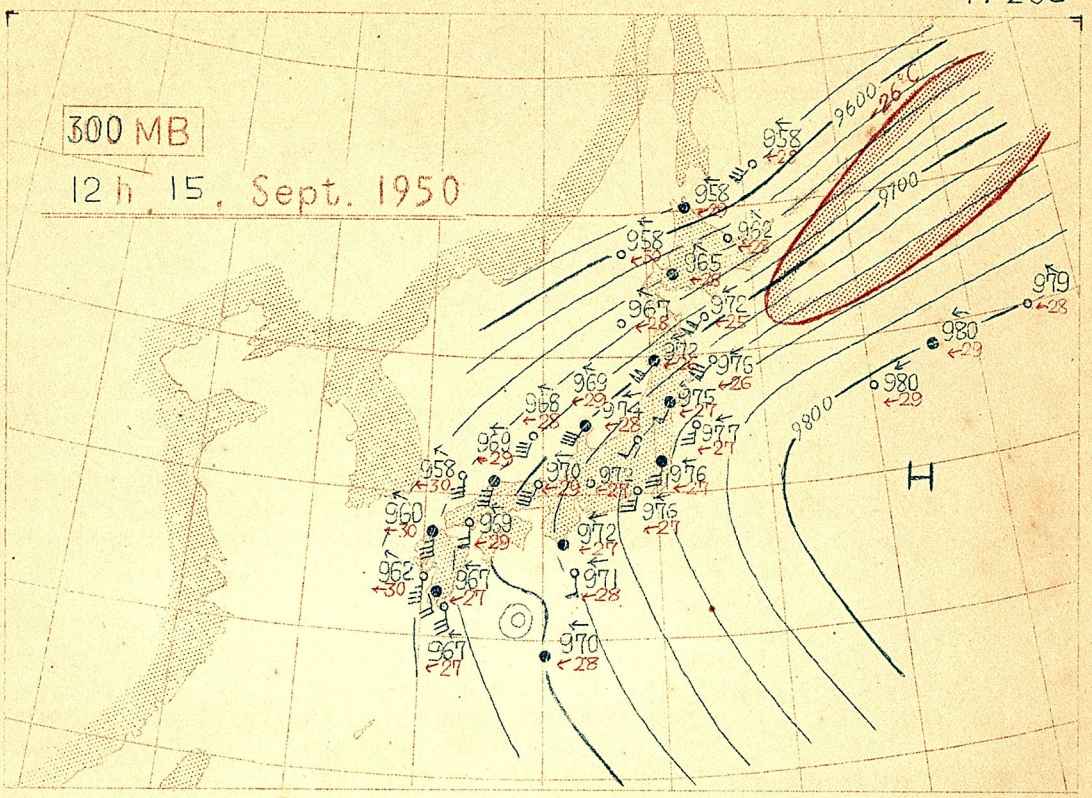
300 MB
12 h 15, Sept. 1950
9600
9700
9800
-26°C
H

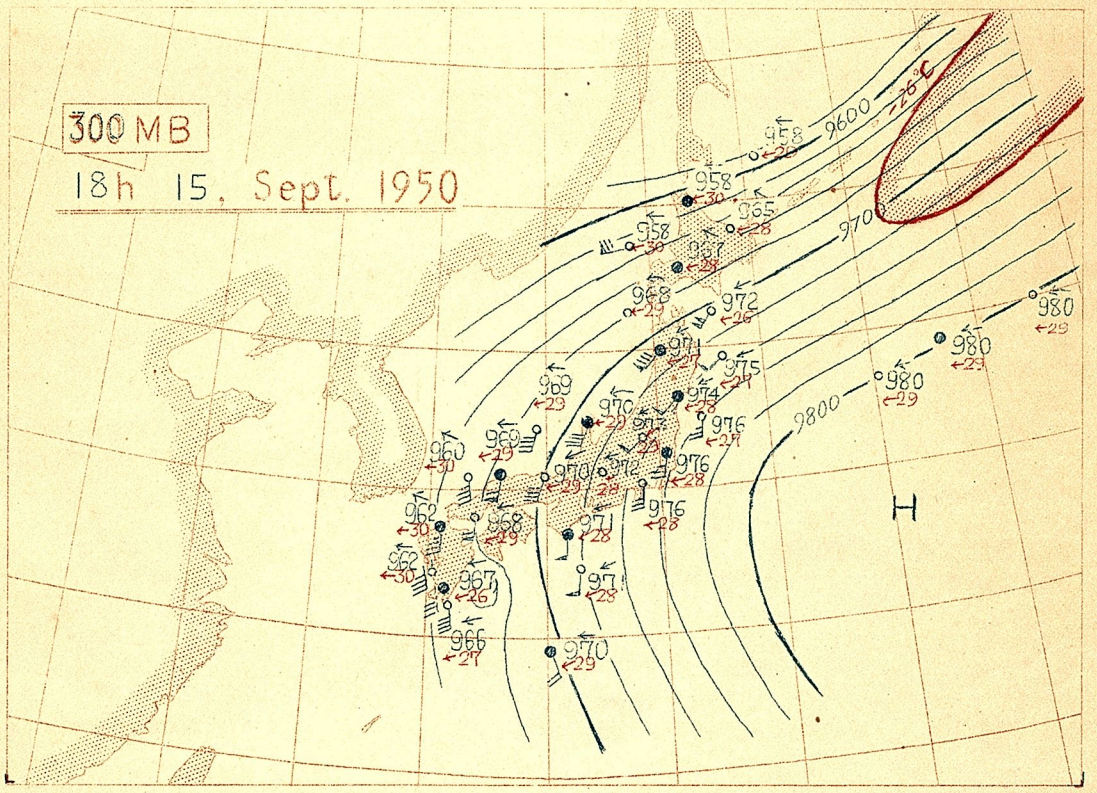
300 MB
18h 15, Sept. 1950
9600
9700
9800
-26°C
H